

GENETIC AND CHEMICAL TARGETING OF THE OUTER MEMBRANE

**GENETIC AND CHEMICAL TARGETING OF THE GRAM-NEGATIVE OUTER
MEMBRANE TO POTENTIATE LARGE-SCAFFOLD ANTIBIOTICS**

By Kristina Klobucar, Hons. B.Sc.

A thesis submitted to the School of Graduate Studies in partial fulfillment of the
requirements for the degree of Doctor of Philosophy

McMaster University © Kristina Klobucar, April 2022

Ph.D. Thesis – K. Klobucar; McMaster University – Biochemistry & Biomedical Sciences

DOCTOR OF PHILOSOPHY (2022) McMaster University

(Biochemistry and Biomedical Sciences) Hamilton, Ontario

TITLE: Genetic and chemical targeting of the Gram-negative outer membrane to potentiate large-scaffold antibiotics

AUTHOR: Kristina Klobucar, Hons. B.Sc.

SUPERVISOR: Eric D. Brown, Ph.D.

PAGES: xiii, 206

Abstract

The outer membrane (OM) is a formidable barrier that has made antibiotic drug discovery in Gram-negatives exceedingly difficult. Many antibiotics which are effective against Gram-positive bacteria cannot permeate the Gram-negative OM to reach their intracellular targets. Thus, it is important to explore unconventional approaches to overcome the intrinsic resistance conferred by the OM. Herein, we used both genetic and chemical means to compromise OM integrity to potentiate the activity of large-scaffold antibiotics against *Escherichia coli*. First, we mapped the genetic interaction network of OM biosynthetic genes using synthetic genetic arrays (SGAs) to reveal permeability determinants of the *E. coli* OM. This led to the creation of a publicly accessible dataset of ~155,400 double deletion strains with growth data in the presence of the large-scaffold antibiotics rifampicin and vancomycin. Investigations of a subset of synthetic sick interactions revealed connectivity in the context of permeability between lipopolysaccharide (LPS) inner core biosynthetic genes and an enigmatic gene involved in enterobacterial common antigen (ECA) regulation. Second, we leveraged a chemical screening platform based on the observation that disruption of the *E. coli* OM leads to antagonism of vancomycin activity at cold temperatures to uncover molecules that potentiate Gram-positive-targeting antibiotics at 37 °C. Two of these compounds, liproxstatin-1 and MAC-0568743, were characterized to bind to LPS and disrupt OM integrity specifically without impacting the inner membrane (IM). Third, we performed genetic and chemical screening to unearth

targets capable of potentiating the activity of Gram-positive-targeting antibiotics against *E. coli*. This validated the OM as a valuable target for antibiotic adjuvants and led to the discovery of two membrane active compounds and an inhibitor of lipid A biosynthesis. Overall, this thesis emphasizes the importance of elucidating biological factors contributing to OM permeability and the attractiveness of the OM as a target for antibiotic potentiators.

Acknowledgements

Dr. Eric Brown – thank you for giving me the opportunity to perform my graduate research in your lab. Your guidance and mentorship have helped to shape me into the more confident and driven scientist that I am today. I will never forget this experience.

Drs. Marie Elliot and Mike Surette – thank you for your scientific guidance and support along the way. I appreciate the time you've given me and the positivity you both bring to our meetings.

Brownies, past and present – thank you to everyone who has taken the time to share their expertise with me and lend a helping hand. Thanks for always being there for me, both in science and in friendship.

My dearest friends – thank you for reminding me that there's more to life than just lab. I appreciate all our life chats and rants and laughs.

Daniel – thank you for all the love and encouragement you've given me throughout graduate school. The walks and smiles in stressful times helped get me through it. I am so glad that we have gone on this journey together. Words cannot describe how much you mean to me. I love you.

Mom and Dad – this is for you. Thank you for always believing in me and encouraging my pursuit of education. I could not have made it this far without you. Your love and support are everything to me. I love you both.

Table of contents

Foreword	
Abstract.....	iii
Acknowledgements.....	v
Table of contents	vi
List of figures	ix
List of tables.....	xi
List of abbreviations.....	xii
Chapter I – Introduction	
Preface	2
The history of antibiotics: An evolutionary arms race	3
Synthetic interactions as probes of complexity in cell systems	4
Investigating genetic synthetic lethality using synthetic genetic arrays	7
Chemical-genetic synthetic lethality.....	10
The Gram-negative outer membrane as a barrier to antibiotic entry	12
Lipopolysaccharide biosynthesis	13
Targeting the outer membrane to overcome intrinsic antibiotic resistance.....	15
Research objectives: From understanding outer membrane biology to drug discovery.....	19
References	20
Figures.....	31
Chapter II - Genetic and chemical-genetic interactions map biogenesis and permeability determinants of the outer membrane of <i>Escherichia coli</i>	
Preface	38
Abstract.....	39
Importance.....	40
Introduction	40
Results.....	44
Synthetic genetic arrays of outer membrane-related genes	44
Frequent interactors in SGA analysis	46
Profound differences in interactions when probed with Gram-positive targeting antibiotics.....	47
OMI Explorer: An online, searchable database for genome-wide interactions of outer membrane biosynthetic genes	49
An interaction between $\Delta yhdP$ and deletions in LPS inner core biosynthesis	50
Discussion	55
Materials and methods	61
References	67
Figures.....	75
Tables.....	83
Supplementary figures.....	84
Supplementary tables.....	90

Chapter III – Chemical screen for vancomycin antagonism uncovers probes of the Gram-negative outer membrane

Preface	94
Abstract.....	95
Introduction	96
Results and Discussion	101
A high-throughput screen to uncover compounds that perturb the outer membrane.....	101
Liproxstatin-1 and MAC-0568743 potentiate Gram-positive-targeting antibiotics in Gram-negatives	104
The potentiation of Gram-positive-targeting antibiotics is due to outer membrane disruption	105
Liproxstatin-1 and MAC-0568743 interact with the outer membrane by binding to LPS	108
Liproxstatin-1 and MAC-0568743 minimally impact inner membrane integrity	111
Potentiation activity of structural analogues of liproxstatin-1 and MAC-0568743.....	113
Conclusion	116
Methods	117
Funding.....	123
Acknowledgements.....	124
References	124
Figures.....	129
Tables.....	139
Supplementary figures.....	140
Supplementary tables	145
Chapter IV – Genetic and chemical screening reveals targets and compounds to potentiate Gram-positive antibiotics against Gram-negative bacteria	
Preface	150
Abstract.....	151
Introduction	152
Results and Discussion	154
Genetic requirements for resistance of <i>E. coli</i> to Gram-positive-targeting antibiotics.....	154
Chemical screening for potentiation of Gram-positive-targeting antibiotics in <i>E. coli</i>	157
MAC-0493157 and MAC-0483351 potentiate linezolid through outer and inner membrane disruption	159
MAC-0485042 potentiates rifampicin and vancomycin by inhibition of LpxC	161
LpxC inhibitors are synergistic with rifampicin in Gram-negative pathogens.....	164
Conclusion	166

Methods	167
Funding	173
Acknowledgements.....	173
References	174
Figures.....	179
Tables	185
Supplementary figures.....	186
Supplementary tables	189
Chapter V – Conclusion	
Summary	191
Lessons learned	192
Future directions	193
Exploiting synthetic interactions in antibacterial drug discovery	196
Targeting the outer membrane for antibiotic potentiation in the clinic	198
Concluding remarks.....	201
References	202
Figures.....	206

List of figures

Chapter I

Figure 1: The principle of synthetic lethal interactions	31
Figure 2: A synthetic genetic array workflow	32
Figure 3: Classes of Gram-positive-targeting antibiotics which are ineffective against Gram-negative bacteria with an intact OM.....	33
Figure 4: Increased OM permeability leads to potentiation of the activity of impermeable antibiotics	34
Figure 5: Lipid A biosynthesis and LPS core assembly in <i>E. coli</i>	35

Chapter II

Figure 1: Synthetic genetic arrays of outer membrane-related gene deletions	75
Figure 2: Frequent interactors in SGAs have conjugation and recombination defects	76
Figure 3: Synthetic genetic interactions are altered in the presence of subinhibitory concentrations of large-scaffold antibiotics.....	77
Figure 4: Example of a search output in OMI Explorer.....	78
Figure 5: A synthetic sick interaction between $\Delta yhdP$ and LPS inner core deletion strains results in increased susceptibility to cell wall active antibiotics	79
Figure 6: The increased susceptibility, of strains with deletions in <i>yhdP</i> and LPS inner core genes, to vancomycin is due to both outer membrane permeability and Und-P flux.....	81
Figure S1: The workflow used to generate SGAs.....	84
Figure S2: SGAs of outer membrane-related gene deletions in subinhibitory concentrations of rifampicin and vancomycin	85
Figure S3: Network interaction map for SSL gene pairs for no drug, rifampicin, and vancomycin	86
Figure S4: t-SNE clustering of SGAs under rifampicin stress compared to no drug.....	87
Figure S5: Deletion of <i>yhdP</i> in LPS inner core deletion strains leads to a growth defect	88
Figure S6: Deletion of ECA production suppresses vancomycin MIC in $\Delta yhdP \Delta lpcA$, $\Delta yhdP \Delta rfaE$, $\Delta yhdP \Delta waaF$, and $\Delta yhdP \Delta waaP$	89

Chapter III

Figure 1: High-throughput chemical screen for molecules that antagonize the activity of vancomycin at cold temperatures	129
Figure 2: Liproxstatin-1 and MAC-0568743 potentiate Gram-positive-targeting antibiotics in Gram-negative bacteria	131
Figure 3: Potentiation of large-scaffold antibiotics by liproxstatin-1 and MAC-0568743 was due to OM disruption.....	133
Figure 4: Liproxstatin-1 and MAC-0568743 disrupt the bacterial OM by physically interacting with LPS	135

Figure 5: Liproxstatin-1 and MAC-0568743 exhibit minimal IM disruption ...	137
Figure S1: Liproxstatin-1 and MAC-0569743 do not potentiate the large, hydrophilic antibiotic, vancomycin	140
Figure S2: Treatment with subinhibitory liproxstatin-1 and MAC-0568743 results in regions of accumulation of membrane stain FM4-64 in <i>E. coli</i>	141
Figure S3: MAC-0568743 is able to physically perturb the OM of stationary phase cells.....	142
Figure S4: Liproxstatin-1 is able to physically perturb the OM of stationary phase cells.....	143
Figure S5: Liproxstatin-1 and MAC-0568743 are effective OM perturbants in polymyxin-resistant environmental and clinical isolates of <i>E. coli</i>	144
Chapter IV	
Figure 1: Genetic requirements for resistance to Gram-positive-targeting antibiotics in <i>E. coli</i>	179
Figure 2: Workflow of the chemical screens for potentiation of Gram-positive-targeting antibiotics	180
Figure 3: MAC-0493157 and MAC-0483351 potentiate the activity of linezolid against <i>E. coli</i> through outer and inner membrane disruption	181
Figure 4: MAC-0485042 potentiates rifampicin and vancomycin activity in <i>E. coli</i> through inhibition of LpxC	183
Figure 5: LpxC inhibitors can be used to potentiate the activity of rifampicin in pathogens	184
Figure S1: Replica plots of normalized <i>E. coli</i> growth in all five primary chemical screens performed in duplicate	186
Figure S2: Chemical structures of A22 analogues detected as actives from the primary potentiation screens.....	187
Figure S3: Chemical structures of sulfonamides detected as actives from the primary vancomycin potentiation screen	187
Figure S4: The hydroxamate moiety is required for potentiation activity of MAC-0485042.....	188
Figure S5: The <i>E. coli lpxC101</i> D22 mutant strain is hypersensitive to rifampicin and vancomycin	188
Chapter V	
Figure 1: Compounds that target LPS, both physically and its biosynthesis, are synergistic with vancomycin in a $\Delta yhdP$ background	206

List of tables

Chapter II	
Table 1: Summary of SSL interactions across all SGAs performed	83
Table S1: Background information on query gene deletion strains	90
Table S2: All synthetic interaction values for SGAs performed in no drug, vancomycin, and rifampicin	90
Table S3: Gene list from t-SNE cluster highlighted in green in Figure 3	91
Table S4: Antibiotic susceptibility testing of a diverse panel of antibiotics against double and single deletion strains of $\Delta yhdP$ and LPS inner core.....	92
Chapter III	
Table 1: Potentiation and inner membrane activity of lipoxstatin-1 analogues in <i>E. coli</i> BW25113.....	139
Table S1: Physicochemical properties of active and inactive compounds screened	145
Table S2: Potentiation activity of D-Series MAC-0568743 analogues in <i>E. coli</i> BW25113	146
Table S3: Characterization and potentiation activity of B-series MAC-0568743 analogues in <i>K. pneumoniae</i> C026	147
Chapter IV	
Table 1: Minimum inhibitory concentrations of Gram-positive-targeting antibiotics in wild type, hyperporinated, and efflux-deficient strains of <i>E. coli</i> BW25113	185
Table S1: Potentiation activity of MAC-0493157 and MAC-0483351 analogues in <i>E. coli</i> BW25113.....	189

List of abbreviations

Ab	<i>Acinetobacter baumannii</i>
ACP	acyl carrier protein
AFM	atomic force microscopy
Apra	apramycin
ATP	adenosine triphosphate
CIP	chromosomal integrative plasmid
DiSC ₃₍₅₎	3,3'-dipropylthiacarbocyanine
DMEM	Dulbecco's modified eagle medium
DMSO	dimethyl sulfoxide
DNA	deoxyribonucleic acid
ECA	enterobacterial common antigen
ECA _{cyc}	cyclic ECA
ECA _{LPS}	lipopolysaccharide-linked ECA
ECA _{PG}	phosphatidylglycerol-linked ECA
EDTA	ethylenediaminetetraacetic acid
Erm	erythromycin
FBS	fetal bovine serum
FIC	fractional inhibitory concentration
FICI	fractional inhibitory concentration index
Gal	galactose
Glc	glucose
GlcNAc	<i>N</i> -acetylglucosamine
GO	Gene Ontology
Hep	<i>L-glycero-D-manno</i> -heptose
HEPES	4-(2-hydroxyethyl)-1-piperazineethanesulfonic acid
Hfr	high-frequency recombination
IC ₅₀	half-maximal inhibitory concentration
IM	inner membrane
IPTG	isopropyl β -D-1-thiogalactopyranoside
Kan	kanamycin
Kdo	3-deoxy- <i>D-manno</i> -octulosonic acid
Kp	<i>Klebsiella pneumoniae</i>
LB	lysogeny broth
LDH	lactate dehydrogenase
Lin	linezolid
LPS	lipopolysaccharide
MEM	minimal essential medium
MES	morpholinoethanesulfonic acid
MHA	Mueller Hinton Agar
MHB	Mueller Hinton Broth
MIC	minimum inhibitory concentration
Mla	maintenance of lipid asymmetry

Novo	novobiocin
O/N	overnight
OD	optical density
OM	outer membrane
OMI	Outer Membrane Interaction
ONPG	ortho-nitrophenyl- β -galactoside
OS	oligosaccharide
Pa	<i>Pseudomonas aeruginosa</i>
PA β N	phenylalanine-arginine β -naphthylamide
PBS	phosphate-buffered saline
PCR	polymerase chain reaction
PMB	polymyxin B
PMBN	polymyxin B nonapeptide
Rif	rifampicin
RNA	ribonucleic acid
RT	room temperature
SDS	sodium dodecyl sulfate
SGA	synthetic genetic array
SIV	synthetic interaction value
SMILES	simplified molecular-input line-entry system
sRNA	small RNA
SSL	synthetic sick or lethal
t-SNE	t-distributed stochastic neighbour embedding
UDP	uridine diphosphate
UMP	uridine monophosphate
Und-P	undecaprenyl-phosphate
UPEC	uropathogenic <i>Escherichia coli</i>
Vanco or Van	vancomycin
WHO	World Health Organization
WT	wild type

CHAPTER I – Introduction

Preface

Some parts of this chapter were adapted from two previously published reviews:

Klobucar K, Brown ED. 2018. Use of genetic and chemical synthetic lethality as probes of bacterial cell systems. *FEMS Microbiol Rev.* 42: fux054. Copyright 2018 Oxford University Press. Reused with permission.

Klobucar K, Brown ED. 2022. New potentiators of ineffective antibiotics: Targeting the Gram-negative outer membrane to overcome intrinsic resistance. *Curr Opin Chem Biol.* 66: 102099. Copyright 2022 Elsevier. Reused with permission.

I wrote and edited both manuscripts with input from Brown ED.

The history of antibiotics: An evolutionary arms race

The discovery of antibiotics has had an immense impact on modern medicine, providing the ability to treat and prevent bacterial infections, originating with the discovery of penicillin in 1928 and its widescale use in 1945 (1). This spurred the golden era of antibiotics, which focused on the discovery of natural product antibiotics, which are produced by bacteria and fungi to protect themselves from environmental competitors (2). Whole cell screening of natural product extracts led to the successful discovery of many antibiotics which were effective in treating bacterial infections *in vivo* and were well-tolerated in hosts (3). However, this reservoir of antibiotics was quickly depleted by the 1960s. Research efforts shifted from the discovery of new scaffolds to the improvement of existing scaffolds via medicinal chemistry efforts and screening of synthetic compounds. Later antibiotic drug discovery efforts were met with little success; leads discovered in target-based discovery platforms did not translate to whole cell activity (2, 4). This is especially true for Gram-negative bacteria, as no novel classes of antibiotics have been approved to treat Gram-negative infections since the quinolone antibiotics in 1962 (3, 5).

With the sparse antibiotic pipeline and increasing levels of bacterial resistance, we are in the modern resistance era (2). In fact, soon after the discovery of the first antibiotic, bacteria with resistance to penicillin were detected (6). Bacteria have developed many resistance mechanisms to antibiotics including modifications to the cellular targets of antibiotics, inactivation of the

antibiotics themselves, and upregulation of efflux pumps (7). Antimicrobial resistance has been responsible for millions of deaths worldwide (8) and public health organizations have highlighted the need for new treatments against pathogens including *Acinetobacter baumannii*, *Pseudomonas aeruginosa*, and Enterobacteriaceae, which have been listed as critical priority pathogens by the World Health Organization (WHO) (9, 10). Notably, these critical priority pathogens are Gram-negative, which are intrinsically resistant to many antibiotics; this will be further discussed in a later section of this chapter.

Since there are widespread bacterial resistance mechanisms to most currently available antibiotics, more research needs to be done to find unconventional ways to target bacterial cells (2). These unconventional approaches can include the discovery of druggable targets that have previously been overlooked, exploiting multiple weaknesses of bacterial cells in combination, and repurposing existing antibiotics in combination with other compounds, like adjuvants, to increase their efficacy in the face of resistance determinants. In order to accomplish this, more work must be done in the scope of gene or target essentiality in different contexts to truly understand the weaknesses in complex bacterial cell systems which can be exploited.

Synthetic interactions as probes of complexity in cell systems

Our classic understanding of gene essentiality is that some genes are indispensable, meaning that they are required for growth and cannot be deleted;

others are dispensable and can be mutated. This is a vast oversimplification as there are many different conditions and genomic contexts that can lead to a non-essential gene becoming essential for viability (11). Genetic interactions can alter gene essentiality, thus it is important to consider the complexity of the biological system under study (11).

Formally, a synthetic interaction is known as a phenotype that is produced by a combination of perturbations (genetic, chemical, or both) that differs from the expected phenotype based on the effect of each perturbing agent individually (12). In the study of microbial synthetic interactions, the phenotype that tends to be measured is fitness or growth (13–18). A synthetic interaction can be either positive or negative (Figure 1A). Positive genetic interactions (also referred to as synthetic viable interactions or alleviating epistasis) occur when the combination of perturbations leads to greater fitness than expected. An example of a synthetic viable interaction could involve a toxin-antitoxin system. Deleting both the toxin and corresponding antitoxin gene, would result in cell viability, whereas if the antitoxin gene was deleted alone, the cell would die (19). Negative genetic interactions (also referred to as aggravating epistasis, synergistic interactions, or synthetic lethality/sickness depending on the extent) occur when the combination of perturbations leads to a lower fitness than expected, or even a lethal phenotype (Figure 1B). Negative or synthetic sick/lethal (SSL) interactions tend to occur if both perturbations target genes in parallel or redundant pathways (Figure 1C) (20, 21). In this case, an essential precursor that is made only by these

redundant pathways will no longer have a means of being synthesized, resulting in synthetic lethality.

SSL interactions have been studied in eukaryotic organisms such as fruit flies, nematodes, yeast, and cancer cells, as well as prokaryotes, including many model bacterial organisms (13, 14, 22–27). Investigating these interactions provides insight into complex biological systems and allows the characterization of genes of unknown function and cellular pathways within the organism. For example, certain pairwise combinations of null mutations of *surA*, *degP*, and *skp*, genes predicted to be involved in periplasmic chaperone activity in *E. coli*, could not be constructed as they formed synthetic lethal pairs (28). Inferences based around the synthetic lethal combinations allowed Rizzitello *et al.* to propose a model with two periplasmic chaperone pathways – one pathway involving DegP and Skp, and the other being a redundant and parallel pathway that requires SurA (28).

Although low-throughput synthetic interaction experiments are effective in lending support to very specific hypotheses, in the last decade it has become increasingly more common to perform genetic interaction experiments in high-throughput using automated instrumentation and computational approaches. The first high-throughput, large-scale genetic interaction mapping study was performed in *Saccharomyces cerevisiae*, which found an average of 34 SSL interactions per gene (15, 22). Methodologies such as the ones used in yeast have been adapted for use in bacteria, and other bacterial-specific approaches

have been designed. This has allowed us to take systems-based approaches when attempting to understand the genetic interaction networks of bacterial species. Our toolbox for performing genomic and chemical genomic studies to understand the synthetic interaction networks in bacteria is ever expanding, especially with the creation of genome-wide deletion and transposon mutant libraries in bacterial organisms (29–35).

Investigating genetic synthetic lethality using synthetic genetic arrays

Genetic SSL screening involves the testing of combinations of gene deletions or mutations that lead to a fitness defect greater than expected based on the effects of each gene disruption alone. The use of synthetic genetic arrays (SGAs) for probing SSL genetic interactions was first developed in yeast (22). SGAs have since been modified for use in bacteria, with similar methods being released simultaneously by two groups—genetic interaction analysis technology for *E. coli* (GIANT-*coli*) and *E. coli* synthetic genetic array (eSGA) (13, 14). For ease, these protocols will be grouped and referred to as SGAs (Figure 2). Performing an SGA involves the crossing of a query gene deletion or mutant bacterial strain with an arrayed collection of single gene deletion strains, like the Keio collection in *E. coli* (29), or other mutant strains to generate double mutants in high-throughput (13, 14). The query gene deletions must be marked with a different selectable marker than the mutant collection it is being crossed with and be made Hfr (high-frequency recombination) using a chromosomal integrative

plasmid, if it is not already capable of acting as a donor in conjugation (13). The query gene deletion must be close to the Hfr origin of transfer to ensure transfer of the query gene deletion from donor to recipient strains. Double mutants are then created via high-throughput conjugation, are selected for, and the size or fitness of the colonies is measured by computer software (16, 36) and compared to the expected value based on that of the single mutants. The colonies on the plates must be normalized for edge effects (16) as well as linkage effects (37–39). Most SGA studies use interaction or S-scores (37) and some calculate synthetic interaction values (SIVs) (39) to classify interactions. In essence, both tactics apply the multiplicative rule to determine the expected growth of the double deletion strain based on the product of the growths of the individual deletions (40, 41). If the observed growth is significantly higher than the expected growth, a synthetic viable interaction is categorized. If the observed growth is significantly lower than the expected growth, an SSL interaction is categorized (Figure 1B).

Generating systematic genome-wide genetic interaction maps in *E. coli* has enabled the discovery of unknown connections between pathways and rich new biology in general. Certainly, the first two studies describing an SGA in *E. coli* made some interesting observations in their method validation (13, 14). Typas *et al.* uncovered that the gene encoding Pal, a lipoprotein known to tether the outer membrane (OM) to peptidoglycan, formed SSL interactions with genes involved in various aspects of lipopolysaccharide (LPS) core, enterobacterial

common antigen (ECA), and other OM or envelope proteins (13). This hinted toward a larger role for Pal in cell envelope organization than previously suspected. Butland *et al.* chose to focus their proof-of-concept on the genetic interactions involving the *isc* and *suf* operons, two redundant pathways in Fe-S cluster biosynthesis (14, 42). They discovered that *ydhD* formed SSL interactions with the *isc* operon, but not the *suf* operon, suggesting a role in the Suf system (14).

Other studies and groups have since applied the SGA methodology to probe different interactions in *E. coli*. In a large-scale study where OM-related genes were crossed with each other, it was uncovered that SSL interactions occurred between colanic acid biosynthetic pathways and the pathways that synthesize ECA and LPS (43). The authors concluded that these pathways interact by means of shared intermediates (43). SGA technology was also used as a starting point in the characterization of *lepA*, a gene of unknown physiological function (44). The gene's SSL interactions led the research group to investigate the role of *lepA* in ribosome function, and it was determined to encode a GTPase involved in translation initiation (44). Another study found that gene deletions leading to cell shape defects displayed extreme enrichment in SSL interactions with genes involved in redox processes (45).

It is also possible for SGAs to be performed on media containing chemical stressors to probe the interactions under these conditions, as demonstrated by studies in yeast (46–48). In an attempt to characterize the genetic interactions of

E. coli in DNA-damaging conditions, one research group performed SGAs on a variety of query genes and compared the interactions in methyl methanesulfonate to the untreated condition (49). Synthetic interactions were vastly different between these conditions hinting at a “rewiring” of the genome integrity machinery (49). Brown and colleagues probed genes required for growth in nutrient-limited conditions for genome-wide interactions using SGAs (39). SSL interactions were detected between nutrient biosynthesis and transport genes such as those involved in pantothenate biosynthesis and transport, and between pairs of genes functioning in redundant pathways such as *metL* and *thrA*, which are involved in parallel pathways leading to homoserine biosynthesis (39).

Chemical-genetic synthetic lethality

Chemical-genetic SSL screening involves the combination of genetic perturbations with chemicals and observing the pairs that lead to a more extreme growth defect than expected based on the individual effects of the perturbations. Although genetic synthetic lethality can be approached from a solely biological discovery perspective, as soon as chemicals are introduced into the equation, the applications become increasingly about drug discovery and combination therapies, as well as probing drug mechanism of action (50). Chemical-genetic approaches rely on the use of chemicals to probe bacterial gene functions. In addition to genetic approaches to study essential genes such as knockdowns and

conditional essentiality, chemicals are another way to probe these genes. The amount of a chemical probe introduced can be both varied and reversed (51).

An extremely high-throughput way to study chemical-genomic interactions is to take an arrayed bacterial collection of single gene deletion strains or transposon mutants and grow them in the presence of various drugs to see which mutants give an SSL phenotype with the drug. Gene-compound SSL interactions have been widely studied in *E. coli*, as it is a model organism with an extremely well-characterized, widely available, arrayed, single gene deletion Keio collection (29, 52, 53). Large-scale phenomic profiling of the Keio collection was performed by Gross and colleagues, who screened the collection in 114 different conditions including many chemical compounds, at varying concentrations, using colony size on solid media to determine SSL interactions of the gene deletion and drug combinations (54). French *et al.* also performed a large-scale chemical genomics study, arraying the Keio collection onto sub-MIC levels of 15 different antibiotics to probe any SSL interactions by monitoring both growth rate and endpoint colony biomass (16). Notably, deletions in *pal* and *lpoB*, which encode OM proteins, were more sensitive to antibiotics targeting the cell wall, and deletion of some exonuclease subunits were synergistic with topoisomerase inhibitors (16). The quantitative nature and high number of chemical-genetic interactions observed when testing dozens of different chemicals across a mutant library enables inferences to be made about drug mechanism of action and gene function at an unprecedented level.

Generating a phenotypic or chemical interaction profile of various deletion strains produces highly useful information. Deciphering which mutants lead to an SSL phenotype with drugs that either are ineffective or are becoming ineffective due to a rise in resistance allows us to propose potential combination therapies. Theoretically, if a gene is identified to be SSL with a drug, it should be possible to either use known inhibitors of that target or screen for inhibitors of that target in order to potentiate the drug (55). This would translate from studies of chemical-genetic synthetic interactions to studies of chemical-chemical interactions, aiming to identify drug-drug synergy or drug-adjuvant synergy. As well, generating a chemical-genomic profile for antibiotics can increase our understanding of their mechanism of action, just as genetic interactions can unveil the function of an unknown gene.

The Gram-negative outer membrane as a barrier to antibiotic entry

As mentioned earlier in this chapter, it is of critical importance to explore new avenues for antibiotic discovery due to the diminishing availability of effective treatments for bacterial pathogens (2). Gram-negative bacteria are particularly worrisome, as they are intrinsically resistant to many antibiotics, such as glycopeptides, macrolides, aminocoumarins, rifamycins, and oxazolidinones, which are effective against Gram-positive organisms (56) (Figure 3). This intrinsic resistance is largely due to the OM, an asymmetric bilayer consisting of phospholipids on the inner leaflet and LPS on the outer leaflet (57). Generally,

the OM excludes compounds which are hydrophobic, as well as compounds greater than ~600 Da in size (58). Although the intracellular targets of many antibiotics are present in Gram-negative bacteria, entry of such drugs into cells is largely hindered by the OM, requiring higher concentrations for growth inhibition than those achievable in clinical practice (Figure 4A). Notably, many of these antibiotics become drastically more effective *in vitro* when tested against Gram-negative bacteria with a compromised OM (Figure 4B,C).

Lipopolysaccharide biosynthesis

The impenetrability of the Gram-negative OM has been attributed to the presence of LPS, which comprises approximately 75% of the bacterial cell surface (59). Adjacent molecules of LPS pack together tightly and are stabilized by divalent cations to reduce their negative charge, creating a barrier to entry (57). LPS molecules are composed of a 3-deoxy-D-*manno*-octulosonic acid (Kdo)₂-lipid A moiety, inner and outer core oligosaccharides (OS), and O-antigenic polysaccharide (60). However, since O-antigen is not present in *E. coli* K-12 strains due to disruption of the gene encoding the WbbL rhamnosyltransferase (61), the biosynthesis of O-antigen will not be discussed here. In contrast, the presence of lipid A-Kdo₂ is essential for viability of *E. coli* and is synthesized in nine steps as described by the Raetz pathway (Figure 5A) (59). Lipid A is synthesized at the interface between the inner membrane (IM) and the cytosol, where uridine diphosphate-*N*-acetylglucosamine (UDP-GlcNAc)

is acylated by LpxA, with a 14-carbon chain from β -hydroxymyristoyl-acyl carrier protein (ACP), at the 3-OH (62, 63). The second step, and first committed step, in the pathway is catalyzed by LpxC, a metalloenzyme which deacetylates UDP-3-O-acyl-GlcNAc to form UDP-3-O-acyl-GlcN (64, 65). LpxC has been widely explored as an antibacterial target, where inhibitors have mainly been hydroxamic acids that coordinate on the zinc ion to occupy the active site (66). A second acyl chain, again from β -hydroxymyristate, is added by LpxD to form UDP-2,3-diacyl-GlcN (67, 68). LpxH then hydrolyzes UDP-2,3-diacyl-GlcN to form uridine monophosphate (UMP) and lipid X (69). Subsequently, lipid X and UDP-2,3-diacyl-GlcN are condensed by the glycosyltransferase LpxB, creating a β -1',6-glycosidic bond to form a disaccharide, releasing UDP (70). The 4' position of the disaccharide is then phosphorylated by LpxK to form lipid IV_A (71). Two Kdo residues are added to lipid IV_A by WaaA, in the last essential step of the Raetz pathway (72). Secondary acyl chains are added to lipid IV_A-Kdo₂ by LpxL and LpxM, which transfer lauroyl to the 2' acyl and myristoyl to the 3' acyl, respectively, to form hexa-acylated lipid A-Kdo₂ (73, 74). Notably, the phosphates on lipid A can be modified with 4-amino-4-deoxy-L-arabinose or phosphoethanolamine through intrinsic and acquired polymyxin resistance mechanisms, decreasing the net negative charge of LPS (75).

Core OS is assembled onto Kdol by a series of glycosyltransferases (Figure 5B) (76). The inner core is composed of L-*glycero*-D-*manno*-heptose (Hep), which is synthesized by the enzymes LpcA (GmhA), RfaE (HldE), GmhB,

RfaD (HldD) (77–79). HepI, HepII, and side chain HepIII are added sequentially by WaaC, WaaF, and WaaQ, with HepI and HepII being phosphorylated by kinases WaaP and WaaY, respectively (80–82). Phosphorylation of HepI is required for the phosphorylation of HepII and the addition of HepIII (82). The constituents of the outer core OS are more variable among Gram-negatives, even within *E. coli* (76). In *E. coli* K-12, outer core OS addition begins by the addition of glucose (Glc) I by WaaG to HepII, followed by addition of a galactose (Gal) I side chain by WaaB, GlcII by WaaO, GlcIII by WaaJ, and HepIV by WaaU (83–85). The rough-type LPS is fully synthesized at this point in the inner leaflet of the IM and is then transferred to the outer leaflet of the IM by the MsbA flippase (86, 87). In strains expressing O-antigen it would be added to HepIV by WaaL on the outer leaflet of the IM (88). LPS molecules can then be transported across the periplasm to their terminal location of the outer leaflet of the OM by the Lpt transport system (89, 90).

Targeting the outer membrane to overcome intrinsic antibiotic resistance

Uncovering potentiator or adjuvant compounds which improve the activity of existing antibiotics by increasing the permeability of the OM is an avenue in drug discovery which is gathering increased attention. Combination therapies spare the dose of both the antibiotic and the potentiator when compared to antibiotic monotherapies, which is promising for toxicity reduction. Further, it has recently been shown that OM perturbation decreases the frequency of

spontaneous resistance for the partner antibiotic and is sufficient to overcome acquired resistance elements such as efflux pumps and antibiotic inactivation enzymes (91).

The most prevalent potentiator molecules in the literature are peptides. Cationic antimicrobial peptides, along with other LPS binding molecules, have long been known to bind to the negatively charged phosphates of lipid A and disrupt the OM (92). Most notably, last-resort cyclic cationic peptides polymyxin B and polymyxin E (colistin) bind to lipid A and accumulate in the OM, displacing divalent cations and thus destabilizing the OM. This allows their access to the IM, where they exert their lethal effects (92). Even in the presence of *mcr-1* mediated phosphoethanolamine modification to lipid A, which abrogates the killing effect of polymyxins, these drugs are still able to disrupt the OM and act as potentiators (93). Although targeting both the OM and IM can lead to reduced resistance frequency and broaden the potentiation spectrum, these compounds can also be cytotoxic to mammalian cells. Indeed, the nephrotoxicity of polymyxins has prompted the design of less toxic derivatives, which maintain potentiation activity but are less active on the IM and, therefore, display reduced antibacterial activity (94–97). One such derivative molecule, SPR741, is capable of potentiating several antibiotic classes against *E. coli*, *Klebsiella pneumoniae*, *A. baumannii*, and *Enterobacter cloacae*, however it is ineffective against *P. aeruginosa* and polymyxin-resistant Gram-negatives (94, 95, 98–100). Although SPR741 showed promising results in Phase I clinical trials, advancement into Phase II is unknown.

In addition to polymyxin derivatives, other OM disrupting peptides and peptidomimetics have been recently investigated as potentiators of Gram-positive-targeting antibiotics (101–104). Some of these peptides and peptidomimetics have also been shown to impair efflux, in addition to their OM disruption activity (101, 104). As peptides are commonly physical membrane disruptors, it is important to determine whether they act exclusively on the OM or display indiscriminate activity on all membranes. A study investigating a library of peptides created by proline-scanning mutagenesis found that peptides that were most potent against Gram-negatives exhibited substantial hemolysis due to non-selective membrane disruption, while those which exhibited no hemolysis had increased hydrophilicity and specificity for the Gram-negative OM (103).

Large libraries of diverse small molecules provide another collection of chemical matter widely explored for compounds that increase OM permeability in Gram-negatives. Small molecule potentiators can be either physical OM disruptors or inhibitors of enzymes involved in OM biosynthesis and integrity (Figure 4B,C). An unconventional screening platform for antagonism of vancomycin activity at cold temperatures in *E. coli* has uncovered OM active compounds capable of antibiotic potentiation (105, 106). From a screen of previously approved drugs for this phenotype, the anti-protozoal and anti-fungal drug pentamidine was found to be an effective OM disrupting adjuvant for impermeable antibiotics (105). Pentamidine showed strong *in vivo* efficacy in combination with novobiocin against a strain of colistin-resistant *A. baumannii*

with phosphoethanolamine-modified LPS, in a systemic murine infection model (105). Other studies include focused medicinal chemistry efforts on generating analogues of known OM permeabilizers, such as phenylalanine-arginine β -naphthylamide (PA β N) and spermine, which minimize cytotoxicity and IM disruption, while maximizing potentiation (107–109). Some groups have also repurposed membrane active compounds with potent Gram-positive activity for antibiotic potentiation in Gram-negative bacteria (110, 111).

Enzyme inhibitors are also highly desirable for drug discoverers in the field of OM permeability. In theory, an inhibitor of an enzyme involved in OM biogenesis or integrity maintenance would produce a narrow-spectrum drug, unlike physical membrane disruptors that may lack specificity for the OM over the IM and host membranes. A majority of the work in this field has focused on targeting OM enzymes with essential phenotypes rather than their non-essential counterparts, where the goal is to uncover a growth inhibitory compound (100). However, potent inhibitors of essential OM processes can be used at sub-inhibitory concentrations or against less sensitive pathogens to compromise OM integrity and potentiate impermeable antibiotics. For instance, the potent inhibitor of LpxC PF-5081090 has poor antibacterial activity against *A. baumannii*, in which LPS is non-essential for viability, but can potentiate the activity of azithromycin, rifampicin, and vancomycin in this organism (112). Treatment with PF-5081090 in *A. baumannii* led to a decrease in lipid A levels in the OM, giving rise to the increased permeability of the OM to large-scaffold antibiotics. Another

small molecule with an intracellular target, MAC13243, has been shown to sensitize *E. coli* to the hydrophobic antibiotics erythromycin and novobiocin by increasing the permeability of the OM (113). MAC13243 has been shown to interact with the OM lipoprotein chaperone LolA and the cytoskeletal protein MreB, resulting in OM barrier defects (114, 115). In contrast to the aforementioned molecules with intracellular targets, Hart *et al.* (116) discovered an inhibitor of BamA, MRL-494, which acts at the cell surface to block OM protein biogenesis. Interestingly, MRL-494 was shown to be membrane active in Gram-positive bacteria, but it is precluded from entry into Gram-negative bacteria and exhibits no physical membrane disruption. Rather, it potentiates rifampicin by increasing OM permeability via its inhibition of BamA (116). While membrane active molecules may have an advantage in suppression of antibiotic resistance development and activity against biofilms, the inhibition of OM biosynthesis can potentially provide a narrower spectrum solution to OM perturbation, with little impact on host cell membranes. In all, both physical OM perturbants and inhibitors of OM biosynthesis are encouraging leads for antibiotic potentiators.

Research objectives: From understanding outer membrane biology to drug discovery

The goal of this thesis is to explore genetic and chemical perturbations which lead to increased permeability of the Gram-negative OM to Gram-positive-targeting antibiotics. Chapter 2 focuses on mapping the genetic and chemical-

genetic interactions of *E. coli* OM biogenesis to uncover previously uncharacterized permeability determinants (117). In chapters 3 and 4 the focus shifts toward chemical screening to find antibiotic potentiators. Chapter 3 describes a chemical screening platform for antagonism of vancomycin activity at cold temperatures in *E. coli* which led to the discovery of OM active compounds (106). Chapter 4 describes a chemical screen for compounds that potentiate five Gram-positive targeting antibiotics against *E. coli* which led to the discovery of membrane active compounds and an inhibitor of lipid A biosynthesis. Lastly, chapter 5 discusses the future of genetic and chemical synthetic lethality approaches to drug discovery, with a focus on subverting the Gram-negative OM.

References

1. **Fleming A.** 1929. On the antibacterial action of cultures of a *Penicillium*, with special reference to their use in the isolation of *B. influenzae*. *Br J Exp Pathol* **10**:226–236.
2. **Brown ED, Wright GD.** 2016. Antibacterial drug discovery in the resistance era. *Nature* **529**:336–343.
3. **Lewis K.** 2020. The science of antibiotic discovery. *Cell* **181**:29–45.
4. **Payne DJ, Gwynn MN, Holmes DJ, Pompliano DL.** 2007. Drugs for bad bugs: Confronting the challenges of antibacterial discovery. *Nat Rev Drug Discov* **6**:29–40.
5. **Deak D, Outterson K, Powers JH, Kesselheim AS.** 2016. Progress in the fight against multidrug-resistant bacteria? A review of U.S. food and drug administration-approved antibiotics, 2010-2015. *Ann Intern Med* **165**:363–372.
6. **Rammelkamp CH, Maxon T.** 1942. Resistance of *Staphylococcus aureus* to the action of penicillin. *Exp Biol Med* **51**:386–389.
7. **Wright GD.** 2010. Q&A: Antibiotic resistance: Where does it come from and what can we do about it? *BMC Biol* **8**.
8. **Murray CJL, Ikuta KS, Sharara F, Swetschinski L, Robles Aguilar G, Gray A, Han C, Bisignano C, Rao P, Wool E, Johnson SC, Browne AJ, Chipeta MG, Fell F, Hackett S, Haines-Woodhouse G, Kashef**

- Hamadani BH, Kumaran EAP, McManigal B, Agarwal R, Akech S, Albertson S, Amuasi J, Andrews J, Aravkin A, Ashley E, Bailey F, Baker S, Basnyat B, Bekker A, Bender R, Bethou A, Bielicki J, Boonkasidecha S, Bukosia J, Carvalho C, Castañeda-Orjuela C, Chansamouth V, Chaurasia S, Chiurchiù S, Chowdhury F, Cook AJ, Cooper B, Cressey TR, Criollo-Mora E, Cunningham M, Darboe S, Day NPJ, De Luca M, Dokova K, Dramowski A, Dunachie SJ, Eckmanns T, Eibach D, Emami A, Feasey N, Fisher-Pearson N, Forrest K, Garrett D, Gastmeier P, Giref AZ, Greer RC, Gupta V, Haller S, Haselbeck A, Hay SI, Holm M, Hopkins S, Iregbu KC, Jacobs J, Jarovsky D, Javanmardi F, Khorana M, Kissoon N, Kobeissi E, Kostyanev T, Krapp F, Krumkamp R, Kumar A, Kyu HH, Lim C, Limmathurotsakul D, Loftus MJ, Lunn M, Ma J, Mturi N, Munera-Huertas T, Musicha P, Mussi-Pinhata MM, Nakamura T, Nanavati R, Nangia S, Newton P, Ngoun C, Novotney A, Nwakanma D, Obiero CW, Olivas-Martinez A, Olliaro P, Ooko E, Ortiz-Brizuela E, Peleg AY, Perrone C, Plakkal N, Ponce-de-Leon A, Raad M, Ramdin T, Riddell A, Roberts T, Robotham JV, Roca A, Rudd KE, Russell N, Schnall J, Scott JAG, Shivamallappa M, Sifuentes-Osornio J, Steenkeste N, Stewardson AJ, Stoeva T, Tasak N, Thaiprakong A, Thwaites G, Turner C, Turner P, van Doorn HR, Velaphi S, Vongpradith A, Vu H, Walsh T, Waner S, Wangrangsimakul T, Wozniak T, Zheng P, Sartorius B, Lopez AD, Stergachis A, Moore C, Dolecek C, Naghavi M. 2022. Global burden of bacterial antimicrobial resistance in 2019: a systematic analysis. *Lancet*.**
9. **Santajit S, Indrawattana N. 2016. Mechanisms of antimicrobial resistance in ESKAPE pathogens. *Biomed Res Int* 2475067.**
10. **Tacconelli E, Carrara E, Savoldi A, Harbarth S, Mendelson M, Monnet DL, Pulcini C, Kahlmeter G, Kluytmans J, Carmeli Y, Ouellette M, Outterson K, Patel J, Cavalieri M, Cox EM, Houchens CR, Grayson ML, Hansen P, Singh N, Theuretzbacher U, Magrini N, Aboderin AO, Al-Abri SS, Awang Jalil N, Benzonana N, Bhattacharya S, Brink AJ, Burkert FR, Cars O, Cornaglia G, Dyar OJ, Friedrich AW, Gales AC, Gandra S, Giske CG, Goff DA, Goossens H, Gottlieb T, Guzman Blanco M, Hryniewicz W, Kattula D, Jinks T, Kanj SS, Kerr L, Kieny MP, Kim YS, Kozlov RS, Labarca J, Laxminarayan R, Leder K, Leibovici L, Levy-Hara G, Littman J, Malhotra-Kumar S, Manchanda V, Moja L, Ndoye B, Pan A, Paterson DL, Paul M, Qiu H, Ramon-Pardo P, Rodríguez-Baño J, Sanguinetti M, Sengupta S, Sharland M, Si-Mehand M, Silver LL, Song W, Steinbakk M, Thomsen J, Thwaites GE, van der Meer JW, Van Kinh N, Vega S, Villegas MV, Wechsler-Fördös A, Wertheim HFL, Wesangula E, Woodford N, Yilmaz FO, Zorzet A. 2018. Discovery, research, and development of new antibiotics: the WHO priority list of antibiotic-resistant bacteria and tuberculosis. *Lancet Infect Dis* 18:318–327.**

11. **D'Elia MA, Pereira MP, Brown ED.** 2009. Are essential genes really essential? *Trends Microbiol* **17**:433–438.
12. **Prabakaran S.** 2015. Precision medicine by synthetic lethality. *Sci Signal* **8**:ec345 LP-ec345.
13. **Typas A, Nichols RJ, Siegele DA, Shales M, Collins SR, Lim B, Braberg H, Yamamoto N, Takeuchi R, Wanner BL, Mori H, Weissman JS, Krogan NJ, Gross CA.** 2008. High-throughput, quantitative analyses of genetic interactions in *E. coli*. *Nat Methods* **5**:781–787.
14. **Butland G, Babu M, Díaz-Mejía JJ, Bohdana F, Phanse S, Gold B, Yang W, Li J, Gagarinova AG, Pogoutse O, Mori H, Wanner BL, Lo H, Wasniewski J, Christopolous C, Ali M, Venn P, Safavi-Naini A, Sourour N, Caron S, Choi J-Y, Laigle L, Nazarians-Armavil A, Deshpande A, Joe S, Datsenko KA, Yamamoto N, Andrews BJ, Boone C, Ding H, Sheikh B, Moreno-Hagelseib G, Greenblatt JF, Emili A.** 2008. eSGA: *E. coli* synthetic genetic array analysis. *Nat Methods* **5**:789–795.
15. **Tong AHY, Lesage G, Bader GD, Ding H, Xu H, Xin X, Young J, Berriz GF, Brost RL, Chang M.** 2004. Global mapping of the yeast genetic interaction network. *Science* **303**:808–813.
16. **French S, Mangat C, Bharat A, Côté J-P, Mori H, Brown ED.** 2016. A robust platform for chemical genomics in bacterial systems. *Mol Biol Cell* **27**:1015–1025.
17. **Schuldiner M, Collins SR, Thompson NJ, Denic V, Bhamidipati A, Punna T, Ihmels J, Andrews B, Boone C, Greenblatt JF, Weissman JS, Krogan NJ.** 2005. Exploration of the function and organization of the yeast early secretory pathway through an epistatic miniarray profile. *Cell* **123**:507–519.
18. **Costanzo M, VanderSluis B, Koch EN, Baryshnikova A, Pons C, Tan G, Wang W, Usaj M, Hanchard J, Lee SD, Pelechano V, Styles EB, Billmann M, van Leeuwen J, van Dyk N, Lin Z-Y, Kuzmin E, Nelson J, Piotrowski JS, Srikumar T, Bahr S, Chen Y, Deshpande R, Kurat CF, Li SC, Li Z, Usaj MM, Okada H, Pascoe N, San Luis B-J, Sharifpoor S, Shuteriqi E, Simpkins SW, Snider J, Suresh HG, Tan Y, Zhu H, Malod-Dognin N, Janjic V, Przulj N, Troyanskaya OG, Stagljar I, Xia T, Ohya Y, Gingras A-C, Raught B, Boutros M, Steinmetz LM, Moore CL, Rosebrock AP, Caudy AA, Myers CL, Andrews B, Boone C.** 2016. A global genetic interaction network maps a wiring diagram of cellular function. *Science* **353**:aaf1420.
19. **Yamaguchi Y, Inouye M.** 2011. Toxin-antitoxin systems in bacteria and archaea. *Annu Rev Genet* **45**:61–79.
20. **Beltrao P, Cagney G, Krogan NJ.** 2010. Quantitative genetic interactions reveal biological modularity. *Cell* **141**:739–745.
21. **Ryan CJ, Cimermančič P, Szpiech ZA, Sali A, Hernandez RD, Krogan NJ.** 2013. High-resolution network biology: connecting sequence with

- function. *Nat Rev Genet* **14**:865–879.
22. **Tong AH, Evangelista M, Parsons AB, Xu H, Bader GD, Page N, Robinson M, Ragibizadeh S, Hogue CW, Bussey H, Andrews B, Tyers M, Boone C.** 2001. Systematic genetic analysis with ordered arrays of yeast deletion mutants. *Science* **294**:2364–2368.
 23. **Baugh LR, Wen JC, Hill AA, Slonim DK, Brown EL, Hunter CP.** 2005. Synthetic lethal analysis of *Caenorhabditis elegans* posterior embryonic patterning genes identifies conserved genetic interactions. *Genome Biol* **6**:R45.
 24. **Dobzhansky T.** 1946. Genetics of natural populations. XIII. Recombination and variability in populations of *Drosophila pseudoobscura*. *Genetics* **31**:269–290.
 25. **Kaelin WG.** 2005. The concept of synthetic lethality in the context of anticancer therapy. *Nat Rev Cancer* **5**:689–698.
 26. **Dörr T, Möll A, Chao MC, Cava F, Lam H, Davis BM, Waldor MK.** 2014. Differential requirement for PBP1a and PBP1b in *in vivo* and *in vitro* fitness of *Vibrio cholerae*. *Infect Immun* **82**:2115–2124.
 27. **Farha MA, Leung A, Sewell EW, D’Elia MA, Allison SE, Ejim L, Pereira PM, Pinho MG, Wright GD, Brown ED.** 2013. Inhibition of WTA synthesis blocks the cooperative action of PBPs and sensitizes MRSA to β -lactams. *ACS Chem Biol* **8**:226–233.
 28. **Rizzitello AE, Harper JR, Silhavy TJ.** 2001. Genetic evidence for parallel pathways of chaperone activity in the periplasm of *Escherichia coli*. *J Bacteriol* **183**:6794–6800.
 29. **Baba T, Ara T, Hasegawa M, Takai Y, Okumura Y, Baba M, Datsenko KA, Tomita M, Wanner BL, Mori H.** 2006. Construction of *Escherichia coli* K-12 in-frame, single-gene knockout mutants: the Keio collection. *Mol Syst Biol* **2**:2006.0008.
 30. **de Berardinis V, Vallenet D, Castelli V, Besnard M, Pinet A, Cruaud C, Samair S, Lechaplais C, Gyapay G, Richez C, Durot M, Kreimeyer A, Le Fèvre F, Schächter V, Pezo V, Döring V, Scarpelli C, Médigue C, Cohen GN, Marlière P, Salanoubat M, Weissenbach J.** 2008. A complete collection of single-gene deletion mutants of *Acinetobacter baylyi* ADP1. *Mol Syst Biol* **4**:174.
 31. **Porwollik S, Santiviago CA, Cheng P, Long F, Desai P, Fredlund J, Srikumar S, Silva CA, Chu W, Chen X, Canals R, Reynolds MM, Bogomolnaya L, Shields C, Cui P, Guo J, Zheng Y, Endicott-Yazdani T, Yang HJ, Maple A, Ragoza Y, Blondel CJ, Valenzuela C, Andrews-Polymenis H, McClelland M.** 2014. Defined single-gene and multi-gene deletion mutant collections in *Salmonella enterica* sv Typhimurium. *PLoS One* **9**:e99820.
 32. **Jacobs MA, Alwood A, Thaipisuttikul I, Spencer D, Haugen E, Ernst S, Will O, Kaul R, Raymond C, Levy R, Chun-Rong L, Guenther D, Bovee D, Olson M V., Manoil C.** 2003. Comprehensive transposon mutant

- library of *Pseudomonas aeruginosa*. Proc Natl Acad Sci **100**:14339–14344.
33. **Liberati NT, Urbach JM, Miyata S, Lee DG, Drenkard E, Wu G, Villanueva J, Wei T, Ausubel FM.** 2006. An ordered, nonredundant library of *Pseudomonas aeruginosa* strain PA14 transposon insertion mutants. Proc Natl Acad Sci **103**:2833–2838.
 34. **Salama NR, Shepherd B, Falkow S.** 2004. Global transposon mutagenesis and essential gene analysis of *Helicobacter pylori*. J Bacteriol **186**:7926–7935.
 35. **Koo BM, Kritikos G, Farelli JD, Todor H, Tong K, Kimsey H, Wapinski I, Galardini M, Cabal A, Peters JM, Hachmann AB, Rudner DZ, Allen KN, Typas A, Gross CA.** 2017. Construction and analysis of two genome-scale deletion libraries for *Bacillus subtilis*. Cell Syst **4**:291–305.
 36. **Kritikos G, Banzhaf M, Herrera-Dominguez L, Koumoutsi A, Wartel M, Zietek M, Typas A.** 2017. A tool named Iris for versatile high-throughput phenotyping in microorganisms. Nat Microbiol **2**:17014.
 37. **Collins SR, Schuldiner M, Krogan NJ, Weissman JS.** 2006. A strategy for extracting and analyzing large-scale quantitative epistatic interaction data. Genome Biol **7**:R63.
 38. **Baryshnikova A, Costanzo M, Kim Y, Ding H, Koh J, Toufighi K, Youn J-Y, Ou J, San Luis B-J, Bandyopadhyay S, Hibbs M, Hess D, Gingras A-C, Bader GD, Troyanskaya OG, Brown GW, Andrews B, Boone C, Myers CL.** 2010. Quantitative analysis of fitness and genetic interactions in yeast on a genome scale. Nat Meth **7**:1017–1024.
 39. **Côté J-P, French S, Gehrke SS, MacNair CR, Mangat CS, Bharat A, Brown ED.** 2016. The genome-wide interaction network of nutrient stress genes in *Escherichia coli*. mBio **7**:e01714-16.
 40. **Mani R, St Onge RP, Hartman JL, Giaever G, Roth FP.** 2008. Defining genetic interaction. Proc Natl Acad Sci **105**:3461–3466.
 41. **Phillips PC, Otto SP, Whitlock MC.** 2000. Beyond the average: the evolutionary importance of gene interactions and variability of epistatic effects, p. 20–38. In Epistasis and the Evolutionary Process. University Press, Oxford/New York.
 42. **Py B, Barras F.** 2010. Building Fe–S proteins: bacterial strategies. Nat Rev Micro **8**:436–446.
 43. **Babu M, Díaz-Mejía JJ, Vlasblom J, Gagarinova A, Phanse S, Graham C, Yousif F, Ding H, Xiong X, Nazarians-Armavil A, Alamgir M, Ali M, Pogoutse O, Pe'er A, Arnold R, Michaut M, Parkinson J, Golshani A, Whitfield C, Wodak SJ, Moreno-Hagelsieb G, Greenblatt JF, Emili A.** 2011. Genetic interaction maps in *Escherichia coli* reveal functional crosstalk among cell envelope biogenesis pathways. PLoS Genet **7**:e1002377.
 44. **Balakrishnan R, Oman K, Shoji S, Bundschuh R, Fredrick K.** 2014. The conserved GTPase LepA contributes mainly to translation initiation in *Escherichia coli*. Nucleic Acids Res **42**:13370–13383.

45. **French S, Côté J-P, Stokes JM, Truant R, Brown ED.** 2017. Bacteria getting into shape: genetic determinants of *E. coli* morphology. *mBio* **8**:e01977-16.
46. **Martin H, Shales M, Fernandez-Piñar P, Wei P, Molina M, Fiedler D, Shokat KM, Beltrao P, Lim W, Krogan NJ.** 2015. Differential genetic interactions of yeast stress response MAPK pathways. *Mol Syst Biol* **11**:800.
47. **Guénolé A, Srivas R, Vreeken K, Wang ZZ, Wang S, Krogan NJ, Ideker T, van Attikum H.** 2013. Dissection of DNA damage responses using multiconditional genetic interaction maps. *Mol Cell* **49**:346–358.
48. **Bandyopadhyay S, Mehta M, Kuo D, Sung M-K, Chuang R, Jaehnig EJ, Bodenmiller B, Licon K, Copeland W, Shales M, Fiedler D, Dutkowski J, Guénolé A, van Attikum H, Shokat KM, Kolodner RD, Huh W-K, Aebersold R, Keogh M-C, Krogan NJ, Ideker T.** 2010. Rewiring of genetic networks in response to DNA damage. *Science* **330**:1385–1389.
49. **Kumar A, Beloglazova N, Bundalovic-Torma C, Phanse S, Deineko V, Gagarinova A, Musso G, Vlasblom J, Lemak S, Hooshyar M, Minic Z, Wagih O, Mosca R, Aloy P, Golshani A, Parkinson J, Emili A, Yakunin AF, Babu M.** 2016. Conditional epistatic interaction maps reveal global functional rewiring of genome integrity pathways in *Escherichia coli*. *Cell Rep* **14**:648–661.
50. **Cacace E, Kritikos G, Typas A.** 2017. Chemical genetics in drug discovery. *Curr Opin Syst Biol* **4**:35–42.
51. **Sharom JR, Bellows DS, Tyers M.** 2004. From large networks to small molecules. *Curr Opin Chem Biol* **8**:81–90.
52. **Tamae C, Liu A, Kim K, Sitz D, Hong J, Becket E, Bui A, Solaimani P, Tran KP, Yang H, Miller JH.** 2008. Determination of antibiotic hypersensitivity among 4,000 single-gene-knockout mutants of *Escherichia coli*. *J Bacteriol* **190**:5981–5988.
53. **Liu A, Tran L, Becket E, Lee K, Chinn L, Park E, Tran K, Miller JH.** 2010. Antibiotic sensitivity profiles determined with an *Escherichia coli* gene knockout collection: generating an antibiotic bar code. *Antimicrob Agents Chemother* **54**:1393–1403.
54. **Nichols RJ, Sen S, Choo YJ, Beltrao P, Zietek M, Chaba R, Lee S, Kazmierczak KM, Lee KJ, Wong A, Shales M, Lovett S, Winkler ME, Krogan NJ, Typas A, Gross CA.** 2011. Phenotypic landscape of a bacterial cell. *Cell* **144**:143–156.
55. **Wright GD.** 2012. Antibiotics: A new hope. *Chem Biol* **19**:3–10.
56. **Delcour AH.** 2009. Outer membrane permeability and antibiotic resistance. *Biochim Biophys Acta* **1794**:808–816.
57. **Nikaido H.** 2003. Molecular basis of bacterial outer membrane permeability revisited. *Microbiol Mol Biol Rev* **67**:593–656.
58. **Decad GM, Nikaido H.** 1976. Outer membrane of Gram-negative bacteria. XII. Molecular-sieving function of cell wall. *J Bacteriol* **128**:325–336.

59. **Whitfield C, Stephen Trent M.** 2014. Biosynthesis and export of bacterial lipopolysaccharides. *Annu Rev Biochem* **83**:99–128.
60. **Raetz CRH, Whitfield C.** 2002. Lipopolysaccharide endotoxins. *Annu Rev Biochem* **71**:635–700.
61. **Liu D, Reeves PR.** 1994. *Escherichia coli* K12 regains its O antigen. *Microbiology* **140**:49–57.
62. **Anderson MS, Raetz CR.** 1987. Biosynthesis of lipid A precursors in *Escherichia coli*. A cytoplasmic acyltransferase that converts UDP-*N*-acetylglucosamine to UDP-3-*O*-(*R*-3-hydroxymyristoyl)-*N*-acetylglucosamine. *J Biol Chem* **262**:5159–5169.
63. **Wyckoff TJO, Lin S, Cotter RJ, Dotson GD, Raetz CRH.** 1998. Hydrocarbon rulers in UDP-*N*-acetylglucosamine acyltransferases. *J Biol Chem* **273**:32569–32372.
64. **Young K, Silver LL, Bramhill D, Cameron P, Eveland SS, Raetz CRH, Hyland SA, Anderson MS.** 1995. The *envA* permeability/cell division gene of *Escherichia coli* encodes the second enzyme of lipid A biosynthesis: UDP-3-*O*-(*R*-3-hydroxymyristoyl)-*N*-acetylglucosamine deacetylase. *J Biol Chem* **270**:30384–30391.
65. **Jackman JE, Raetz CRH, Fierke CA.** 1999. UDP-3-*O*-(*R*-3-hydroxymyristoyl)-*N*-acetylglucosamine deacetylase of *Escherichia coli* is a zinc metalloenzyme. *Biochemistry* **38**:1902–1911.
66. **Erwin AL.** 2016. Antibacterial drug discovery targeting the lipopolysaccharide biosynthetic enzyme LpxC. *Cold Spring Harb Perspect Med* **6**:a025304.
67. **Bartling CM, Raetz CRH.** 2008. Steady-state kinetics and mechanism of LpxD, the *N*-acyltransferase of lipid A biosynthesis. *Biochemistry* **47**:5290–5302.
68. **Kelly TM, Stachula SA, Raetz CRH, Anderson MS.** 1993. The *firA* gene of *Escherichia coli* encodes UDP-3-*O*-(*R*-3-hydroxymyristoyl)-glucosamine *N*-acyltransferase. The third step of endotoxin biosynthesis. *J Biol Chem* **268**:19866–19874.
69. **Babinski KJ, Ribeiro AA, Raetz CRH.** 2002. The *Escherichia coli* gene encoding the UDP-2,3-diacylglucosamine pyrophosphatase of lipid A biosynthesis. *J Biol Chem* **277**:25937–25946.
70. **Crowell DN, Anderson MS, Raetz CRH.** 1986. Molecular cloning of the genes for lipid A disaccharide synthase and UDP-*N*-acetylglucosamine acyltransferase in *Escherichia coli*. *J Bacteriol* **168**:152–159.
71. **Garrett TA, Kadrmaz JL, Raetz CRH.** 1997. Identification of the gene encoding the *Escherichia coli* lipid A 4'-kinase: Facile phosphorylation of endotoxin analogs with recombinant LpxK. *J Biol Chem* **272**:21855–21864.
72. **Clementz T, Raetz CRH.** 1991. A gene coding for 3-deoxy-D-*manno*-octulosonic-acid transferase in *Escherichia coli*: Identification, mapping, cloning, and sequencing. *J Biol Chem* **266**:9687–9696.
73. **Clementz T, Bednarski JJ, Raetz CRH.** 1996. Function of the *htrB* high

- temperature requirement gene of *Escherichia coli* in the acylation of lipid A: HtrB catalyzed incorporation of laurate. J Biol Chem **271**:12095–12102.
74. **Clementz T, Zhou Z, Raetz CRH.** 1997. Function of the *Escherichia coli* *msbB* gene, a multicopy suppressor of *htrB* knockouts, in the acylation of lipid A. Acylation by MsbB follows laurate incorporation by HtrB. J Biol Chem **272**:10353–10360.
 75. **Jeannot K, Bolard A, Plésiat P.** 2017. Resistance to polymyxins in Gram-negative organisms. Int J Antimicrob Agents **49**:526–535.
 76. **Bertani B, Ruiz N.** 2018. Function and biogenesis of lipopolysaccharides. EcoSal Plus **8**.
 77. **Valvano MA, Marolda CL, Bittner M, Glaskin-Clay M, Simon TL, Klena JD.** 2000. The *rfaE* gene from *Escherichia coli* encodes a bifunctional protein involved in biosynthesis of the lipopolysaccharide core precursor ADP-L-glycero-D-manno-heptose. J Bacteriol **182**:488–497.
 78. **Brooke JS, Valvano MA.** 1996. Biosynthesis of inner core lipopolysaccharide in enteric bacteria identification and characterization of a conserved phosphoheptose isomerase. J Biol Chem **271**:3608–3614.
 79. **Kneidinger B, Marolda C, Graninger M, Zamyatina A, McArthur F, Kosma P, Valvano MA, Messner P.** 2002. Biosynthesis pathway of ADP-L-glycero- β -D-manno-heptose in *Escherichia coli*. J Bacteriol **184**:363–369.
 80. **Kadrmas JL, Raetz CRH.** 1998. Enzymatic synthesis of lipopolysaccharide in *Escherichia coli*. Purification and properties of heptosyltransferase I. J Biol Chem **273**:2799–2807.
 81. **Gronow S, Brabetz W, Brade H.** 2000. Comparative functional characterization *in vitro* of heptosyltransferase I (WaaC) and II (WaaF) from *Escherichia coli*. Eur J Biochem **267**:6602–6611.
 82. **Yethon JA, Heinrichs DE, Monteiro MA, Perry MB, Whitfield C.** 1998. Involvement of *waaY*, *waaQ*, and *waaP* in the modification of *Escherichia coli* lipopolysaccharide, and their role in the formation of a stable outer membrane. J Biol Chem **273**:26310–26316.
 83. **Parker CT, Kloser AW, Schnaitman CA, Stein MA, Gottesman S, Gibson BW.** 1992. Role of the *rfaG* and *rfaP* genes in determining the lipopolysaccharide core structure and cell surface properties of *Escherichia coli* K-12. J Bacteriol **174**:2525–2538.
 84. **Pradel E, Parker CT, Schnaitman CA.** 1992. Structures of the *rfaB*, *rfaI*, *rfaJ*, and *rfaS* genes of *Escherichia coli* K-12 and their roles in assembly of the lipopolysaccharide core. J Bacteriol **174**:4736–4745.
 85. **Qian J, Garrett TA, Raetz CRH.** 2014. *In vitro* assembly of the outer core of the lipopolysaccharide from *Escherichia coli* K-12 and *Salmonella typhimurium*. Biochemistry **53**:1250–1262.
 86. **Zhou Z, White KA, Polissi A, Georgopoulos C, Raetz CRH.** 1998. Function of *Escherichia coli* MsbA, an essential ABC family transporter, in lipid A and phospholipid biosynthesis. J Biol Chem **273**:12466–12475.
 87. **Mi W, Li Y, Yoon SH, Ernst RK, Walz T, Liao M.** 2017. Structural basis of

- MsbA-mediated lipopolysaccharide transport. *Nature* **549**:233–237.
88. **Whitfield C, Amor PA, Köplin R.** 1997. Modulation of the surface architecture of Gram-negative bacteria by the action of surface polymer:lipid A-core ligase and by determinants of polymer chain length. *Mol Microbiol* **23**:629–638.
 89. **Li Y, Orlando BJ, Liao M.** 2019. Structural basis of lipopolysaccharide extraction by the LptB₂FGC complex. *Nature* **567**:486–490.
 90. **Owens TW, Taylor RJ, Pahil KS, Bertani BR, Ruiz N, Kruse AC, Kahne D.** 2019. Structural basis of unidirectional export of lipopolysaccharide to the cell surface. *Nature* **567**:550–553.
 91. **MacNair CR, Brown ED.** 2020. Outer membrane disruption overcomes intrinsic, acquired, and spontaneous antibiotic resistance. *mBio* **11**:e01615-20.
 92. **Hancock REW, Chapple DS.** 1999. Peptide antibiotics. *Antimicrob Agents Chemother* **43**:1317–1323.
 93. **MacNair CR, Stokes JM, Carfrae LA, Fiebig-Comyn AA, Coombes BK, Mulvey MR, Brown ED.** 2018. Overcoming *mcr-1* mediated colistin resistance with colistin in combination with other antibiotics. *Nat Commun* **9**:458.
 94. **Vaara M.** 2019. Polymyxin derivatives that sensitize Gram-negative bacteria to other antibiotics. *Molecules* **24**:249.
 95. **French S, Farha MA, Ellis MJ, Sameer Z, Côté J-P, Cotroneo N, Lister T, Rubio A, Brown ED.** 2020. Potentiation of antibiotics against Gram-negative bacteria by polymyxin B analogue SPR741 from unique perturbation of the outer membrane. *ACS Infect Dis* **6**:1405–1412.
 96. **Tyrrell JM, Aboklaish AF, Walsh TR, Vaara T, Vaara M.** 2019. The polymyxin derivative NAB739 is synergistic with several antibiotics against polymyxin-resistant strains of *Escherichia coli*, *Klebsiella pneumoniae* and *Acinetobacter baumannii*. *Peptides* **112**:149–153.
 97. **Brown P, Abbott E, Abdulle O, Boakes S, Coleman S, Divall N, Duperchy E, Moss S, Rivers D, Simonovic M, Singh J, Stanway S, Wilson A, Dawson MJ.** 2019. Design of next generation polymyxins with lower toxicity: the discovery of SPR206. *ACS Infect Dis* **5**:1645–1656.
 98. **Corbett D, Wise A, Langley T, Skinner K, Trimby E, Birchall S, Dorali A, Sandiford S, Williams J, Warn P, Vaara M, Lister T.** 2017. Potentiation of antibiotic activity by a novel cationic peptide: Potency and spectrum of activity of SPR741. *Antimicrob Agents Chemother* **61**:e00200-17.
 99. **Mendes RE, Rhomberg PR, Lister T, Cotroneo N, Parr TR, Castanheira M.** 2021. *In vitro* activity analysis of a new polymyxin, SPR741, tested in combination with antimicrobial agents against a challenge set of *Enterobacteriaceae*, including molecularly characterized strains. *Antimicrob Agents Chemother* **65**:e00742-20.
 100. **MacNair CR, Tsai CN, Brown ED.** 2020. Creative targeting of the Gram-

- negative outer membrane in antibiotic discovery. *Ann N Y Acad Sci* **1459**:69–85.
101. **Si Z, Lim HW, Tay MYF, Du Y, Ruan L, Qiu H, Zamudio-Vazquez R, Reghu S, Chen Y, Tiong WS, Marimuthu K, De PP, Ng OT, Zhu Y, Gan YH, Chi YR, Duan H, Bazan GC, Greenberg EP, Chan-Park MB, Pethe K.** 2020. A glycosylated cationic block poly(β -peptide) reverses intrinsic antibiotic resistance in all ESKAPE Gram-negative Bacteria. *Angew Chem Int Ed* **59**:6819–6826.
 102. **Song M, Liu Y, Huang X, Ding S, Wang Y, Shen J, Zhu K.** 2020. A broad-spectrum antibiotic adjuvant reverses multidrug-resistant Gram-negative pathogens. *Nat Microbiol* **5**:1040–1050.
 103. **Hyun S, Choi Y, Jo D, Choo S, Park TW, Park SJ, Kim S, Lee S, Park S, Jin SM, Cheon DH, Yoo W, Arya R, Chong YP, Kim KK, Kim YS, Lee Y, Yu J.** 2020. Proline hinged amphipathic α -helical peptide sensitizes Gram-negative bacteria to various Gram-positive antibiotics. *J Med Chem* **63**:14937–14950.
 104. **Ramirez D, Berry L, Domalaon R, Brizuela M, Schweizer F.** 2020. Dilipid ultrashort tetrabasic peptidomimetics potentiate novobiocin and rifampicin against multidrug-resistant Gram-negative bacteria. *ACS Infect Dis* **6**:1413–1426.
 105. **Stokes JM, MacNair CR, Ilyas B, French S, Côté J-P, Bouwman C, Farha MA, Sieron AO, Whitfield C, Coombes BK, Brown ED.** 2017. Pentamidine sensitizes Gram-negative pathogens to antibiotics and overcomes acquired colistin resistance. *Nat Microbiol* **2**:17028.
 106. **Klobucar K, Côté J-P, French S, Borrillo L, Guo ABY, Serrano-Wu MH, Lee KK, Hubbard B, Johnson JW, Gaulin JL, Magolan J, Hung DT, Brown ED.** 2021. Chemical screen for vancomycin antagonism uncovers probes of the Gram-negative outer membrane. *ACS Chem Biol* **16**:929–942.
 107. **Blankson GA, Parhi AK, Kaul M, Pilch DS, LaVoie EJ.** 2019. Advances in the structural studies of antibiotic potentiators against *Escherichia coli*. *Bioorganic Med Chem* **27**:3254–3278.
 108. **Blankson G, Parhi AK, Kaul M, Pilch DS, LaVoie EJ.** 2019. Structure-activity relationships of potentiators of the antibiotic activity of clarithromycin against *Escherichia coli*. *Eur J Med Chem* **178**:30–38.
 109. **Cadelis MM, Li SA, Bourguet-Kondracki M-L, Blanchet M, Douafer H, Brunel JM, Copp BR.** 2021. Spermine derivatives of indole-3-carboxylic acid, indole-3-acetic acid and indole-3-acrylic acid as Gram-negative antibiotic adjuvants. *ChemMedChem* **16**:513–523.
 110. **Konai MM, Haldar J.** 2020. Lysine-based small molecule sensitizes rifampicin and tetracycline against multidrug-resistant *Acinetobacter baumannii* and *Pseudomonas aeruginosa*. *ACS Infect Dis* **6**:91–99.
 111. **Liu Y, Jia Y, Yang K, Li R, Xiao X, Zhu K, Wang Z.** 2020. Metformin restores tetracyclines susceptibility against multidrug resistant bacteria.

- Adv Sci **7**:1902227.
112. **García-Quintanilla M, Caro-Vega JM, Pulido MR, Moreno-Martínez P, Pachón J, McConnell MJ.** 2016. Inhibition of LpxC increases antibiotic susceptibility in *Acinetobacter baumannii*. *Antimicrob Agents Chemother* **60**:5076–5079.
 113. **Muheim C, Götzke H, Eriksson AU, Lindberg S, Lauritsen I, Nørholm MHH, Daley DO.** 2017. Increasing the permeability of *Escherichia coli* using MAC13243. *Sci Rep* **7**:17629.
 114. **Barker CA, Allison SE, Zlitni S, Nguyen ND, Das R, Melacini G, Capretta AA, Brown ED.** 2013. Degradation of MAC13243 and studies of the interaction of resulting thiourea compounds with the lipoprotein targeting chaperone LolA. *Bioorg Med Chem Lett* **23**:2426–2431.
 115. **Buss JA, Baidin V, Welsh MA, Flores-Kim J, Cho H, Wood BM, Uehara T, Walker S, Kahne D, Bernhardt TG.** 2019. Pathway-directed screen for inhibitors of the bacterial cell elongation machinery. *Antimicrob Agents Chemother* **63**:e101530-18.
 116. **Hart EM, Mitchell AM, Konovalova A, Grabowicz M, Sheng J, Han X, Rodriguez-Rivera FP, Schwaid AG, Malinverni JC, Balibar CJ, Bodea S, Si Q, Wang H, Homsher MF, Painter RE, Ogawa AK, Sutterlin H, Roemer T, Black TA, Rothman DM, Walker SS, Silhavy TJ.** 2019. A small-molecule inhibitor of BamA impervious to efflux and the outer membrane permeability barrier. *Proc Natl Acad Sci* **116**:21748–21757.
 117. **Klobucar K, French S, Côté J-P, Howes JR, Brown ED.** 2020. Genetic and chemical-genetic interactions map biogenesis and permeability determinants of the outer membrane of *Escherichia coli*. *mBio* **11**:e00161-20.

Figures

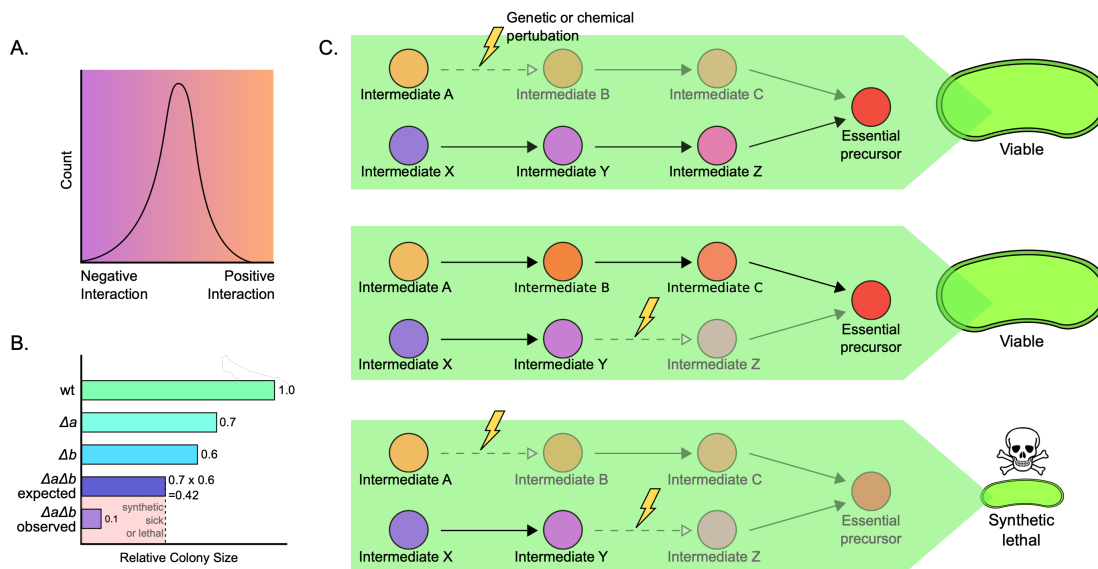


Figure 1: The principle of synthetic lethal interactions. (A) Data for genome-wide interactions tend to be symmetrical around a central value as most interactions are indifferent and only small subsets are positive or negative. (B) Negative or synthetic lethal interactions can be classified using the multiplicative rule (40, 41). Colony sizes shown are relative to wild type. Assuming no interaction exists between the two perturbations (in this case deletions are used) the multiplicative rule states that the growth in the presence of two perturbations should be the product of the growths for each perturbation alone. An observed value that is less than the expected value is a synthetic lethal interaction. (C) A schematic of how synthetic lethal interactions can occur is shown. Individually, perturbations targeting one of the pathways that synthesize an essential precursor for the cell should not change the viability of the cell, as long as the parallel pathway leading to the synthesis of that precursor is functional. When both pathways are non-functional, the essential precursor is not produced and the cell cannot survive, resulting in a synthetic lethal phenotype.

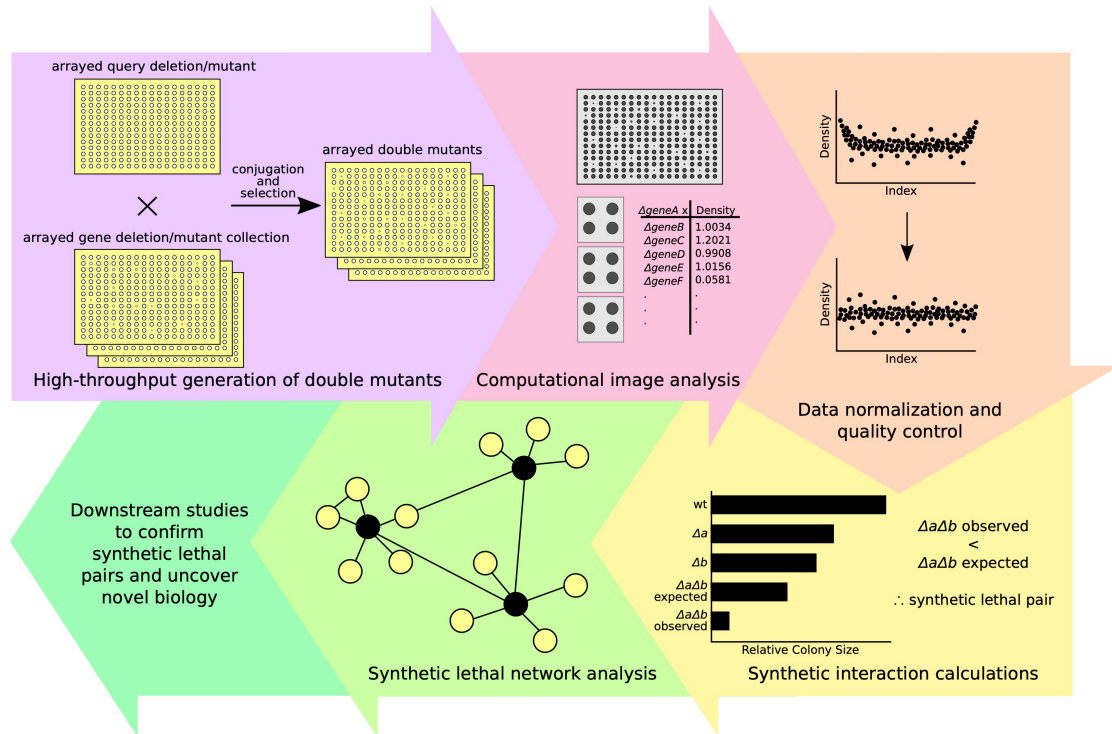


Figure 2: A synthetic genetic array workflow. The query deletion is conjugated with a gene deletion or mutant collection, with each carrying a different selectable marker in high-throughput using automated colony printing to generate arrayed double mutants. The plates can be scanned and images converted to grayscale to more easily detect colony margins and determine relative colony sizes or densities. These must be normalized for edge effects, which can be done as described in (16). SSL interactions can be identified by comparing the growth of the double deletion to the product of the growths of the single deletions on control plates. Network interactions maps can be created and used to find interesting interactions to follow up on.

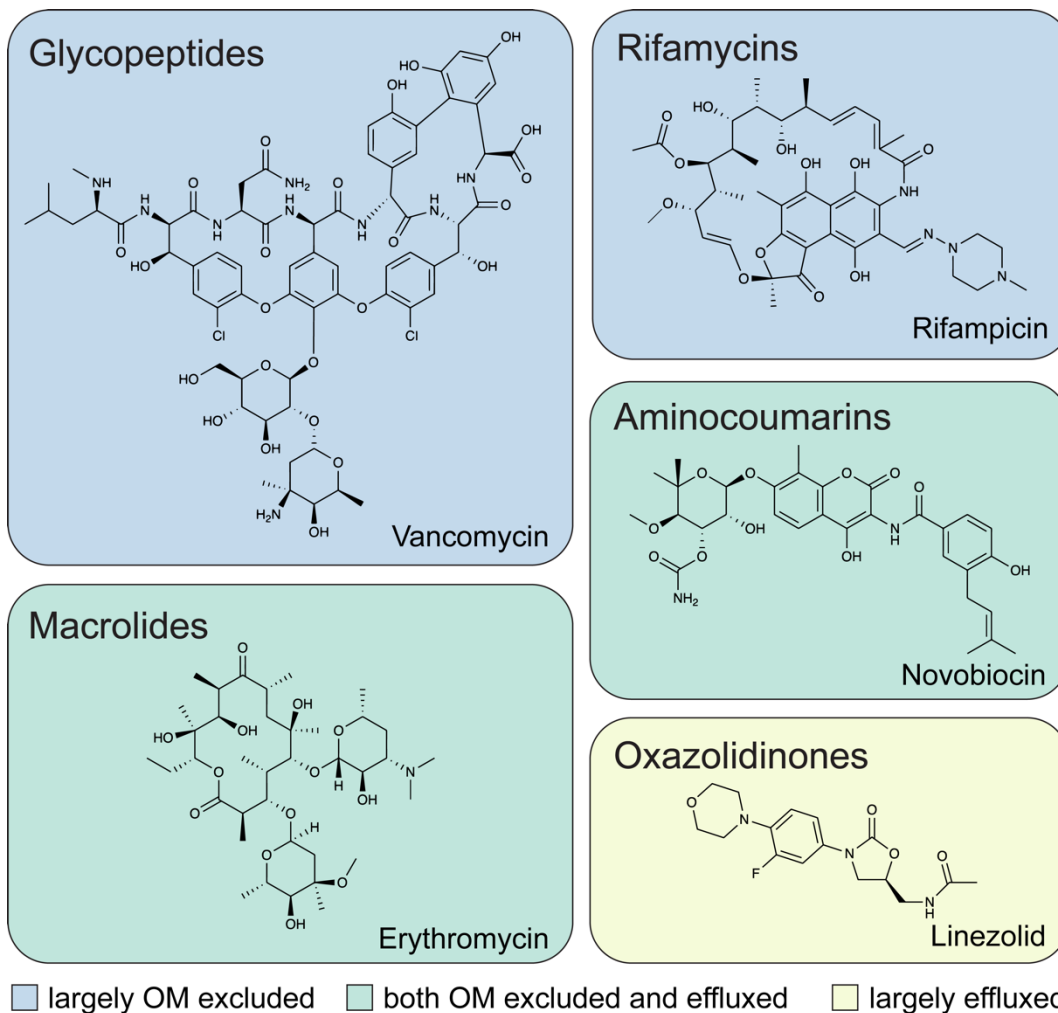


Figure 3: Classes of Gram-positive-targeting antibiotics which are ineffective against Gram-negative bacteria with an intact OM. The structure of a representative antibiotic of each class is shown. Permeabilization of the OM leads to increased intracellular accumulation of these antibiotics.

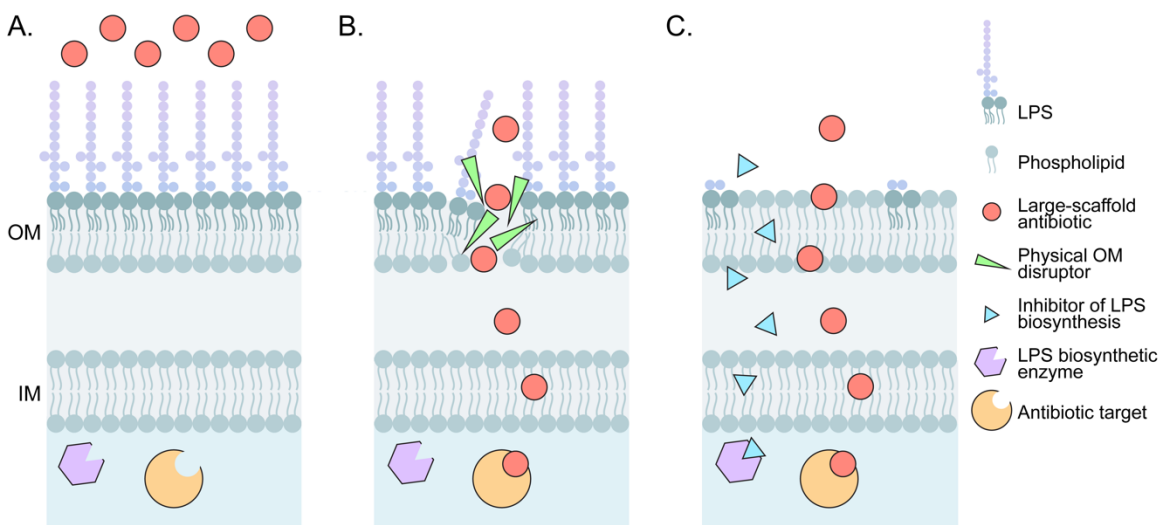


Figure 4: Increased OM permeability leads to potentiation of the activity of impermeable antibiotics. (A.) In Gram-negative bacteria with an intact OM, large-scaffold antibiotics are unable to sufficiently penetrate the OM barrier to reach their intracellular targets and inhibit bacterial growth. (B.) Compounds capable of physically disrupting OM integrity allow increased influx of these normally impermeable antibiotics into cells where they can access their targets and lead to growth inhibition. (C.) Treatment with non-lethal compounds that increase OM permeability via inhibition of an OM biosynthetic enzyme can also allow for increased influx of large-scaffold antibiotics without physical membrane disruption. For example, inhibition of an enzyme which leads to truncated LPS and/or reduced LPS content in the OM results in a more permeable OM.

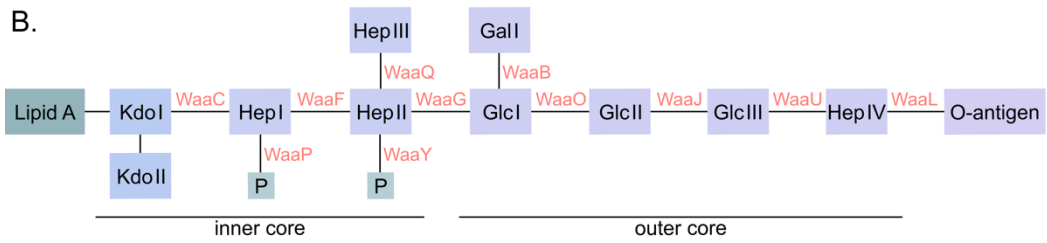
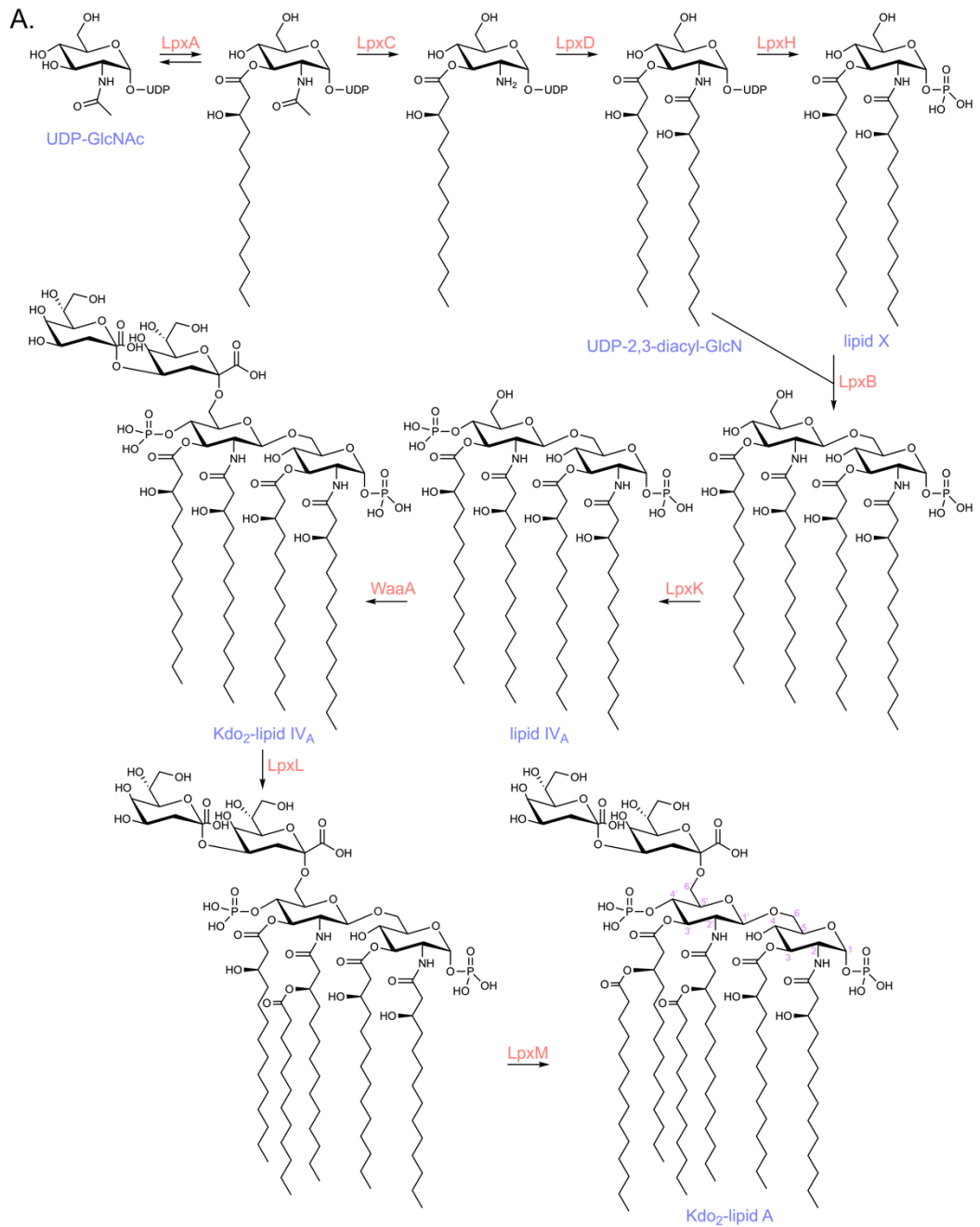


Figure 5: Lipid A biosynthesis and LPS core assembly in *E. coli*. (A.) The Raetz pathway describes the nine steps of Kdo₂-lipid A biosynthesis. Enzymes performing each step are shown with each arrow. (B.) The structure of core OS and the enzymes involved in its biosynthesis.

**CHAPTER II – Genetic and chemical-genetic interactions map biogenesis
and permeability determinants of the outer membrane of *Escherichia coli***

Preface

The work presented in this chapter was previously published in:

Klobucar K, French S, Côté J-P, Howes JR, Brown ED. 2020. Genetic and chemical-genetic interactions map biogenesis and permeability determinants of the outer membrane of *Escherichia coli*. mBio. 11: e00161-20. Reused with permission (CC BY 4.0).

I performed all experiments, with assistance from Côté J-P in performing synthetic genetic arrays and Howes JR in performing antimicrobial susceptibility testing. French S performed machine learning analysis. French S and Howes JR assisted with online data explorer creation. I wrote and edited the manuscript with input from all authors.

Abstract

Gram-negative bacteria are intrinsically resistant to many antibiotics due to their outer membrane (OM) barrier. Although the OM has been studied for decades, there is much to uncover about the biology and permeability of this complex structure. Investigating synthetic genetic interactions can reveal a great deal of information about genetic function and pathway interconnectivity. Here, we performed synthetic genetic arrays (SGAs) in *Escherichia coli* by crossing a subset of gene deletion strains implicated in OM permeability with non-essential gene and small RNA (sRNA) deletion collections. Some 155,400 double deletion strains were grown on rich microbiological media with and without subinhibitory concentrations of two antibiotics excluded by the OM, vancomycin and rifampicin, to probe both genetic interactions and permeability. The genetic interactions of interest were synthetic sick or lethal (SSL) gene deletions that were detrimental to the cell in combination but had negligible impact on viability individually. On average there were ~30, ~36, and ~40 SSL interactions per gene in the no drug, rifampicin, and vancomycin conditions, respectively, however many of these involved frequent interactors. Our datasets have been compiled into an interactive database called the Outer Membrane Interaction (OMI) Explorer, where genetic interactions can be searched, visualized across the genome, compared between conditions, and enriched for Gene Ontology (GO) terms. A set of SSL interactions revealed connectivity and permeability links between enterobacterial common antigen (ECA) and lipopolysaccharide (LPS) of the OM.

This dataset provides a novel platform to generate hypotheses about OM biology and permeability.

Importance

Gram-negative bacteria are a major concern for public health, particularly due to the rise of antibiotic resistance. It is important to understand the biology and permeability of the outer membrane (OM) of these bacteria in order to increase the efficacy of antibiotics which have difficulty penetrating this structure. Here, we studied the genetic interactions of a subset of OM-related gene deletions in the model Gram-negative bacterium *E. coli*. We systematically combined these mutants with 3,985 non-essential gene and small RNA deletion mutations in the genome. We examined the viability of these double deletion strains and probed their permeability characteristics using two antibiotics that have difficulty crossing the OM barrier. Understanding the genetic basis for OM integrity can assist in the development of new antibiotics with favourable permeability properties, and the discovery of compounds capable of increasing OM permeability to enhance the activity of existing antibiotics.

Introduction

The Gram-negative outer membrane (OM) confers an intrinsic resistance to some antibiotics (1, 2). This OM structure is an asymmetric bilayer with a phospholipid inner leaflet and lipopolysaccharide (LPS) outer leaflet, which is

typically composed of lipid A, inner and outer core oligosaccharides, and O-antigenic polysaccharide, the last being absent in K-12 strains of *Escherichia coli* (3–5). Negatively charged LPS molecules exhibit strong lateral interactions and are stabilized by divalent cations such as Mg^{2+} and Ca^{2+} , creating a strong permeability barrier to protect the cell from toxins (5–8). As such, diffusion of hydrophobic molecules through the OM is hindered, and hydrophilic molecules over ~600 Daltons are excluded from entry through OM porins (9–11). Thus, any molecules that are hydrophobic or large and hydrophilic are prevented from cell entry, including many antibiotics that are otherwise effective against Gram-positive bacteria, rendering these drugs useless in the treatment of Gram-negative infections (12).

In order to potentiate antibiotics conventionally used to treat Gram-positive infections in Gram-negative bacteria, the permeability of the OM must be altered. As the divalent cations that reduce the negative charge of LPS are required for OM stability, chelation of these ions with compounds such as ethylenediaminetetraacetic acid (EDTA) results in membrane permeabilization (8, 13). Cationic compounds such as polymyxins are also known to bind LPS to physically disrupt the OM (8, 14). Mutations in certain OM biosynthetic genes, such as LPS inner core, are likewise known to potentiate hydrophobic antibiotics, as these mutants tend to have more phospholipids in the outer leaflet of their OM (5). Additionally, cold temperatures have been shown to increase the rigidity of the Gram-negative OM and increase its susceptibility to “cracking” that

compromises the permeability barrier (5). Indeed, we previously demonstrated that *E. coli* could be sensitized to the Gram-positive targeting antibiotic vancomycin at cold temperatures (15). In a systematic search for suppressors of this phenotype, we found that deletion of certain OM-related genes leads to antagonism of vancomycin activity in the cold. Since many of those genes encoded LPS biosynthetic functions, we reasoned that altered LPS packing could make the OM more resistant to cracking (15). Although the Gram-negative OM has been studied for decades, there is still much to learn about this complex barrier.

A great deal of information can be uncovered about genes of interest by investigating their synthetic interactions. A synthetic interaction is a phenotype produced by a combination of genetic and/or chemical perturbations that differs from the phenotype expected based on the effect of each perturbation alone (16). Synthetic interactions in which the result is better growth than expected are referred to as suppressing or synthetic viable. Conversely, those interactions which result in worse growth than expected or lethality to the cell are referred to as enhancing or synthetic sick/lethal (SSL) interactions (17–21). SSL interactions tend to occur if both perturbations target genes in parallel or redundant pathways to abrogate a process that is essential for growth (22). Studying these interactions in high-throughput using synthetic genetic arrays (SGAs) (17–19) can provide a wealth of complex information about genetic involvement in cellular pathways and crosstalk between pathways, which can help characterize genes of

unknown function. Further, including small RNA (sRNA) deletions (23) in SGAs can provide some clarity on regulation of SSL interactions. Previous SGA studies in *E. coli* have characterized the roles of certain OM proteins (19, 24), iron-sulfur cluster biosynthetic genes (18), ribosome biogenesis factors (25, 26), nutrient stress genes (21), and cell shape related genes (27). Interactions have also previously been probed in different conditions such as DNA damage (28) and nutrient and temperature stressors (29).

Here, we performed SGAs by focusing on a subset of *E. coli* gene deletion strains that have been implicated in OM permeability; mutations in these genes led to suppression of the cold-sensitive phenotype of vancomycin (15). We systematically constructed double deletions with these 39 query genes and each of the *E. coli* single gene deletion (Keio) (30) and sRNA deletion (23) collections. Other studies have performed genome-wide SGAs by crossing query deletions with the Keio collection, however this study also includes a large collection of sRNA deletions, increasing the scope of interactions probed. Once generated, the double deletion strains were grown on rich microbiological media with and without subinhibitory concentrations of two Gram-positive targeting antibiotics, rifampicin and vancomycin, to probe both genetic interactions and OM permeability. High-density arrays of double deletion strains were carefully analyzed for growth (21, 27, 31) and the resulting dataset has been compiled into a searchable, interactive database called the Outer Membrane Interaction (OMI) Explorer (https://edbrowlab.shinyapps.io/omi_explorer/) where genetic

interactions of these OM implicated genes can be visualized across the genome. Herein, we have also explored a curious synthetic sick interaction on solid media between strains with truncated LPS inner core and $\Delta yhdP$, an enigmatic gene implicated in stationary phase stress response (32) and the production of enterobacterial common antigen (ECA) (33).

Results

Synthetic genetic arrays of outer membrane-related genes

In order to gain insight into the permeability of the OM and the interconnectivity of its biosynthetic pathways, we crossed 39 query gene deletion strains, previously implicated in OM permeability in *E. coli* (15), with genome-wide single gene and sRNA deletion collections (23, 30). The 39 query gene deletion strains include those involved in LPS biosynthesis, maintenance of lipid asymmetry, ECA biosynthesis, flagella biosynthesis, curli biosynthesis, efflux pump components, and genes of unknown function (Table S1). These crosses were performed in high-throughput using standard SGA procedures (18, 19, 21), whereby a query gene deletion was transferred to each gene and sRNA deletion strain using conjugation at 1,536 colony density to generate double deletion strains (see Methods and Figure S1A-B for workflow). Double deletion strains were pinned in quadruplicate to 6,144 colony density onto assay plates containing no drug, 1/8th of the minimum inhibitory concentration (MIC) of vancomycin, or 1/8th MIC of rifampicin (see Table S1 for solid media MIC values

of query strains) and growth was measured at endpoint. Vancomycin and rifampicin were chosen as they are both large scaffold antibiotics with widely different physical-chemical properties that are precluded from entry into Gram-negative bacteria by the OM (34, 35).

Experiments were performed in biological duplicates, with four technical replicates, which correlated well (Figure S1B), and the average standard deviation across all SGAs was 0.068. Synthetic interaction values (SIVs) for each double deletion strain were calculated using a multiplicative approach and the dips in the regions of the query genes due to decreased recombination efficiency were corrected as described in (21) and the materials and methods section. The majority of the SIVs are around 1 which indicates no interaction, while less than 1 is an enhancing interaction and greater than 1 is a suppressing interaction. A total of ~155,400 double deletion strains were generated and probed in rich media with no drug, vancomycin, and rifampicin. SIVs for all generated double deletion strains can be found in Table S2. A hierarchically clustered heatmap showing all SIVs of double deletion strains in the no drug condition is presented in Figure 1. Synthetic growth profiles changed when exposed to antibiotic probes of membrane permeability (Figure S2), indicating that certain double deletion strains may be viable in the no drug condition but are hyperpermeable to either vancomycin and/or rifampicin. We focused on SSL interactions, which were defined as double deletion strains with SIVs three standard deviations (3σ) below the mean of the SGA, excluding outliers in the σ calculation. From our 39 SGAs,

we observed approximately 30 SSL interactions on average per gene, with approximately six and ten more interactions per gene in the presence of rifampicin and vancomycin, respectively (Table 1). The high density of SSL interactions is shown in the centre of the network maps in Figure S3, where larger nodes indicate high network connectivity. However, many outer nodes only have a single connection showing an interaction that is specific to that gene pair (Figure S3).

Frequent interactors in SGA analysis

As previously noted in SGA studies, e.g., (21), several recipient strains frequently formed SSL interactions with our query genes. Many of these were strains with deletions in genes that are known to be important for conjugation or recombination and are therefore unable to form double deletion strains in SGAs. Working with only a specific subset of query genes, such as those implicated in OM structure and function, makes it challenging to decipher whether the gene deletions that were frequently SSL with our query genes are simply conjugation or recombination deficient or are meaningful interactions. Gene deletion strains which appear as frequent interactors in SGAs are an important class of interactors to examine to determine the reason for the frequently detected genetic interactors and whether these should be further studied.

Thus, we compared the frequent SSL interactors between our OM SGA dataset in the no drug condition and two previously published SGA datasets generated in our laboratory, one of which focused on nutrient biosynthetic query

gene deletions (21) and the other which focused on query gene deletions producing shape defects (27) (Figure 2A). A cross-gene deletion was deemed a frequent interactor if it was SSL in at least 25% of SGAs in that study. Many of the frequent interactors common between at least two of the three datasets were linked directly to having recombination or conjugation defects. For example, $\Delta recG$ and $\Delta recA$, appear as frequent interactors as the deletions in these strains are both in genes encoding double-strand break repair enzymes, which are needed for homologous recombination (36, 37). As well, $\Delta ompA$ and $\Delta bamB$ also appear as frequent interactors as OmpA encodes an OM protein that stabilizes mating pairs and BamB assists in inserting OmpA into the OM, leading to conjugation deficiencies in strains lacking these proteins (38, 39) (Figure 2B). Several frequent interactors were also indirectly linked to conjugation such as $\Delta fabH$, as FabH is involved in fatty acid biosynthesis which is important for membranes and cell size (40, 41), and $\Delta envC$, as EnvC is a peptidoglycan hydrolase activator that when deleted results in cell division and peptidoglycan defects (42).

Profound differences in interactions when probed with Gram-positive targeting antibiotics

As the number of SSL interactions increased in the presence of subinhibitory concentrations of vancomycin and rifampicin, this indicated that there were double deletion strains that were more sensitive or permeable to at least one of these two antibiotics. This increased sensitivity arose from either the

combined effect of both gene deletions or was a property of the single deletion strain that was not one of our query strains since the concentrations of vancomycin and rifampicin used were subinhibitory for the queries.

To uncover how genetic interactions were altered in the presence of Gram-positive targeting antibiotics, the SIVs from the vancomycin and rifampicin datasets were compared to the no drug dataset using a t-distributed stochastic neighbour embedding (t-SNE) machine learning algorithm to find clusters of cross gene deletions that differed most between datasets. When comparing the SIVs between the vancomycin and no drug conditions, t-SNE produces clusters of cross gene deletions that are more SSL in the presence of vancomycin (Figure 3A; Table S3). One of these clusters is enriched for Gene Ontology (GO) terms notably related to OM assembly, protein folding, 3-deoxy-D-manno-octulosonic acid (Kdo)₂-lipid A biosynthesis, and lipid metabolism (Figure 3B). One of the genes from this highlighted cluster encodes the β -barrel assembly-enhancing protease, *bepA*. The BepA protein is known to be involved in OM integrity and deletion of the gene encoding it results in higher permeability to large scaffold antibiotics (43). As $\Delta b e p A$ is frequently SSL with the query gene deletion strains in the presence of vancomycin and rifampicin, this confirms the increased sensitivity of the strain to these antibiotics (Figure 3C-E).

An additional cluster showing large differences between the vancomycin and the no drug datasets is highlighted in Figure 3A. One of the gene deletions from this cluster is the sRNA *ryjB*. Based on the frequent SSL interactions of

$\Delta ryjB$ with the query gene deletion strains which exclusively occur in the rifampicin and vancomycin conditions, this implicates the sRNA in OM permeability. Although this sRNA is largely uncharacterized, one group has predicted the genes it regulates using context likelihood of relatedness, an algorithm which uses transcriptional profiles to infer regulatory interactions (44). One of the inferred potential targets of RyjB was *rfaH*, a transcription antiterminator which regulates LPS production (44–46). Interestingly, $\Delta rfaH$ also shows frequent SSL interactions under rifampicin and vancomycin stress. The same clustering method was performed comparing the rifampicin dataset to the no drug dataset, and the bottom right cluster of red points also contains many genes involved in the OM, especially LPS biogenesis, among others (Figure S4).

OMI Explorer: An online, searchable database for genome-wide interactions of outer membrane biosynthetic genes

Our accumulated dataset has a total of ~466,200 datapoints across all three conditions. We created an online, user friendly database called the OMI Explorer (https://edbrowlab.shinyapps.io/omi_explorer/) to increase the accessibility of our datasets. This database allows the user to view all SGAs which can be selected by choosing the OM probe of interest (none, vancomycin, or rifampicin). The user can select the desired cutoff value for which to call SSL or enhancing interactions and suppressing interactions and select the query gene of interest (Figure 4A). In real time, a plot will be generated displaying the SIVs of all double deletion strains for that selected query gene along the position of the

genome (Figure 4B). Gene names of any cross-gene deletions of interest can be individually selected to appear highlighted on the plot (Figure 4A-B). Additionally, gene names and their corresponding GO term annotations appear below the plot for significant enhancers and suppressors depending on the chosen cutoff (Figure 4C). The gene names in these enrichment tables are hyperlinked to the gene's corresponding EcoCyc (47) page. Enhancing and suppressing interactions can be compared between conditions using the Venn diagram tab and the genes in each region of intersection are displayed below. Furthermore, a table tab is included which shows all SIVs for double deletion strains with conditional formatting to highlight enhancers and suppressors based on the chosen standard deviation. A gene of interest can be searched within this table in order to easily view its interaction values with all query gene deletions. In all, this tool makes the dataset approachable without the need for the user to be familiar with programming.

An interaction between $\Delta yhdP$ and deletions in LPS inner core biosynthesis

Using the OMI Explorer, we noticed that $\Delta yhdP$ showed SSL interactions with query deletion strains in LPS inner core biosynthesis: $\Delta lpcA$ ($\Delta gmhA$), $\Delta rfaE$ ($\Delta hldE$), $\Delta waaF$, $\Delta waaP$ (Figure 5A). Deletion of *lpcA* and *rfaE* results in a heptoseless LPS consisting only of Kdo₂-lipid A (48, 49), while deletion of *waaF* results in only one heptose on LPS (50). Deletion of *waaP* leads to loss of core phosphates, loss of the third heptose, as well as a lower percentage of full length core oligosaccharide (51, 52). The function of YhdP in the cell has not yet been

fully elucidated. The YhdP protein is predicted to have a transmembrane domain in the inner membrane with the majority of its structure in the periplasmic space; it contains a domain of unknown function (DUF3971) near the middle of the protein and an AsmA2 domain at the C-terminus. Recent characterization of YhdP has implicated it in stationary phase stress response, acting downstream of RpoS to strengthen the permeability barrier in response to sodium dodecyl sulfate (SDS) in carbon-limited media (32). Furthermore, YhdP has been linked to a role in ECA regulation (33). ECA consists of repeats of *N*-acetylglucosamine, *N*-acetyl-d-mannosaminuronic acid, and 4-acetamido-4,6-dideoxy-d-galactose, and there are three different forms: cyclic ECA (ECA_{cyc}) contained in the periplasm, LPS-linked ECA (ECA_{LPS}), and phosphatidylglycerol-linked ECA (ECA_{PG}), reviewed in (53). The deletion of *yhdP* results in permeability defects and suppression of these defects has been linked specifically to ECA_{cyc}, for which the function is not well understood (33, 53). Levels of the linear LPS-linked ECA (ECA_{LPS}) and phosphatidylglycerol-linked ECA (ECA_{PG}) have also been shown to be altered upon deletion of *yhdP* (33).

To confirm that $\Delta yhdP$ is synthetic sick with LPS inner core truncations, the double deletion strains $\Delta yhdP \Delta lpcA$, $\Delta yhdP \Delta rfaE$, $\Delta yhdP \Delta waaF$, and $\Delta yhdP \Delta waaP$ were remade by conjugation and PCR confirmed. Growth kinetics of the double and single deletion strains were monitored in solid media (31) and the double deletion strains showed a growth defect relative to the corresponding single deletion strains (Figure 5B-C, S5A-B). In the $\Delta yhdP \Delta lpcA$ and $\Delta yhdP$

ΔrfaE strains the most prominent defect is in the endpoint amplitude, while in *ΔyhdP ΔwaaF* and *ΔyhdP ΔwaaP* along with the defect in endpoint amplitude there also appears to be a slight defect in growth rate (Figure 5B-C). However, in liquid media the growth defect is only evidenced by a slight increase in lag time in the double deletion strains compared to the slowest growing strain of the single deletions (Figure S5C).

Since these double deletion strains of *ΔyhdP* with LPS inner core truncations are able to grow in liquid media, antibiotic susceptibility testing was performed using a large panel of diverse antibiotics to determine whether the double deletion strains were hyperpermeable (Table S4). High levels of sensitivity to the large scaffold antibiotic vancomycin were observed in the double deletion strains relative to the single deletion strains (Figure 5D-E). Increased sensitivity to bacitracin was also observed, as well as a slight increase in rifampicin and erythromycin sensitivity in one of the strains (Figure 5E). This suggests a potential increase in OM permeability allowing entry to these Gram-positive targeting antibiotics. However, enhanced MICs were also observed for other cell wall targeting antibiotics such as ampicillin and piperacillin, suggesting that the antibiotic susceptibility of the double deletion strains may also be due to weakened peptidoglycan (Figure 5E).

To determine whether the increased susceptibility of the double deletion strains in *yhdP* and LPS inner core to vancomycin was due to increased OM permeability, the effect of Mg^{2+} on the MIC of vancomycin was tested. Increasing

levels of divalent cations such as Mg^{2+} should strengthen the OM by increasing bridging of phosphates and carboxyl functional groups between adjacent LPS molecules (15, 54). A Mg^{2+} concentration dependent increase in vancomycin MIC was observed in the double deletion strains, with at least a 2- to 4-fold shift for each increase of 10 mM Mg^{2+} (Figure 6A). Thus, OM permeability is one aspect which alters vancomycin potency in these double deletion strains.

As vancomycin targets the D-alanyl-D-alanine portion of the peptidoglycan crosslinks, it is possible that the increased susceptibility of the double deletion strains to vancomycin was also due to a weakened cell wall. The deletion of *yhdP* has previously been shown to increase the levels of ECA_{LPS} and ECA_{PG} together (33). Thus, it is possible that when LPS is altered or truncated, deletion of *yhdP* causes an accumulation of dead end ECA intermediates on the undecaprenyl-phosphate (Und-P) carrier as they cannot be displayed on truncated LPS, decreasing the flux of Und-P for peptidoglycan synthesis. Indeed, this phenomenon has previously been noted for dispensable cell surface polymers, such as O-antigen and ECA, that require Und-P for synthesis (53, 55, 56). To test this, we overexpressed *murA* in the double deletion strains. MurA catalyzes the first committed step of peptidoglycan synthesis and competes for uridine diphosphate-N-acetylglucosamine (UDP-GlcNAc) with the ECA biosynthetic pathway (57). Therefore, increased levels of MurA should increase Und-P availability for peptidoglycan and decrease it for ECA (55). Indeed, overexpression of *murA* suppressed the MIC of vancomycin by between 8- and

16-fold in each of the double deletion strains (Figure 6B). Thus, the susceptibility of the double deletion strains in *yhdP* and LPS inner core to vancomycin can also be attributed to decreased flux of Und-P for cell wall biosynthesis as a result of ECA intermediate accumulation.

Another way to test whether the accumulation of ECA intermediates could explain, in part, the vancomycin sensitivity of double deletions between *yhdP* and LPS inner core genes was to eliminate ECA production in these strains. Rfe (WecA) transfers GlcNAc-1-phosphate onto Und-P to initiate ECA biosynthesis (58, 59). In the absence of Rfe, ECA production in the cell is abolished (55) and thus should relieve pressure on the competing peptidoglycan pathway, decreasing susceptibility to vancomycin. We constructed triple deletion strains in which *rfe* was deleted in the $\Delta yhdP$ LPS mutants. The triple deletion strains lacking ECA showed suppression of vancomycin activity, supporting the hypothesis that in strains with truncated or altered inner core LPS lacking *yhdP* leads to sequestration of ECA by dead end intermediates, weakening peptidoglycan (Figure S6). However, overexpressing *murA*, disrupting ECA biosynthesis by the deletion of *rfe*, and increasing Mg^{2+} levels were unable to restore the growth defects observed in these double deletion strains (data not shown). Overall, the evidence suggests that double deletions between *yhdP* and LPS inner core genes leads to increased sensitivity of cell wall active antibiotics like vancomycin due to hyperpermeability of the OM and weakened peptidoglycan due to competition with ECA for Und-P.

Discussion

Herein, we probed the synthetic genetic interactions of 39 OM-related genes previously implicated in permeability in *E. coli* (15). This was done using high-throughput bacterial conjugation to move the 39 query gene deletions into the rest of the genome-wide single gene and sRNA deletion backgrounds (23, 30), generating double deletion strains which were observed for SSL interactions. To increase the scope of interactions probed, the double deletion strains were also grown in the presence of two Gram-positive targeting antibiotics, vancomycin and rifampicin, capturing double deletions that are SSL and those which result in a viable but hyperpermeable cell. Two antibiotics of different properties were chosen as sensitivity is not necessarily generalizable across all large scaffold antibiotics (60). This is the first *E. coli* genetic interaction study, to our knowledge, that probes growth of double deletion strains generated through SGAs on antibiotics, and it also includes the largest scale of sRNAs in the deletions crossed with the query strains. The percentage of SSL interactions detected in this study in the no drug condition is on the higher end of a similar range to previous SGA studies in *E. coli*, where ~0.6-0.8% of all double deletion strains generated were SSL (21, 27). This suggests that the processes supporting OM integrity are highly connected with each other and the rest of the cell.

In and of itself, this dataset can be mined to advance knowledge gaps in the biology and interconnectivity *E. coli* OM pathways, as well as in the

permeability of the OM to large scaffold antibiotics. The dataset has particular utility as a hypothesis generation tool for researchers working to further characterize OM biosynthetic genes, including genes of unknown or poorly described functions. Due to the complexity and size of this dataset, it has been made publicly available at https://edbrownlab.shinyapps.io/omi_explorer/ in an interactive and easily searchable format in order to encourage its use among researchers who are not versed in programming languages. Several other genetic interaction databases exist, with the most comprehensive being BioGRID (61), however most of them do not enable visualization of the screening data for the SGAs from which they originated.

The number of SGAs in this dataset provides information about frequent interactors, in addition to genetic interactions, both for the no drug and drug conditions. Determining the frequent SSL interactions in the no drug condition reveals either genes that interact with many of the query genes in the study or those which are unable to form double recombinant strains, either due to defects in recombination or conjugation. By comparing the frequent interactors in this dataset with those from other datasets with unrelated query genes, it is possible to infer that these common frequent interactors result in one of these defects. Thus, any conjugation- or recombination-defective deletion strains discovered in low-throughput studies are likely to appear as frequent interactors here. In addition, the dataset produced herein reveals there are frequent interactors in the presence of subinhibitory concentrations of vancomycin and rifampicin but not in

the no drug condition. This suggests that there are underlying sensitivities of the individual deletions to these antibiotics and that growth defects become evident in the SGAs where they might not be detected with traditional broth microdilution assays to determine MIC changes. For example, $\Delta maIQ$ is frequently SSL with the query genes in the presence of vancomycin, however it does not have a different MIC from WT (data not shown). As expected, interactions which become more intense in the presence of the Gram-positive targeting antibiotics show enrichment for OM biogenesis-related GO terms. Since the OM precludes hydrophobic and large hydrophilic molecules, altering the OM should increase sensitivity to these antibiotics.

In the work reported here, we reveal new chemical and genetic interactions important to our understanding of the role of YhdP, an enigmatic inner membrane protein that has been implicated in stationary phase stress response (32), and suggested to have a role in ECA_{cyc} regulation (33). Recently, deletion of the *yhdP* gene alone was found to result in sensitivity to SDS EDTA and vancomycin (33). Suppressor mutants that reversed this phenotype mapped exclusively to enterobacterial common antigen (ECA) biosynthetic genes, that encode synthesis of the three forms of ECA, phosphatidylglycerol-bound (ECA_{PG}), LPS-associated (ECA_{LPS}), and cyclic (ECA_{cyc}). Further, strains lacking YhdP were shown to have decreased levels of ECA_{cyc} and increased levels of ECA_{PG} and ECA_{LPS} . Selective perturbation of the three forms of ECA led to the

conclusion that ECA_{cyc} in the absence of YhdP led to OM damage, independent of Und-P pools (33).

Herein, we report new interactions that shed light on the function of YhdP. Foremost were the synthetic sick interactions between $\Delta yhdP$ and deletions in LPS inner core genes in solid media, in the absence of drugs. Further, we revealed profound sensitivities in these double deletion strains to several large scaffold antibiotics and cell wall targeting antibiotics, including vancomycin, which falls into both categories. This is in contrast to the comparatively subtle change in sensitivity of the single gene deletion mutant $\Delta yhdP$ to vancomycin, i.e., a two-fold change in MIC (33). Indeed, we have leveraged our discovery of a strong synthetic sensitivity to vancomycin that results from deletions in LPS inner core genes in the $\Delta yhdP$ genetic background to further probe the function of the YhdP protein. In strains lacking LPS inner core, LPS cannot be substituted with ECA (53), amplifying the significance of the regulation of ECA biosynthesis. Thus, in strains where $yhdP$ is deleted, and LPS inner core is truncated, ECA_{LPS} cannot be attached to its LPS destination and likely leads to the accumulation of dead end ECA intermediates on undecaprenyl-phosphate (Und-P), a substrate common to both ECA and peptidoglycan synthesis. Indeed, our work suggests these dead end intermediates reduce the availability of Und-P for peptidoglycan biosynthesis and lead to a weakened cell wall which can be damaged more easily by cell wall active antibiotics such as vancomycin. The vancomycin sensitivity in these double mutants is partially reversed by *murA* overexpression,

to increase precursor availability for peptidoglycan biosynthesis, and by *rfe* deletion, to prevent ECA production. Vancomycin activity is also antagonized in these double deletion strains by the addition of Mg^{2+} , indicating that OM permeability is an additional factor. Divalent cations are well-known to strengthen OM integrity (15, 54). In addition to these peptidoglycan- and permeability-related phenotypes, other factors may also influence vancomycin potency in the double deletion strains. While cell wall defects have been linked to slower growth (62), overexpressing *murA*, disrupting ECA biosynthesis, and increasing Mg^{2+} levels were unable to restore the growth defects of the double deletion strains in solid media while restoring vancomycin MIC. Nevertheless, despite previous findings showing that Und-P could not restore the permeability defect of $\Delta yhdP$ due to ECA_{cyc} (33), Und-P becomes important in $\Delta yhdP$ strains in a genetic context where LPS is truncated, revealing a connection between YhdP and ECA_{LPS} . This previously unknown interaction offers further insight into the enigmatic role of YhdP in *E. coli*.

In addition to further describing OM biology in the model organism *E. coli*, the data described herein could also provide a platform to design new antibacterial therapies for Gram-negative pathogens. SSL gene pairs could inspire chemical screens targeting those gene products. So discovered, combinations of chemicals could be used to treat pathogens in which that SSL gene pair is considered an Achilles heel (reviewed in (16)). Moreover, single or double deletion strains which are sensitized to vancomycin and/or rifampicin

provide a conceivable route to enhancing the activity of large scaffold Gram-positive-only antibiotics against Gram-negative bacteria. In fact, biochemical inhibitors of some of these OM biosynthetic enzymes have shown promise to this end but often lack whole cell activity due to poor permeability or efflux (63, 64). The dataset described herein provides a particularly compelling discovery path that uses phenotypic screens to generate compounds with activity on whole cells. These genetic interactions have special utility as a tool for elucidating mechanism of action of compounds thought to target one of the query deletion strains. Such compounds would not inhibit the growth of wild-type *E. coli* but would have signature growth inhibitory capacity when screened against the single gene and sRNA deletion collections. A chemical-genetic fingerprint similar to one of the query genes would provide a strong hypothesis regarding the target of such a compound. Indeed, new chemical probes of known mechanisms that target OM biosynthetic processes would provide great tools for further research and may have utility as leads for new therapies directed at Gram-negative pathogens (65–70).

In all, the genetic and chemical-genetic interaction networks described herein provide a useful tool for the exploration of Gram-negative OM biology and permeability. Further, the dataset provides additional opportunities for the discovery of new chemical compounds with value as probes of the biology and as leads for new drugs that target the permeability barrier of Gram-negative pathogens.

Materials and methods

Strains, gene deletions, and growth conditions

Escherichia coli BW25113 [$F^- \Delta(araD-araB)567 lacZ4787\Delta::rrnB-3$ LAM $^- rph-1 \Delta(rhaD-rhaB)568 hsdR514$] was used throughout this study to create gene deletions using an apramycin, kanamycin, or chloramphenicol resistance cassette and was used to perform all assays. Apramycin-resistant strains were crossed with the kanamycin-resistant Keio collection (non-essential single gene deletions in *E. coli* BW25113) and sRNA and small peptide deletion collection in *E. coli* MG1655 [F^- LAM $^- rph-1$] (23, 30). Bacteria were grown at 37 °C for 18-24 hours in LB (Lysogeny Broth) or LB agar (1.5%) with ampicillin (50 µg/mL), spectinomycin (100 µg/mL), kanamycin (50 µg/mL), apramycin (100 µg/mL), and/or chloramphenicol (25 µg/mL) if needed, unless otherwise stated. All antibiotics used in this study were purchased from Sigma-Aldrich.

The PCR products for gene deletions were generated by amplifying the apramycin resistance cassette from pSET152 linearized by EcoRI digestion (New England Biolabs). PCR amplification was performed using Phusion polymerase (Life Technologies, Inc.) and the apramycin amplification primers in Table S1 with a melting temperature of 65 °C and an elongation time of 30 s. Amplification primers contain a 50 bp region of homology with the targeted region followed by 5'-AGCAAAGGGGATGATAAGTTTATC-3' (forward primer) and 5'-TCAGCCAATCGACTGGCGAGCGG-3' (reverse primer).

Single gene deletions were generated using homologous recombination (71, 72) as described in Côté et al. (21). Briefly, *E. coli* BW25113 was transformed with pSim6 (71), cells were grown at 30 °C to an optical density at 600 nm (OD₆₀₀) of 0.8, and heat shocked at 42 °C for 20 min to induce expression of λ phage genes *exo*, *beta*, and *gam* on pSim6. Cells were made electrocompetent, transformed with the PCR products described above, and plated on LB agar with selection. Deletions were confirmed by three PCR reactions using primers upstream, downstream, and internal to the apramycin resistance cassette (forward: 5'-CAGAGATGATCTGCTCTGCCTG-3'; reverse: 5'-CAGGCAGAGCAGATCATCTCTG-3'), kanamycin resistance cassette (forward: 5'-CACGTACTCGGATGGAAGC-3'; reverse: 5'-CTTCCATCCGAGTACGTG-3'), or chloramphenicol resistance cassette (forward: 5'-CGATGCCATTGGGATATATC-3'; reverse: 5'-CAATCCCTGGGTGAGTTTCAC-3') (Table S1).

Synthetic genetic arrays and MIC determination on solid media

Synthetic genetic arrays (18, 19) were performed as described in Côté et al. (21). Briefly, apramycin-resistant query deletion strains were made competent for conjugation through mating with pseudo-F⁺ *E. coli* strains carrying a chromosomal integrative plasmid (CIP) containing the machinery required for conjugation (73). Overnight cultures of the apramycin-resistant query deletion strains (in LB with apramycin) and the CIP strain (in LB with 0.3 mM diaminopimelic acid and spectinomycin) with an integration site close to the query

gene were co-spotted in a 1:1 ratio and incubated at 37 °C overnight. Hfr strains were recovered by plating on another LB agar plate with apramycin and spectinomycin.

To determine the MICs of vancomycin and rifampicin in solid LB agar medium for each apramycin-resistant Hfr query strain, cultures of the query strains in LB were arrayed in a 384-well plate in quadruplicate and pinned to 1,536-colony density on LB agar with apramycin. Upon incubation overnight at 37 °C, strains were upscaled to 6,144-colony density on LB agar plates with varying concentrations of vancomycin and rifampicin (12 two-fold dilutions from 512 µg/mL to 0 µg/mL).

For the SGAs, each apramycin-resistant Hfr query strain was arrayed on LB agar with apramycin at 1,536-colony density using the Singer Rotor HDA (Singer Instruments) and incubated overnight at 37 °C. The gene and sRNA deletion collections were also arrayed at 1,536 density on LB agar with kanamycin and grown at 37 °C. The query strain and deletion collection colonies were co-pinned onto LB agar without antibiotic selection at 1,536 density and incubated at 30 °C for 24 hours. Colonies were transferred to LB agar with apramycin and kanamycin to select for the double deletion strains at the same colony density and incubated overnight at 37 °C. Double mutants were pinned in quadruplicate at 6,144 density onto LB agar, LB agar with 1/8th MIC of vancomycin, and LB agar with 1/8th MIC of rifampicin (as determined in the query strain), and incubated at 37 °C for 18 hours. The fraction 1/8th MIC was chosen

because this concentration did not inhibit growth and maximized the available amplitude to detect growth inhibition in all genetic backgrounds sensitive to the antibiotics. The deletion collections were also pinned at 6,144 density in parallel to be used as controls.

Plate imaging, quantification, and analysis

Plates were imaged using Epson Perfection V750 scanners and analyzed as previously described in (31) and (21). Briefly, images were analyzed using ImageJ (74) to extract integrated density values for each colony. Edge effects were normalized using a two-pass rows and columns normalization system (31). A SIV was calculated for each double deletion strain by dividing the observed normalized integrated density of the double deletion strain by the expected integrated density of the double deletion based on the product of integrated densities of the corresponding single deletion collection strains. For the SIVs in the vancomycin and rifampicin conditions, double deletions were normalized as in the no drug condition above, then the normalized observed integrated density of that double deletion strain as the new query strain in the triple factor interaction calculation. Here, the effect of the drug is represented by Δc , which acts as a third deletion would in a triple mutant analysis (75), and the growth of the double deletion strain ($\Delta a \Delta b$) on the drug condition is represented by $\Delta a \Delta b \Delta c$:

$$SIV(no\ drug) = \frac{\Delta a \Delta b}{\Delta a \times \Delta b} ; SIV(drug) = \frac{\Delta a \Delta b \Delta c}{\Delta a \Delta b \times \Delta c}.$$

The dip in the index plot in the region of the query gene is corrected using a rolling median. SSL interactions are indicated by a SIV <1 and significant interactions were identified using a 3σ cutoff.

Data visualization

SGA datasets were visualized in a heatmap, using the heatmap.2 function from the gplots package in R. Batch effect correction was performed using the ComBat function from the sva package in R (76, 77). Genetic interaction networks were generated using R programming language and Cytoscape (78). SSL interactions were mined using Gene Ontology (GO) term enrichments through EcoCyc (47) and REVIGO (79) to determine dispensability and uniqueness of GO terms.

To visualize the overall genetic interactions within the SGAs under vancomycin and rifampicin stress, we utilized t-SNE machine learning (80). This collapsed the number of dimensions to three, while also providing a spatial structure to the data. t-SNE visualizations were prepared in OSIRIS Datawarrior (81), using a perplexity of 20, 50 source dimensions, and 1000 iterations to structure the data.

Solid media growth kinetics

Glycerol stocks of *E. coli* strains in a 96-well plate were pinned using the Singer Rotor HDA in quadruplicate to 384 density using 96 long pins onto an LB agar plate and incubated overnight at 37 °C. The 384 source plate was pinned in duplicate using 384 short pins onto fresh LB agar plates. Plates were incubated

at 37 °C for 24 hours and scanned every 20 minutes in Epson Perfection V750 scanners as described in (31), and integrated densities were extracted for each colony. Values were background subtracted, averaged, and LOESS smoothed.

Liquid media growth kinetics

Overnight cultures of *E. coli* strains were grown in LB media with the appropriate antibiotic selection, if applicable. Strains were subcultured 1:50 in LB and grown at 37 °C with aeration at 250 rpm to mid-log phase ($OD_{600} \sim 0.4$). Cells were diluted 1:10,000 in fresh LB, added to a 96-well assay plate, and OD_{600} was monitored for 18 hours at 37 °C with shaking using a Tecan Sunrise plate reader.

Antibiotic susceptibility testing

Overnight cultures of *E. coli* strains were grown in LB media with the appropriate antibiotic selection, if applicable. Strains were subcultured 1:50 in LB media and grown at 37 °C with shaking at 250 rpm to mid-exponential phase ($OD_{600} \sim 0.4$). Cells were diluted 1:10,000 in fresh LB and added to a 96-well assay plate containing 2-fold dilutions of antibiotic in either water or DMSO. Prior to incubation, OD_{600} of assay plates was measured using the Tecan Infinite M1000 plate reader. Assay plates were incubated at 37 °C with shaking (250 rpm) for 18 hours and OD_{600} was measured. Final measurements were background subtracted and normalized to the 0 µg/mL well. The MIC was determined to be the lowest concentration that resulted in less than or equal to 10% residual growth.

Acknowledgements

We thank Hirotada Mori (Nara Institute of Science and Technology) for providing the Keio collection clones and Gisela Storz (NICHD, National Institutes for Health) for providing the sRNA and small peptide deletion collection used in this work. We thank Chris Whitfield and Caitlin Sande (University of Guelph) for helpful discussions and providing the *rfe*::Cm cassette to generate the triple deletions. We thank Madeline Tong for providing code for analysis of solid media growth curves. We also thank the current and former members of the Brown laboratory for the helpful discussions.

This work was supported by a Foundation grant from the Canadian Institutes of Health Research (FRN-143215) to E.D.B., a Tier I Canada Research Chair award to E.D.B., a grant from the Ontario Research Fund (RE09-047) and by scholarships to K.K. from the Natural Sciences and Engineering Research Council Canada Graduate Scholarships program (CGS-M) and Canadian Institutes for Health Research Canada Graduate Scholarships (CGS-D).

The funders had no role in study design, data collection and interpretation, or the decision to submit the work for publication.

References

1. **Silver LL.** 2016. A Gestalt approach to Gram-negative entry. *Bioorg Med Chem* **24**:6379–6389.
2. **Rex JH.** 2014. ND4BB: addressing the antimicrobial resistance crisis. *Nat Rev Microbiol* **12**:231–232.
3. **Ruiz N, Kahne D, Silhavy TJ.** 2006. Advances in understanding bacterial outer-membrane biogenesis. *Nat Rev Microbiol* **4**:57–66.

4. **Silhavy TJ, Kahne D, Walker S.** 2010. The bacterial cell envelope. *Cold Spring Harb Perspect Biol* **2**:a000414.
5. **Nikaido H.** 2003. Molecular basis of bacterial outer membrane permeability revisited. *Microbiol Mol Biol Rev* **67**:593–656.
6. **Takeuchi Y, Nikaido H.** 1981. Persistence of segregated phospholipid domains in phospholipid-lipopolysaccharide mixed bilayers: studies with spin-labeled phospholipids. *Biochemistry* **20**:523–529.
7. **Labischinski H, Barnickel G, Bradaczek H, Naumann D, Rietschel ET, Giesbrecht P.** 1985. High state of order of isolated bacterial lipopolysaccharide and its possible contribution to the permeation barrier property of the outer membrane. *J Bacteriol* **162**:9–20.
8. **Vaara M.** 1992. Agents that increase the permeability of the outer membrane. *Microbiol Rev* **56**:395–411.
9. **Plésiat P, Nikaido H.** 1992. Outer membranes of Gram-negative bacteria are permeable to steroid probes. *Mol Microbiol* **6**:1323–1333.
10. **Decad GM, Nikaido H.** 1976. Outer membrane of Gram-negative bacteria. XII. Molecular-sieving function of cell wall. *J Bacteriol* **128**:325–336.
11. **Nikaido H.** 2001. Preventing drug access to targets: cell surface permeability barriers and active efflux in bacteria. *Semin Cell Dev Biol* **12**:215–23.
12. **Delcour AH.** 2009. Outer membrane permeability and antibiotic resistance. *Biochim Biophys Acta* **1794**:808–816.
13. **Leive L.** 1965. Release of lipopolysaccharide by EDTA treatment of *E. coli*. *Biochem Biophys Res Commun* **21**:290–296.
14. **Rosenthal KS, Storm DR.** 1977. Disruption of the *Escherichia coli* outer membrane permeability barrier by immobilized polymyxin B. *J Antibiot (Tokyo)* **30**:1087–1092.
15. **Stokes JM, French S, Ovchinnikova OG, Bouwman C, Whitfield C, Brown ED.** 2016. Cold stress makes *Escherichia coli* susceptible to glycopeptide antibiotics by altering outer membrane integrity. *Cell Chem Biol* **23**:267–277.
16. **Klobucar K, Brown ED.** 2018. Use of genetic and chemical synthetic lethality as probes of complexity in bacterial cell systems. *FEMS Microbiol Rev* **42**:fux054.
17. **Tong AH, Evangelista M, Parsons AB, Xu H, Bader GD, Page N, Robinson M, Ragibizadeh S, Hogue CW, Bussey H, Andrews B, Tyers M, Boone C.** 2001. Systematic genetic analysis with ordered arrays of yeast deletion mutants. *Science* **294**:2364–2368.
18. **Butland G, Babu M, Díaz-Mejía JJ, Bohdana F, Phanse S, Gold B, Yang W, Li J, Gagarinova AG, Pogoutse O, Mori H, Wanner BL, Lo H, Wasniewski J, Christopolous C, Ali M, Venn P, Safavi-Naini A, Sourour N, Caron S, Choi J-Y, Laigle L, Nazarians-Armavil A, Deshpande A, Joe S, Datsenko KA, Yamamoto N, Andrews BJ, Boone C, Ding H, Sheikh B, Moreno-Hagelseib G, Greenblatt JF, Emili A.**

2008. eSGA: *E. coli* synthetic genetic array analysis. *Nat Methods* **5**:789–795.
19. **Typas A, Nichols RJ, Siegele DA, Shales M, Collins SR, Lim B, Braberg H, Yamamoto N, Takeuchi R, Wanner BL, Mori H, Weissman JS, Krogan NJ, Gross CA.** 2008. High-throughput, quantitative analyses of genetic interactions in *E. coli*. *Nat Methods* **5**:781–787.
 20. **Costanzo M, VanderSluis B, Koch EN, Baryshnikova A, Pons C, Tan G, Wang W, Usaj M, Hanchard J, Lee SD, Pelechano V, Styles EB, Billmann M, van Leeuwen J, van Dyk N, Lin Z-Y, Kuzmin E, Nelson J, Piotrowski JS, Srikumar T, Bahr S, Chen Y, Deshpande R, Kurat CF, Li SC, Li Z, Usaj MM, Okada H, Pascoe N, San Luis B-J, Sharifpoor S, Shuteriqi E, Simpkins SW, Snider J, Suresh HG, Tan Y, Zhu H, Malod-Dognin N, Janjic V, Przulj N, Troyanskaya OG, Stagljar I, Xia T, Ohya Y, Gingras A-C, Raught B, Boutros M, Steinmetz LM, Moore CL, Rosebrock AP, Caudy AA, Myers CL, Andrews B, Boone C.** 2016. A global genetic interaction network maps a wiring diagram of cellular function. *Science* **353**:aaf1420.
 21. **Côté J-P, French S, Gehrke SS, MacNair CR, Mangat CS, Bharat A, Brown ED.** 2016. The genome-wide interaction network of nutrient stress genes in *Escherichia coli*. *MBio* **7**:e01714-16.
 22. **Beltrao P, Cagney G, Krogan NJ.** 2010. Quantitative genetic interactions reveal biological modularity. *Cell* **141**:739–745.
 23. **Hobbs EC, Astarita JL, Storz G.** 2010. Small RNAs and small proteins involved in resistance to cell envelope stress and acid shock in *Escherichia coli*: analysis of a bar-coded mutant collection. *J Bacteriol* **192**:59–67.
 24. **Babu M, Díaz-Mejía JJ, Vlasblom J, Gagarinova A, Phanse S, Graham C, Yousif F, Ding H, Xiong X, Nazarians-Armavil A, Alamgir M, Ali M, Pogoutse O, Pe'er A, Arnold R, Michaut M, Parkinson J, Golshani A, Whitfield C, Wodak SJ, Moreno-Hagelsieb G, Greenblatt JF, Emili A.** 2011. Genetic interaction maps in *Escherichia coli* reveal functional crosstalk among cell envelope biogenesis pathways. *PLoS Genet* **7**:e1002377.
 25. **Babu M, Arnold R, Bundalovic-Torma C, Gagarinova A, Wong KS, Kumar A, Stewart G, Samanfar B, Aoki H, Wagih O, Vlasblom J, Phanse S, Lad K, Yeou Hsiung Yu A, Graham C, Jin K, Brown E, Golshani A, Kim P, Moreno-Hagelsieb G, Greenblatt J, Houry WA, Parkinson J, Emili A.** 2014. Quantitative genome-wide genetic interaction screens reveal global epistatic relationships of protein complexes in *Escherichia coli*. *PLoS Genet* **10**:e1004120.
 26. **Balakrishnan R, Oman K, Shoji S, Bundschuh R, Fredrick K.** 2014. The conserved GTPase LepA contributes mainly to translation initiation in *Escherichia coli*. *Nucleic Acids Res* **42**:13370–13383.
 27. **French S, Côté J-P, Stokes JM, Truant R, Brown ED.** 2017. Bacteria getting into shape: genetic determinants of *E. coli* morphology. *MBio*

- 8:e01977-16.
28. **Kumar A, Beloglazova N, Bundalovic-Torma C, Phanse S, Deineko V, Gagarinova A, Musso G, Vlasblom J, Lemak S, Hooshyar M, Minic Z, Wagih O, Mosca R, Aloy P, Golshani A, Parkinson J, Emili A, Yakunin AF, Babu M.** 2016. Conditional epistatic interaction maps reveal global functional rewiring of genome integrity pathways in *Escherichia coli*. *Cell Rep* **14**:648–661.
 29. **Gagarinova A, Stewart G, Samanfar B, Phanse S, White CA, Aoki H, Deineko V, Beloglazova N, Yakunin AF, Golshani A, Brown ED, Babu M, Emili A.** 2016. Systematic genetic screens reveal the dynamic global functional organization of the bacterial translation machinery. *Cell Rep* **17**:904–916.
 30. **Baba T, Ara T, Hasegawa M, Takai Y, Okumura Y, Baba M, Datsenko KA, Tomita M, Wanner BL, Mori H.** 2006. Construction of *Escherichia coli* K-12 in-frame, single-gene knockout mutants: the Keio collection. *Mol Syst Biol* **2**:2006.0008.
 31. **French S, Mangat C, Bharat A, Côté J-P, Mori H, Brown ED.** 2016. A robust platform for chemical genomics in bacterial systems. *Mol Biol Cell* **27**:1015–1025.
 32. **Mitchell AM, Wang W, Silhavy TJ.** 2017. Novel RpoS-dependent mechanisms strengthen the envelope permeability barrier during stationary phase. *J Bacteriol* **199**:e00708-16.
 33. **Mitchell AM, Srikumar T, Silhavy TJ.** 2018. Cyclic enterobacterial common antigen maintains the outer membrane permeability barrier of *Escherichia coli* in a manner controlled by YhdP. *MBio* **9**:e01321-18.
 34. **Shlaes DM, Shlaes JH, Davies J, Williamson R.** 1989. *Escherichia coli* susceptible to glycopeptide antibiotics. *Antimicrob Agents Chemother* **33**:192–197.
 35. **Vaara M.** 1993. Antibiotic-supersusceptible mutants of *Escherichia coli* and *Salmonella typhimurium*. *Antimicrob Agents Chemother* **37**:2255–2260.
 36. **Whitby MC, Vincent SD, Lloyd RG.** 1994. Branch migration of Holliday junctions: identification of RecG protein as a junction specific DNA helicase. *EMBO J* **13**:5220–5228.
 37. **Courcelle J, Hanawalt PC.** 2004. RecA-dependent recovery of arrested DNA replication forks. *Annu Rev Genet* **37**:611–646.
 38. **van Alphen L, Havekes L, Lugtenberg B.** 1977. Major outer membrane protein *d* of *Escherichia coli* K12. *FEBS Lett* **75**:285–290.
 39. **Reusch RN.** 2012. Insights into the structure and assembly of *Escherichia coli* outer membrane protein A. *FEBS J* **279**:894–909.
 40. **Lai CY, Cronan JE.** 2003. β -ketoacyl-acyl carrier protein synthase III (FabH) is essential for bacterial fatty acid synthesis. *J Biol Chem* **278**:51494–51503.
 41. **Yao Z, Davis RM, Kishony R, Kahne D, Ruiz N.** 2012. Regulation of cell size in response to nutrient availability by fatty acid biosynthesis in

- Escherichia coli*. Proc Natl Acad Sci **109**:E2561–E2568.
42. **Uehara T, Parzych KR, Dinh T, Bernhardt TG.** 2010. Daughter cell separation is controlled by cytokinetic ring-activated cell wall hydrolysis. EMBO J **29**:1412–1422.
 43. **Narita S, Masui C, Suzuki T, Dohmae N, Akiyama Y.** 2013. Protease homolog BepA (YfgC) promotes assembly and degradation of β -barrel membrane proteins in *Escherichia coli*. Proc Natl Acad Sci **110**:E3612–E3621.
 44. **Pandey SP, Winkler JA, Li H, Camacho DM, Collins JJ, Walker GC.** 2014. Central role for RNase YbeY in Hfq-dependent and Hfq-independent small-RNA regulation in bacteria. BMC Genomics **15**:121.
 45. **Beutin L, Manning PA, Achtman M, Willetts N.** 1981. *sfrA* and *sfrB* products of *Escherichia coli* K-12 are transcriptional control factors. J Bacteriol **145**:840–844.
 46. **Creeger ES, Schulte T, Rothfield LI.** 1984. Regulation of membrane glycosyltransferases by the *sfrB* and *rfaH* genes of *Escherichia coli* and *Salmonella typhimurium*. J Biol Chem **259**:3064–3069.
 47. **Keseler IM, Mackie A, Santos-Zavaleta A, Billington R, Bonavides-Martínez C, Caspi R, Fulcher C, Gama-Castro S, Kothari A, Krummenacker M, Latendresse M, Muñiz-Rascado L, Ong Q, Paley S, Peralta-Gil M, Subhraveti P, Velázquez-Ramírez DA, Weaver D, Collado-Vides J, Paulsen I, Karp PD.** 2017. The EcoCyc database: reflecting new knowledge about *Escherichia coli* K-12. Nucleic Acids Res **45**:D543–D550.
 48. **Tamaki S, Sato T, Matsushashi M.** 1971. Role of lipopolysaccharides in antibiotic resistance and bacteriophage adsorption of *Escherichia coli* K-12. J Bacteriol **105**:968–975.
 49. **Valvano MA, Marolda CL, Bittner M, Glaskin-Clay M, Simon TL, Kléna JD.** 2000. The *rfaE* gene from *Escherichia coli* encodes a bifunctional protein involved in biosynthesis of the lipopolysaccharide core precursor ADP-L-glycero-D-manno-heptose. J Bacteriol **182**:488–497.
 50. **Gronow S, Brabetz W, Brade H.** 2000. Comparative functional characterization *in vitro* of heptosyltransferase I (WaaC) and II (WaaF) from *Escherichia coli*. Eur J Biochem **267**:6602–6611.
 51. **Yethon JA, Heinrichs DE, Monteiro MA, Perry MB, Whitfield C.** 1998. Involvement of *waaY*, *waaQ*, and *waaP* in the modification of *Escherichia coli* lipopolysaccharide, and their role in the formation of a stable outer membrane. J Biol Chem **273**:26310–26316.
 52. **Yethon JA, Malo D, Whitfield C, Gunn JS, Ernst RK, Miller SI, Laroche L.** 2000. *Salmonella enterica* serovar Typhimurium *waaP* mutants show increased susceptibility to polymyxin and loss of virulence *in vivo*. Infect Immun **68**:4485–4491.
 53. **Kuhn H-M, Meier-Dieter U, Mayer H.** 1988. ECA, the enterobacterial common antigen. FEMS Microbiol Rev **54**:195–222.

54. **Clifton LA, Skoda MW, Le Brun AP, Ciesielski F, Kuzmenko I, Holt SA, Lakey JH.** 2015. Effect of divalent cation removal on the structure of Gram-negative bacterial outer membrane models. *Langmuir* **31**:404–412.
55. **Jorgenson MA, Kannan S, Laubacher ME, Young KD.** 2016. Dead-end intermediates in the enterobacterial common antigen pathway induce morphological defects in *Escherichia coli* by competing for undecaprenyl phosphate. *Mol Microbiol* **100**:1–14.
56. **Jorgenson MA, Young KD.** 2016. Interrupting biosynthesis of O antigen or the lipopolysaccharide core produces morphological defects in *Escherichia coli* by sequestering undecaprenyl phosphate. *J Bacteriol* **198**:3070–3079.
57. **Marquardt JL, Siegele DA, Kolter R, Walsh CT.** 1992. Cloning and sequencing of *Escherichia coli murZ* and purification of its product, a UDP-*N*-acetylglucosamine enolpyruvyl transferase. *J Bacteriol* **174**:5748–5752.
58. **Barr K, Rick PD.** 1985. Biosynthesis of enterobacterial common antigen. *J Bacteriol* **162**:494–503.
59. **Meier-Dieter U, Barr K, Starman R, Hatch L, Rick PD.** 1992. Nucleotide sequence of the *Escherichia coli rfe* gene involved in the synthesis of enterobacterial common antigen. Molecular cloning of the *rfe-rff* gene cluster. *J Biol Chem* **267**:746–753.
60. **Dörr T, Delgado F, Umans BD, Gerding MA, Davis BM, Waldor MK.** 2016. A transposon screen identifies genetic determinants of *Vibrio cholerae* resistance to high-molecular-weight antibiotics. *Antimicrob Agents Chemother* **60**:4757–4763.
61. **Oughtred R, Stark C, Breitzkreutz BJ, Rust J, Boucher L, Chang C, Kolas N, O'Donnell L, Leung G, McAdam R, Zhang F, Dolma S, Willems A, Coulombe-Huntington J, Chatr-Aryamontri A, Dolinski K, Tyers M.** 2019. The BioGRID interaction database: 2019 update. *Nucleic Acids Res* **47**:D529–D541.
62. **Glover WA, Yang Y, Zhang Y.** 2009. Insights into the molecular basis of L-form formation and survival in *Escherichia coli*. *PLoS One* **4**:e7316.
63. **De Leon GP, Elowe NH, Koteva KP, Valvano MA, Wright GD.** 2006. An *in vitro* screen of bacterial lipopolysaccharide biosynthetic enzymes identifies an inhibitor of ADP-heptose biosynthesis. *Chem Biol* **13**:437–441.
64. **Durka M, Tikad A, Périon R, Bosco M, Andaloussi M, Floquet S, Malacain E, Moreau F, Oxoby M, Gerusz V, Vincent SP.** 2011. Systematic synthesis of inhibitors of the two first enzymes of the bacterial heptose biosynthetic pathway: towards antivirulence molecules targeting lipopolysaccharide biosynthesis. *Chem Eur J* **17**:11305–11313.
65. **Beceiro A, Moreno A, Fernández N, Vallejo JA, Aranda J, Adler B, Harper M, Boyce JD, Bou G.** 2014. Biological cost of different mechanisms of colistin resistance and their impact on virulence in *Acinetobacter baumannii*. *Antimicrob Agents Chemother* **58**:518–526.
66. **Weirich J, Bräutigam C, Mühlenkamp M, Franz-Wachtel M, Macek B, Meuskens I, Skurnik M, Leskinen K, Bohn E, Autenrieth I, Schütz M.**

2017. Identifying components required for OMP biogenesis as novel targets for anti-infective drugs. *Virulence* **8**:1170–1188.
67. **Trent MS, Stead CM, Tran AX, Hankins JV**. 2006. Diversity of endotoxin and its impact on pathogenesis. *J Endotoxin Res* **12**:205–223.
68. **Raetz CRH, Whitfield C**. 2002. Lipopolysaccharide endotoxins. *Annu Rev Biochem* **71**:635–700.
69. **Ellis TN, Kuehn MJ**. 2010. Virulence and immunomodulatory roles of bacterial outer membrane vesicles. *Microbiol Mol Biol Rev* **74**:81–94.
70. **Stokes JM, MacNair CR, Ilyas B, French S, Côté J-P, Bouwman C, Farha MA, Sieron AO, Whitfield C, Coombes BK, Brown ED**. 2017. Pentamidine sensitizes Gram-negative pathogens to antibiotics and overcomes acquired colistin resistance. *Nat Microbiol* **2**:17028.
71. **Datta S, Costantino N, Court DL**. 2006. A set of recombineering plasmids for Gram-negative bacteria. *Gene* **379**:109–115.
72. **Datsenko KA, Wanner BL**. 2000. One-step inactivation of chromosomal genes in *Escherichia coli* K-12 using PCR products. *Proc Natl Acad Sci U S A* **97**:6640–6645.
73. **Mori H, Takeuchi R, Otsuka Y, Bowden S, Yokoyama K, Muto A, Libourel I, Wanner BL**. 2015. Toward network biology in *E. coli* cell, p. 155–168. In Krogan, NJ, Babu, M (eds.), *Prokaryotic Systems Biology. Advances in Experimental Medicine and Biology*. Springer International Publishing, Cham.
74. **Schneider CA, Rasband WS, Eliceiri KW**. 2012. NIH Image to ImageJ: 25 years of image analysis. *Nat Methods* **9**:671–675.
75. **Braberg H, Alexander R, Shales M, Xu J, Franks-Skiba KE, Wu Q, Haber JE, Krogan NJ**. 2014. Quantitative analysis of triple-mutant genetic interactions. *Nat Protoc* **9**:1867–1881.
76. **Leek JT, Johnson WE, Parker HS, Jaffe AE, Storey JD**. 2012. The SVA package for removing batch effects and other unwanted variation in high-throughput experiments. *Bioinformatics* **28**:882–883.
77. **Johnson WE, Li C, Rabinovic A**. 2007. Adjusting batch effects in microarray expression data using empirical Bayes methods. *Biostatistics* **8**:118–127.
78. **Shannon P, Markiel A, Ozier O, Baliga NS, Wang JT, Ramage D, Amin N, Schwikowski B, Ideker T**. 2003. Cytoscape: a software environment for integrated models of biomolecular interaction networks. *Genome Res* **13**:2498–2504.
79. **Supek F, Bošnjak M, Škunca N, Šmuc T**. 2011. REVIGO summarizes and visualizes long lists of Gene Ontology terms. *PLoS One* **6**:e21800.
80. **van der Maaten L, Hinton G**. 2008. Visualizing Data using t-SNE. *J Mach Learn Res* **9**:2579–2605.
81. **Sander T, Freyss J, Von Korff M, Rufener C**. 2015. DataWarrior: An open-source program for chemistry aware data visualization and analysis. *J Chem Inf Model* **55**:460–473.

82. **Kitagawa M, Ara T, Arifuzzaman M, Ioka-Nakamichi T, Inamoto E, Toyonaga H, Mori H.** 2005. Complete set of ORF clones of *Escherichia coli* ASKA library (A complete set of *E. coli* K-12 ORF archive): unique resources for biological research. *DNA Res* **12**:291–299.

Figures

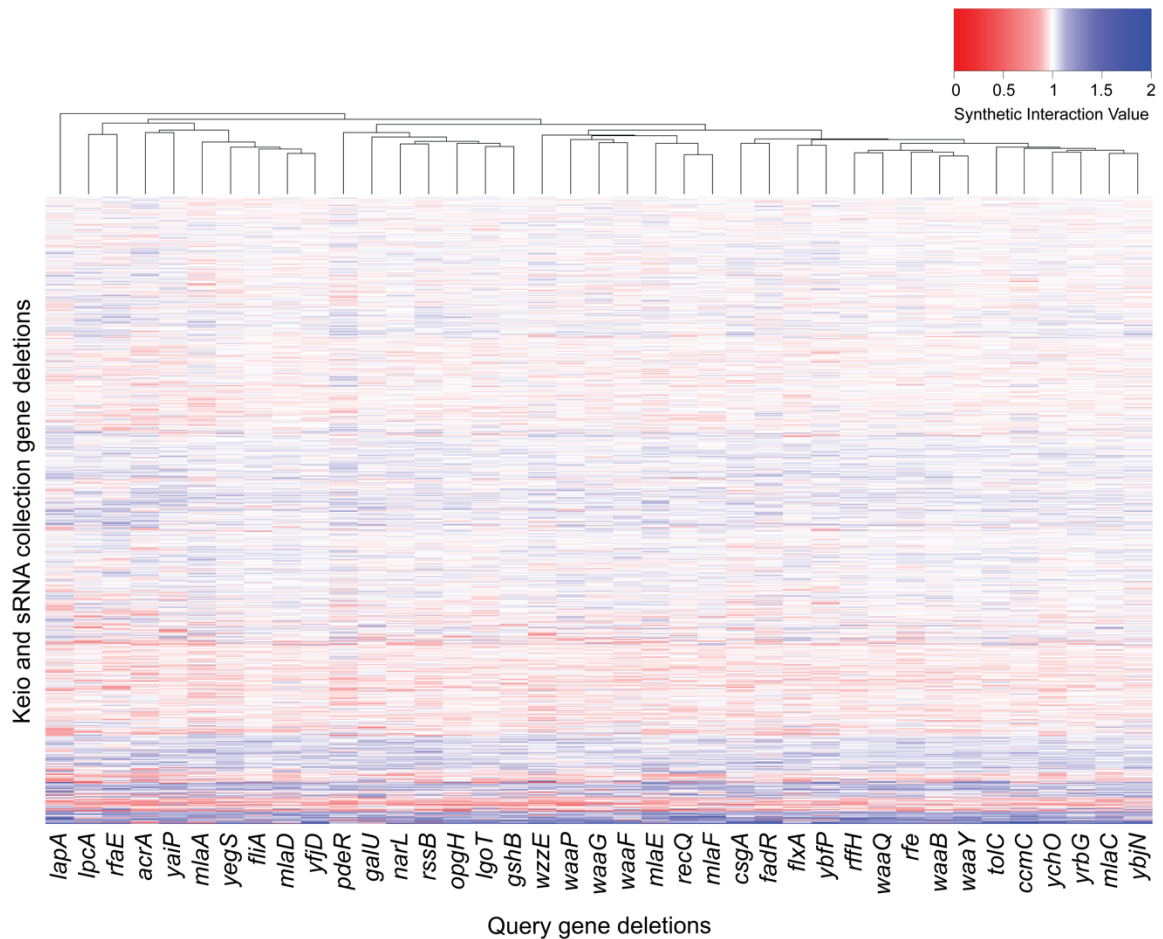


Figure 1: Synthetic genetic arrays of outer membrane-related gene deletions. A heat map showing the genome-wide SIVs for each double deletion strain in rich microbiological media in the no drug condition. Interactions are colour coded with enhancement in red (SSL) and suppression of growth defect in blue. Hierarchical clustering was performed using interaction profiles for both query deletion strains and the deletion collection strains.

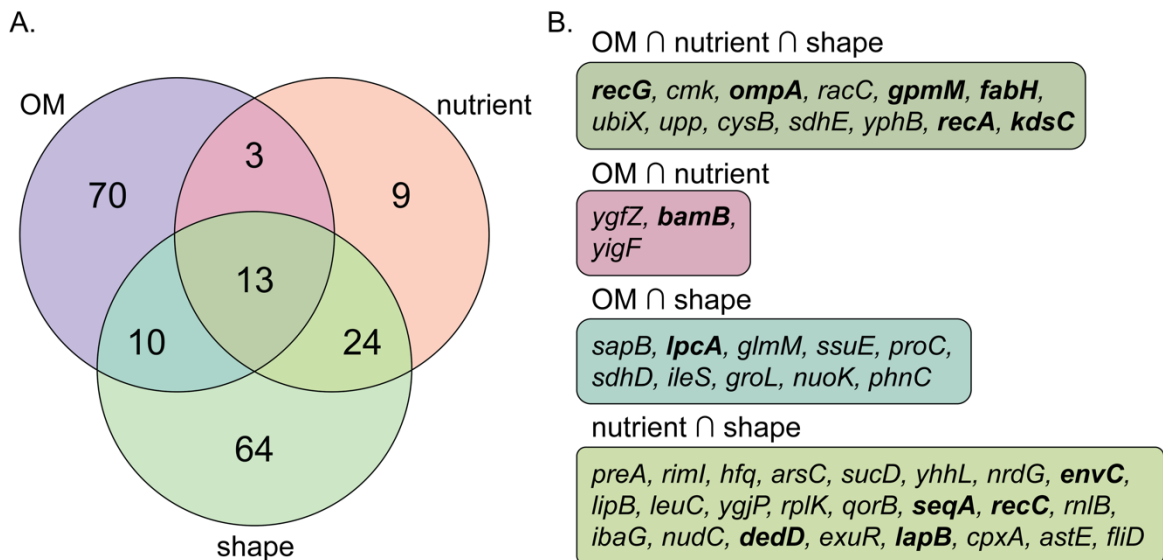


Figure 2: Frequent interactors in SGAs have conjugation and recombination defects. (A.) A Venn diagram of single deletion strains that are frequently SSL with query strains in SGA datasets. The studies compared are the OM SGAs in the no drug condition published here in purple, the nutrient biosynthesis SGAs from (21) in orange, and the shape-related SGAs from (27) in green. Single deletion strains that were SSL (using a 2.5σ cutoff for the nutrient and shape datasets and 3σ cutoff for the OM dataset) in at least 25% of crosses by SGA dataset were deemed frequent interactors. (B.) Gene deletion strains that were common frequent SSL interactors between the datasets in (A.). Bolded gene names are those which have been previously linked to conjugation and recombination deficiencies in the literature, either directly or indirectly.

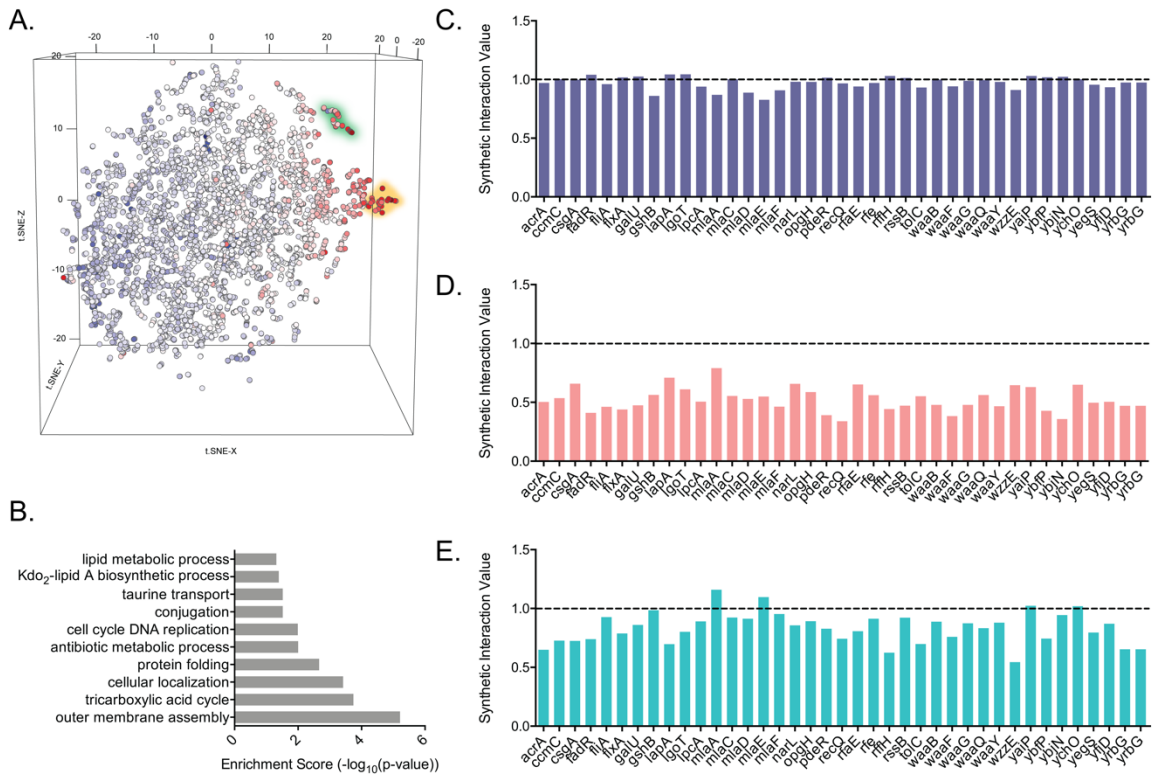


Figure 3: Synthetic genetic interactions are altered in the presence of subinhibitory concentrations of large-scaffold antibiotics. (A.) Cluster visualization of SGAs under vancomycin stress. Dimensionality reduction using t-SNE reveals a structure to genetic interaction data specific to vancomycin stress. To highlight interactions across the vancomycin-treated array, points are colored based on the median SIV for each gene in the deletion collections. Highlighted here are two small clusters that are more SSL under vancomycin stress than in no drug. (B.) GO term enrichment of the single gene deletions from the deletion collections in the highlighted green cluster shown in (A.). Full gene list of this green cluster in (A.) can be found in Table S3. (C.-E.) SIVs of $\Delta bepA$ with every query gene deletion in (C.) no drug, (D.) vancomycin, and (E.) rifampicin. The horizontal dotted line at 1.0 indicates no interaction.

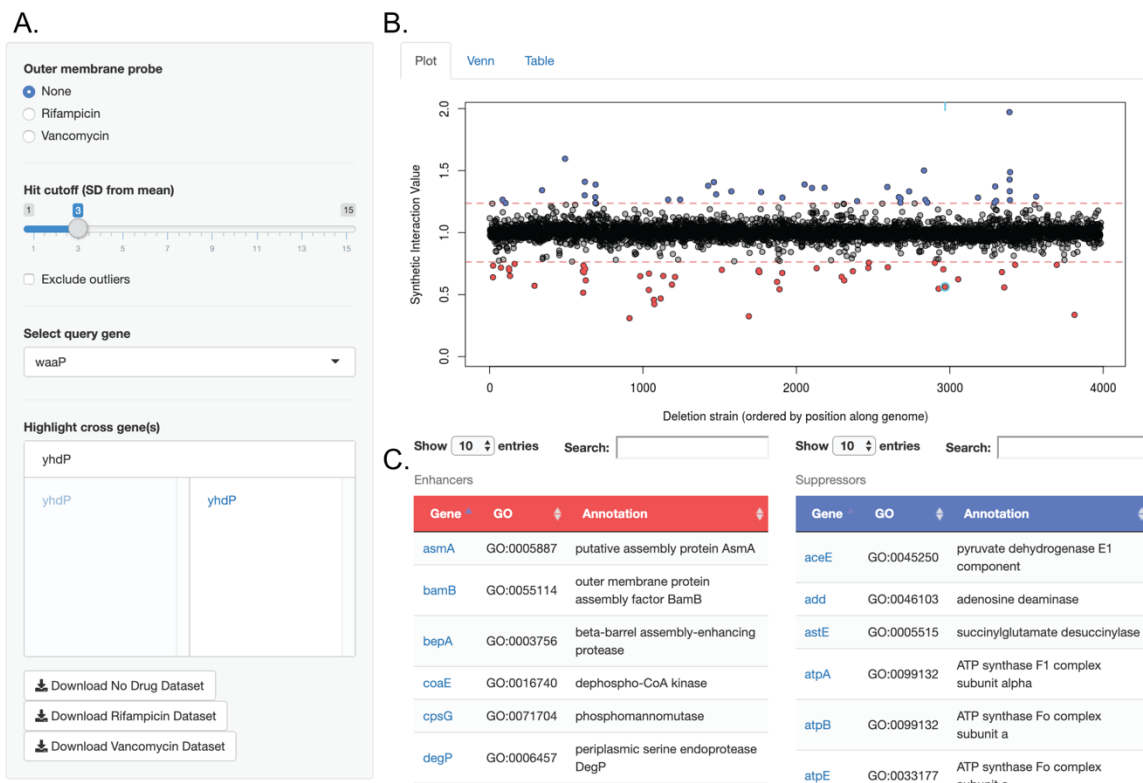


Figure 4: Example of a search output in OMI Explorer. (A.) The search window allows the specification of the OM probe of interest, selection of the hit cutoff value based on number of standard deviation from the mean, selection of the query gene deletion strain of interest, and which gene deletions strains in the cross are to be highlighted. (B.) A plot is generated showing the SIVs of all double deletion strains with the specified query gene deletion. (C.) GO terms and annotations for strains classified as enhancers (SSL) and suppressors based on the hit cutoff. Gene names are hyperlinked to the corresponding gene information page on EcoCyc.

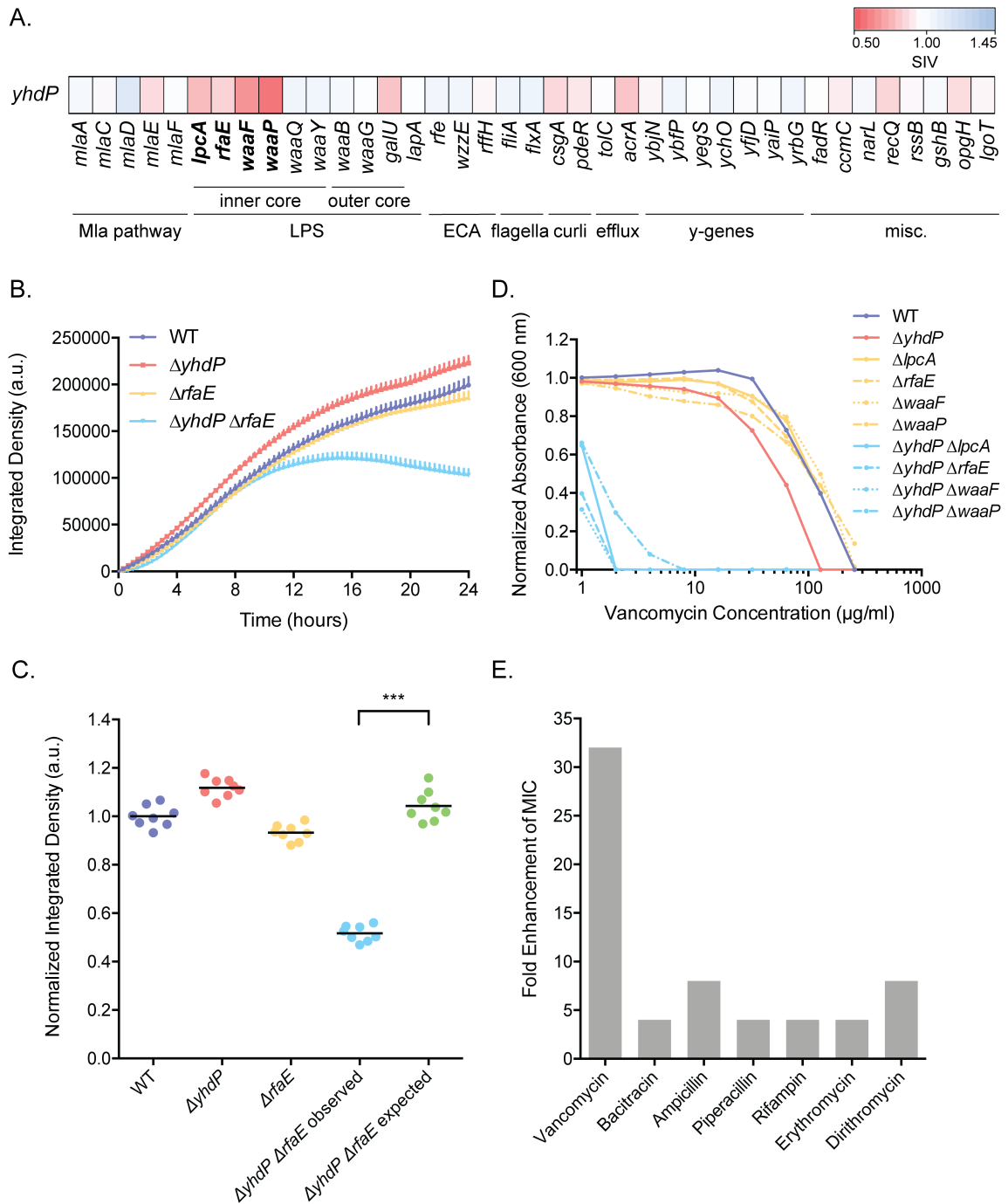


Figure 5: A synthetic sick interaction between $\Delta yhdP$ and LPS inner core deletion strains results in increased susceptibility to cell wall active antibiotics. (A.) A heatmap of SIVs between $\Delta yhdP$ and the query gene deletion strains. Red represents a lower SIV, white represents neutral interactions, and blue represents a higher SIV. (B.) Growth kinetics in solid media of the single

deletion strains compared to the double deletion strain, $n = 8$. Error bars represent standard deviation from the mean. (C.) Endpoint (24 hour) normalized integrated densities of the strains in (B.). Expected growth was calculated as the product of the growths of each single deletion based on the multiplicative rule. Each point represents the individual replicate and the line indicates the mean; $***P < 0.001$, two-tailed Mann-Whitney test. (D.) Potency analysis of vancomycin in the single and double deletion strains. In order to determine differences in MICs, strains were grown in the presence of two-fold dilutions of vancomycin from 0-256 $\mu\text{g}/\text{mL}$ where the normalized absorbance is the background subtracted endpoint OD_{600} divided by the background subtracted endpoint OD_{600} in the 0 $\mu\text{g}/\text{mL}$ well. The average value of three technical replicates is shown from one experiment, although experiments were performed in biological duplicate. (E.) Fold enhancement (decrease) in MIC of a subset of antibiotics in the $\Delta yhdP \Delta waaP$ double strain compared to the corresponding single deletions. MIC tests were performed in triplicate. All MIC values for all strains can be found in Table S4.

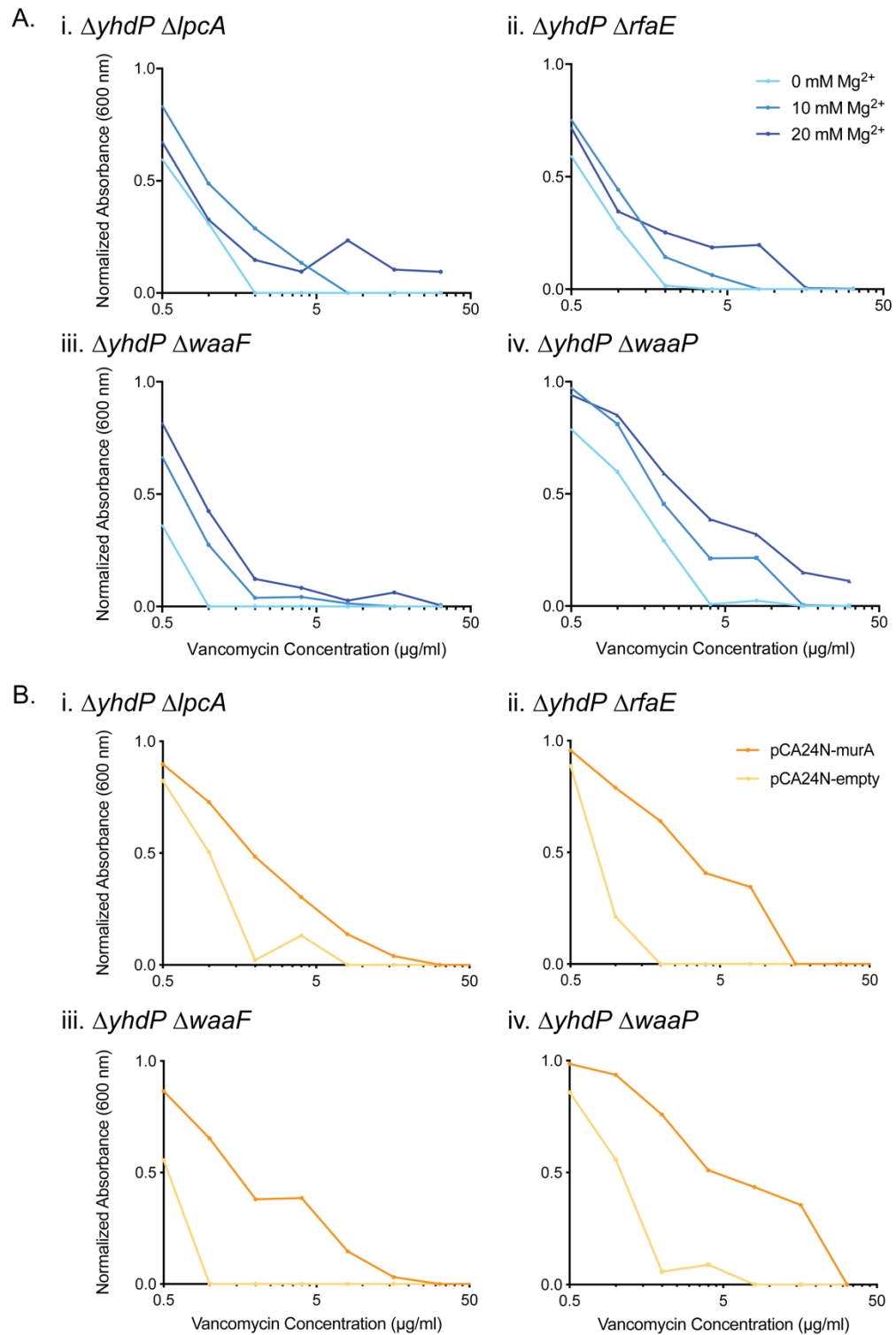


Figure 6: The increased susceptibility, of strains with deletions in *yhdP* and LPS inner core genes, to vancomycin is due to both outer membrane permeability and Und-P flux. (A.) Suppression of vancomycin activity by

addition of magnesium in (i) $\Delta yhdP \Delta lpcA$, (ii) $\Delta yhdP \Delta rfaE$, (iii) $\Delta yhdP \Delta waaF$, (iv) $\Delta yhdP \Delta waaP$. (B.) Suppression of vancomycin activity by overexpression of *murA* in (i) $\Delta yhdP \Delta lpcA$, (ii) $\Delta yhdP \Delta rfaE$, (iii) $\Delta yhdP \Delta waaF$, (iv) $\Delta yhdP \Delta waaP$. Induction using 0.1 mM IPTG was performed for both pCA24N-*murA* and pCA24N-empty (82). Strains were grown in the presence of two-fold dilutions of vancomycin from 0-128 $\mu\text{g/mL}$ where the normalized absorbance is the background subtracted endpoint OD_{600} divided by the background subtracted endpoint OD_{600} in the 0 $\mu\text{g/mL}$ well. Values shown are averages of three technical replicates. Experiments were performed in at least biological duplicate and one representative example is shown.

Tables

Table 1: Summary of SSL interactions across all SGAs performed.
 Interactions 3σ below the mean, excluding outliers, were classified as SSL interactions.

Condition	Interactions	
	Total	Per gene
No drug	1173	30.077
Rifampicin	1409	36.128
Vancomycin	1564	40.103

Supplementary Material

Figures

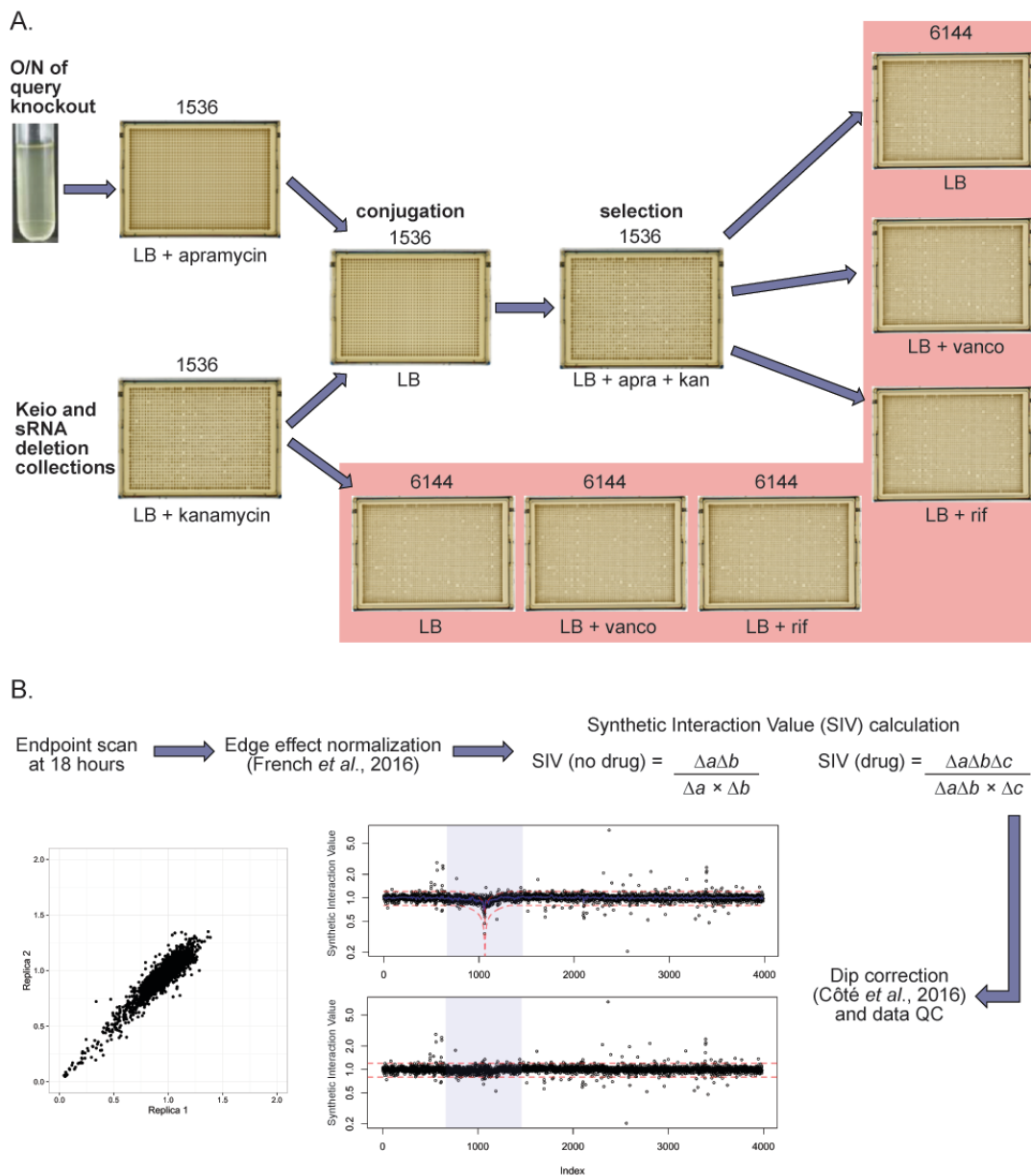


Figure S1: The workflow used to generate SGAs. (A.) Shown are the steps to perform a single replicate of a query deletion strain crossed with the one plate of the Keio collection using the Singer Rotor HDA. Drug plates pinned at 6144 density are at 1/8th MIC of the query strain. (B.) Data analysis steps for determination of synthetic interactions. apra: apramycin, kan: kanamycin, vanco: vancomycin, rif: rifampicin

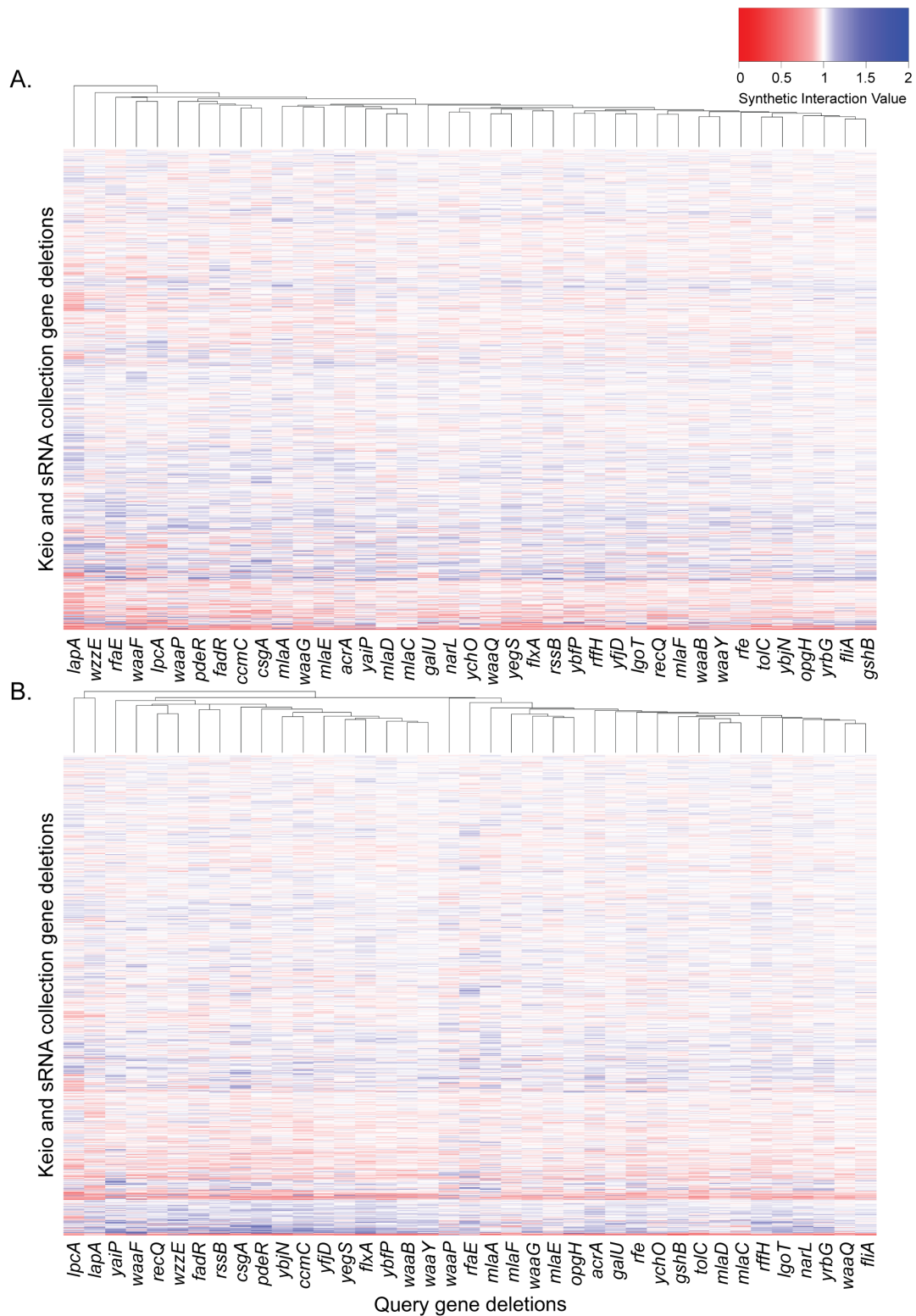


Figure S2: SGAs of outer membrane-related gene deletions in subinhibitory concentrations of (A.) rifampicin and (B.) vancomycin. Related to Figure 1.

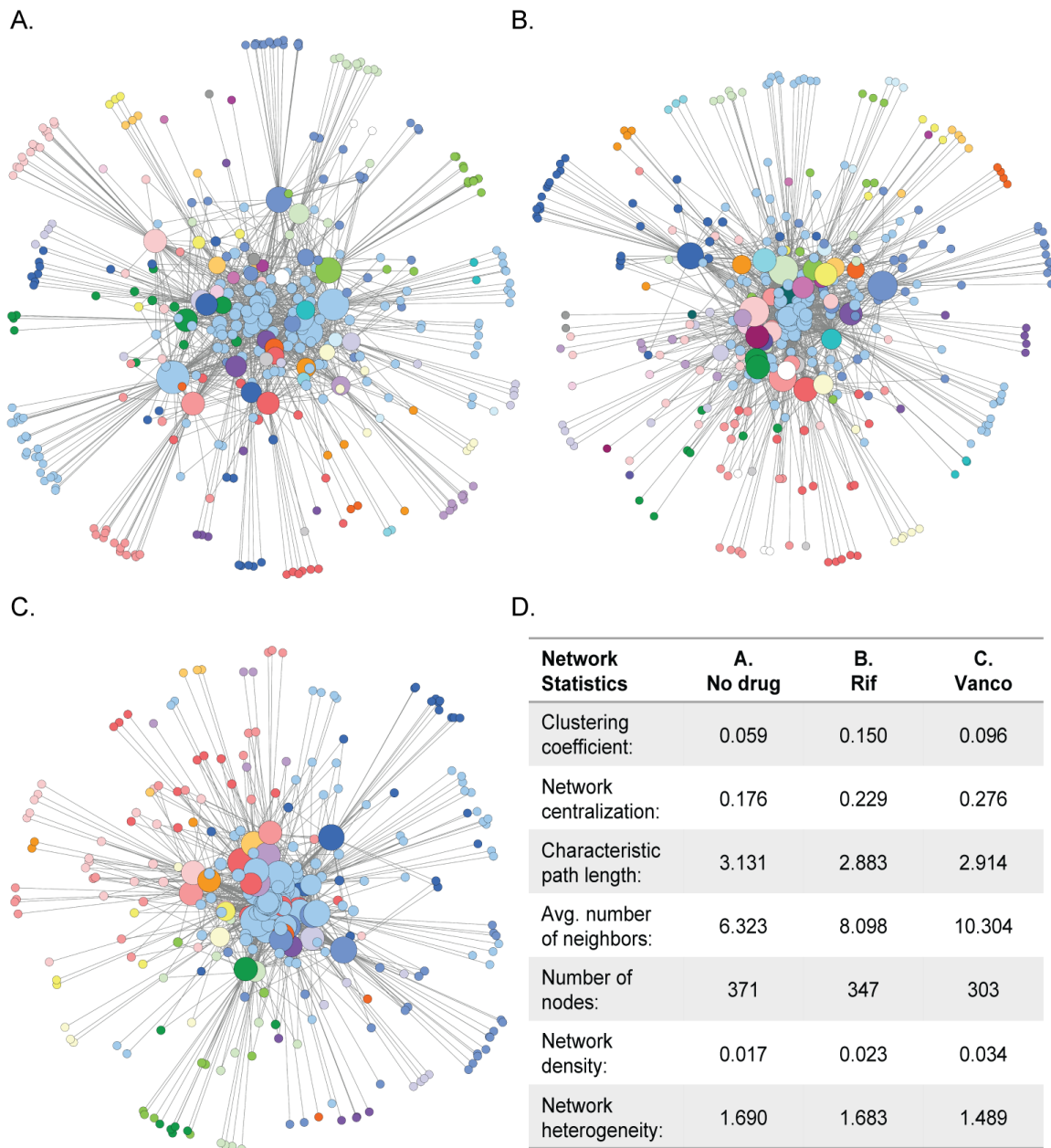


Figure S3: Network interaction map for SSL gene pairs for (A.) no drug, (B.) rifampicin, (C.) vancomycin. Network maps were generated in Cytoscape using an edge-weighted spring embedded layout. Nodes were sized according to their number of edges and coloured by Markov cluster (using a granularity/inflation value of 2). Self loops due to incomplete dip correction were removed. (D.) Network statistics output from Cytoscape’s NetworkAnalyzer for genetic interaction network maps in (A.-C.).

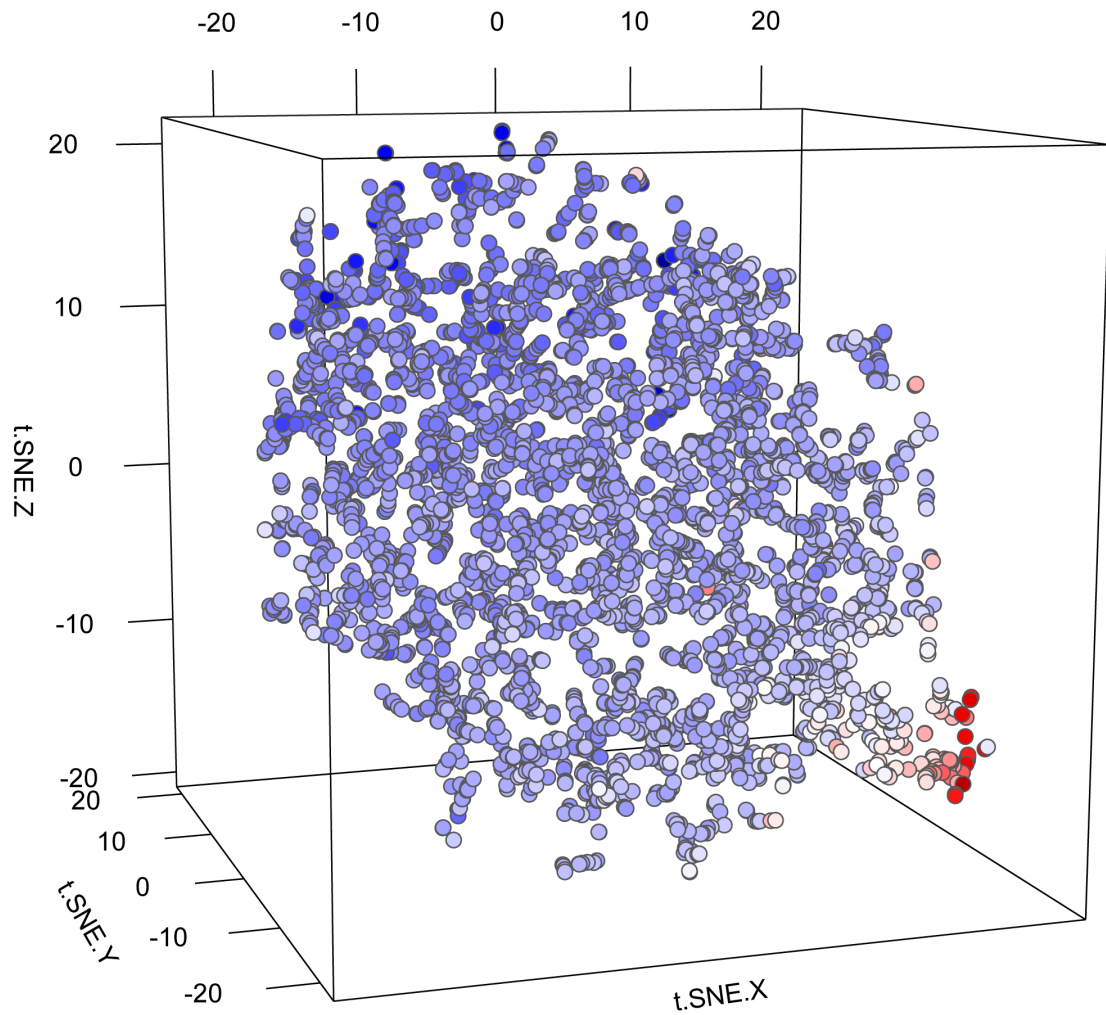


Figure S4: t-SNE clustering of SGAs under rifampicin stress compared to no drug. To highlight interactions across the rifampicin-treated array, points are colored based on the median genetic interaction score for each gene in the deletion collections. Related to Figure 3.

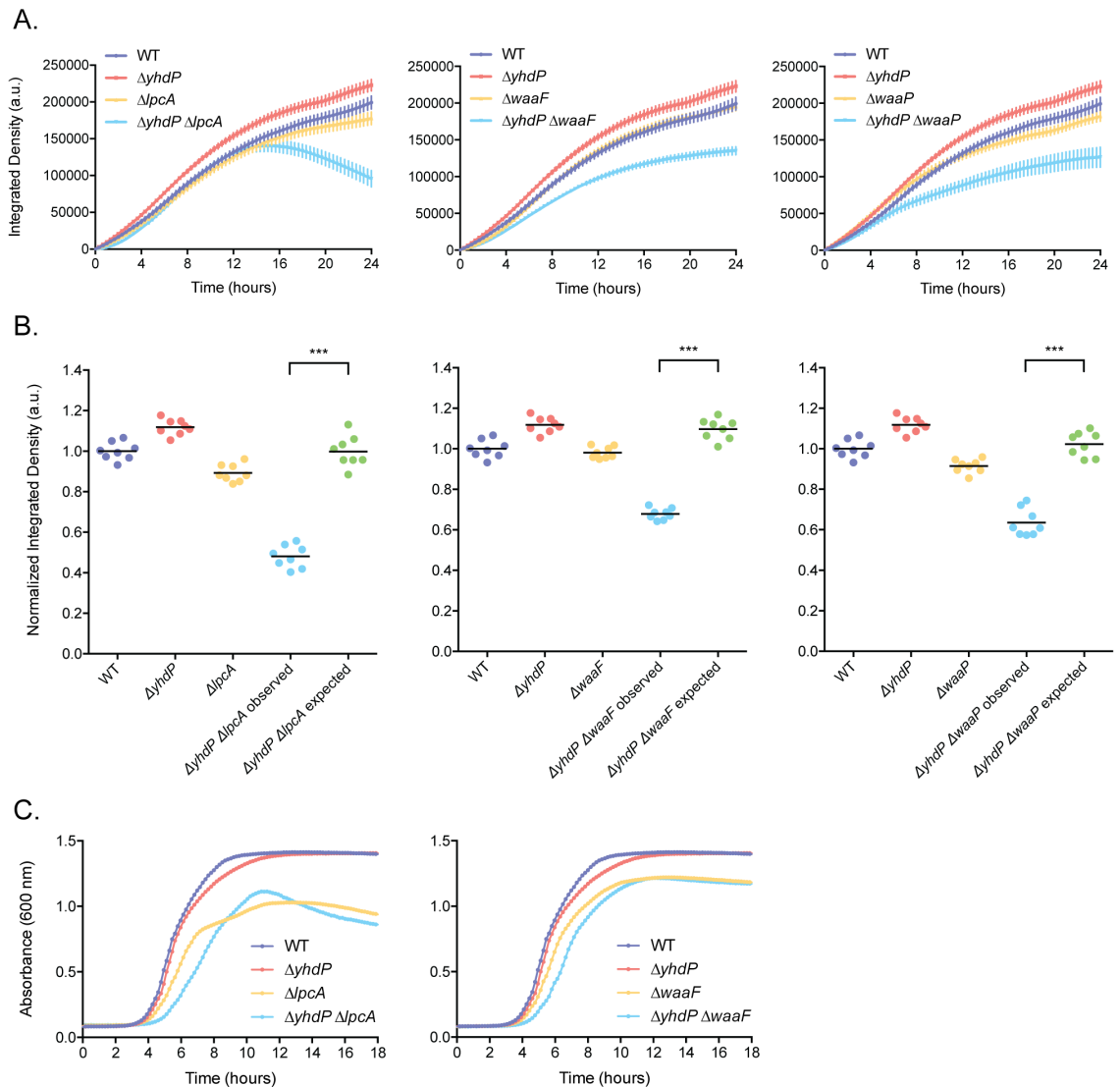


Figure S5: Deletion of *yhdP* in LPS inner core deletion strains leads to a growth defect. (A.) Growth kinetics in solid media of the single deletion strains compared to the double deletion strain, $n = 8$. Error bars represent standard deviation from the mean. (B.) Endpoint (24 hour) normalized integrated densities of the strains in (A.). Expected growth was calculated as the product of the growths of each single deletion based on the multiplicative rule. Each point represents the individual replicate and the line indicates the mean; $***P < 0.001$, two-tailed Mann-Whitney test. (C.) Growth kinetics in liquid media of the single deletions compared to the double deletions, $n = 2$. Related to Figure 5.

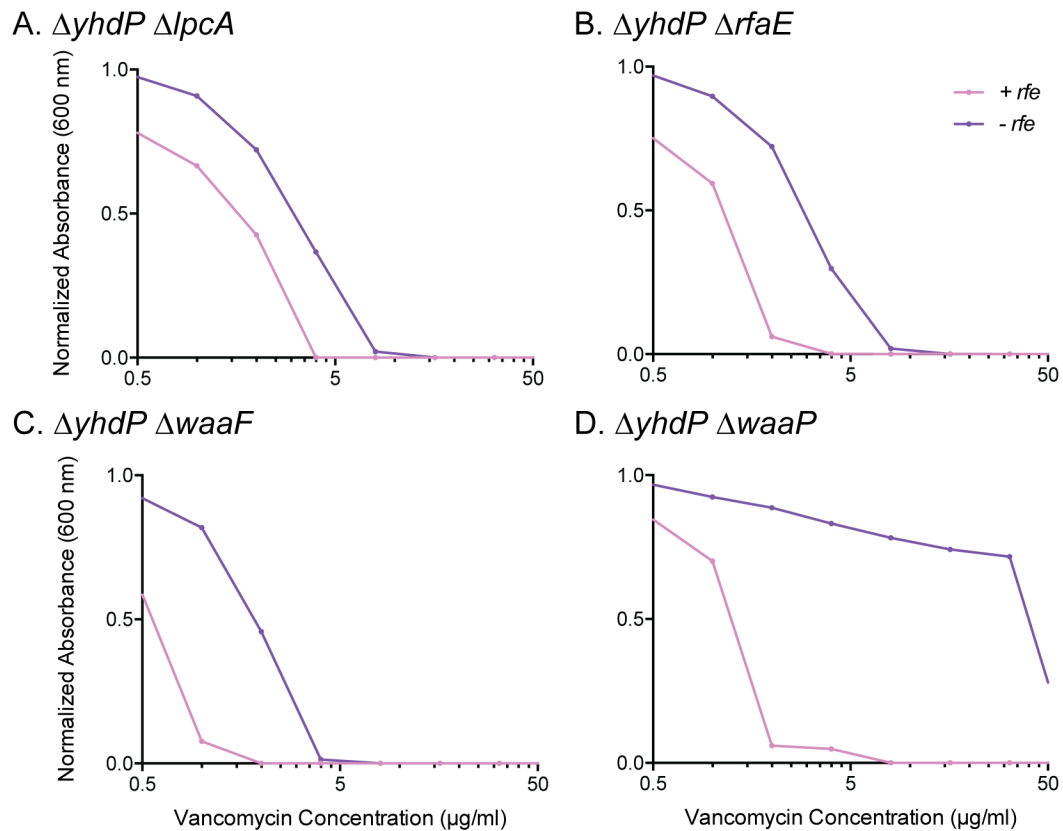


Figure S6: Deletion of ECA production suppresses vancomycin MIC in (A.) $\Delta yhdP \Delta lpcA$, (B.) $\Delta yhdP \Delta rfaE$, (C.) $\Delta yhdP \Delta waaF$, (D.) $\Delta yhdP \Delta waaP$. Triple deletions were constructed by replacing *rfe* with a chloramphenicol resistance cassette using lambda red recombineering in the double deletion backgrounds. Values shown are averages of three technical replicates. Experiments were performed in at least biological duplicate and one representative example is shown.

Tables

Table S1: Background information on query gene deletion strains. Selected CIP strains used to making query gene deletion strains Hfr are shown. Primers for amplifying the apramycin resistance cassette to generate deletion strains and confirmation of cassette are listed. Solid MICs of vancomycin and rifampicin are also listed. *This supplementary table is a spreadsheet file which can be found at <https://mbio.asm.org/content/11/2/e00161-20>.

Table S2: All synthetic interaction values for SGAs performed in no drug, vancomycin, and rifampicin. Included are SSL interactions and their corresponding SIV used to generate the network maps in Figure S3. *This supplementary table is a spreadsheet file which can be found at <https://mbio.asm.org/content/11/2/e00161-20>.

Table S3: Gene list from t-SNE cluster highlighted in green in Figure 3.

Gene deletion	Product
<i>asmA</i>	putative assembly protein AsmA
<i>atl</i>	DNA base-flipping protein
<i>bamB</i>	outer membrane protein assembly factor BamB
<i>bamC</i>	outer membrane protein assembly factor BamC
<i>bepA</i>	β -barrel assembly-enhancing protease
<i>clpX</i>	ATP-dependent Clp protease ATP-binding subunit ClpX
<i>cydB</i>	cytochrome <i>bd</i> -I ubiquinol oxidase subunit II
<i>dksA</i>	RNA polymerase-binding transcription factor DksA
<i>fepD</i>	ferric enterobactin ABC transporter membrane subunit FepD
<i>gpmM</i>	2,3-bisphosphoglycerate-independent phosphoglycerate mutase
<i>hns</i>	DNA-binding transcriptional dual regulator H-NS
<i>hupA</i>	DNA-binding protein HU- α
<i>icd</i>	isocitrate dehydrogenase
<i>ihfB</i>	integration host factor subunit β
<i>lapB</i>	lipopolysaccharide assembly protein B
<i>lpp</i>	murein lipoprotein
<i>lpxL</i>	lauroyl acyltransferase
<i>ninE</i>	DLP12 prophage; NinE family prophage protein
<i>nuoJ</i>	NADH:quinone oxidoreductase subunit J
<i>pgpB</i>	phosphatidylglycerophosphatase B
<i>ptsI</i>	PTS enzyme I
<i>rep</i>	ATP-dependent DNA helicase Rep
<i>rodZ</i>	transmembrane component of cytoskeleton
<i>rpiA</i>	ribose-5-phosphate isomerase A
<i>rseA</i>	anti-sigma-E factor RseA
<i>sdhB</i>	succinate:quinone oxidoreductase, iron-sulfur cluster binding protein
<i>sdhD</i>	succinate:quinone oxidoreductase, membrane protein SdhD
<i>secB</i>	SecB chaperone
<i>skp</i>	periplasmic chaperone Skp
<i>sucC</i>	succinyl-CoA synthetase subunit β
<i>tauA</i>	taurine ABC transporter periplasmic binding protein
<i>tolB</i>	Tol-Pal system periplasmic protein TolB
<i>ybcN</i>	DLP12 prophage; DNA base-flipping protein
<i>ybcO</i>	DLP12 prophage; putative nuclease YbcO
<i>ybgC</i>	esterase/thioesterase
<i>yedF</i>	putative sulfurtransferase YedF
<i>yegQ</i>	putative peptidase YegQ
<i>yhdP</i>	outer membrane permeability factor YhdP

Table S4: Antibiotic susceptibility testing of a diverse panel of antibiotics against double and single deletion strains of $\Delta yhdP$ and LPS inner core. MIC values are in $\mu\text{g}/\text{mL}$. *This supplementary table is a spreadsheet file which can be found at <https://mbio.asm.org/content/11/2/e00161-20>.

**CHAPTER III – Chemical screen for vancomycin antagonism uncovers
probes of the Gram-negative outer membrane**

Preface

The work presented in this chapter was previously published in:

Klobucar K*, Côté J-P*, French S, Borrillo L, Guo ABY, Serrano-Wu MH, Hubbard B, Johnson JW, Gaulin JL, Magolan J, Hung DT, Brown ED. 2021. Chemical screen for vancomycin antagonism uncovers probes of the Gram-negative outer membrane. ACS Chem Biol. 16: 929-942. *co-first authors
Copyright 2021 American Chemical Society. Reused with permission.

<http://pubs.acs.org/articlesonrequest/AOR-TQKSXTSPC2AHTXMBTUWX>

I performed all physicochemical property analysis, membrane integrity assays, and LPS displacement assays. Côté J-P and I performed all checkerboard broth microdilution assays. Côté J-P performed the high-throughput chemical screening and prioritization of compounds. French S performed atomic force microscopy experiments and Guo ABY performed live cell microscopy. Liproxstatin-1 analogue design, synthesis, and characterization was performed by Borrillo L and Johnson JW. MAC-0568743 analogue design and characterization was performed by Serrano-Wu MH, Lee KK, Hubbard B, and Gaulin JL. Serrano-Wu MH and Magolan J assisted with writing the results for structural analogues of MAC-0568743 and liproxstatin-1, respectively. I wrote and edited the manuscript with input from all authors.

Abstract

The outer membrane of Gram-negative bacteria is a formidable permeability barrier which allows only a small subset of chemical matter to penetrate. This outer membrane barrier can hinder the study of cellular processes and compound mechanism of action, as many compounds including antibiotics are precluded from entry despite having intracellular targets. Consequently, outer membrane permeabilizing compounds are invaluable tools in such studies. Many existing compounds known to perturb the outer membrane also impact inner membrane integrity, such as polymyxins and their derivatives, making these probes non-specific. We performed a screen of ~140,000 diverse synthetic compounds, for those that antagonized the growth inhibitory activity of vancomycin at 15 °C in *Escherichia coli*, to enrich for chemicals capable of perturbing the outer membrane. This led to the discovery that liproxstatin-1, an inhibitor of ferroptosis in human cells, and MAC-0568743, a novel cationic amphiphile, could potentiate the activity of large-scaffold antibiotics with low permeation into Gram-negative bacteria at 37 °C. Liproxstatin-1 and MAC-0568743 were found to physically disrupt the integrity of the outer membrane through interactions with lipopolysaccharide in the outer leaflet of the outer membrane. We showed that these compounds selectively disrupt the outer membrane while minimally impacting inner membrane integrity, particularly at the concentrations needed to potentiate Gram-positive-targeting antibiotics. Further

exploration of these molecules and their structural analogues is a promising avenue for the development of outer membrane specific probes.

Introduction

Gram-negative bacteria are intrinsically resistant to many compounds due to the outer membrane (OM) component of their cell envelopes. The Gram-negative cell envelope is composed of an inner membrane (IM), which is a canonical phospholipid bilayer, a thin layer of rigid peptidoglycan in the periplasmic space, and the OM, which is an asymmetric bilayer composed of phospholipids on the inner leaflet and lipopolysaccharide (LPS) molecules on the outer leaflet (1). LPS molecules are principally composed of a lipid A component which anchors the LPS molecules into the membrane, a core oligosaccharide region, and a negatively charged, O-polysaccharide; however, O-polysaccharide is absent in *Escherichia coli* K-12 strains (2). The LPS molecules in the outer leaflet pack together tightly, with adjacent molecules being stabilized by divalent cations like Mg^{2+} and Ca^{2+} , producing a barrier that is difficult to penetrate by many antibiotics (3, 4). The chemical matter capable of cell penetration is limited. The molecules that tend to be able to pass through the OM barrier are small (less than ~600 Da) and hydrophilic, passing through porins rather than diffusing across the OM (5–8). To explore the use of small molecules to knock down cellular processes, this OM obstacle needs to be circumvented.

OM permeability has proven to be especially problematic to modern target-based antibacterial drug discovery efforts. Biochemical screening campaigns have no shortage of tightly-binding enzyme inhibitors, however, their targets are often unreachable due to the OM barrier. These sorts of inhibitors are often ineffective against Gram-negative cells, as the chemical properties favoured for target inhibition are largely incompatible with OM permeability (8). Regardless, antibiotics often require high concentrations to produce any detectable growth inhibitory effect on Gram-negative bacteria, despite being effective against Gram-positive bacteria. In particular, antibiotics such as macrolides, rifamycins, aminocoumarins, oxazolidinones, and glycopeptides have high minimum inhibitory concentrations (MICs) against Gram-negative bacteria with an intact OM (9, 10). The targets of these antibiotic classes are present in Gram-negative bacteria (11), including the model bacterium *E. coli*, for which there is a strong foundational understanding of bacterial genetics and physiology as well as a plethora of omics tools to address the mode of action of antibacterial compounds. Thus, chemical probes capable of permeabilizing the OM can facilitate mechanism of action studies which can be otherwise challenging. Further, such probes of OM processes have broad potential for OM permeability studies across a spectrum of Gram-negative pathogens.

OM perturbation can be achieved *in vitro* through a variety of genetic means. Genetic lesions in OM biosynthetic genes, such as those involved in LPS biogenesis, tend to result in increased OM permeability (3). There is utility in

libraries of systematic gene disruptions, particularly in well-annotated and characterized organisms such as *E. coli* (12). Indeed, this translates well to approaches using such libraries to explore the biology of the OM (13). However, the effects of genetic perturbation are permanent in most instances, and conditional mutations are challenging to engineer (14, 15). Further, disruption of essential processes must always be partial or conditional in some way, as knocking out essential processes ultimately results in growth inhibition. This can be achieved using complementation systems, or CRISPR-Cas disruption, but these approaches can be imprecise under control of promoters prone to basal levels of transcription. While mutants with hyperpermeable OM phenotypes are useful in conjunction with small molecule probes of biology, such as cytoplasmic membrane activity (16, 17) or assaying efflux (18), chemical perturbation of the OM has many advantages. For example, it is fast-acting and does not require complex genetic disruption to achieve the desired effect.

Chemical perturbation of the OM is often an organism-agnostic approach, with utility in explorations of biology as well as antimicrobial combination therapies. The level of perturbation can be altered by tuning probe concentration, in contrast to the complex systems of regulation outlined above. Such probes are powerful tools for exploring cell biology, particularly when combined with genomic libraries in model organisms. Compounds like EDTA increase the permeability of the OM by chelating the divalent cations that stabilize LPS (19, 20). Other chemical compounds, most notably polymyxins and polymyxin derivatives, are

known to physically bind to the OM and disrupt its integrity. For example, polymyxins, which are cationic antimicrobial peptides, are known to bind to the lipid A component of LPS, displacing the divalent cations which stabilize the OM (21, 22). Subsequently, these compounds promote their own uptake, through deficiencies in the OM caused by their accumulation, and interact with the IM leading to cell death (21). Thus, despite being good OM permeabilizers, their IM activity makes these compounds non-specific as OM probes. Derivatives of polymyxin B such as polymyxin B nonapeptide (PMBN) and SPR741 have been designed to retain OM disruption while reducing IM activity (23–25).

In an effort to discover new compounds capable of perturbing the Gram-negative OM, our group developed an unconventional screening platform to enrich for non-lethal molecules that are likely to potentiate molecules such as large-scaffold antibiotics. The basis for this chemical screening platform originated with the observation that *E. coli* becomes susceptible to vancomycin at sub-physiological growth temperatures (26). Normally, the *E. coli* OM is impervious to large, hydrophilic antibiotics like vancomycin; however, phase transitions in the OM under cold stress create fissures that allow entry of vancomycin into cells (27). Interestingly, at low temperatures the activity of vancomycin was antagonized by deletions in OM biosynthetic genes, notably those involved in LPS biogenesis (28). These deletion strains were also more sensitive to other large-scaffold antibiotics like rifampicin, novobiocin, and erythromycin at 37 °C, indicating compromised OM integrity (29). Previously, our

group performed a pilot screen of ~1,500 approved drugs for those that antagonized the growth-inhibitory activity of vancomycin at 15 °C in *E. coli* and discovered that pentamidine, an antiprotozoal drug, had the cryptic ability to physically perturb the OM and potentiate Gram-positive-targeting antibiotics against Gram-negative pathogens (29).

Here, we extended our previously published vancomycin antagonism screening platform to a diverse library of ~140,000 synthetic compounds, in an effort to uncover more probes of the OM. We began by performing a high-throughput screen for growth in the presence of a lethal concentration of vancomycin at 15 °C in *E. coli*. An analysis of active compounds revealed unique physicochemical properties of these presumed OM perturbing compounds. We chose to focus on two compounds which were found to potentiate Gram-positive-targeting antibiotics in several Gram-negative organisms, a hallmark for OM disruption, namely, MAC-0568743 and liproxstatin-1. Characterization of these two compounds revealed that they potentiate large-scaffold antibiotics by physically disrupting the OM through interactions with LPS, while exhibiting minimal disruption of the IM. Altogether, this work describes two new, selective, chemical perturbants of the Gram-negative OM, liproxstatin-1 and MAC-0568743, and their structural analogues.

Results and Discussion

A high-throughput screen to uncover compounds that perturb the outer membrane

As shown previously, screening for antagonists of the growth inhibition by vancomycin at cold temperatures has the potential to uncover molecules that perturb the OM, either physically or by altering its biogenesis (28, 29). A pilot screen of ~1,500 previously approved drugs for vancomycin antagonism at cold temperatures led to the discovery of pentamidine, a known antifungal drug, with the cryptic capacity to perturb the bacterial OM and potentiate large-scaffold antibiotics against Gram-negative bacteria (29). Here we have expanded this screen to include a collection of ~140,000 diverse synthetic compounds, sourced from four different vendors, Asinex, ChemDiv, ChemBridge, and Enamine. These compounds were screened at a concentration of 10 μ M against *E. coli* K-12 BW25113 in the presence of 16 μ g/mL of vancomycin at 15 °C for 96 h in rich microbiological media (Figure 1A). The concentration of vancomycin used in the screen was lethal to *E. coli* cells grown under cold stress (28). Any compounds which promoted growth in the presence of vancomycin at 15 °C in both replicates of the screen were deemed active (Figure 1B). Of the ~140,000 compounds screened, only 39 molecules were found to antagonize the activity of vancomycin in the cold (Figure 1A-B). This resulted in an active rate of ~0.027%, which was much lower than is typical for screens, for example, where growth inhibition is the phenotype of interest (30).

For the resulting 39 active compounds, physicochemical properties were calculated in order to determine which characteristics distinguished the actives from the rest of the screened compounds which did not antagonize vancomycin in these conditions. Active compounds had significantly lower $\log D$ and $\log S$ values compared to the inactive compounds, where D is the distribution coefficient of ionizable species between octanol and water and S is the water solubility (Figure 1C; Table S1). Interestingly, the active compounds also had significantly lower topological polar surface area values than the rest of the library, despite similarity in total surface area. The distribution of pK_a values was also higher, and active compounds possessed more basic nitrogens, compared to the inactive ones (Figure 1C; Table S1). Accordingly, most compounds which were active against the OM tended to be positively charged, presumably because LPS is negatively charged and molecules with positive charge are more likely to bind to the LPS component of the Gram-negative OM (31). Additionally, active compounds had more sp^3 hybridization and molecular flexibility relative to the inactive molecules in the screen (Table S1). Several properties did not significantly differ between groups, including molecular weight and total surface area. Although these molecules themselves were not antibacterial, the physicochemical properties followed some of the same trends observed with antibacterials, which tend to have lower $\log D$ and higher polar surface areas on average than general drugs (7, 8).

Of the 39 actives, 17 compounds were resupplied based on structural diversity and availability for purchase from the vendors. These reordered compounds were assessed for synergy with rifampicin, a large-scaffold antibiotic, using checkerboard broth microdilution assays. Seven of the tested compounds were found to be synergistic with rifampicin (Figure 1A). Of these compounds we chose to focus on two: (1) a commercially available analogue of the active MAC-0549481, liproxstatin-1 (Figure 2A), and (2) MAC-0568743, which produced the greatest suppression of vancomycin activity in the primary screen (Figures 1B, 2B). Liproxstatin-1, which is a spiroquinoxaline derivative, differs from the screening active only in the position of the chlorine group on the phenyl ring, which is in the meta position as opposed to the ortho position in MAC-0549481 (Figure 2A). Several molecules with quinoxaline moieties have been shown to have biological activity, including activity against human chronic and metabolic diseases as well as antimicrobial activity (32). Liproxstatin-1 has been shown to inhibit ferroptosis, a form of programmed cell death in mammalian cells that is characterized by the accumulation of lipid hydroperoxides in an iron-dependent manner, by acting as a radical-trapping antioxidant in lipid bilayers (33–35). However, liproxstatin-1 has not previously been reported to have any activity against bacterial cells. The other compound of focus, MAC-0568743, *N*'-[2-(2-benzyl-4-chlorophenoxy)ethyl]propane-1,3-diamine, has not been previously described to have any biological or antimicrobial activity. Notably, neither of these compounds are peptides.

Liproxstatin-1 and MAC-0568743 potentiate Gram-positive-targeting antibiotics in Gram-negatives

As these prioritized compounds were found to potentiate the large-scaffold antibiotic rifampicin, other antibiotics which have low permeability or accumulation in Gram-negatives were tested in combination with liproxstatin-1 and MAC-0568743. Despite having a high MIC alone, liproxstatin-1 was able to potentiate the activity of the large, hydrophobic antibiotics, rifampicin, novobiocin and erythromycin, as well as the small, hydrophilic antibiotic, linezolid, in *E. coli* BW25113 at 37 °C at workable concentrations (Figure 2C). However, liproxstatin-1 was unable to sensitize *E. coli* cells to vancomycin which is large and hydrophilic (Figure S1A). In addition to its potentiation activity in *E. coli*, liproxstatin-1 was also able to potentiate rifampicin in *Klebsiella pneumoniae* and *Acinetobacter baumannii*, but was ineffective against *Pseudomonas aeruginosa* (Figure 2D). MAC-0568743 was also able to potentiate rifampicin, novobiocin, erythromycin, and linezolid in *E. coli* (Figure 2E), and was similarly unable to potentiate vancomycin (Figure S1B). MAC-0568743 maintained its potentiation activity in *K. pneumoniae*, *A. baumannii*, and *P. aeruginosa* (Figure 2F). Indeed, tool compounds of any kind that are effective potentiators of Gram-positive-targeting antibiotics against *P. aeruginosa* are rare, with PMBN being one of the few available (36). Commonly used OM disrupting compounds such as SPR741 and pentamidine lack activity against this organism (29, 37). Thus,

MAC-0568743 is able to fulfill the need for an effective potentiator compound in this organism.

The potentiation of Gram-positive-targeting antibiotics is due to outer membrane disruption

As liproxstatin-1 and MAC-0568743 antagonized the activity of vancomycin at 15 °C and were synergistic with large-scaffold antibiotics with poor permeability in Gram-negatives, we sought to investigate whether these compounds were physically disrupting the OM barrier. Lysozyme is a ~14 kDa protein that hydrolyzes peptidoglycan effectively in Gram-positive bacteria; however, it is only effective against Gram-negative bacteria that have a compromised OM. A permeabilized OM enables increased uptake of lysozyme, allowing it to access its target, resulting in cell lysis (38, 39). Exposure of whole cells to subinhibitory concentrations of liproxstatin-1 and MAC-0568743, as well as the known OM perturbant SPR741, resulted in cell lysis by lysozyme in comparison to the untreated control (Figure 3A). The compounds did not lyse cells in the absence of lysozyme under these conditions. An additional assay for measuring OM perturbation was performed by measuring nitrocefin cleavage by a strain of *E. coli* constitutively expressing periplasmic β -lactamase. Disruption of the OM allows the periplasmic β -lactamase to come into contact with and cleave the extracellular nitrocefin substrate, producing a detectable colour change. Cells treated with MAC-0568743 showed a strong increase in absorbance, comparable to the positive control, SPR741, while liproxstatin-1 exhibited a much weaker

increase in absorbance that was only detectable at the highest concentration (Figure 3B). Additionally, although both compounds increased the permeability of cells to lysozyme, the permeability of liproxstatin-1 treated cells to nitrocefin was lower than the MAC-0568743 treated cells, suggesting differing permeability properties. Overall, it is likely that liproxstatin-1 and MAC-0568743 physically impair the structural integrity of the OM since these results are produced upon brief exposure to the compounds rather than exclusively with extended growth in their presence.

Since these compounds increase the permeability of the OM, it is possible that they would produce visible changes to the architecture of the OM. Cells grown in the presence of subinhibitory concentrations of liproxstatin-1 and MAC-0568743, and then stained with the membrane dye, FM4-64, displayed regions of concentrated FM4-64 which are not present in the untreated control (Figure S2). This phenotype has previously been reported for a peptide found to disrupt the OM (40). Consistent with this observation and an increase in permeability, the topology of the OM of cells treated with liproxstatin-1 and MAC-0568743 showed striking changes, revealed using atomic force microscopy (Figure 3C-I). MAC-0568743 treatment resulted in a dose-dependent increase in the roughness of the OM of treated cells, with undulations up to 17 nm in amplitude detected at 8 $\mu\text{g}/\text{mL}$, relative to the untreated cells with a maximum roughness of 8 nm (Figure 3C-F). Perhaps more striking was the abundance of ~ 10 nm wide crevices that appeared in a dose-dependent manner when grown in the presence of MAC-

0568743. The effects of MAC-0568743 on stationary phase cells were noticeable in the first 10 minutes upon treatment, with more visible undulations on the cell surface (Figure S3), suggesting disruption via physical interactions with the OM, rather than through inhibition of OM biosynthesis. Similarly, liproxstatin-1 treatment produced a dose-dependent increase in roughness of the OM, with an increase of 11 nm in undulation amplitude between the 32 $\mu\text{g}/\text{mL}$ and 64 $\mu\text{g}/\text{mL}$ concentrations (Figure 3G-I). In the presence of 128 $\mu\text{g}/\text{mL}$ of liproxstatin-1, blebs or vesicles were observed on the OM of whole cells (Figure 3I). The surface area-to-volume ratio for these structures was much higher than where absent, with a 31% increase in the surface area in the blebbing region with a roughness (R_{max}) of 26 nm. The region without the presence of blebbing was notably smoother, with a surface area difference of 6% and R_{max} of 13 nm. Interestingly, there were a large number of released vesicles accumulated on the filter paper existing independently from the cells. Surface topologies of these exogenous vesicles were indistinguishable from those appearing on the surface of whole cells (data not shown). Furthermore, time course imaging upon treatment of stationary phase cells with liproxstatin-1 revealed that vesicles were detected within 60 minutes after exposure to the compound (Figure S4). Based on these results, both liproxstatin-1 and MAC-0568743 appeared to disrupt the physical architecture of the Gram-negative OM, producing phenotypic changes to the surface topology of cells. Although both compounds resulted in changes to OM

surface architecture, their differing effects suggest that liproxstatin-1 and MAC-0568743 may impact the OM in different ways.

Liproxstatin-1 and MAC-0568743 interact with the outer membrane by binding to LPS

As LPS is a major component of the Gram-negative OM, and most known antibiotic potentiator molecules interact with or disrupt the lateral interactions of adjacent LPS molecules, we hypothesized that liproxstatin-1 and MAC-0568743 were interacting with LPS. To explore whether liproxstatin-1 and MAC-0568743 disrupt lateral interactions between LPS molecules, we investigated the effects of addition of divalent cations like Mg^{2+} on their activities. Divalent cations are known to stabilize the interactions between adjacent LPS molecules in the OM via reduction of negative charge (3, 4). As expected, liproxstatin-1 and MAC-0568743 lost their ability to potentiate rifampicin in the presence of 20 mM $MgCl_2$ (Figure 4A). The ability of these compounds to synergize with large-scaffold antibiotics was also suppressed upon addition of exogenous LPS (Figure 4B), with the fractional inhibitory concentration index (FICI) between rifampicin and liproxstatin-1 increasing from 0.38 to 0.5, and the FICI between rifampicin and MAC-0568743 increasing from 0.16 to ≤ 0.5 . Thus, both liproxstatin-1 and MAC-0568743 likely act by binding to LPS. However, the concentration of LPS required to suppress the activity of MAC-0568743 was lower than that required to observe suppression of liproxstatin-1.

To further investigate the interaction between both compounds and LPS, checkerboard broth microdilution antibiotic susceptibility assays were performed in a strain of *E. coli* possessing a deletion in *waaC*, the gene responsible for the transfer of the first heptose of LPS onto the lipid A-Kdo₂ portion of the inner core (41). The LPS in this strain is deep rough and highly truncated, possessing only the lipid A-Kdo₂ region essential for growth. In this genetic background, the synergies between both lipoxstatin-1 and MAC-0568743 with rifampicin were more pronounced relative to wildtype (Figure 4C). The FICIs decreased from 0.38 (wildtype) to 0.08 ($\Delta waaC$) in the checkerboard assay between lipoxstatin-1 and rifampicin, and ≤ 0.16 (wildtype) to 0.09 ($\Delta waaC$) in the checkerboard assay between MAC-0568743 and rifampicin. This suggests that the LPS core is not required for the interaction of these compounds with LPS. Additionally, we explored whether *mcr-1* mediated phosphoethanolamine modification to lipid A, reducing the anionic charge of LPS molecules, would impair the ability of the potentiator molecules to synergize with their partner antibiotics. In the *E. coli* strain expressing *mcr-1*, lipoxstatin-1 was no longer synergistic with rifampicin, with an FICI of 0.56, greater than the ≤ 0.5 value required for synergy (Figure 4D). On the other hand, the potentiation activity of MAC-0568743 was unchanged, as the FICI with rifampicin was 0.16 regardless of the presence of the *mcr-1* gene (Figure 4D). These results suggest that the lipoxstatin-1 interactions are dependent on phosphoryl sites flanking lipid A on LPS, but that MAC-0568743 is active in a different manner. Nonetheless, despite the suppression of lipoxstatin-

1 activity upon expression of *mcr-1* in wildtype *E. coli* BW25113, liproxstatin-1 was still able to potentiate rifampicin in the three tested environmental isolates of polymyxin resistant *E. coli* and in the polymyxin resistant clinical *E. coli* strain tested, all of which had FICIs of 0.5 or less (Figure S5). MAC-0568743 was also able to potentiate rifampicin in all environmental and clinical polymyxin resistant strains tested (Figure S5).

Recently, the OM perturbant SPR741 was investigated for its ability to impact intrinsic, acquired, and spontaneous resistance development in laboratory and clinical strains of *E. coli*, when used in combination with large-scaffold antibiotics (42). However, a limitation in this study was that polymyxin resistant strains had cross-resistance to SPR741, constraining the use of SPR741 as an OM probe to clinical isolates lacking polymyxin resistance. With the use of MAC-0568743 or liproxstatin-1, the spectrum of bacteria suited to this type of study could be expanded to include polymyxin resistant clinical isolates. Both MAC-0568743 and liproxstatin-1 were shown to be effective OM permeabilizers in the clinical *E. coli* isolate C0244 (Figure S5), one of the strains which SPR741 was ineffective against (42). Additionally, liproxstatin-1 and MAC-0568743 demonstrated utility against *mcr-1* positive environmental *E. coli* isolates which are known to be insensitive to PMBN as a potentiator (29). Interestingly, another polymyxin derivative, NAB739 which is otherwise identical to SPR741 but has an octanoyl residue instead of an acetyl residue at the N-terminal of the linear (tail)

portion of the molecule, is capable of sensitizing target Gram-negatives with acquired polymyxin resistance to several Gram-positive antibiotics (43).

Next, we examined the binding of liproxstatin-1 and MAC-0568743 to LPS using a BODIPY-cadaverine displacement assay (25, 44). BODIPY-tagged cadaverine binds to LPS molecules at the negatively charged phosphates of lipid A, quenching its fluorescence. Upon displacement of the BODIPY-cadaverine probe from LPS by a compound that also binds LPS, an increase in fluorescence intensity is observed. Both MAC-0568743 and liproxstatin-1 resulted in a dose-dependent increase in fluorescence intensity, indicating that both compounds were able to bind LPS and displace the BODIPY-cadaverine probe (Figure 4E). Notably, the increase in fluorescence intensity in MAC-0568743 was at similar levels to SPR741, which is known to bind to LPS. This was an unexpected result, given that MAC-0568743 was not impacted by phosphoethanolamine modifications arising from *mcr-1* mediated resistance. However, liproxstatin-1 treatment produced much lower fluorescence levels, suggesting a weaker binding affinity to LPS (Figure 4E). Along with the AFM data, this may suggest that liproxstatin-1 has other additional mechanisms of action to impair OM integrity.

Liproxstatin-1 and MAC-0568743 minimally impact inner membrane integrity

Historically, it has been difficult to uncover drugs which exclusively permeabilize the OM of Gram-negative bacteria without also impacting the IM. For instance, polymyxin B and colistin are both strong disruptors of the OM,

however these compounds are also highly potent antimicrobials due to their strong activity on the IM (21). These molecules are highly positively charged possessing 5 positively charged amines. Efforts to reduce this IM activity of polymyxin B have produced PMBN, which retains the same number of positive charges but lacks the hydrophobic N-terminal fatty acyl chain (23). Although PMBN has reduced lytic activity relative to its parent compound, recent work has shown that PMBN treatment still results in substantial levels of IM depolarization, albeit less than polymyxin B (25). A derivative of PMBN with only 3 positively charged amines, SPR741, was designed to reduce the nephrotoxicity of the compound, and as a consequence its IM activity was minimized while the OM permeabilization properties were retained (45, 46). SPR741 is substantially less active on the IM, resulting in minimal membrane disruption, making this compound the polymyxin derivative most specific for the OM and an excellent OM perturbant (25). Thus, SPR741 makes a suitable standard for comparison with lipoxstatin-1 and MAC-0568743.

In order to measure IM permeability, a strain of *E. coli* constitutively expressing β -galactosidase in the cytoplasm with a deletion in the lactose permease was used. Any cleavage of the ortho-nitrophenyl- β -galactoside (ONPG) substrate by β -galactosidase is the result of a compromised IM and produces a detectable colour change. As expected based on previous work (25), SPR741 resulted in a relatively small increase in absorbance compared to the high control of polymyxin B, which is known to be highly IM active (Figure 5A).

Both liproxstatin-1 and MAC-0568743 were found to have minimal levels of IM disruption, comparable to or less than that of SPR741 at concentrations where potentiation of large-scaffold antibiotics was possible (Figure 5A). For further validation, the effects of the compounds on IM potential was investigated. This assay employs the use of the fluorescent dye, 3,3'-dipropylthiacarbocyanine [DiSC₃(5)] (16). *E. coli* cells are loaded with DiSC₃(5), which is known to accumulate in the IM and self-quench its fluorescence. Upon IM depolarization or disruption of IM integrity by a compound, release of the dye occurs, leading to an increase in fluorescence. In this assay, SPR741 treatment produced fluorescence intensities drastically lower than the polymyxin B high control, with particularly low levels of fluorescence at large-scaffold antibiotic potentiation concentrations (Figure 5B). Again, both liproxstatin-1 and MAC-0568743 treatment also produced low levels of fluorescence, indicating minimal IM disruption (depolarization), particularly at their potentiation concentrations (Figure 5B). Thus liproxstatin-1 and MAC-0568743 specifically disrupt the OM while sparing the IM.

Potentiation activity of structural analogues of liproxstatin-1 and MAC-0568743

The observed preferential targeting of the Gram-negative OM by liproxstatin-1 and MAC-0568743 led us to initiate a preliminary medicinal chemistry effort to probe the effects of minor modifications to these chemical scaffolds in the context of antibiotic potentiation. Liproxstatin-1 and its analogues are readily accessible via chemical synthesis using a modular three-component

condensation reaction between an *o*-phenylenediamine, a benzyl isocyanate, and a carbonyl derivative (see Supporting Information) (47). Eleven synthetic analogues of liproxstatin-1 were evaluated for synergy with linezolid in *E. coli* (M1-M11, Table 1). Linezolid was chosen as the partner antibiotic for liproxstatin-1, rather than rifampicin, as it showed a stronger synergy in the checkerboard assay, with an FICI of 0.19 compared to 0.38 (Figure 2C). First, modification of the *N*-benzyl moiety resulted in modest reduction in potentiation activity relative to liproxstatin-1 for seven analogues (MAC-0549481, M1-M5, M10) and considerable reduction in potentiation activity for compound M6 (Table 1). The reduced potentiation by compound M6 indicates that chlorine atoms of both liproxstatin-1 and MAC-0549481 have a beneficial effect on this activity. Complete loss of potentiation was observed for the pyridine-containing derivative (M9) (Table 1). Similarly, three modifications to the spirocyclic piperidine moiety of liproxstatin-1 all resulted in complete loss of antibiotic potentiation activity (M7, M8, and M11) (Table 1). All of the compounds with FICI values ≤ 0.5 and potentiation concentrations lower than their respective MICs were tested for IM activity using the β -galactosidase assay. Compound M10, which was the most potent analogue alone, had relatively strong IM activity at 16 $\mu\text{g/ml}$ (Table 1). Four compounds (M1-M4) had no detectable IM activity at the highest concentration tested ($>128 \mu\text{g/ml}$). Of these, compound M3 was the most potent potentiator of linezolid (Table 1). Further medicinal chemistry efforts are underway and will be reported in due course.

A more extensive structure-activity relationship analysis was performed for MAC-0568743, with 29 structural analogues tested for synergy with rifampicin (Tables S2, S3). In contrast to liproxstatin-1, MAC-0568743 can be viewed as a more flexible molecule consisting of a cationic headgroup and a lipophilic tail. With regards to the lipophilic region, conformational flexibility appears to be favored, as the 2-benzyl substituent in MAC-0568743 resulted in superior activity compared to the more rigid biphenyl (D3) or carbazole (B34) analogues (Tables S2, S3). In the cationic headgroup region, the influence of freely-rotatable bonds is more complex: cyclization strategies which reduce conformational freedom of both nitrogen atoms (B2, B3R and B3S, B11-cis/trans) are less active, whereas cyclization designs which preserve the flexibility of the C-N bonds (B8A and B8B) are quite active (Table S3). A series of chiral derivatives were designed to probe any influence of stereochemistry on biological activity. For all optically-pure derivatives (for example B3R and B3S, B5R and B5S, and B35R and B35S), no difference in biological activity was observed between stereoisomers (Table S3), thus making it highly unlikely that these molecules bind to a topologically-complex surface like a protein. A dibasic motif was required for biological synergy, as the di-aniline version B37 was significantly less active (Table S3). In general, however, a wide variety of diamino headgroups were able to confer activity, suggesting the role of this ionic headgroup was predominantly electrostatic in nature.

Conclusion

The OM provides intrinsic resistance in Gram-negative bacteria, acting as a barrier to prevent toxic compounds from entering the cell. Increasing the permeability of the OM should improve the influx of compounds which are typically excluded by this structure. However, many existing chemical disruptors of outer membrane integrity are often also active on the IM due to a lack of specificity. In an effort to expand the available collection of OM perturbants, we performed a ~140,000 compound screen to uncover compounds which perturb the OM of *E. coli* whole cells. Of the actives obtained in this screen, we prioritized two compounds for subsequent studies: liproxstatin-1 and MAC-0568743. These compounds were found to potentiate the activity of the Gram-positive-targeting antibiotics rifampicin, novobiocin, erythromycin, and linezolid, which are typically ineffective against Gram-negative bacteria due to a lack of cell penetration. This potentiation was confirmed to be due to physical disruption of the OM by the two compounds, facilitated through their interactions with LPS, with MAC-0568743 being the stronger LPS binding compound. Despite targeting the outer membrane, liproxstatin-1 and MAC-0568743 were found to spare the IM, a desirable property for a specific chemical probe of the OM. In all, the properties of OM perturbants and the prioritized molecules described here are assets to the study of the Gram-negative OM and processes beyond the OM which are made challenging to study by this impermeable barrier. These compounds and their

structural analogues expand our available repertoire of probes for the study of Gram-negative bacterial cell systems and compounds acting on those systems.

Methods

High-throughput chemical screening

Chemical screening was performed at the McMaster Centre for Microbial Chemical Biology. *E. coli* BW25113 was grown overnight (~18 h) in LB medium (10 g/L trypticase peptone, 5 g/L yeast extract, 10 g/L NaCl) and diluted 1:5000 into fresh LB media containing 16 µg/mL of vancomycin (Sigma-Aldrich). A 49.5 µL volume of cells was subsequently transferred to each well of a clear 384-well flat-bottom plate. A 0.5 µL volume of compound was added to each well for a final concentration of 10 µM. Plates were immediately read for absorbance at 600 nm (OD₆₀₀) on an EnVision plate reader (Perkin-Elmer), then grown in a stationary incubator at 15 °C for 96 h. Plates were read again at 600 nm, and cell growth was calculated by subtracting the initial OD₆₀₀ of each well at 0 h from the final OD₆₀₀ at 96 h. Actives were identified as wells with visible growth.

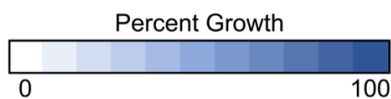
Physicochemical property analysis

The Collective Drug Discovery (CDD) Vault was used to extract the SMILES codes and several physicochemical properties (molecular weight, log P, H-bond donors, H-bond acceptors, Lipinski violations, log D, log S, pKa, CNS MPO score, topological polar surface area, Fsp³, heavy atom count, rotatable bonds) for the screened compound library and the actives in the screen. The rest

of the physicochemical properties were calculated by importing the compound SMILES into OSIRIS DataWarrior (48). Averages and standard deviations for the properties were calculated in Excel and GraphPad Prism was used to perform statistical analyses. Density plots were generating using the R programming language using the default bandwidth.

Checkerboard broth microdilution assays

Overnight cultures (~18 h) of the appropriate strain of bacteria were grown in LB media. Strains were subcultured 1:50 in fresh LB media and grown at 37 °C with shaking at 250 rpm to mid-exponential phase ($OD_{600} \sim 0.4$). Cells were diluted to 1:10,000 in fresh LB (including $MgCl_2$ or LPS from *E. coli* O127:B8 [Sigma-Aldrich] at the indicated concentrations, where appropriate) and added to a clear, flat-bottom 96-well assay plate containing two-fold dilutions of two compounds in 8 by 8 dose-point matrices. OD_{600} was measured using a Tecan Infinite M1000 Pro plate reader prior to incubation in a 37 °C stationary incubator. After incubation for 18 h, OD_{600} was measured again and background (0 h) reads were subtracted. Heat maps were generated by converting OD_{600} to percent growth, with the scale shown here:



The MIC values of the individual drugs were determined to be the concentration of the compound that resulted in a percent residual growth of $\leq 10\%$. The FIC of each compound was determined to be its MIC in combination with the other

compound divided by its MIC alone. The reported FIC indices (FICIs) are the sum of FICs for the two compounds being tested (49). FICI values ≤ 0.5 were considered synergistic.

Lysozyme assay for OM permeability

Assay was performed as previously described (39), with modifications. *E. coli* BW25113 was grown overnight (~18 h) in LB and subcultured 1:50 in fresh LB media at 37 °C with shaking at 250 rpm to mid-log (OD_{600} ~0.4-0.5).

Subcultures were centrifuged and resuspended in 5 mM HEPES pH 7.2 to OD_{600} ~0.5. A volume of 1 mL of cells was added to microfuge tubes containing the appropriate drug at 1/4 MIC and 50 $\mu\text{g}/\text{mL}$ lysozyme (Sigma-Aldrich). Tubes were gently inverted to mix and left at room temperature for ~15 min for any cell debris to settle. A volume of 200 μL was transferred from each tube to a clear, flat bottom 96-well plate, and OD_{600} was read using a Tecan Infinite M1000 Pro plate reader. Controls were included to ensure that the drugs alone did not lyse cells and to find the baseline levels of cell lysis by lysozyme alone.

β -lactamase assay for OM integrity

Assay was performed as previously described (50). *E. coli* ML35 pBR322 cells grown overnight (~18 h) in LB with 50 $\mu\text{g}/\text{mL}$ ampicillin were subcultured 1:50 in fresh LB media and grown at 37 °C with shaking at 250 rpm to mid-log (OD_{600} ~0.4-0.5), centrifuged, washed in PBS, and resuspended to $OD_{600} = 0.02$ in PBS. A volume of 50 μL of the cell suspension was added to a clear, flat bottom 96-well plate containing 50 μL of PBS with a final concentration of 30 μM

nitrocefin (Sigma-Aldrich) and the two-fold dilution of compound. No cell controls were performed in parallel. Plates were incubated at 37 °C in a stationary incubator and read at 0 h and 2 h using a Tecan Infinite M1000 Pro plate reader at 492 nm to monitor nitrocefin hydrolysis. Reads from the corresponding no cell control well were subtracted from the 2 h timepoint.

β-galactosidase assay for IM integrity

Assay was performed as previously described (50). *E. coli* ML35 pBR322 cells grown overnight (~18 h) in LB with 50 µg/mL ampicillin were subcultured 1:50 in fresh LB media and grown at 37 °C with shaking at 250 rpm to mid-log (OD₆₀₀ ~0.4-0.5), centrifuged, washed in PBS, and resuspended to OD₆₀₀ = 0.02 in PBS. A volume of 50 µL of the cell suspension was added to a clear, flat bottom 96-well plate containing 50 µL of PBS with a final concentration of 1.5 mM of ONPG (Sigma-Aldrich) and the two-fold dilution of compound. Plates were incubated at 37 °C in a stationary incubator and read at 0 h and 2 h using a Tecan Infinite M1000 Pro plate reader at 405 nm to monitor ONPG hydrolysis. Reads from the corresponding no cell control well were subtracted from the 2 h timepoint.

DiSC₃(5) assay for IM depolarization

Assay was performed as previously described (25). *E. coli* MC1061 cells (hyperpermeable strain of *E. coli* to allow for dye uptake) grown overnight (~18 h) were subcultured 1:50 in fresh LB media and grown at 37 °C with shaking at 250 rpm to mid-log (OD₆₀₀ ~0.4-0.5). Cells were centrifuged and washed in buffer

containing 5 mM HEPES and 20 mM glucose (pH 7.2). Pellets were resuspended in buffer to $OD_{600} = 0.085$, loaded with 1 μM DiSC₃(5) (Sigma-Aldrich), and allowed to equilibrate for ~1 h. Cells were then added to a black, flat-bottom 96-well assay plate containing two-fold dilutions of compound and fluorescence was read using a Tecan Infinite M1000 Pro plate reader using 620 ± 5 nm excitation and 685 ± 5 nm emission wavelengths.

BODIPY-cadaverine LPS displacement assay

Assay was performed as previously described (25, 44). A solution of BODIPY-cadaverine (Sigma-Aldrich) and LPS from *E. coli* EH100 (Sigma-Aldrich), with final assay concentrations of 2.25 μM and 5.25 $\mu\text{g/mL}$, respectively, in Tris-HCl buffer (50 mM, pH 7.4) was prepared. A volume of 0.5 μL of compound and 49.5 μL of Tris-HCl buffer with BODIPY-cadaverine and LPS were added to a Corning non-binding surface black 384-well polystyrene plate. Fluorescence intensity was measured immediately using a Tecan Infinite M1000 Pro plate reader with an excitation wavelength of 580 ± 5 nm and emission wavelength of 620 ± 5 nm.

Atomic force microscopy (AFM)

Subinhibitory concentrations of MAC-0568743 and liproxstatin-1 were used in AFM scans of surface topology, using the method described previously (29). For long-exposure treatments, *E. coli* BW25113 cultures were prepared as described previously for checkerboard assays in the presence of the compounds. For short-exposure treatments, an overnight culture of *E. coli* BW25113 was

treated with the indicated concentration of compound. A 50 μL volume of culture was transferred to hydrophilic polycarbonate 0.2 μm Millipore Isopore GTTP filters (Merck Millipore) on top of Kimwipes (Kimberly-Clark Professional) to absorb excess liquid from the filter. Salts were flushed from the LB medium in the culture using 50 μL of 25 mM HEPES (pH 7.0), which was absorbed by the Kimwipes. Upon removal of the liquid from the filter, the filter was attached to a glass slide using non-conductive double-sided tape. A Bruker BioScope Catalyst AFM with a NanoScope V controller was used to analyze the samples. For each drug concentration, a 0.65 μm thick Si_3N_4 triangular cantilever was used (Scan Asyst AIR, Bruker), with scan rates of ~ 1 Hz and 256 data points per scan line resolution, in PeakForce quantitative nanomechanical mapping mode. Images were processed and analysed using Nanoscope software (Bruker). Z-Height was used to process images downstream, flattening images to account for subtle cell curvature, with topography calculated from cross sections of these image scans.

Live cell fluorescence microscopy

E. coli BW25113 cells were grown in the presence of subinhibitory concentrations of lipoxstatin-1 and MAC-0568743 as described for checkerboard assays. Cultures were transferred to a black 384-well 0.17 mm glass bottom microwell plate (Brooks Life Sciences). Cells were stained with 20 $\mu\text{g}/\text{mL}$ of FM4-64FX (Invitrogen) and incubated at room temperature for 30 minutes. Fluorescence images were acquired using a Nikon Eclipse Ti inverted microscope, a 100x Plan Fluor Apo λ oil immersion objective, and a FM4-64 filter

(excitation/emission 515nm/740nm). Micrographs were captured using the NIS-Elements AR (v. 4.50 Nikon) software with identical imaging conditions applied for all samples. At least three biological replicates were performed for each condition and representative images were chosen. Images were cropped while maintaining the original aspect ratios.

Chemical synthesis of analogues

MAC-0568743 and its analogues were purchased from ChemBridge (D-series) or synthesized by WuXi AppTec (B-series) according to standard literature procedures. Liproxstatin-1 was purchased from Sigma-Aldrich. Liproxstatin-1 analogues (MAC-0549481 and M-series) were synthesized using the procedures described in the Supporting Information.

Funding

Work in the lab of E.D.B. was supported by a Tier I Canada Research Chair award, a Foundation grant from the Canadian Institutes of Health Research (CIHR; FRN 143215), a grant from the Ontario Research Fund (RE09-047), and grants from GlycoNet (AM-32, ID-02). This research was enabled by an endowed gift to McMaster University from the Boris Family. This work was also supported by a partnership with the Combating Antibiotic-Resistant Bacterial Biopharmaceutical Accelerator program (CARB-X; 5 IDSEP160030-03-00) from the Biomedical Advance Research and Development Authority (BARDA) awarded to Boston University, where Collaborative Hub for Early Antibiotic

Discovery (CHEAD) at the Broad Institute was a sub-awardee. K.K. was supported by a scholarship from the CIHR Canada Graduate Scholarships (CGS-D). J.-P.C. was supported by a Cystic Fibrosis Canada fellowship (500039). A.B.Y.G. was supported by a scholarship from the CIHR Canada Graduate Scholarships (CGS-M) and an Ontario Graduate Scholarship.

The authors declare no competing financial interest.

Acknowledgements

We thank the McMaster Centre for Microbial Chemical Biology (CMCB) for assisting with high-throughput chemical screening. We also thank Spero Therapeutics for providing SPR741, O. El-Halfawy for providing the *E. coli* ML35 pBR322 strain, C. MacNair for providing the *E. coli* BW25113 pGDP2::*mcr-1* strain, M. Mulvey for providing the environmental *mcr-1* positive isolates, and G. Wright for providing the *E. coli*, *K. pneumoniae*, *A. baumannii*, and *P. aeruginosa* clinical isolates. We would also like to thank M. Farha and C. Whitfield for helpful discussions surrounding the project and M. Vaara for feedback on the manuscript.

References

1. **Silhavy TJ, Kahne D, Walker S.** 2010. The bacterial cell envelope. Cold Spring Harb Perspect Biol **2**:a000414.
2. **Raetz CRH, Whitfield C.** 2002. Lipopolysaccharide endotoxins. Annu Rev Biochem **71**:635–700.
3. **Nikaido H.** 2003. Molecular basis of bacterial outer membrane permeability revisited. Microbiol Mol Biol Rev **67**:593–656.

4. **Clifton LA, Skoda MW, Le Brun AP, Ciesielski F, Kuzmenko I, Holt SA, Lakey JH.** 2015. Effect of divalent cation removal on the structure of Gram-negative bacterial outer membrane models. *Langmuir* **31**:404–412.
5. **Decad GM, Nikaido H.** 1976. Outer membrane of Gram-negative bacteria. XII. Molecular-sieving function of cell wall. *J Bacteriol* **128**:325–336.
6. **Nikaido H.** 1976. Outer membrane of *Salmonella typhimurium* transmembrane diffusion of some hydrophobic substances. *Biochim Biophys Acta - Biomembr* **433**:118–132.
7. **O’Shea R, Moser HE.** 2008. Physicochemical properties of antibacterial compounds: Implications for drug discovery. *J Med Chem* **51**:2871–2878.
8. **Tommasi R, Brown DG, Walkup GK, Manchester JI, Miller AA.** 2015. ESKAPEing the labyrinth of antibacterial discovery. *Nat Rev Drug Discov* **14**:529–542.
9. **Vaara M.** 1993. Outer membrane permeability barrier to azithromycin, clarithromycin, and roxithromycin in Gram-negative enteric bacteria. *Antimicrob Agents Chemother* **37**:354–356.
10. **Ofek I, Cohen S, Rahmani R, Kabha K, Tamarkin D, Herzig Y, Rubinstein E.** 1994. Antibacterial synergism of polymyxin B nonapeptide and hydrophobic antibiotics in experimental Gram-negative infections in mice. *Antimicrob Agents Chemother* **38**:374–377.
11. **Kohanski MA, Dwyer DJ, Collins JJ.** 2010. How antibiotics kill bacteria: From targets to networks. *Nat Rev Microbiol* **8**:423–435.
12. **Baba T, Ara T, Hasegawa M, Takai Y, Okumura Y, Baba M, Datsenko KA, Tomita M, Wanner BL, Mori H.** 2006. Construction of *Escherichia coli* K-12 in-frame, single-gene knockout mutants: the Keio collection. *Mol Syst Biol* **2**:2006.0008.
13. **Klobucar K, French S, Côté JP, Howes JR, Brown ED.** 2020. Genetic and chemical-genetic interactions map biogenesis and permeability determinants of the outer membrane of *Escherichia coli*. *MBio* **11**:e00161-20.
14. **Specht KM, Shokat KM.** 2002. The emerging power of chemical genetics. *Curr Opin Cell Biol* **14**:155–159.
15. **Barker CA, Farha MA, Brown ED.** 2010. Chemical genomic approaches to study model microbes. *Chem Biol* **17**:624–632.
16. **Wu M, Maier E, Benz R, Hancock REW.** 1999. Mechanism of interaction of different classes of cationic antimicrobial peptides with planar bilayers and with the cytoplasmic membrane of *Escherichia coli*. *Biochemistry* **38**:7235–7242.
17. **Farha MA, Brown ED.** 2010. Chemical probes of *Escherichia coli* uncovered through chemical-chemical interaction profiling with compounds of known biological activity. *Chem Biol* **17**:852–862.
18. **Krishnamoorthy G, Wolloscheck D, Weeks JW, Croft C, Rybenkov V V., Zgurskaya HI.** 2016. Breaking the permeability barrier of *Escherichia coli* by controlled hyperporination of the outer membrane. *Antimicrob*

- Agents Chemother **60**:7372–7381.
19. **Vaara M.** 1992. Agents that increase the permeability of the outer membrane. *Microbiol Rev* **56**:395–411.
 20. **Repaske R.** 1958. Lysis of Gram-negative organisms and the role of versene. *Biochim Biophys Acta* **30**:225–232.
 21. **Hancock REW.** 1997. Peptide antibiotics. *Lancet* **349**:418–422.
 22. **Schindler M, Osborn MJ.** 1979. Interaction of divalent cations and polymyxin B with lipopolysaccharide. *Biochemistry* **18**:4425–4430.
 23. **Vaara M, Viljanen P.** 1985. Binding of polymyxin B nonapeptide to Gram-negative bacteria. *Antimicrob Agents Chemother* **27**:548–554.
 24. **Corbett D, Wise A, Langley T, Skinner K, Trimby E, Birchall S, Dorali A, Sandiford S, Williams J, Warn P, Vaara M, Lister T.** 2017. Potentiation of antibiotic activity by a novel cationic peptide: Potency and spectrum of activity of SPR741. *Antimicrob Agents Chemother* **61**:e00200-17.
 25. **French S, Farha MA, Ellis MJ, Sameer Z, Côté; J-P, Cotroneo N, Lister T, Rubio A, Brown ED.** 2020. Polymyxin B analog SPR741 potentiates antibiotics against Gram-negative bacteria and uniquely perturbs the outer membrane. *ACS Infect Dis* **6**:1405–1412.
 26. **Stokes JM, Davis JH, Mangat CS, Williamson JR, Brown ED.** 2014. Discovery of a small molecule that inhibits bacterial ribosome biogenesis. *Elife* **3**:e03574.
 27. **Nikaido H.** 2005. Restoring permeability barrier function to outer membrane. *Chem Biol* **12**:507–509.
 28. **Stokes JM, French S, Ovchinnikova OG, Bouwman C, Whitfield C, Brown ED.** 2016. Cold stress makes *Escherichia coli* susceptible to glycopeptide antibiotics by altering outer membrane integrity. *Cell Chem Biol* **23**:267–277.
 29. **Stokes JM, MacNair CR, Ilyas B, French S, Côté J-P, Bouwman C, Farha MA, Sieron AO, Whitfield C, Coombes BK, Brown ED.** 2017. Pentamidine sensitizes Gram-negative pathogens to antibiotics and overcomes acquired colistin resistance. *Nat Microbiol* **2**:17028.
 30. **Campbell J.** 2010. High-throughput assessment of bacterial optical density measurements. *Curr Protoc Chem Biol* **2**:195–208.
 31. **Hancock REW.** 1984. Alterations in outer membrane permeability. *Ann Rev Microbiol* **38**:237–264.
 32. **Pereira JA, Pessoa AM, Cordeiro MNDS, Fernandes R, Prudêncio C, Noronha JP, Vieira M.** 2015. Quinoxaline, its derivatives and applications: A State of the Art review. *Eur J Med Chem* **97**:664–672.
 33. **Friedmann Angeli JP, Schneider M, Proneth B, Tyurina YY, Tyurin VA, Hammond VJ, Herbach N, Aichler M, Walch A, Eggenhofer E, Basavarajappa D, Rådmark O, Kobayashi S, Seibt T, Beck H, Neff F, Esposito I, Wanke R, Förster H, Yefremova O, Heinrichmeyer M, Bornkamm GW, Geissler EK, Thomas SB, Stockwell BR, Odonnell VB,**

- Kagan VE, Schick JA, Conrad M.** 2014. Inactivation of the ferroptosis regulator Gpx4 triggers acute renal failure in mice. *Nat Cell Biol* **16**:1180–1191.
34. **Li J, Cao F, Yin H, Huang Z, Lin Z, Mao N, Sun B, Wang G.** 2020. Ferroptosis: past, present and future. *Cell Death Dis* **11**:88.
35. **Zilka O, Shah R, Li B, Friedmann Angeli JP, Griesser M, Conrad M, Pratt DA.** 2017. On the mechanism of cytoprotection by ferrostatin-1 and liproxstatin-1 and the role of lipid peroxidation in ferroptotic cell death. *ACS Cent Sci* **3**:232–243.
36. **Viljanen P, Vaara M.** 1984. Susceptibility of Gram-negative bacteria to polymyxin B nonapeptide. *Antimicrob Agents Chemother* **25**:701–705.
37. **Vaara M.** 2019. Polymyxin derivatives that sensitize Gram-negative bacteria to other antibiotics. *Molecules* **24**.
38. **Sanderson KE, MacAlister T, Costerton JW, Cheng KJ.** 1974. Permeability of lipopolysaccharide deficient (rough) mutants of *Salmonella typhimurium* to antibodies, lysozyme, and other agents. *Can J Microbiol* **20**:1135–1145.
39. **Hancock REW, Wong PGW.** 1984. Compounds which increase the permeability of the *Pseudomonas aeruginosa* outer membrane. *Antimicrob Agents Chemother* **26**:48–52.
40. **Urfer M, Bogdanovic J, Monte F Lo, Moehle K, Zerbe K, Omasits U, Ahrens CH, Pessi G, Eberl L, Robinson JA.** 2016. A peptidomimetic antibiotic targets outer membrane proteins and disrupts selectively the outer membrane in *Escherichia coli*. *J Biol Chem* **291**:1921–1932.
41. **Gronow S, Brabetz W, Brade H.** 2000. Comparative functional characterization In vitro of heptosyltransferase I (WaaC) and II (WaaF) from *Escherichia coli*. *Eur J Biochem* **267**:6602–6611.
42. **MacNair CR, Brown ED.** 2020. Outer membrane disruption overcomes intrinsic, acquired, and spontaneous antibiotic resistance. *MBio* **11**:e01615-20.
43. **Tyrrell JM, Aboklaish AF, Walsh TR, Vaara T, Vaara M.** 2019. The polymyxin derivative NAB739 is synergistic with several antibiotics against polymyxin-resistant strains of *Escherichia coli*, *Klebsiella pneumoniae* and *Acinetobacter baumannii*. *Peptides* **112**:149–153.
44. **Wood SJ, Miller KA, David SA.** 2004. Anti-endotoxin agents. 1. Development of a fluorescent probe displacement method optimized for high-throughput identification of lipopolysaccharide-binding agents. *Comb Chem High Throughput Screen* **7**:239–249.
45. **Vaara M, Siikanen O, Apajalahti J, Fox J, Frimodt-Møller N, He H, Poudyal A, Li J, Nation RL, Vaara T.** 2010. A novel polymyxin derivative that lacks the fatty acid tail and carries only three positive charges has strong synergism with agents excluded by the intact outer membrane. *Antimicrob Agents Chemother* **54**:3341–3346.
46. **Zabawa TP, Pucci MJ, Parr TR, Lister T.** 2016. Treatment of Gram-

- negative bacterial infections by potentiation of antibiotics. *Curr Opin Microbiol* **33**:7–12.
47. **Shaabani A, Maleki A, Moghimi-Rad J.** 2007. A novel isocyanide-based three-component reaction: Synthesis of highly substituted 1,6-dihydropyrazine-2,3-dicarbonitrile derivatives. *J Org Chem* **72**:6309–6311.
 48. **Sander T, Freyss J, Von Korff M, Rufener C.** 2015. DataWarrior: An open-source program for chemistry aware data visualization and analysis. *J Chem Inf Model* **55**:460–473.
 49. **Lambert RJW, Lambert R.** 2003. A model for the efficacy of combined inhibitors. *J Appl Microbiol* **95**:734–743.
 50. **Farha MA, El-Halfawy OM, Gale RT, Macnair CR, Carfrae LA, Zhang X, Jentsch NG, Magolan J, Brown ED.** 2020. Uncovering the Hidden Antibiotic Potential of Cannabis. *ACS Infect Dis* **6**:338–346.

Figures

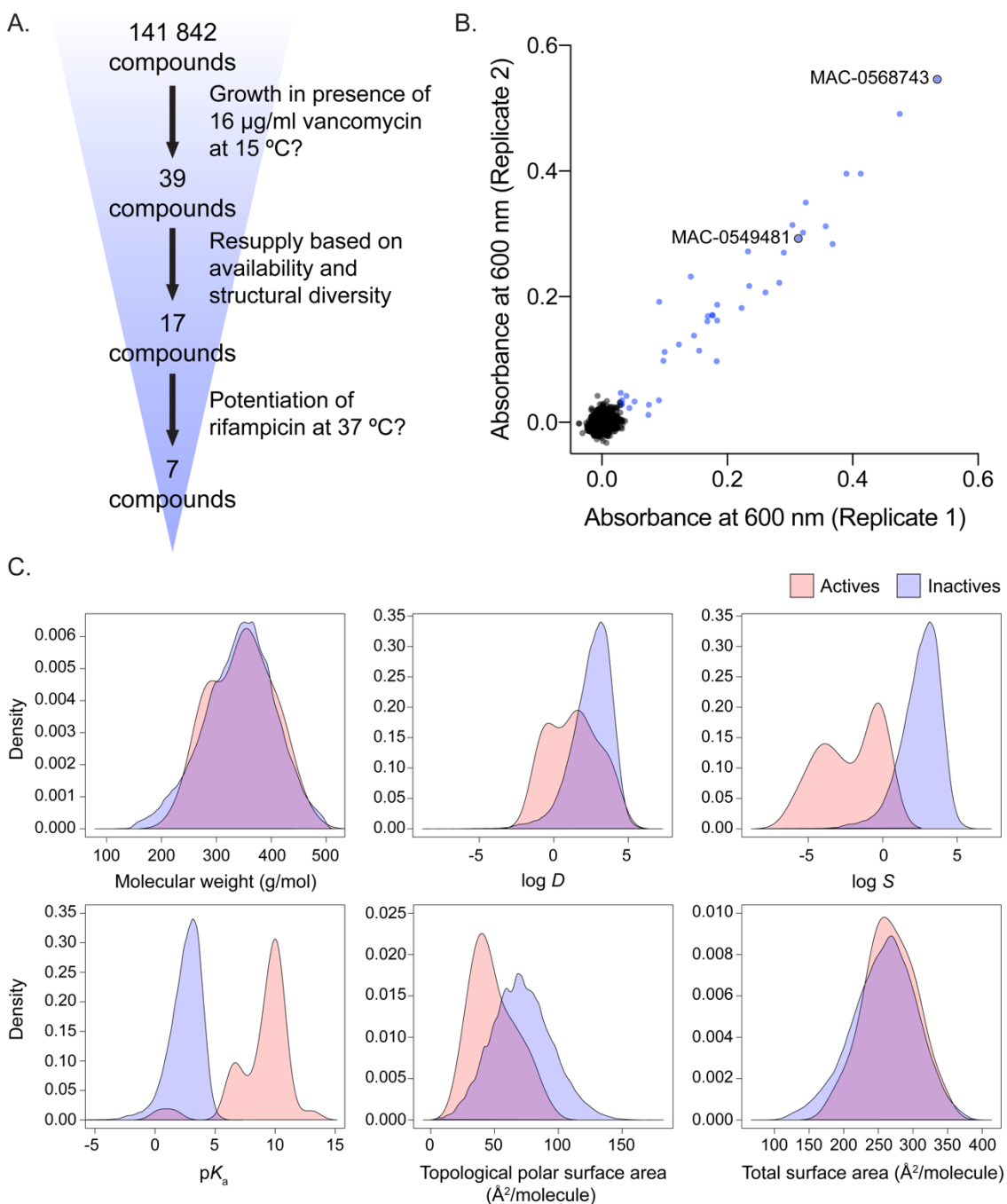


Figure 1: High-throughput chemical screen for molecules that antagonize the activity of vancomycin at cold temperatures. (A.) Shown is the workflow for the screening platform in which ~140,000 compounds were screened for antagonism of vancomycin activity at 15 °C. Reordered compounds were

subsequently tested for rifampicin potentiation at 37 °C. (B.) A replicate plot is shown for the primary screening data, performed in duplicate. Growth was measured as absorbance at 600 nm with the background (0 h) reads subtracted from the endpoint absorbance readings. Blue points represent active compounds that promoted growth in the presence of vancomycin at 15 °C. (C.) Density plots compare the distribution of selected physicochemical properties of active (n=39) and inactive (n=141,803) compounds from the primary screen. Table S1 has details for all calculated physicochemical properties.

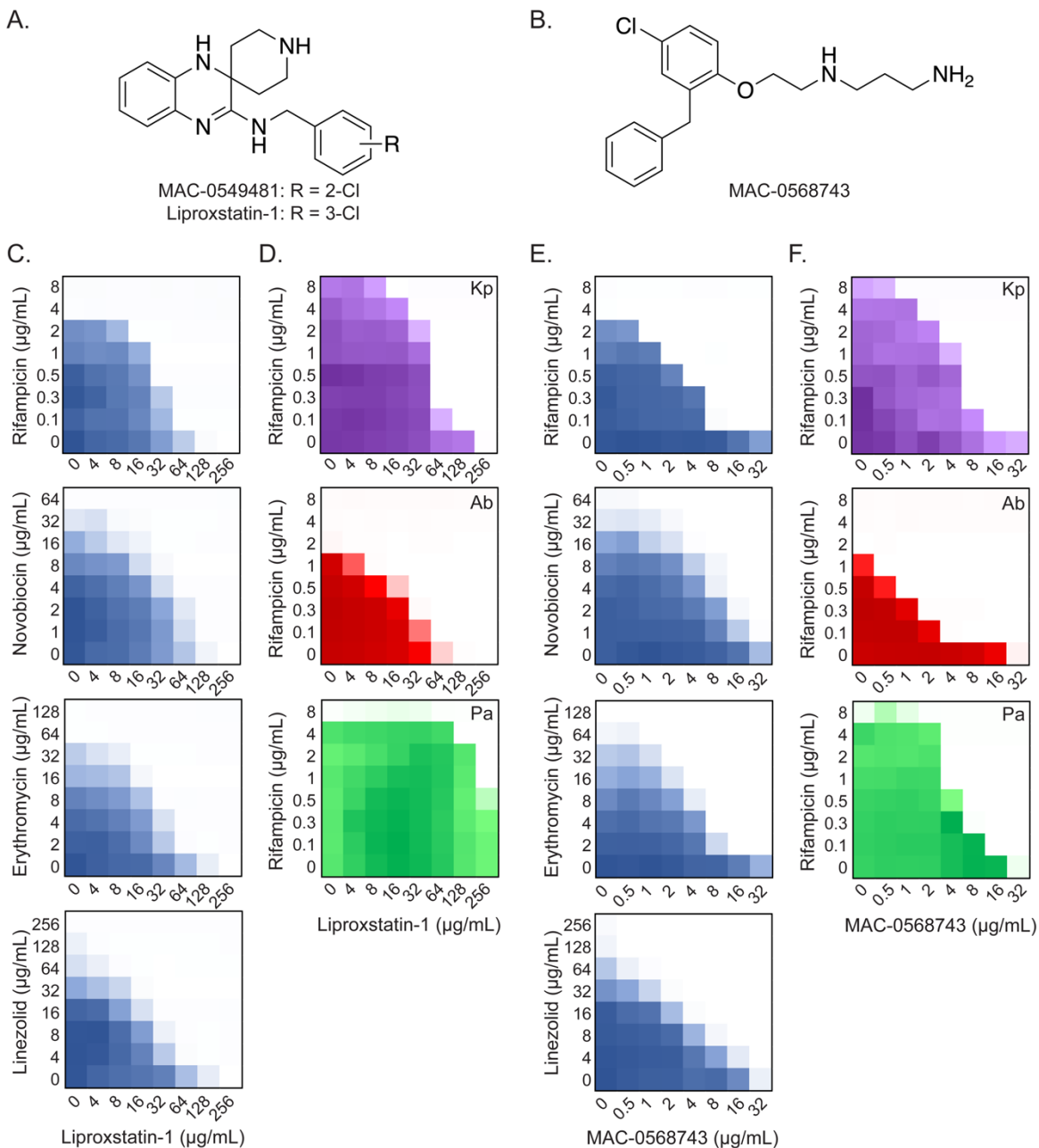


Figure 2: Liproxstatin-1 and MAC-0568743 potentiate Gram-positive-targeting antibiotics in Gram-negative bacteria. Structures shown are: (A.) MAC-0549481, an active from the vancomycin cold antagonism screen, and its close structural analogue liproxstatin-1, and (B.) MAC-0568743. (C.) Checkerboard broth microdilution assays for *E. coli* with liproxstatin-1 and the Gram-positive-targeting antibiotics, rifampicin, novobiocin, erythromycin, and linezolid at 37 °C are shown. (D.) Checkerboard broth microdilution assays for liproxstatin-1 and rifampicin with clinical isolates of *K. pneumoniae* C026 (Kp; purple), *A. baumannii* C015 (Ab; red), and *P. aeruginosa* C028 (Pa; green) at 37

°C are shown. (E.) Checkerboard broth microdilution assays in *E. coli* with MAC-0568743 and rifampicin, novobiocin, erythromycin, and linezolid at 37 °C are shown. (F.) Checkerboard broth microdilution assays between MAC-0568743 and rifampicin in clinical isolates of *K. pneumoniae* C026 (Kp; purple), *A. baumannii* C015 (Ab; red), and *P. aeruginosa* C028 (Pa; green) at 37 °C are shown. Dark regions depicted in the checkerboard assays represent regions of higher cell growth. Checkerboard data are representative of at least two biological replicates.

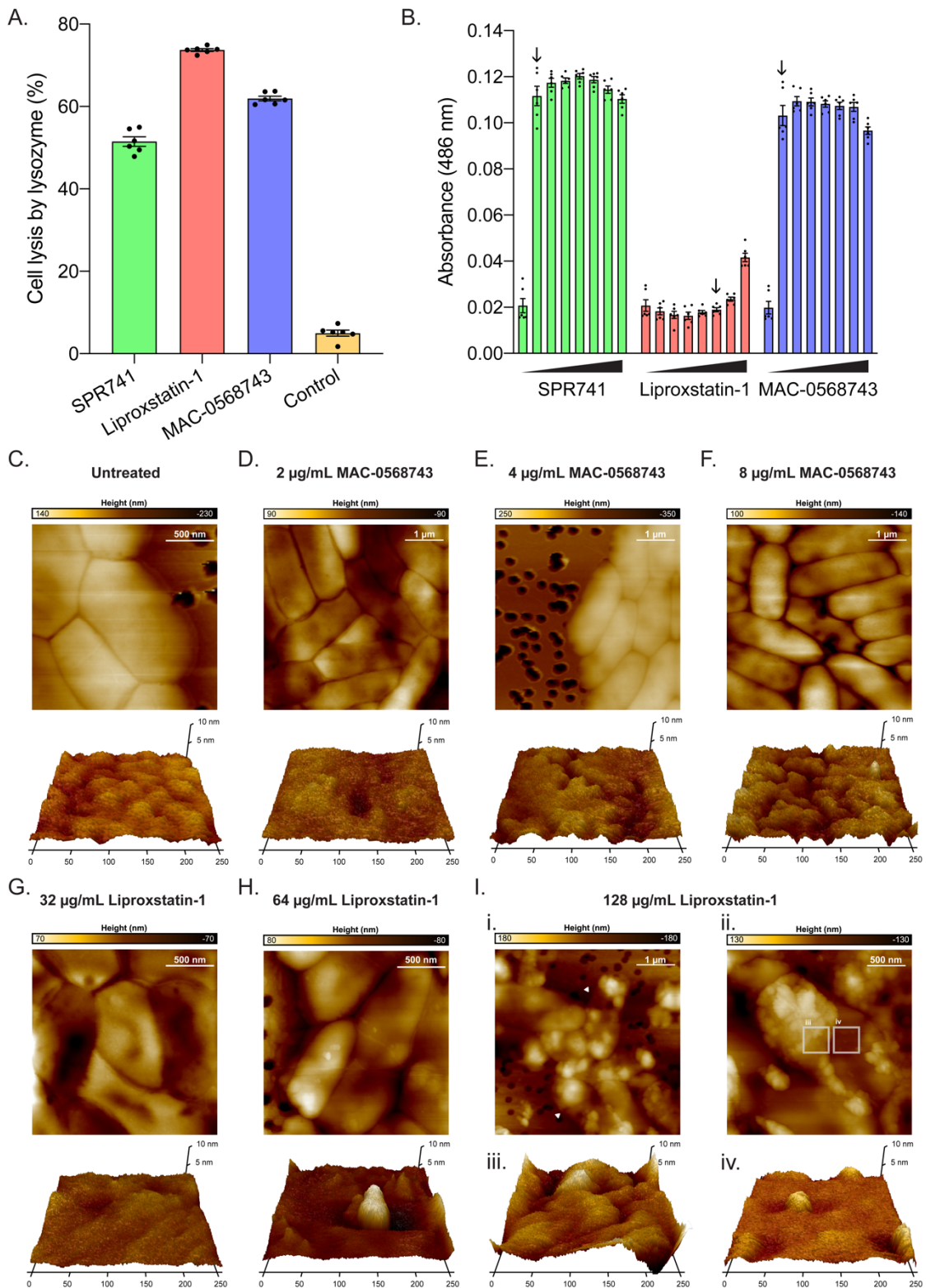


Figure 3: Potentiation of large-scaffold antibiotics by liproxstatin-1 and MAC-0568743 was due to OM disruption. (A.) Disruption of *E. coli* OM was measured by lysozyme permeability using subinhibitory concentrations of SPR741 (2 µg/mL), liproxstatin-1 (32 µg/mL), and MAC-0568743 (16 µg/mL). The control was the percent cell lysis by lysozyme without the addition of potentiator compound. The experiment was performed in biological triplicate. (B.) Disruption of the OM was measured by β-lactamase assay for OM permeability in *E. coli*, where increased absorbance at 486 nm indicated nitrocefin hydrolysis by periplasmic β-lactamase, resulting in the production of a coloured product. Concentrations of each compound shown are two-fold dilutions from 0 (left) to 128 (right) µg/mL. An arrow has been included to indicate the potentiation concentration (MIC of the compound in the presence of 1 µg/mL rifampicin). Experiments were performed in biological triplicate. (C.-I.) Shown are atomic force microscopy images of *E. coli* cell surfaces grown in the presence of increasing concentrations of liproxstatin-1 and of MAC-0568743. (C.) Shown are untreated *E. coli* whole cells (top) and high-resolution 3D surface topology scan (bottom). (D.-F.) Shown are *E. coli* cells treated with (D.) 2 µg/mL, (E.) 4 µg/mL, and (F.) 8 µg/mL MAC-0568743. Scans depict whole cells (top) and high-resolution 3D surface topology of a representative region of the cell (bottom) for each concentration. (G.-I.) Shown are *E. coli* cells treated with (G.) 32 µg/mL, (H.) 64 µg/mL, and (F.) 128 µg/mL liproxstatin-1. Scans depict whole cells (top) and high-resolution 3D surface topology of a representative region of the cell (bottom) for each concentration. (I.) Whole cell scans (i., ii.) show blebbing on the cell surface; (ii.) is zoomed into a region of (i.). Arrows in (i.) indicate membranes of cells that have lysed which still show blebs on their surface. High-resolution 3D surface topology of a region containing (iii.) a bleb and (iv.) one without visible blebbing is shown to emphasize the differences in surface architecture between the two regions.

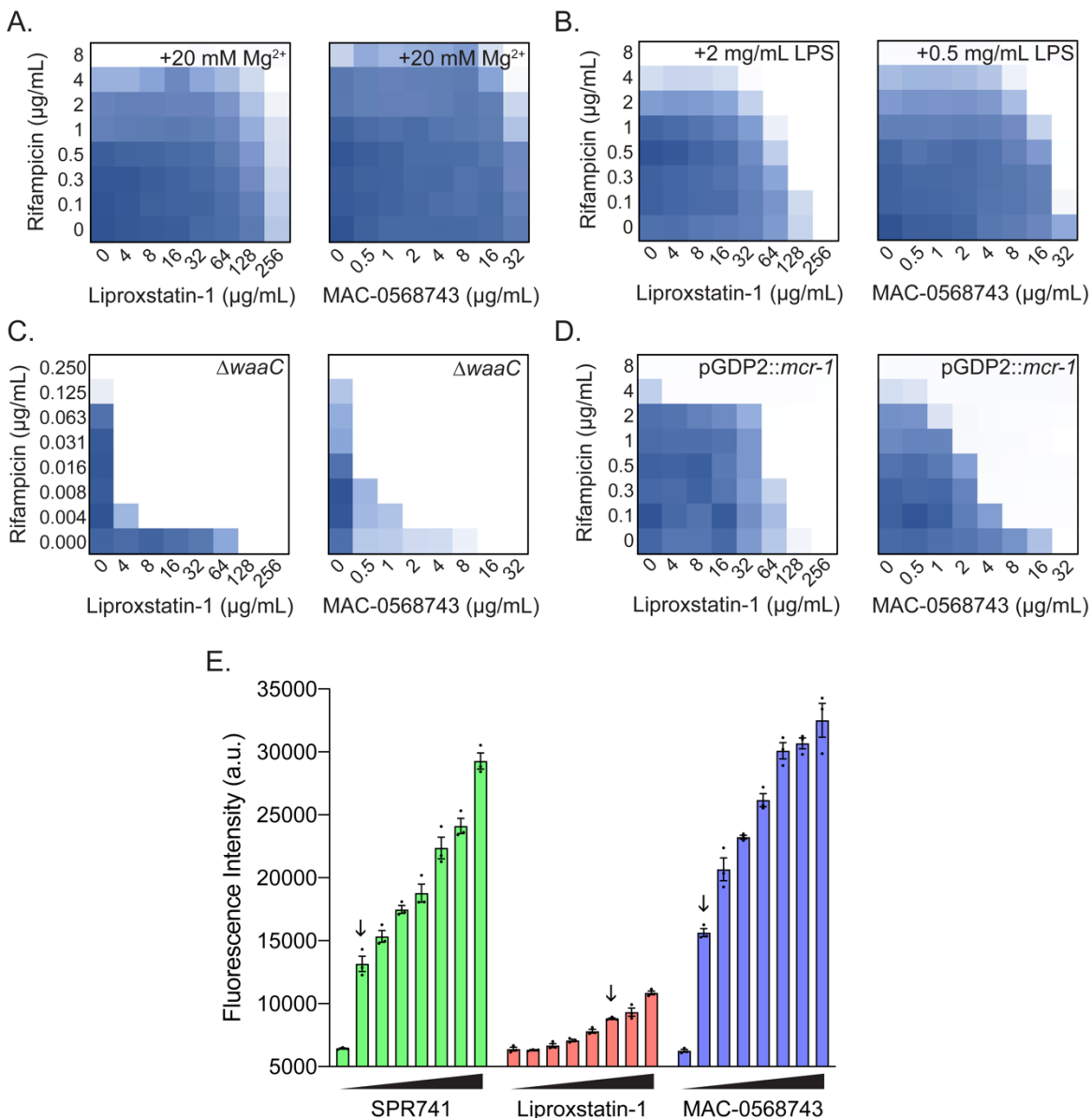


Figure 4: Liproxstatin-1 and MAC-0568743 disrupt the bacterial OM by physically interacting with LPS. (A.-D.) Checkerboard broth microdilution assays are presented for *E. coli* with liproxstatin-1 (left) or MAC-0568743 (right) and rifampicin, with the following: (A.) 20 mM MgCl₂ in wildtype *E. coli*, (B.) 2 mg/mL LPS for liproxstatin-1 and 0.5 mg/mL LPS for MAC-0568743, (C.) *E. coli* ΔwaaC, a strain of *E. coli* with LPS truncated at lipid A-Kdo₂, and (D.) *E. coli* BW25113 expressing the *mcr-1* gene from the pGDP2 plasmid. Dark regions on the checkerboard represent regions of higher cell growth. Data are representative of at least two biological replicates. (E.) Shown is a BODIPY-cadaverine LPS binding assay. Dose-dependent increases in fluorescence by SPR741, liproxstatin-1, and MAC-0568743 indicate that the compounds displaced

BODIPY-cadaverine probe from the phosphates of *E. coli* LPS, with liproxstatin-1 exhibiting the lowest affinity for LPS. Experiments were performed in triplicate. An arrow has been included to indicate the MIC of the compound in the presence of 1 µg/mL rifampicin (the potentiation concentration).

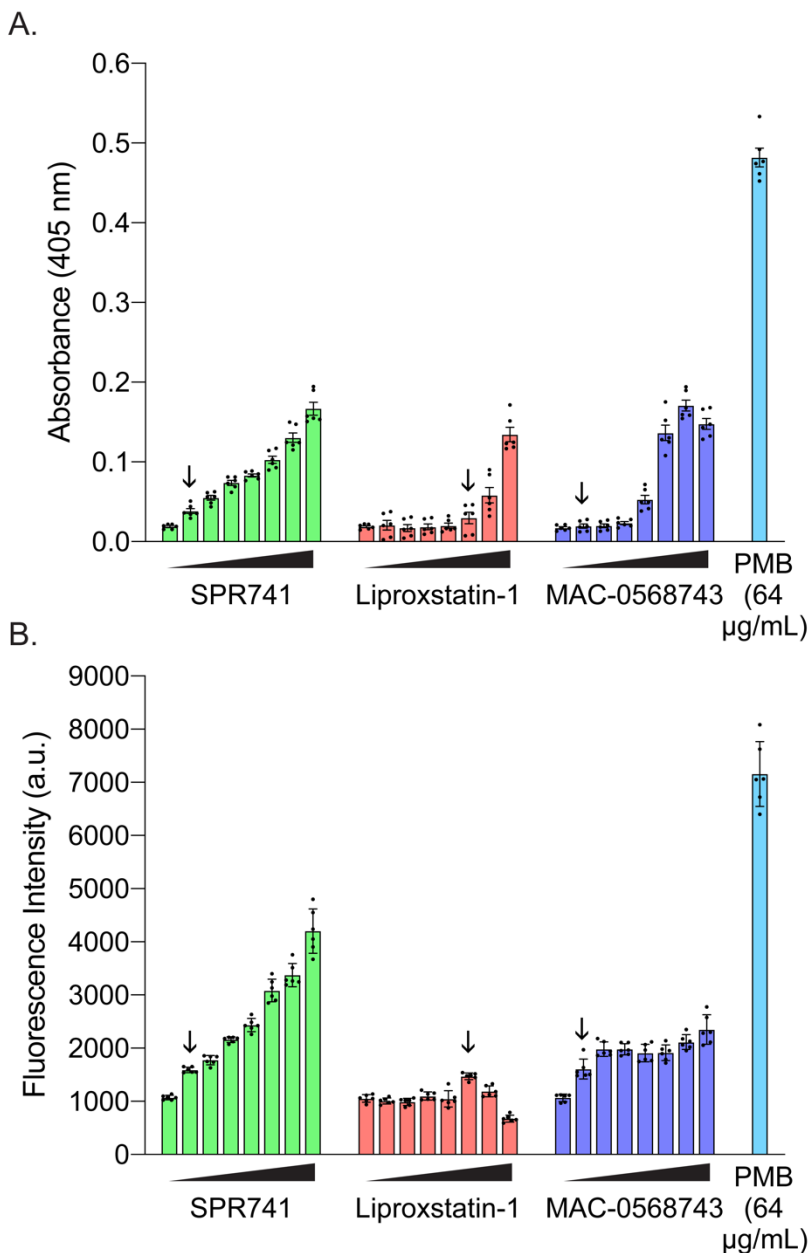
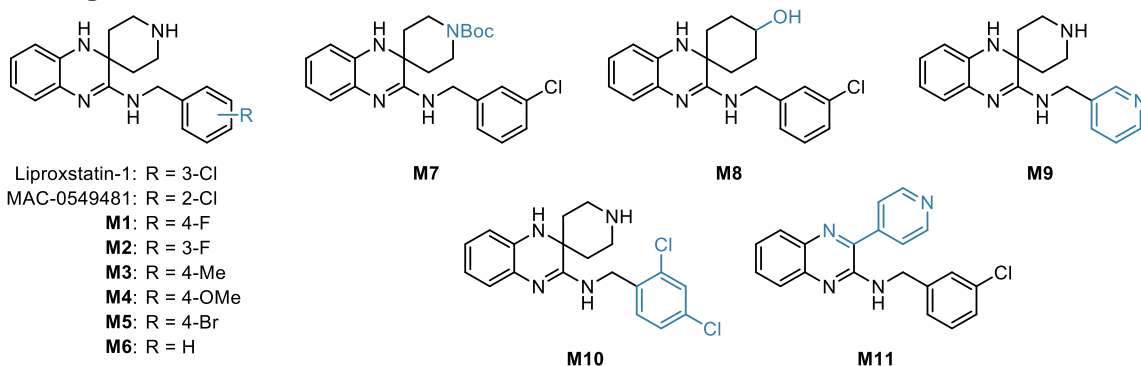


Figure 5: Liproxstatin-1 and MAC-0568743 exhibit minimal IM disruption. (A.) A β -galactosidase assay for IM permeability in *E. coli* measured increased absorbance at 405 nm to indicate ONPG hydrolysis by cytoplasmic β -galactosidase, resulting in the production of a coloured product. SPR741 is known to have minimal activity on the IM and is less IM active than the high control polymyxin B (PMB; 64 μ g/mL). Concentrations of each compound shown are two-fold dilutions from 0 (left) to 128 (right) μ g/mL. An arrow has been included to indicate the potentiation concentration (the MIC of the compound in the presence of 1 μ g/mL rifampicin). Experiments were performed in triplicate.

(B.) A DiSC₃(5) assay for IM depolarization in *E. coli* is shown. Increased fluorescence intensity indicated release of the DiSC₃(5) fluorescent dye from the IM. Concentrations of each compound shown are two-fold dilutions from 0 (left) to 128 (right) µg/mL. An arrow has been included to indicate the potentiation concentration, or the MIC of the compound in the presence of 1 µg/mL rifampicin. Experiments were performed in triplicate. A no cell control was performed to ensure the compounds themselves did not quench DiSC₃(5) fluorescence; any decreases in fluorescence in the absence of cells were less than 3 standard deviations from the mean of the DMSO controls.

Tables

Table 1: Potentiation and inner membrane activity of liproxstatin-1 analogues in *E. coli* BW25113.

Compound	MIC ($\mu\text{g/mL}$)	FICI ^a	Linezolid Potentiation Concentration ^b ($\mu\text{g/mL}$)	Minimum Concentration to Observe IM Activity ^c ($\mu\text{g/mL}$)
Liproxstatin-1	256	0.19	32	128
MAC-0549481	256	0.38	64	64
M1	>256	≤ 0.38	128	>128
M2	>256	≤ 0.38	128	>128
M3	>256	≤ 0.25	64	>128
M4	>256	≤ 0.38	128	>128
M5	128	0.38	32	64
M6	128	≤ 0.5	128	N/A
M7	>256	≤ 1.01	N/A	N/A
M8	>256	≤ 1.01	N/A	N/A
M9	>256	≤ 0.75	N/A	N/A
M10	64	0.31	16	16
M11	>256	≥ 2	N/A	N/A

^a FICI data reported are for liproxstatin-1 analogues in combination with linezolid.

^b Concentration needed to potentiate 16 $\mu\text{g/mL}$ of linezolid for liproxstatin-1 analogues found to be synergistic with linezolid (FICI ≤ 0.5)

^c Concentration needed to elicit 20% of the absorbance at 405 nm of the high control (64 $\mu\text{g/mL}$ polymyxin B) in the β -galactosidase assay for IM integrity

Supplementary Material

Figures

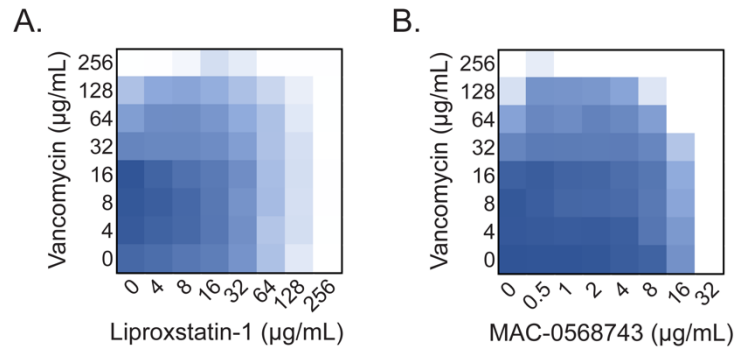


Figure S1: Liproxstatin-1 and MAC-0568743 do not potentiate the large, hydrophilic antibiotic, vancomycin. Checkerboard broth microdilution assays in *E. coli* between (A.) liproxstatin-1 or (B.) MAC-0568743 and vancomycin at 37 °C are shown. Dark regions depicted in the checkerboard assays represent regions of higher cell growth. Checkerboard data are representative of at least two biological replicates.

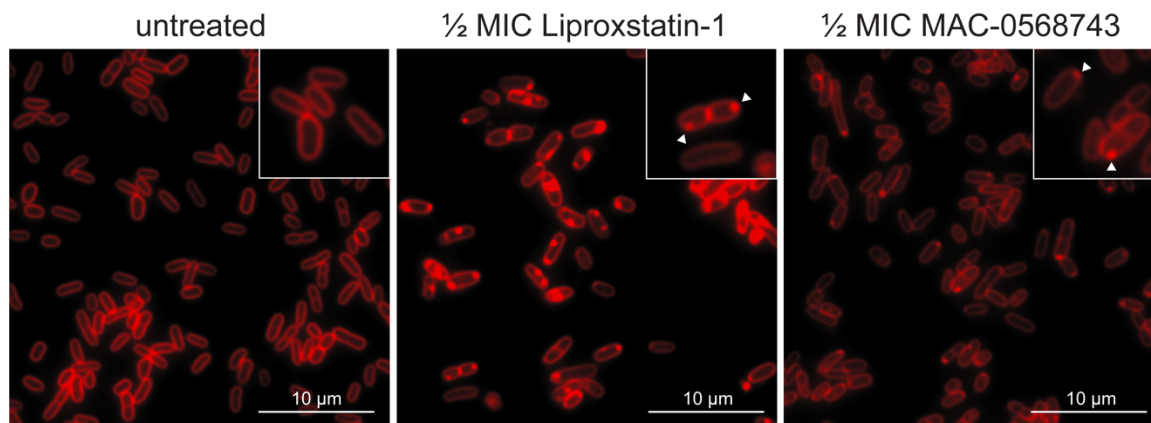


Figure S2: Treatment with subinhibitory liproxstatin-1 and MAC-0568743 results in regions of accumulation of membrane stain FM4-64 in *E. coli*. Cells were grown in the presence of compound for 18 h at 37 °C prior to membrane staining. Arrows in insets mark lipophilic regions of FM4-64 concentrated in the membrane.

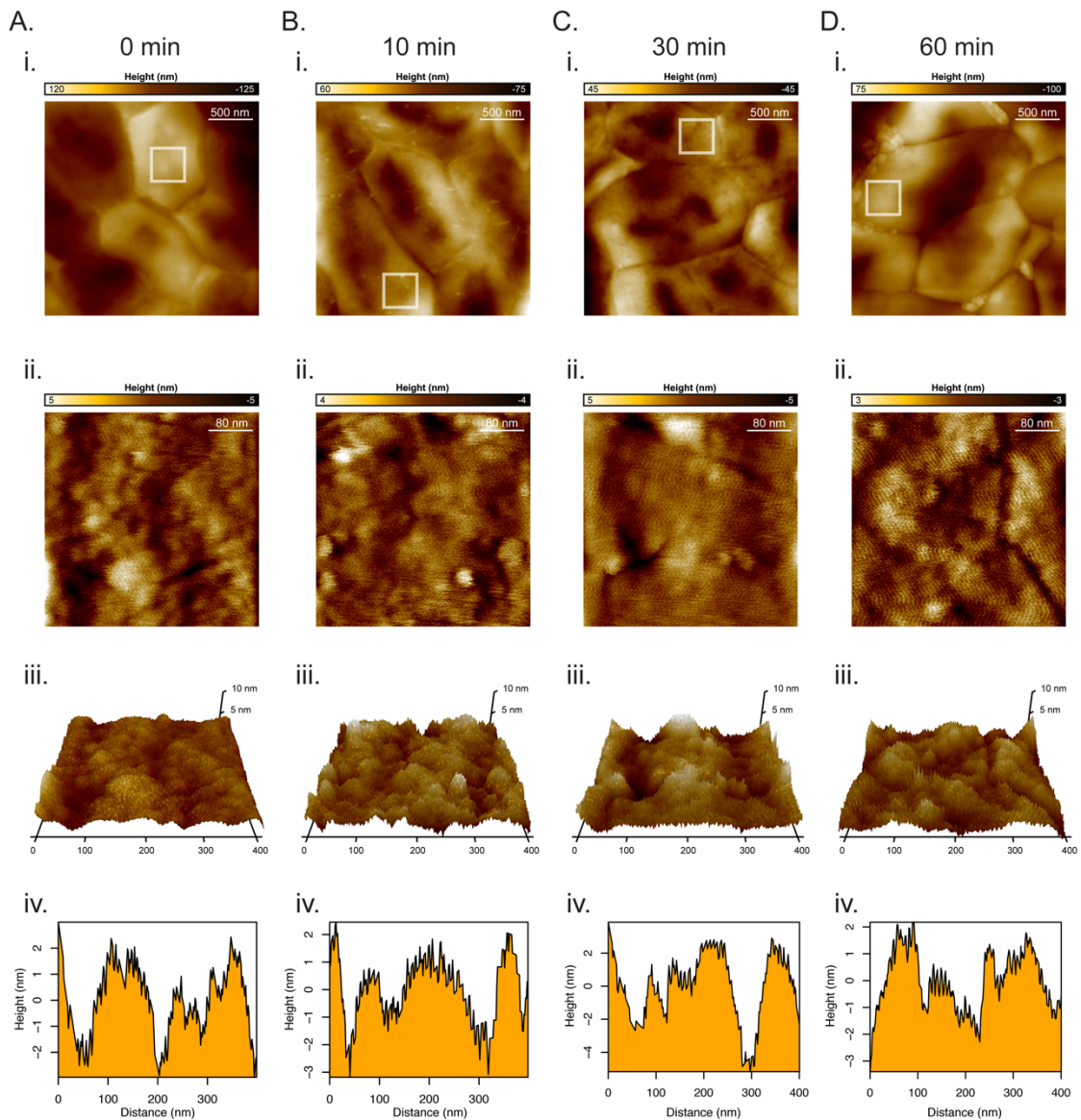


Figure S3: MAC-0568743 is able to physically perturb the OM of stationary phase cells. Atomic force microscopy of stationary phase *E. coli* cells exposed to 8 µg/mL MAC-0568743 for (A.) 0 minutes, (B.) 10 minutes, (C.) 30 minutes, and (D.) 60 minutes. Scans shown for each timepoint depict (i.) whole cells with white squares indicating the region shown at higher resolution in 2D in panel (ii.), (iii.) high-resolution 3D topology scans of a portion of the cell surface shown in (ii.), and (iv.) a plot showing the height along a cross-section of the cell surface.

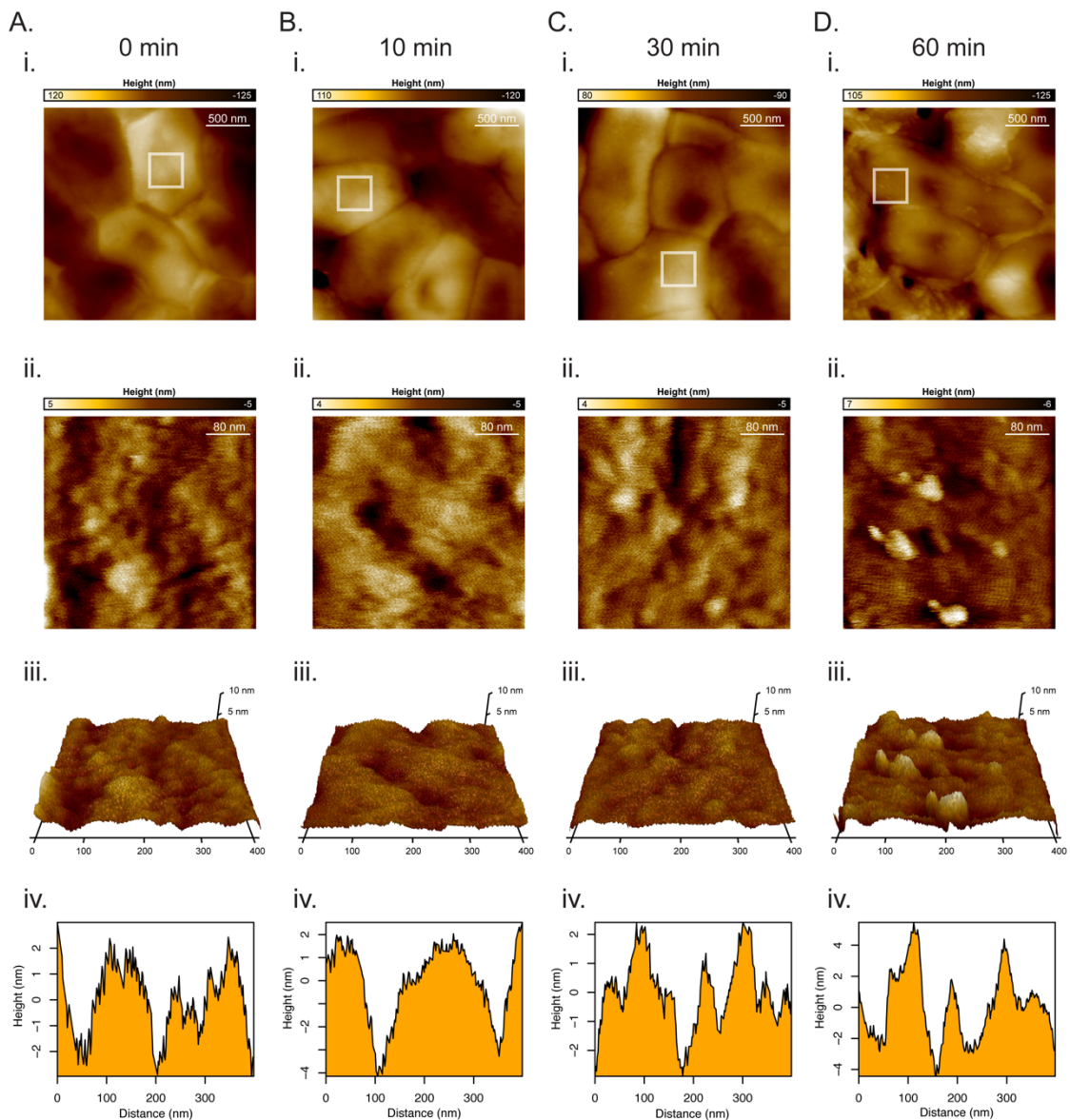


Figure S4: Liproxstatin-1 is able to physically perturb the OM of stationary phase cells. Atomic force microscopy of stationary phase *E. coli* cells exposed to 128 $\mu\text{g}/\text{mL}$ liproxstatin-1 for (A.) 0 minutes, (B.) 10 minutes, (C.) 30 minutes, and (D.) 60 minutes. Scans shown for each timepoint depict (i.) whole cells with white squares indicating the region shown at higher resolution in 2D in panel (ii.), (iii.) high-resolution 3D topography scans of a portion of the cell surface shown in (ii.), and (iv.) a plot showing the height along a cross-section of the cell surface.

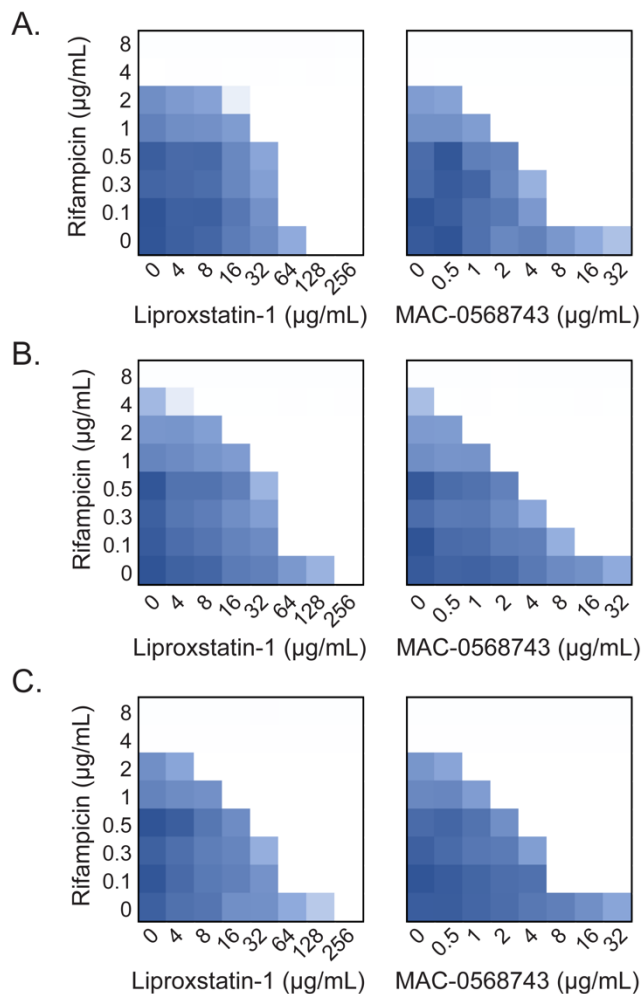


Figure S5: Liproxstatin-1 and MAC-0568743 are effective OM perturbants in polymyxin resistant environmental and clinical isolates of *E. coli*.

Checkerboard broth microdilution assays between liproxstatin-1 (left) or MAC-0568743 (right) and rifampicin in (A.) *E. coli* N15-02865, (B.) *E. coli* N15-02866, and (C.) *E. coli* C0244. Strains N15-02865 and N15-02866 are both *mcr-1* positive isolates from contaminated meat samples. Strain C0244 is a clinical isolate from urine, carrying resistance elements *ugd* and *eptA* resulting in lipid A modified with 4-aminoarabinose and phosphoethanolamine. Dark regions depicted in the checkerboard assays represent regions of higher cell growth. Checkerboard data are representative of at least two biological replicates.

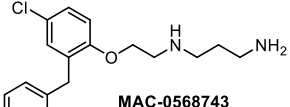
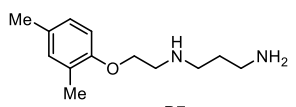
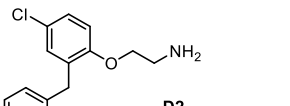
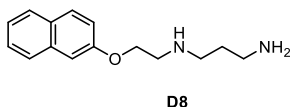
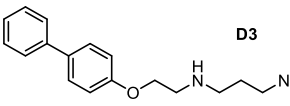
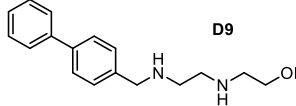
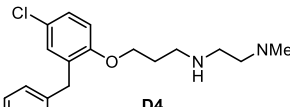
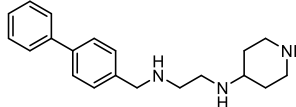
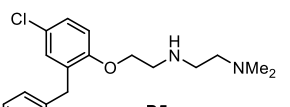
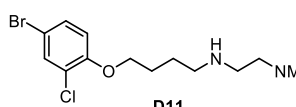
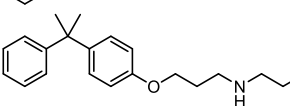
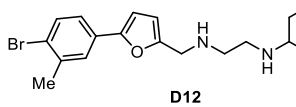
Tables

Table S1: Physicochemical properties of active ($n = 39$) and inactive ($n = 141,803$) compounds screened.

Property	Actives		Inactives		Significance Level (Kolmogorov–Smirnov) ^a
	Average	Std Dev	Average	Std Dev	
Molecular weight (g/mol)	345.9277	56.5750	342.0187	64.1848	ns
Log <i>P</i>	3.2323	0.7522	2.7444	1.1263	*
H-bond donors	1.7436	0.6774	1.1462	0.8293	****
H-bond acceptors	3.2308	1.0628	3.7870	1.3520	*
Lipinski violations	0.0000	0.0000	0.0083	0.0908	ns
Log <i>D</i>	1.3005	1.6659	2.5314	1.3492	****
Log <i>S</i>	-2.1808	2.0073	-3.9567	1.4291	****
p <i>K</i> _a	8.8567	2.4157	7.5304	4.9345	***
CNS MPO score	4.3700	0.5954	4.9047	0.7238	****
Topological polar surface area	49.4697	17.7622	71.3799	23.5721	****
Fsp ³	0.3656	0.1787	0.2753	0.1562	****
Heavy atom count	23.7179	3.9132	24.1285	4.6864	ns
Rotatable bonds	6.3590	2.3112	4.9816	1.8685	**
Total surface area	267.1454	36.9972	258.3576	46.7883	ns
Relative polar surface area	0.1736	0.0618	0.2604	0.0795	****
Druglikeness	0.8210	5.2129	0.4584	5.3368	ns
Shape index	0.6479	0.0946	0.5945	0.0678	****
Molecular flexibility	0.4970	0.0873	0.4457	0.0825	****
Molecular complexity	0.7226	0.0890	0.7649	0.0821	***
Non-C/H atoms	5.4359	1.6669	6.6036	1.8666	*
Metal atoms	0.0000	0.0000	0.0000	0.0038	ns
Electronegative atoms	5.4359	1.6669	6.6035	1.8667	*
Stereocenters	0.2564	0.5946	0.2893	0.5773	ns
Rings closures	2.6410	0.9315	2.9188	0.9414	ns
Small rings	2.6410	0.9315	2.9229	0.9468	ns
Aromatic rings	2.0000	0.6882	2.2304	0.8265	ns
Aromatic atoms	11.3077	3.4577	12.2901	4.1829	ns
sp ³ atoms	8.8205	4.1031	6.2564	3.4088	****
Symmetric atoms	2.4103	1.9963	2.1108	2.1828	ns
Amides	0.3077	0.5691	1.0602	0.8536	****
Amines	1.3077	0.8631	0.3011	0.5577	****
Alkyl amines	1.2564	0.8497	0.1925	0.4474	****
Aromatic amines	0.0513	0.2235	0.1086	0.3299	ns
Aromatic nitrogens	0.4615	0.8840	1.0798	1.3236	**
Basic nitrogens	1.4359	0.8206	0.3227	0.5652	****
Acidic oxygens	0.0000	0.0000	0.1510	0.3783	ns

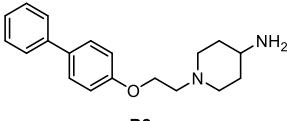
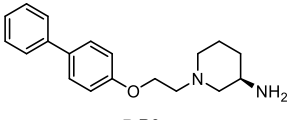
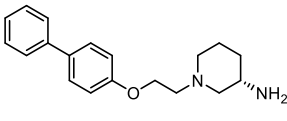
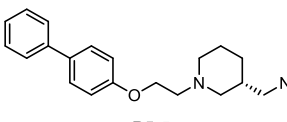
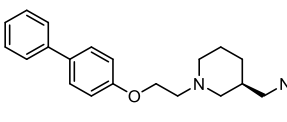
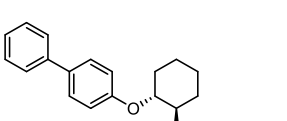
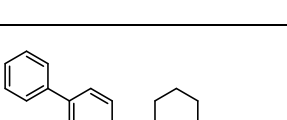
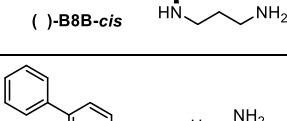
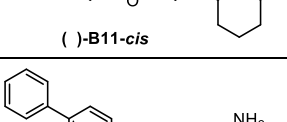
^a ns = not significant ($P > 0.05$); * $P \leq 0.05$; ** $P \leq 0.01$; *** $P \leq 0.001$; **** $P \leq 0.0001$.

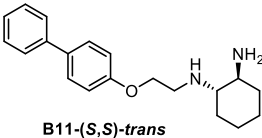
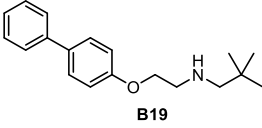
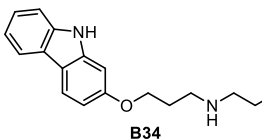
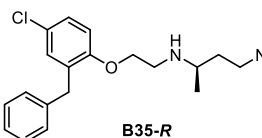
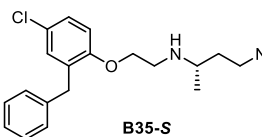
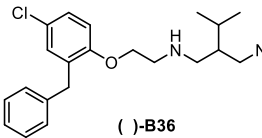
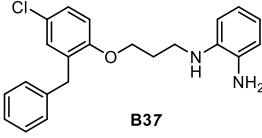
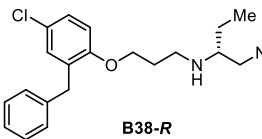
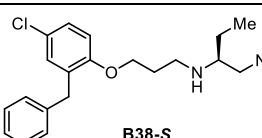
Table S2: Potentiation activity of D-Series MAC-0568743 analogues in *E. coli* BW25113.

Compound	MIC ($\mu\text{g/mL}$)	FICI ^a	Compound	MIC ($\mu\text{g/mL}$)	FICI ^a
 MAC-0568743	64	≤ 0.16	 D7	>128	≤ 0.31
 D2	32	0.5	 D8	>128	≤ 0.25
 D3	>128	≤ 0.19	 D9	>128	≤ 0.5
 D4	16	0.52	 D10	>128	≤ 0.31
 D5	32	0.75	 D11	128	0.25
 D6	32	0.094	 D12	32	0.31

^a FICI data reported are for MAC-0568743 analogues in combination with rifampicin. Refer to the Methods section for FICI determination.

Table S3: Characterization and potentiation activity of B-Series MAC-0568743 analogues in *K. pneumoniae* C026.

Compound	MIC (µg/mL)	FICI ^a	Characterization ^b
 B2	256	0.38	36.9 mg; 34% yield; 98.8% purity (Q. HPLC); LCMS RT 0.928 min; [M+H] ⁺ 297.2; ¹ H NMR (400 MHz, CD ₃ OD): δ 7.59–7.53 (d, 4H), 7.39 (t, <i>J</i> = 8.0 Hz, 2H), 7.29–7.25 (m, 1H), 7.35 (s, 1H), 7.07–7.11 (m, 2H), 4.45 (t, <i>J</i> = 4.8 Hz, 2H), 3.64 (brs, 2H), 3.55–3.49 (m, 2H), 2.32–2.28 (m, 2H), 2.14–2.05 (m, 2H).
 R-B3	256	0.38	88.9 mg; 39% yield; 98.3% purity (Q. HPLC); LCMS RT 0.928 min; [M+H] ⁺ 297.3; ¹ H NMR (400 MHz, CD ₃ OD): δ 7.60–7.54 (m, 4H), 7.42–7.40 (m, 2H), 7.40–7.38 (m, 1H), 7.14–7.12 (m, 2H), 4.51–4.48 (m, 2H), 3.92 (s, 1H), 3.75–3.73 (m, 4H), 3.22 (s, 2H), 2.24–2.15 (m, 2H), 2.08–2.07 (m, 1H), 1.73–1.70 (m, 1H)
 S-B3	256	0.5	75.3 mg; 36% yield; 97.1% purity (Q. HPLC); LCMS RT 0.908 min; [M+H] ⁺ 297.3; ¹ H NMR (400 MHz, CD ₃ OD): δ 7.60–7.54 (m, 4H), 7.42–7.40 (m, 2H), 7.40–7.38 (m, 1H), 7.14–7.11 (m, 2H), 4.51–4.47 (m, 2H), 3.89 (s, 1H), 3.72 (s, 4H), 3.20 (s, 2H), 2.23–2.15 (m, 2H), 2.07–2.00 (m, 1H), 1.73–1.71 (m, 1H)
 B5-R	>256	≤0.25	115 mg; 45% yield; 98.8% purity (Q. HPLC); LCMS RT 0.929 min; [M+H] ⁺ 311.1; ¹ H NMR (400 MHz, CD ₃ OD): δ 7.59–7.55 (m, 4H), 7.42–7.38 (m, 2H), 7.31–7.29 (m, 1H), 7.13–7.11 (m, 2H), 4.52–4.47 (m, 2H), 3.78–3.75 (m, 2H), 3.66–3.64 (m, 2H), 3.11–2.93 (m, 4H), 2.41 (br s, 1H), 2.09–1.96 (m, 3H), 1.39–1.35 (m, 1H)
 B5-S	>256	≤0.25	82.2 mg; 32% yield; 99.4% purity (Q. HPLC); LCMS RT 0.907 min; [M+H] ⁺ 311.1; ¹ H NMR (400 MHz, CD ₃ OD): δ 7.60–7.55 (m, 4H), 7.42–7.38 (m, 2H), 7.31–7.29 (m, 1H), 7.13–7.11 (m, 2H), 4.49–4.47 (m, 2H), 3.74–3.66 (m, 4H), 3.11–2.94 (m, 4H), 2.41 (br s, 1H), 2.09–1.94 (m, 3H), 1.39–1.29 (m, 1H).
 (-)-B8A-trans	>256	≤0.078	54.6 mg; 13% yield; 96.9% purity (Q. HPLC); LCMS RT 0.992 min; [M+H] ⁺ 325.3; ¹ H NMR (400 MHz, DMSO- <i>d</i> ₆): δ 9.66 (s, 1H), 9.03 (s, 1H), 8.16 (s, 3H), 7.59–7.57 (m, 4H), 7.42–7.39 (t, <i>J</i> = 7.6 Hz, 2H), 7.29 (t, <i>J</i> = 7.6 Hz, 1H), 7.14 (d, <i>J</i> = 8.8 Hz, 2H), 4.61–4.56 (m, 1H), 3.27–3.26 (m, 1H), 3.09–3.08 (m, 2H), 2.88–2.83 (m, 2H), 2.24–2.16 (m, 2H), 2.04–2.01 (m, 2H), 1.99–1.65 (m, 2H), 1.59–1.53 (m, 1H), 1.31–1.29 (m, 3H).
 (-)-B8B-cis	>256	≤0.047	75.7 mg; 67% yield; 99.1% purity (Q. HPLC); LCMS RT 0.998 min; [M+H] ⁺ 325.3; ¹ H NMR (400 MHz, DMSO- <i>d</i> ₆): δ 9.35 (s, 1H), 9.18 (s, 1H), 8.25 (s, 3H), 7.60–7.58 (m, 4H), 7.40 (t, <i>J</i> = 7.6 Hz, <i>J</i> = 8.0 Hz, 2H), 7.28 (t, <i>J</i> = 7.2 Hz, <i>J</i> = 7.6 Hz, 1H), 7.19 (d, <i>J</i> = 8.8 Hz, 2H), 5.01 (s, 1H), 3.36 (s, 1H), 3.09–3.87 (m, 2H), 2.84 (d, <i>J</i> = 6.0 Hz, 2H), 2.06–2.03 (m, 4H), 2.01–1.73 (m, 2H), 1.41–1.36 (m, 4H).
 (-)-B11-cis	128	0.62	72.7 mg; 21% yield; 96.2% purity (Q. HPLC); LCMS RT 0.974 min; [M+H] ⁺ 311.3; ¹ H NMR (400 MHz, CD ₃ OD): δ 7.58–7.53 (m, 4H), 7.38 (t, <i>J</i> = 8.0 Hz, 2H), 7.27 (t, <i>J</i> = 8.0 Hz, 1H), 7.11 (d, <i>J</i> = 8.0 Hz, 2H), 4.42 (t, <i>J</i> = 4.0 Hz, 2H), 4.03 (s, 1H), 3.86–3.62 (m, 3H), 2.14–2.04 (m, 2H), 1.94–1.84 (m, 3H), 1.68–1.52 (m, 3H).
 B11-(R,R)-trans	128	0.62	53.6 mg; 10% yield; 97.2% purity (Q. HPLC); LCMS RT 0.96 min; [M+H] ⁺ 311.2; ¹ H NMR (400 MHz, CD ₃ OD): δ 7.59–7.53 (m, 4H), 7.39 (t, <i>J</i> = 8.0 Hz, 2H), 7.27 (t, <i>J</i> = 8.0 Hz, 1H), 7.11 (d, <i>J</i> = 8.0 Hz, 2H), 4.49–4.41 (m, 2H), 3.73–3.67 (m, 1H), 3.54–3.44 (m, 3H), 2.38 (d, <i>J</i> = 8.0 Hz, 1H), 2.19 (d, <i>J</i> = 8.0 Hz, 1H), 1.92–1.84 (m, 2H), 1.62–1.53 (m, 2H), 1.48–1.37 (m, 2H).

	B11-(S,S)-trans	128	0.62	68.4 mg; 19.6% yield; 99.4% purity (Q. HPLC); LCMS RT 0.58 min; [M+H] ⁺ 311.2; ¹ H NMR (400 MHz, CD ₃ OD): δ 7.61–7.56 (m, 4H), 7.42 (t, <i>J</i> = 8.0 Hz, 2H), 7.31 (t, <i>J</i> = 8.0 Hz, 1H), 7.14 (d, <i>J</i> = 8.0 Hz, 2H), 4.54–4.43 (m, 2H), 3.77–3.73 (m, 1H), 3.60–3.52 (m, 3H), 2.41 (d, <i>J</i> = 8.0 Hz, 1H), 2.19 (d, <i>J</i> = 8.0 Hz, 1H), 1.95–1.87 (m, 2H), 1.67–1.61 (m, 2H), 1.49–1.42 (m, 2H).
	B19	>256	≤0.31	99.2 mg; 41% yield; 98.9% purity (Q. HPLC); LCMS RT 0.938 min; [M+H] ⁺ 299.2; ¹ H NMR (400 MHz, CD ₃ OD): δ 7.61–7.55 (m, 4H), 7.42–7.40 (m, 2H), 7.35–7.33 (m, 1H), 7.13–7.11 (m, 2H), 4.45–4.43 (m, 2H), 3.61–3.59 (m, 2H), 3.22 (s, 2H), 3.06 (s, 2H), 1.23 (s, 6H).
	B34	>256	≤0.25	57.5 mg; 46% yield; 100% purity (Q. HPLC); LCMS RT 0.908 min; [M+H] ⁺ 284.2; ¹ H NMR (400 MHz, DMSO- <i>d</i> ₆): δ 10.93–11.23 (m, 1H), 11.09 (s, 1H), 9.58 (br s, 2H), 8.42 (br s, 3H), 8.08 (d, <i>J</i> = 7.58 Hz, 1H), 7.72 (d, <i>J</i> = 2.20 Hz, 1H), 7.45 (d, <i>J</i> = 8.07 Hz, 1H), 7.40 (d, <i>J</i> = 8.56 Hz, 1H), 7.30–7.37 (m, 1H), 7.08–7.16 (m, 1H), 7.01–7.08 (m, 1H), 7.06 (dd, <i>J</i> = 8.80, 2.45 Hz, 1H), 4.18 (t, <i>J</i> = 6.11 Hz, 2H), 3.13–3.30 (m, 6H), 2.11–2.26 (m, 2H)
	B35-R	256	0.078	20 mg; 29% yield; 94.3% purity (Q. HPLC); LCMS RT 0.771 min; [M+H] ⁺ 333.2; ¹ H NMR (400 MHz, DMSO- <i>d</i> ₆): δ = 9.53–9.20 (m, 2H), 8.22–7.96 (m, 3H), 7.34–7.24 (m, 5H), 7.24–7.18 (m, 1H), 7.13 (d, <i>J</i> = 2.6 Hz, 1H), 7.06 (d, <i>J</i> = 8.8 Hz, 1H), 4.31 (t, <i>J</i> = 5.2 Hz, 2H), 4.08–3.93 (m, 2H), 3.47–3.38 (m, 1H), 3.38–3.27 (m, 2H), 3.06–2.81 (m, 2H), 2.22–2.07 (m, 1H), 1.95–1.77 (m, 1H), 1.30 (d, <i>J</i> = 6.6 Hz, 3H)
	B35-S	128	0.12	21.1 mg; 20% yield; 99.5% purity (Q. HPLC); LCMS RT 0.776 min; [M+H] ⁺ 333.1; ¹ H NMR (400 MHz, DMSO- <i>d</i> ₆): δ 9.53 (br s, 2H), 8.21 (br s, 3H), 7.33–7.23 (m, 5H), 7.22–7.17 (m, 1H), 7.11 (d, <i>J</i> = 2.6 Hz, 1H), 7.04 (d, <i>J</i> = 8.8 Hz, 1H), 4.32 (br t, <i>J</i> = 5.1 Hz, 2H), 4.05–3.94 (m, 2H), 3.32 (br s, 3H), 2.99–2.82 (m, 2H), 2.22–2.12 (m, 1H), 1.97–1.85 (m, 1H), 1.30 (d, <i>J</i> = 6.5 Hz, 3H)
	(-)-B36	64	0.38	51.8 mg; 33% yield; 100% purity (Q. HPLC); LCMS RT 0.795 min; [M+H] ⁺ 361.3; ¹ H NMR (400 MHz, CD ₃ OD): δ 7.34–7.27 (m, 2H), 7.26–7.16 (m, 4H), 7.07–6.99 (m, 2H), 4.42–4.26 (m, 2H), 4.05 (s, 2H), 3.61–3.38 (m, 2H), 3.24 (br dd, <i>J</i> = 5.6, 13.6 Hz, 1H), 3.18–3.08 (m, 2H), 3.08–3.00 (m, 1H), 2.20–1.90 (m, 2H), 1.00 (dd, <i>J</i> = 6.8, 16.8 Hz, 6H).
	B37	>256	≤3	45.7 mg; 38% yield; 99.5% purity (Q. HPLC); LCMS RT 0.931 min; [M+H] ⁺ 367.2; ¹ H NMR (400 MHz, DMSO- <i>d</i> ₆): δ 7.27–7.19 (m, 6H), 7.19–7.05 (m, 3H), 7.02–6.95 (m, 1H), 6.78 (br s, 2H), 4.12 (t, <i>J</i> = 6.0 Hz, 2H), 3.90 (s, 2H), 3.61–3.54 (m, 1H), 3.20 (br t, <i>J</i> = 7.0 Hz, 2H), 2.08 (q, <i>J</i> = 6.3 Hz, 2H).
	B38-R	32	0.56	58.9 mg; 21% yield; 100% purity (Q. HPLC); LCMS RT 0.792 min; [M+H] ⁺ 347.3; ¹ H NMR (400 MHz, DMSO- <i>d</i> ₆): δ 9.76 (br s, 1H), 9.53 (br s, 1H), 8.60 (br s, 3H), 7.32–7.26 (m, 2H), 7.25–7.16 (m, 5H), 6.98 (d, <i>J</i> = 8.4 Hz, 1H), 4.07 (br t, <i>J</i> = 5.6 Hz, 2H), 3.90 (s, 2H), 3.34 (br s, 1H), 3.26–3.13 (m, 2H), 3.13–2.93 (m, 2H), 2.19 (br s, 2H), 1.84–1.72 (m, 1H), 1.71–1.57 (m, 1H), 0.94 (t, <i>J</i> = 7.6 Hz, 3H).
	B38-S	32	0.56	45.9 mg; 39% yield; 100% purity (Q. HPLC); LCMS RT 0.791 min; [M+H] ⁺ 347.3; ¹ H NMR (400 MHz, DMSO- <i>d</i> ₆): δ 9.85–9.25 (m, 2H), 8.54 (br s, 3H), 7.35–7.12 (m, 7H), 6.98 (d, <i>J</i> = 8.6 Hz, 1H), 4.14–4.01 (m, 2H), 3.90 (s, 2H), 3.18 (br s, 2H), 3.12–2.94 (m, 2H), 2.18 (br d, <i>J</i> = 2.7 Hz, 2H), 1.84–1.53 (m, 2H), 0.94 (t, <i>J</i> = 7.4 Hz, 3H).

^a FICI data reported are for MAC-0568743 analogues in combination with rifampicin.

Refer to the Methods section for FICI determination ^b Instrument for LCMS: Shimadzu LCMS-2020; Software: LabSolution Version 5.82 SP1; Method A: 0.0375% TFA in water (v/v); 0/01875% TFA in acetonitrile (v/v), 10% B to 90% B.

**CHAPTER IV – Genetic and chemical screening reveals targets and
compounds to potentiate Gram-positive antibiotics against Gram-negative
bacteria**

Preface

The work presented in this chapter is in preparation for submission, as of April 25, 2022:

Klobucar K, Jardine E, Farha MA, MacKinnon MR, Fragis M, Nkonge B, Bhandu T, Borrillo L, Tsai CN, Coombes BK, Magolan J, Brown ED. 2022. Genetic and chemical screening reveals targets and compounds to potentiate Gram-positive antibiotics against Gram-negative bacteria. In preparation.

I performed all antibiotic susceptibility testing, checkerboard assays, membrane integrity assays, and enzyme assays. I performed chemical-genetic screening with assistance from Jardine E. Chemical screening and dose-response experiments were performed by Jardine E. I performed compound prioritization with significant input from Farha MA, Jardine E, and Brown ED. Hyperporinated strains were constructed by Bhandu T. Cytotoxicity assays were performed by Tsai CN. MAC-0485042 and analogues were synthesized and chemically characterized by MacKinnon MR and Borrillo L. MAC-0493157 and MAC-0483351 analogues were synthesized and chemically characterized by Fragis M. and Nkonge B. I wrote and edited the manuscript with input from all authors.

Abstract

Gram-negative bacteria are intrinsically resistant to a plethora of antibiotics which effectively inhibit the growth of Gram-positive bacteria. The intrinsic resistance of Gram-negative bacteria to classes of antibiotics including rifamycins, aminocoumarins, macrolides, glycopeptides, and oxazolidinones, has largely been attributed to their lack of accumulation within cells due to poor permeability across the outer membrane, susceptibility to efflux pumps, or a combination of these factors. Due to the difficulty in discovering antibiotics which can bypass these barriers, finding targets and compounds that increase the activity of these ineffective antibiotics against Gram-negative bacteria has the potential to expand antibiotic spectrum. In this study, we investigated the genetic determinants for resistance to rifampicin, novobiocin, erythromycin, vancomycin, and linezolid, to determine potential targets of antibiotic potentiating compounds. We subsequently performed a high-throughput screen of ~50,000 diverse, synthetic compounds to uncover molecules that potentiate the activity of at least one of the five Gram-positive-targeting antibiotics. This led to the discovery of two membrane active compounds capable of potentiating linezolid, and an inhibitor of lipid A biosynthesis capable of potentiating rifampicin and vancomycin. Furthermore, we characterized the ability of known inhibitors of lipid A biosynthesis to potentiate the activity of rifampicin against Gram-negative pathogens.

Introduction

The lack of available effective antibiotics to treat Gram-negative pathogens is one of the greatest current threats to medicine (1, 2). Treatments using the existing antibiotics which are effective against Gram-negative bacteria are plagued by widespread resistance elements, making their use increasingly obsolete. The void in discovery of new antibiotics has produced no new classes of antibiotics to treat Gram-negative infections in over 50 years (3, 4). It is exceedingly difficult to find antibiotics which target Gram-negative bacteria as cell envelopes of these microbes provide a formidable permeability barrier (5). The Gram-negative cell envelope consists of a canonical phospholipid inner membrane (IM), a thin layer of peptidoglycan, and an asymmetric outer membrane (OM) composed of phospholipids in the inner leaflet and lipopolysaccharide (LPS) molecules in the outer leaflet (6). LPS typically consists of a 3-deoxy-D-manno-octulosonic acid (Kdo)₂-lipid A moiety, inner and outer core oligosaccharides, and O-polysaccharide; however, O-polysaccharide is absent in *Escherichia coli* K-12 strains (7, 8). LPS contributes to the impenetrability of the OM barrier, which hinders the entry of hydrophobic molecules and molecules greater than ~600 Da in size (8, 9). An additional barrier to antibiotic accumulation in Gram-negative bacteria is the presence of multidrug efflux pumps, such as the AcrAB-TolC system, whereby much of the chemical matter capable of entry is still susceptible to removal by these pumps, limiting intracellular concentrations (10, 11).

As a result of the OM barrier, as well as the presence of efflux pumps, many antibiotics which are effective against Gram-positive bacteria are unable to reach their targets and lack any growth inhibitory activity against Gram-negative bacteria. Gram-positive-targeting antibiotics include rifamycins (e.g. rifampicin), aminocoumarins (e.g. novobiocin), macrolides (e.g. erythromycin), glycopeptides (e.g. vancomycin), and oxazolidinones (e.g. linezolid) (12, 13). Our research group has previously explored genetic and chemical approaches to understand and overcome the permeability barrier of the model Gram-negative *E. coli* (14–18). Chemical perturbation of intrinsic resistance mechanisms is an avenue with broad application across multiple pathogens and with the potential to expand the spectrum of Gram-positive-targeting antibiotics to include Gram-negative bacteria. Therapeutically, this could be accomplished through a combinatorial, dose-sparing approach, in which a Gram-positive-targeting antibiotic is co-administered with an enhancing agent (13, 19, 20). Potentiators could target OM biogenesis or impact OM integrity through physical perturbation to increase antibiotic influx. Such agents could also target efflux pumps to reduce antibiotic removal from cells. In principle, potentiator compounds might also impact specific cellular processes that enhance efficacy without affecting antibiotic accumulation within cells.

In the work described here, we investigated the genetic requirements for resistance of *E. coli* to rifampicin, novobiocin, erythromycin, vancomycin, and linezolid, antibiotics that have intracellular targets in Gram-negative bacteria but

are only effective against Gram-positive bacteria. Similarly, we screened a library of ~50,000 diverse, synthetic compounds for growth inhibitory activity against *E. coli* in the presence subinhibitory concentrations of the five Gram-positive-targeting antibiotics. Some 12 compounds were determined to be synergistic with at least one of the antibiotics and we characterized the mechanism of potentiation of three of these. Two were structural analogues that physically disrupted both the OM and IM to potentiate linezolid. One compound was a weakly potent inhibitor of the lipid A biosynthetic enzyme, LpxC, that potentiated rifampicin and vancomycin. The latter finding led us to characterize the synergy between known LpxC inhibitors and rifampicin in various Gram-negative pathogens.

Results and Discussion

Genetic requirements for resistance of *E. coli* to Gram-positive-targeting antibiotics

As Gram-negative bacteria are intrinsically resistant to several Gram-positive-targeting antibiotics due to the presence of the OM barrier and efflux, we sought to confirm the relative contribution of each to antibiotic activity. We began by selecting five antibiotics of different classes which are effective against Gram-positive bacteria but are ineffective against Gram-negative bacteria despite the presence of otherwise susceptible intracellular targets: rifampicin (a rifamycin), novobiocin (an aminocoumarin), erythromycin (a macrolide), vancomycin (a glycopeptide), and linezolid (an oxazolidinone). We performed susceptibility

testing of these antibiotics in four different strains of *E. coli* BW25113: wild type (WT), a hyperporinated strain constitutively expressing a truncated form of the FhuA pore (WT-pore) (21, 22), an efflux-deficient strain ($\Delta toIC$), and a hyperporinated, efflux-deficient strain ($\Delta toIC$ -pore). Both rifampicin and vancomycin are largely OM excluded as their minimum inhibitory concentrations (MICs) were ≥ 32 -fold lower in the hyperporinated strains compared to wild type, while the efflux-deficient strains were no more susceptible to either antibiotic (Table 1). Erythromycin, novobiocin, and linezolid activities were all improved by both hyperporination and a lack of efflux, to varying extents (Table 1). These findings were largely in line with previous observations (22). Linezolid resistance in Gram-negative bacteria has generally been attributed to efflux (23), however our data suggested, as has other recent work (15, 18, 24), that a compromised OM barrier can also increase its activity, albeit to a lesser extent. While efflux and permeability are closely linked, these strains provided valuable benchmarking for the impact of these elements on the five chosen antibiotics.

Next, we sought to identify the genetic determinants for resistance to these antibiotics in *E. coli* using high-throughput genetic screens. We measured the growth of a collection of single gene deletion strains (25), as well as a collection of small RNA deletion strains (26), in the presence of subinhibitory concentrations (1/4 of the solid media MIC) of five Gram-positive-targeting antibiotics, rifampicin, novobiocin, erythromycin, vancomycin, and linezolid, and compared the growth to that with no drug added. Strains with impaired growth in the presence of

subinhibitory concentrations of antibiotic compared to the no drug condition, defined as 2 standard deviations (σ) below the mean, were deemed to be sensitive to the respective antibiotic (Figure 1A). Of the 222 gene deletion strains that were sensitive to at least one of the five antibiotics, 134 were uniquely sensitive to one of the antibiotics (Figure 1A). Some of these sensitive strains reflected the mechanism of action or cellular response to the antibiotic. For instance, deletions in *ruvA* and *uvrA*, which are genes involved in the SOS response, as well as *trxA*, a regulator of DNA replication, resulted in sensitivity to rifampicin which targets DNA-dependent RNA polymerase. Deletions in *glmZ* and *hfq*, elements of small RNA regulated gene expression, were more sensitive to linezolid which targets protein synthesis. Increased sensitivity to vancomycin, which targets peptidoglycan synthesis, was also observed in deletions of peptidoglycan metabolism genes *ldtC*, *pgpB*, and *mltD*, as well as the nucleotide metabolism gene deletions *atpE*, *atpB*, *sucB*, *sucC*, and *upp*. The remaining 88 gene deletion strains were sensitive to at least two of the antibiotics. Interestingly, rifampicin and vancomycin showed the most overlap, despite having widely different mechanisms of action and hydrophobicities (Figure 1A). An analysis of gene ontology (GO) terms of the genes that were important for resistance to at least two of the Gram-positive-targeting antibiotics revealed an enrichment in a variety of processes including LPS core metabolism (*waaP*, *waaF*, *lpcA*, *gmhB*, *rfaE*, *galU*), bile acid and bile salt transport (*acrA*, *acrB*, *tolC*, *ygiS*), protein folding (*skp*, *dnaK*, *bepA*, *dppA*, *elfD*, *dsbB*), protein insertion into membrane

(*skp*, *secG*, *bamE*), and peptidoglycan turnover (*murQ*, *ldcA*, *nagE*) (Figure 1B).

Based on these GO terms, increased sensitivity to these different classes of antibiotics was commonly due to increased cell permeation and decreased efflux. Consequently, these processes represent potential targets for chemicals which increase the sensitivity of *E. coli* to these Gram-positive-targeting antibiotics.

Chemical screening for potentiation of Gram-positive-targeting antibiotics in *E. coli*

Given the varied genetic targets which led to sensitivity to the five different Gram-positive-targeting antibiotics, we undertook a chemical screening campaign to uncover molecules which are capable of potentiating each of the antibiotics in Gram-negative *E. coli*. We screened a library of ~50,000 diverse synthetic compounds at 10 μ M for growth inhibitory activity against *E. coli* BW25113 in the presence of the five antibiotics, rifampicin, novobiocin, erythromycin, vancomycin, and linezolid, at subinhibitory concentrations in rich microbiological media (Figure 2). Compounds which resulted in *E. coli* growth less than 4σ below the mean for each screen were deemed active (Figure S1). For each of the five screens there were between 100 and 200 actives, resulting in active rates of ~0.2-0.4% (Figure 2). As the primary screen was unable to differentiate between compounds with growth inhibitory activity alone and those which increased the growth inhibitory activity of the partner antibiotic, all active compounds were tested in dose-response assays to determine their MICs in the presence and absence of the corresponding antibiotic. Compounds which had an unchanged MIC in the

presence and absence of the antibiotic were eliminated from further study (Figure 2).

From all screens, 45 compounds were found to potentiate the activity of at least one of the five antibiotics tested (Figure 2). Five of these compounds were structural analogues of *S*-(3,4-dichlorobenzyl) isothiourea, also known as A22 (Figure S2). A22 and other thiourea compounds have been shown to potentiate the activity of large-scaffold antibiotics via their inhibitory activity on the bacterial cytoskeletal protein MreB, resulting in increased permeability (27–30). Similarly, the A22 analogue MAC13243, and related compounds are likely to break down to expose the active thiourea fragment of the molecule (29). Additionally, seven of the actives were sulfonamides found to be synergistic with the peptidoglycan targeting antibiotic vancomycin (Figure S3). Sulfonamide antibiotics target the enzyme dihydropteroate synthase involved in folic acid biosynthesis by competing with the native substrate of the enzyme, *p*-aminobenzoic acid (31). A similar observation by Zhou *et al.* (32) revealed that vancomycin was synergistic with trimethoprim, another antibiotic which targets folic acid biosynthesis. The observed synergy was speculated to be due to a small amount of vancomycin entering cells, causing DNA damage through generation of hydroxyl radicals, and acting synergistically with compounds which deplete thymine from cells, such as inhibitors of the folic acid biosynthetic pathway (32).

Excluding the five A22 analogues and seven sulfonamides, 25 compounds were resupplied based on commercial availability (Figure 2). All 25 resupplied

compounds were tested in combination with the five Gram-positive-targeting antibiotics against *E. coli* using checkerboard broth microdilution assays, which were used to calculate a fractional inhibitory concentration index (FICI) for each antibiotic-compound combination. The FICI is the sum of the fractional inhibitory concentration (FIC) of each tested compound, which is the MIC of the compound in combination divided by the MIC of the compound alone (33). FICIs less than or equal to 0.5 are deemed synergistic (34). Of the 25 compounds tested, 12 compounds were synergistic with at least one of the antibiotics tested (Figure 2).

MAC-0493157 and MAC-0483351 potentiate linezolid through outer and inner membrane disruption

In our screen, we identified two potentiators of linezolid in *E. coli* that were structural analogues of one another, MAC-0493157 and MAC-0483351 (Figure 3A). Interestingly, MAC-0493157 was also active in the novobiocin potentiation screen, while MAC-0483351 was not. This was confirmed in the checkerboard assays, with MAC-0493157 being most synergistic with novobiocin and linezolid, while MAC-0483351 was synergistic with linezolid but not novobiocin (Figure 3B). MAC-0493157 was also weakly synergistic with rifampicin and erythromycin, and MAC-0483351 was weakly synergistic with vancomycin (Figure 3B). To test the effects of these compounds on OM integrity, a β -lactamase assay was performed. Upon OM disruption of a strain of *E. coli* constitutively expressing β -lactamase in the periplasm, the β -lactamase enzyme can encounter the nitrocefin substrate, resulting in its cleavage, to produce a detectable colour change. Both

compounds were found to physically disrupt OM integrity in the β -lactamase assay (Figure 3C). In this assay, MAC-0493157 disrupted the OM to a similar extent as the known OM perturbant, SPR741 (35), while MAC-0483351 exhibited a lower maximal observed level of OM disruption (Figure 3C).

As many physical membrane disruptors act indiscriminately on all membranes, we also tested whether MAC-0493157 and MAC-0483351 perturb IM integrity using a β -galactosidase assay. To measure their effects on IM permeability, a strain of *E. coli* constitutively expressing β -galactosidase in the cytoplasm was used. If the IM integrity of cells is disrupted, the β -galactosidase can come into contact with the chromogenic substrate, *o*-nitrophenyl- β -galactoside (ONPG) and cleave it to produce a detectable colour change. Indeed, both MAC-0493157 and MAC-0483351 disrupted the integrity of the IM as measured in the β -galactosidase assay at levels approaching the polymyxin B high control (Figure 3D). In accordance with these findings, MAC-0493157 and MAC-0483351 were potently growth inhibitory against *Staphylococcus aureus*, a Gram-positive bacterium, which possesses a cytoplasmic membrane similar to the Gram-negative IM (Figure 3E). As expected for compounds which indiscriminately disrupt cell membranes, both compounds were also cytotoxic against the HEK293 mammalian cell line in a lactate dehydrogenase (LDH) release assay at the concentrations which would be useful for potentiation of linezolid (Figure 3F). Thus, both MAC-0493157 and MAC-0483351 are capable of potentiating linezolid against Gram-negatives, however, would require

considerable medicinal chemistry optimization to maintain OM activity while decreasing activity against canonical phospholipid membranes that is presumably the mechanism of cytotoxicity. Based on preliminary structure-activity relationship efforts, modifications to the carbazole group including removal of one of the benzene rings and removal of the halogen substituents resulted in loss of potentiation activity (Table S1).

MAC-0485042 potentiates rifampicin and vancomycin by inhibition of LpxC

One of the hit compounds detected in the vancomycin potentiation screen was MAC-0485042, a hydroxamic acid containing compound (Figure 4A). Hydroxamic acid containing drugs have been used in a variety of therapeutic applications due to their ability to form complexes with metal ions (36, 37). Additionally, hydroxamic acids have been explored as inhibitors of bacterial metalloenzymes (37). Such enzymes include UDP-3-O-(*R*-3-hydroxymyristoyl)-*N*-acetylglucosamine deacetylase (LpxC), a zinc-binding metalloenzyme which catalyzes the first committed step of lipid A biosynthesis in Gram-negative bacteria (38–40), and peptide deformylase, a metalloenzyme which catalyzes the removal of the formyl group from the N-terminal methionine residue of nascent peptides (41). MAC-0485042 has previously been reported to inhibit *E. coli* peptide deformylase in an *in vitro* biochemical assay (42).

Since MAC-0485042 was discontinued by the supplier, the compound was synthesized in house for further studies. As discovered in the potentiation screen, MAC-0485042 was synergistic with vancomycin (Figure 4B). MAC-0485042

displayed enhanced synergy with rifampicin compared to vancomycin (Figure 4B), however was undetected in the rifampicin potentiation screen due to depletion of the stock in the cherry-picking source plate. MAC-0485042 also showed borderline synergy with erythromycin and linezolid (Figure 4B). Notably, MAC-0485042 lacked growth inhibitory activity against *E. coli* on its own, with an MIC of 256 $\mu\text{g/mL}$, suggesting either a non-essential target or weak inhibition of an essential target. We set out to eliminate the possibility of the compound acting via physical OM perturbation. Indeed, MAC-0485042 lacked any physical OM disruption in the β -lactamase assay, unlike the SPR741 positive control (Figure 4C). Interestingly, there was a decrease in absorbance in this assay with increasing concentrations of MAC-0485042 upon subtraction of the corresponding no cell control wells, since the compound alone resulted in nitrocefin cleavage (data not shown). A lysozyme assay was performed as an additional method to confirm the lack of OM disruption by MAC-0485042 observed in the β -lactamase assay. Lysozyme, an ~ 14 kDa protein, only lyses Gram-negative cells with a compromised OM facilitating its entry (43, 44). MAC-0485042 was unable to produce cell lysis by lysozyme, confirming the lack of physical OM disruption by this compound (Figure 4D). Thus, MAC-0485042 was capable of potentiating rifampicin and vancomycin without physically perturbing the OM.

Due to the high concentration of MAC-0485042 required for growth inhibition, we postulated that the compound could be susceptible to efflux or have

difficulty permeating the OM. Thus, we tested the potency of MAC-0485042 in the efflux-deficient and hyperporinated strains of *E. coli*. MAC-0485042 was ≥ 4 -fold more potent with an MIC of 64 $\mu\text{g}/\text{mL}$ in the efflux-deficient strain relative to wild type *E. coli*, with little difference in MIC in the hyperporinated strain (Figure 4E). These results suggested MAC-0485042 was susceptible to efflux by TolC-dependent efflux pumps and inhibited an intracellular target. Additionally, MAC-0485042 did not inhibit the growth of *S. aureus* (MIC $>256 \mu\text{g}/\text{mL}$), suggesting a Gram-negative specific target.

Since inhibition of LpxC, a Gram-negative specific target with numerous known hydroxamate-containing inhibitors (40), would increase the permeability of the OM, we hypothesized that MAC-0485042 was able to potentiate the activity of rifampicin and vancomycin through weak inhibition of LpxC. To confirm that the hydroxamic acid portion of the molecule which would interact with this bacterial metalloenzyme was required for the potentiation of rifampicin by MAC-0485042, we synthesized and tested two structural analogues which lacked the hydroxamate group. Both analogues lacked any synergy with rifampicin, suggesting that the hydroxamic acid portion of MAC-0485042 is critical to its biological activity (Figure S4). To explore whether LpxC inhibition was indeed the reason for potentiation of Gram-positive-targeting antibiotics by MAC-0485042, we tested the potency of MAC-0485042 against a strain of *E. coli* possessing a mutation in the *lpxC* gene (*lpxC101*) resulting in reduced lipid A biosynthesis (39). The *lpxC101* mutation is known to increase the sensitivity of cells to LpxC

inhibitors, along with other impermeant antibiotics (Figure S5) (45). MAC-0485042 was observed to be >64-fold more potent against the *lpxC101* mutant compared to the parental strain (Figure 4F). This increase in potency is substantially larger than any increase in potency due to reduction in efflux and permeability barriers (Figure 4E). Therefore, it is likely that the *lpxC101* mutant is more susceptible to MAC-0485042 due to LpxC being the target of the compound rather than due to increased permeability of the compound in this mutant background. To test whether MAC-0485042 was able to inhibit the activity of the *E. coli* LpxC enzyme, the use of an *in vitro* biochemical assay was employed. This fluorescence-based assay measures the conversion of the UDP-3-O-(*R*-3-hydroxymyristoyl)-*N*-acetylglucosamine substrate into UDP-glucosamine which is detected with *o*-phthaldialdehyde (45). In this assay, MAC-0485042 was able to weakly inhibit the activity of the LpxC enzyme, with an IC₅₀ value of ~333 μM (Figure 4G). Thus, MAC-0485042 may be capable of potentiating rifampicin and vancomycin through its weak inhibition of LpxC. Although the mechanism of synergy between MAC-0485042 appeared to be due to inhibition of LpxC, this does not exclude the possibility of peptide deformylase as an additional cellular target of this compound.

LpxC inhibitors are synergistic with rifampicin in Gram-negative pathogens

As LpxC is an essential enzyme for viability in most Gram-negative pathogens, drug discovery efforts in this area have largely focused on targeting LpxC as a monotherapy. A plethora of chemical matter targeting this enzyme has

been uncovered and many of these characterized inhibitors are highly potent on their own, with MICs typically in the single digit $\mu\text{g}/\text{mL}$ range, with some being less than 1 $\mu\text{g}/\text{mL}$ in certain strains (40). Additionally, since compromising LpxC function is known to increase OM permeability (39, 45), inhibitors of LpxC have potential for use in combination therapies with antibiotics excluded by the OM. One of the LpxC inhibitors discovered by Pfizer, PF-05081090, has also previously been shown to potentiate Gram-positive-targeting antibiotics in *A. baumannii*, in which inhibition of lipid A biosynthesis results in increased OM permeability but is not lethal (46). To further validate the use of LpxC inhibitors in combination with Gram-positive-targeting antibiotics against Gram-negative pathogens, we tested MAC-0485042 and the commercially available LpxC inhibitors ACHN-975, CHIR-090, PF-04753299, and PF-05081090, in combination with rifampicin in uropathogenic *E. coli* (UPEC), *Klebsiella pneumoniae*, and *Pseudomonas aeruginosa*. MAC-0485042 was synergistic with rifampicin in UPEC and *K. pneumoniae*, but not in *P. aeruginosa* (Figure 5). All other LpxC inhibitors tested were synergistic with rifampicin in all three pathogens tested, with the strongest synergy detected between PF-05081090 and rifampicin in *K. pneumoniae* (Figure 5). LpxC inhibitors have faced difficulty entering clinical trials, with ACHN-975 being the only one of its class to reach Phase I (40, 47). However, the compound was found to have issues due to cardiovascular toxicity (48). Despite concerns surrounding the hydroxamic acid moiety resulting in toxicity, it was found that the cardiovascular toxicity of the LpxC inhibitor was not

exclusively due to the hydroxamate (48). Thus, opportunities still exist in this area through the use of these compounds in combination with other large-scaffold antibiotics that could enable further dose-sparing, as well as investigation of analogues which are less potent and less toxic on their own while exhibiting synergy with other antibiotics.

Conclusion

The intrinsic antibiotic resistance mechanisms of Gram-negative bacteria must be subverted to potentiate the activity of antibiotics which are currently limited to use against Gram-positive bacteria. Through studies of the contribution of efflux and OM permeability, as well as the genetic determinants of resistance to these antibiotics, we have described potential processes which can be targeted for antibiotic potentiation. We performed high-throughput chemical screening for antibiotic potentiation and uncovered two membrane active compounds with a shared scaffold, MAC-0493157 and MAC-0483351, which are synergistic with linezolid, as well as MAC-0485042 which is capable of potentiating rifampicin and vancomycin through weak inhibition of LpxC. MAC-0485042 and other commercially available LpxC inhibitors have utility in potentiating antibiotics against Gram-negative pathogens which is an avenue that should be explored further for *in vivo* potential.

Methods

Bacterial strains and chemicals

Bacterial strains used in this study include *E. coli* BW25113, *E. coli* BW25113 $\Delta toIC$ (Keio collection) (25), *E. coli* ML35 pBR322 (49), *S. aureus* Newman, *E. coli* D21 (CGSC #5158) (50), *E. coli* D22 (CGSC #5163) (51), *E. coli* CFT073, *K. pneumoniae* ATCC 43816, *P. aeruginosa* PAO1. The hyperporinated *E. coli* BW25113 (*E. coli* WT-pore) and hyperporinated, efflux-deficient *E. coli* BW25113 (*E. coli* $\Delta toIC$ -pore) were generated by moving the pore, as described previously (21), into *E. coli* BW25113 and *E. coli* BW25113 $\Delta toIC$, respectively.

Chemicals were purchased from Sigma-Aldrich (rifampicin, vancomycin, novobiocin, erythromycin, CHIR-090, PF-04753299, polymyxin B), AvaChem Scientific (linezolid), MedChem Express (ACHN-975), Maybridge (MAC-0493157, MAC-0483351), and Axon Medchem (PF-05081090). SPR741 was supplied by Spero Therapeutics and Northern Antibiotics. MAC-0485042 and its analogues, as well as analogues of MAC-0493157 and MAC-0483351 were synthesized in house. Stock solutions of compounds were routinely dissolved in DMSO, except for polymyxin B and SPR741 which were dissolved in sterile deionized H₂O, and stored at -20 °C.

Chemical-genetic screening

The Keio collection (25) was pinned from Mueller Hinton agar (MHA) at 1,536-colony density to 6,144-colony density using the Singer Rotor onto MHA plates containing the following concentrations of antibiotics (1/4 of the solid media

MIC as determined using the method described in French *et al.* (52)), in duplicate: 4 µg/mL rifampicin, 128 µg/mL novobiocin, 128 µg/mL linezolid, 64 µg/mL vancomycin, 64 µg/mL erythromycin. A no drug control condition was also included. Plates were incubated at 37 °C for 18 h and imaged at endpoint using Epson Perfection V750 scanners. Data was analyzed and normalized as previously described (52). The normalized integrated density of each colony in the presence of antibiotic was divided by its normalized integrated density in the no drug condition. Colonies which grew less than 2σ below the mean in each antibiotic were defined as sensitive. GO term enrichment and P value calculations (using a Fisher exact test) were performed using EcoCyc (53). REVIGO was used to reduce the redundancy of GO term enrichments (54).

High-throughput chemical screening and dose-response assays

Chemical screening was performed at the McMaster Centre for Microbial Chemical Biology. *E. coli* BW25113 was grown overnight (~18 h) in cation-adjusted Mueller Hinton II Broth (MHB), subcultured 1:50 into fresh MHB, and grown at 37 °C with shaking at 250 rpm to mid-exponential phase (absorbance at 600 nm or OD₆₀₀ ~0.4). Cells were diluted to 1:10,000 in fresh MHB containing the following antibiotics, where applicable: 2 µg/mL rifampicin, 8 µg/mL novobiocin, 25 µg/mL linezolid, 8 µg/mL vancomycin, 4 µg/mL erythromycin. A 100 nL volume of compound was added to each well of a clear 384-well flat-bottom plate for a final concentration of 10 µM (or two-fold dilutions from 0-100 µM for dose-response assays) using the Echo 550 (LabCyte). A 50 µL volume of

cells was subsequently transferred to each well using the Tempest liquid dispenser (Formulatrix). Plates were then placed in a stationary incubator at 37 °C for 18 h and were subsequently read for absorbance at 600 nm. Normalization was performed as described previously in Mangat *et al.* (55). Active compounds were defined as those which resulted in growth less than 4σ below the mean.

Checkerboard broth microdilution assays and MIC determination

Overnight cultures (~18 h) of the appropriate strain of bacteria were grown in cation-adjusted MHB. Strains were subcultured 1:50 in fresh MHB and grown at 37 °C with shaking at 250 rpm to mid-exponential phase ($OD_{600} \sim 0.4$). Cells were diluted to 1:10,000 in fresh MHB and added to a clear, flat-bottom 96-well assay plate containing two-fold dilutions of two compounds in 8 by 8 dose-point matrices (or one compound for MIC determination). OD_{600} was measured using a Tecan Infinite M1000 Pro plate reader prior to incubation in a 37 °C stationary incubator. After incubation for 18 h, OD_{600} was measured again and background (0 h) reads were subtracted. The MIC values of the individual drugs were determined to be the concentration of the compound that resulted in a percent residual growth of $\leq 10\%$. The FIC of each compound was determined to be its MIC in combination with the other compound divided by its MIC alone. The reported FIC indices (FICIs) are the sum of FICs for the two compounds being tested (33). FICI values ≤ 0.5 were considered synergistic. Checkerboards and MICs were performed in at least duplicate.

Lysozyme assay for OM permeability

Assay was performed as previously described in Klobucar *et al.* (15). Briefly, *E. coli* BW25113 was grown overnight (~18 h) in MHB and subcultured 1:50 in fresh MHB media at 37 °C with shaking at 250 rpm to mid-exponential phase (OD₆₀₀ ~0.5). Subcultures were centrifuged and resuspended in 5 mM HEPES pH 7.2 to OD₆₀₀ 0.5. A 1 mL volume of cells was added to microfuge tubes containing the appropriate compound at 1/4 MIC and 50 µg/mL lysozyme (Sigma Aldrich, Fluka Analytical). Tubes were gently inverted to mix and left at room temperature for ~1 h for any cell debris to settle. A volume of 200 µL was transferred from each tube to a clear, flat bottom 96-well plate, and OD₆₀₀ was read using a Tecan Infinite M1000 Pro plate reader. Controls were included to ensure that the compound alone did not lyse cells and to find the baseline cell lysis by lysozyme alone.

β-lactamase assay for OM integrity

Assay was performed as previously described (15, 49). *E. coli* ML35 pBR322 cells grown overnight (~18 h) in MHB with 50 µg/mL ampicillin were subcultured 1:50 in fresh MHB and grown at 37 °C with shaking at 250 rpm to mid-exponential phase (OD₆₀₀ ~0.4-0.5), centrifuged, washed in 1x phosphate-buffered saline (PBS), and resuspended to OD₆₀₀ = 0.02 in PBS. A volume of 50 µL of the cell suspension was added to a clear, flat bottom 96-well plate containing 50 µL of PBS with a final concentration of 30 µM nitrocefin (Sigma-Aldrich) and the two-fold dilution of compound in DMSO or H₂O. No cell controls

were performed in parallel. Plates were incubated at 37 °C in a stationary incubator and read at 4 h using a Tecan Infinite M1000 Pro plate reader at 492 nm to monitor nitrocefin hydrolysis. Reads from the corresponding no cell control wells were subtracted from the 4 h timepoint.

β-galactosidase assay for IM integrity

Assay was performed as previously described (15, 49). *E. coli* ML35 pBR322 cells grown overnight (~18 h) in MHB with 50 µg/mL ampicillin were subcultured 1:50 in fresh MHB and grown at 37 °C with shaking at 250 rpm to mid-exponential phase (OD₆₀₀ ~0.4-0.5), centrifuged, washed in PBS, and resuspended to OD₆₀₀ = 0.02 in PBS. A volume of 50 µL of the cell suspension was added to a clear, flat bottom 96-well plate containing 50 µL of PBS with a final concentration of 1.5 mM of ONPG (Sigma-Aldrich) and the two-fold dilution of compound in DMSO or H₂O. Plates were incubated at 37 °C in a stationary incubator and read at 4 h using a Tecan Infinite M1000 Pro plate reader at 405 nm to monitor ONPG hydrolysis. Reads from the corresponding no cell control well were subtracted from the 4 h timepoint.

Cytotoxicity assays

Cytotoxicity was measured using the Gbiosciences Cytoscan-LDH cytotoxicity (Cat. #786-210, 786-324), which measures LDH release upon cell death. Briefly, HEK293 cells were maintained in DMEM supplemented with 10% FBS, 0.1 mM MEM non-essential amino acids, 6 mM L-glutamine, and 1 mM MEM sodium pyruvate. Cells were seeded at 5×10⁴ cells per well of a 384-well

tissue culture plate and incubated for ~20 h at 37 °C with 5% CO₂. Cherry-picked compound was added to each well in two-fold dilutions from 0-100 µM using the Echo 550 (LabCyte), and cells were incubated for 48 h. Plates were centrifuged at 500×g for 2 min and LDH release was measured according to manufacturer's instructions.

LpxC assay

LpxC assay was performed as previously described in Clements *et al.*, with slight modifications (45). Assays were performed in a 96-well black non-binding surface plate with a total volume of 100 µl per well containing 40 mM sodium morpholinoethanesulfonic acid (MES) buffer (pH 6.0), 0.02% Brij 35, 80 µM dithiothreitol, 25 µM UDP-3-O-(*R*-3-hydroxymyristoyl) GlcNAc Tris salt (Toronto Research Chemicals), 50 ng/mL *E. coli* LpxC (BPS Bioscience), 1% DMSO vehicle with or without MAC-0485042. Reactions were started upon LpxC addition and incubated at 37 °C for 60 min prior to stopping with 40 µl 0.625 M sodium hydroxide. After 10 min at 37 °C, 40 µl of 0.625 M acetic acid was added to hydrolyze the 3-O-acyl ester. A volume of 33.5 µl of *o*-phthaldialdehyde solution complete (Sigma-Aldrich) was added to detect the UDP-glucosamine. Fluorescence was measured using a Tecan Infinite M1000 Pro plate reader using 340 nm excitation and 455 nm emission wavelengths. CHIR-090 at 0.25 µg/mL was used as a control for full enzyme inhibition. The IC₅₀ was calculated using GraphPad Prism.

Funding

Work in the lab of E.D.B. was supported by a Tier I Canada Research Chair award, a Foundation grant from the Canadian Institutes of Health Research (CIHR; FRN 143215), a grant from the Ontario Research Fund (RE09-047), and grants from GlycoNet (AM-32, ID-02). This research was enabled by an endowed gift to McMaster University from the Boris Family. K.K. was supported by a scholarship from the CIHR Canada Graduate Scholarships (CGS-D).

Acknowledgements

We thank the McMaster Centre for Microbial Chemical Biology (CMCB) for assisting with high-throughput chemical screening, as well as S. French and S. El Zahed for providing the screening analysis code. We thank Spero Therapeutics and Northern Antibiotics for providing SPR741, H. Mori for providing the Keio collection, G. Storz for providing the sRNA and small peptide deletion collection, and O. El-Halfawy for providing the *E. coli* ML35 pBR322 strain. We also thank B. Clarke, C. Whitfield, and R. Gordzevich for helpful discussions surrounding the project.

References

1. Tacconelli E, Carrara E, Savoldi A, Harbarth S, Mendelson M, Monnet DL, Pulcini C, Kahlmeter G, Kluytmans J, Carmeli Y, Ouellette M, Outtersson K, Patel J, Cavalieri M, Cox EM, Houchens CR, Grayson ML, Hansen P, Singh N, Theuretzbacher U, Magrini N, Aboderin AO, Al-Abri SS, Awang Jalil N, Benzonana N, Bhattacharya S, Brink AJ, Burkert FR, Cars O, Cornaglia G, Dyar OJ, Friedrich AW, Gales AC, Gandra S, Giske CG, Goff DA, Goossens H, Gottlieb T, Guzman Blanco M, Hryniewicz W, Kattula D, Jinks T, Kanj SS, Kerr L, Kieny MP, Kim YS, Kozlov RS, Labarca J, Laxminarayan R, Leder K, Leibovici L, Levy-Hara G, Littman J, Malhotra-Kumar S, Manchanda V, Moja L, Ndoye B, Pan A, Paterson DL, Paul M, Qiu H, Ramon-Pardo P, Rodríguez-Baño J, Sanguinetti M, Sengupta S, Sharland M, Si-Mehand M, Silver LL, Song W, Steinbakk M, Thomsen J, Thwaites GE, van der Meer JW, Van Kinh N, Vega S, Villegas MV, Wechsler-Fördös A, Wertheim HFL, Wesangula E, Woodford N, Yilmaz FO, Zorzet A. 2018. Discovery, research, and development of new antibiotics: the WHO priority list of antibiotic-resistant bacteria and tuberculosis. *Lancet Infect Dis* 18:318–327.
2. Murray CJL, Ikuta KS, Sharara F, Swetschinski L, Robles Aguilar G, Gray A, Han C, Bisignano C, Rao P, Wool E, Johnson SC, Browne AJ, Chipeta MG, Fell F, Hackett S, Haines-Woodhouse G, Kashef Hamadani BH, Kumaran EAP, McManigal B, Agarwal R, Akech S, Albertson S, Amuasi J, Andrews J, Aravkin A, Ashley E, Bailey F, Baker S, Basnyat B, Bekker A, Bender R, Bethou A, Bielicki J, Boonkasidecha S, Bukosia J, Carvalho C, Castañeda-Orjuela C, Chansamouth V, Chaurasia S, Chiurchiù S, Chowdhury F, Cook AJ, Cooper B, Cressey TR, Criollo-Mora E, Cunningham M, Darboe S, Day NPJ, De Luca M, Dokova K, Dramowski A, Dunachie SJ, Eckmanns T, Eibach D, Emami A, Feasey N, Fisher-Pearson N, Forrest K, Garrett D, Gastmeier P, Giref AZ, Greer RC, Gupta V, Haller S, Haselbeck A, Hay SI, Holm M, Hopkins S, Iregbu KC, Jacobs J, Jarovsky D, Javanmardi F, Khorana M, Kissoon N, Kobeissi E, Kostyanov T, Krapp F, Krumkamp R, Kumar A, Kyu HH, Lim C, Limmathurotsakul D, Loftus MJ, Lunn M, Ma J, Mturi N, Munera-Huertas T, Musicha P, Mussi-Pinhata MM, Nakamura T, Nanavati R, Nangia S, Newton P, Ngoun C, Novotney A, Nwakanma D, Obiero CW, Olivas-Martinez A, Olliaro P, Ooko E, Ortiz-Brizuela E, Peleg AY, Perrone C, Plakkal N, Ponce-de-Leon A, Raad M, Ramdin T, Riddell A, Roberts T, Robotham JV, Roca A, Rudd KE, Russell N, Schnall J, Scott JAG, Shivamallappa M, Sifuentes-Osornio J, Steenkeste N, Stewardson AJ, Stoeva T, Tasak N, Thaiprakong A, Thwaites G, Turner C, Turner P, van Doorn HR, Velaphi S, Vongpradith A, Vu H, Walsh T, Waner S, Wangrangsimakul

- T, Wozniak T, Zheng P, Sartorius B, Lopez AD, Stergachis A, Moore C, Dolecek C, Naghavi M.** 2022. Global burden of bacterial antimicrobial resistance in 2019: a systematic analysis. *Lancet*.
3. **Silver LL.** 2011. Challenges of antibacterial discovery. *Clin Microbiol Rev* **24**:71–109.
 4. **Emmerson AM.** 2003. The quinolones: decades of development and use. *J Antimicrob Chemother* **51**:13–20.
 5. **Silver LL.** 2016. A Gestalt approach to Gram-negative entry. *Bioorg Med Chem* **24**:6379–6389.
 6. **Silhavy TJ, Kahne D, Walker S.** 2010. The bacterial cell envelope. *Cold Spring Harb Perspect Biol* **2**:a000414.
 7. **Raetz CRH, Whitfield C.** 2002. Lipopolysaccharide endotoxins. *Annu Rev Biochem* **71**:635–700.
 8. **Nikaido H.** 2003. Molecular basis of bacterial outer membrane permeability revisited. *Microbiol Mol Biol Rev* **67**:593–656.
 9. **Clifton LA, Skoda MW, Le Brun AP, Ciesielski F, Kuzmenko I, Holt SA, Lakey JH.** 2015. Effect of divalent cation removal on the structure of Gram-negative bacterial outer membrane models. *Langmuir* **31**:404–412.
 10. **Nikaido H.** 1994. Prevention of drug access to bacterial targets: Permeability barriers and active efflux. *Science* **264**:382–388.
 11. **Du D, Wang Z, James NR, Voss JE, Klimont E, Ohene-Agyei T, Venter H, Chiu W, Luisi BF.** 2014. Structure of the AcrAB-TolC multidrug efflux pump. *Nature* **509**:512–515.
 12. **Delcour AH.** 2009. Outer membrane permeability and antibiotic resistance. *Biochim Biophys Acta* **1794**:808–816.
 13. **Klobucar K, Brown ED.** 2021. New potentiators of ineffective antibiotics: Targeting the Gram-negative outer membrane to overcome intrinsic resistance. *Curr Opin Chem Biol* **66**:102099.
 14. **Klobucar K, French S, Côté J-P, Howes JR, Brown ED.** 2020. Genetic and chemical-genetic interactions map biogenesis and permeability determinants of the outer membrane of *Escherichia coli*. *mBio* **11**:e00161-20.
 15. **Klobucar K, Côté J-P, French S, Borrillo L, Guo ABY, Serrano-Wu MH, Lee KK, Hubbard B, Johnson JW, Gaulin JL, Magolan J, Hung DT, Brown ED.** 2021. Chemical screen for vancomycin antagonism uncovers probes of the Gram-negative outer membrane. *ACS Chem Biol* **16**:929–942.
 16. **Stokes JM, MacNair CR, Ilyas B, French S, Côté J-P, Bouwman C, Farha MA, Sieron AO, Whitfield C, Coombes BK, Brown ED.** 2017. Pentamidine sensitizes Gram-negative pathogens to antibiotics and overcomes acquired colistin resistance. *Nat Microbiol* **2**:17028.
 17. **MacNair CR, Farha MA, Serrano-Wu MH, Lee KK, Hubbard B, Côté J-P, Carfrae LA, Tu MM, Gaulin JL, Hunt DK, Hung DT, Brown ED.** 2022. Preclinical development of pentamidine analogs identifies a potent and

- nontoxic antibiotic adjuvant. *ACS Infect Dis* **8**:768–777.
18. **MacNair CR, Brown ED.** 2020. Outer membrane disruption overcomes intrinsic, acquired, and spontaneous antibiotic resistance. *mBio* **11**:e01615-20.
 19. **Opperman TJ, Nguyen ST.** 2015. Recent advances toward a molecular mechanism of efflux pump inhibition. *Front Microbiol* **6**:421.
 20. **Cox G, Wright GD.** 2013. Intrinsic antibiotic resistance: Mechanisms, origins, challenges and solutions. *Int J Med Microbiol* **303**:287–292.
 21. **Johnson JW, Ellis MJ, Piquette ZA, MacNair C, Carfrae L, Bhandu T, Ritchie NE, Saliba P, Brown ED, Magolan J.** 2022. Antibacterial activity of metergoline analogues: revisiting the ergot alkaloid scaffold for antibiotic discovery. *ACS Med Chem Lett* **13**:284–291.
 22. **Krishnamoorthy G, Wolloscheck D, Weeks JW, Croft C, Rybenkov V V., Zgurskaya HI.** 2016. Breaking the permeability barrier of *Escherichia coli* by controlled hyperporination of the outer membrane. *Antimicrob Agents Chemother* **60**:7372–7381.
 23. **Hung LW, Kim HB, Murakami S, Gupta G, Kim CY, Terwilliger TC.** 2013. Crystal structure of AcrB complexed with linezolid at 3.5 Å resolution. *J Struct Funct Genomics* **14**:71–75.
 24. **Ferreira RJ, Kasson PM.** 2019. Antibiotic uptake across Gram-negative outer membranes: better predictions towards better antibiotics. *ACS Infect Dis* **5**:2096–2104.
 25. **Baba T, Ara T, Hasegawa M, Takai Y, Okumura Y, Baba M, Datsenko KA, Tomita M, Wanner BL, Mori H.** 2006. Construction of *Escherichia coli* K-12 in-frame, single-gene knockout mutants: the Keio collection. *Mol Syst Biol* **2**:2006.0008.
 26. **Hobbs EC, Astarita JL, Storz G.** 2010. Small RNAs and small proteins involved in resistance to cell envelope stress and acid shock in *Escherichia coli*: analysis of a bar-coded mutant collection. *J Bacteriol* **192**:59–67.
 27. **Taylor PL, Rossi L, De Pascale G, Wright GD.** 2012. A forward chemical screen identifies antibiotic adjuvants in *Escherichia coli*. *ACS Chem Biol* **7**:1547–1555.
 28. **Muheim C, Götzke H, Eriksson AU, Lindberg S, Lauritsen I, Nørholm MHH, Daley DO.** 2017. Increasing the permeability of *Escherichia coli* using MAC13243. *Sci Rep* **7**:17629.
 29. **Barker CA, Allison SE, Zlitni S, Nguyen ND, Das R, Melacini G, Capretta AA, Brown ED.** 2013. Degradation of MAC13243 and studies of the interaction of resulting thiourea compounds with the lipoprotein targeting chaperone LolA. *Bioorg Med Chem Lett* **23**:2426–2431.
 30. **Buss JA, Baidin V, Welsh MA, Flores-Kim J, Cho H, Wood BM, Uehara T, Walker S, Kahne D, Bernhardt TG.** 2019. Pathway-directed screen for inhibitors of the bacterial cell elongation machinery. *Antimicrob Agents Chemother* **63**:e101530-18.
 31. **Sköld O.** 2010. Sulfonamides and trimethoprim. *Expert Rev Anti Infect*

- Ther **8**:1–6.
32. **Zhou A, Kang TM, Yuan J, Beppler C, Nguyen C, Mao Z, Nguyen MQ, Yeh P, Miller JH.** 2015. Synergistic interactions of vancomycin with different antibiotics against *Escherichia coli*: trimethoprim and nitrofurantoin display strong synergies with vancomycin against wild-type *E. coli*. *Antimicrob Agents Chemother* **59**:276–281.
 33. **Lambert RJW, Lambert R.** 2003. A model for the efficacy of combined inhibitors. *J Appl Microbiol* **95**:734–743.
 34. **Odds FC.** 2003. Synergy, antagonism, and what the checkerboard puts between them. *J Antimicrob Chemother* **52**:1.
 35. **French S, Farha MA, Ellis MJ, Sameer Z, Côté J-P, Cotroneo N, Lister T, Rubio A, Brown ED.** 2020. Potentiation of antibiotics against Gram-negative bacteria by polymyxin B analogue SPR741 from unique perturbation of the outer membrane. *ACS Infect Dis* **6**:1405–1412.
 36. **Neilands JB.** 1967. Hydroxamic acids in nature. *Science* **156**:1443–1447.
 37. **Keth J, Johann T, Frey H.** 2020. Hydroxamic acid: An underrated moiety? Marrying bioinorganic chemistry and polymer science. *Biomacromolecules* **21**:2546–2556.
 38. **Whittington DA, Rusche KM, Shin H, Fierke CA, Christianson DW.** 2003. Crystal structure of LpxC, a zinc-dependent deacetylase essential for endotoxin biosynthesis. *Proc Natl Acad Sci U S A* **100**:8146–8150.
 39. **Young K, Silver LL, Bramhill D, Cameron P, Eveland SS, Raetz CRH, Hyland SA, Anderson MS.** 1995. The *envA* permeability/cell division gene of *Escherichia coli* encodes the second enzyme of lipid A biosynthesis: UDP-3-O-(*R*-3-hydroxymyristoyl)-*N*-acetylglucosamine deacetylase. *J Biol Chem* **270**:30384–30391.
 40. **Erwin AL.** 2016. Antibacterial drug discovery targeting the lipopolysaccharide biosynthetic enzyme LpxC. *Cold Spring Harb Perspect Med* **6**:a025304.
 41. **Guay DRP.** 2007. Drug forecast - the peptide deformylase inhibitors as antibacterial agents. *Ther Clin Risk Manag* **3**:513–525.
 42. **Grant SK, Green BG, Kozarich JW.** 2001. Inhibition and structure-activity studies of methionine hydroxamic acid derivatives with bacterial peptide deformylase. *Bioorg Chem* **29**:211–222.
 43. **Sanderson KE, MacAlister T, Costerton JW, Cheng KJ.** 1974. Permeability of lipopolysaccharide deficient (rough) mutants of *Salmonella typhimurium* to antibodies, lysozyme, and other agents. *Can J Microbiol* **20**:1135–1145.
 44. **Hancock REW, Wong PGW.** 1984. Compounds which increase the permeability of the *Pseudomonas aeruginosa* outer membrane. *Antimicrob Agents Chemother* **26**:48–52.
 45. **Clements JM, Coignard F, Johnson I, Chandler S, Palan S, Waller A, Wijkmans J, Hunter MG.** 2002. Antibacterial activities and characterization of novel inhibitors of LpxC. *Antimicrob Agents Chemother* **46**:1793–1799.

46. **García-Quintanilla M, Caro-Vega JM, Pulido MR, Moreno-Martínez P, Pachón J, McConnell MJ.** 2016. Inhibition of LpxC increases antibiotic susceptibility in *Acinetobacter baumannii*. *Antimicrob Agents Chemother* **60**:5076–5079.
47. **MacNair CR, Tsai CN, Brown ED.** 2020. Creative targeting of the Gram-negative outer membrane in antibiotic discovery. *Ann N Y Acad Sci* **1459**:69–85.
48. **Cohen F, Aggen JB, Andrews LD, Assar Z, Boggs J, Choi T, Dozzo P, Easterday AN, Haglund CM, Hildebrandt DJ, Holt MC, Joly K, Jubb A, Kamal Z, Kane TR, Konradi AW, Krause KM, Linsell MS, Machajewski TD, Miroshnikova O, Moser HE, Nieto V, Phan T, Plato C, Serio AW, Seroogy J, Shakhmin A, Stein AJ, Sun AD, Sviridov S, Wang Z, Wlasichuk K, Yang W, Zhou X, Zhu H, Cirz RT.** 2019. Optimization of LpxC inhibitors for antibacterial activity and cardiovascular safety. *ChemMedChem* **14**:1560–1572.
49. **Farha MA, El-Halfawy OM, Gale RT, Macnair CR, Carfrae LA, Zhang X, Jentsch NG, Magolan J, Brown ED.** 2020. Uncovering the hidden antibiotic potential of cannabis. *ACS Infect Dis* **6**:338–346.
50. **Boman H, Eriksson-Greenberg K, Normark S, Matsson E.** 1968. Resistance of *Escherichia coli* to penicillins. *Genet Res (Camb)* **12**:169–185.
51. **Normark S, Boman HG, Matsson E.** 1969. Mutant of *Escherichia coli* with anomalous cell division and ability to decrease episomally and chromosomally mediated resistance to ampicillin and several other antibiotics. *J Bacteriol* **97**:1334–1342.
52. **French S, Mangat C, Bharat A, Côté J-P, Mori H, Brown ED.** 2016. A robust platform for chemical genomics in bacterial systems. *Mol Biol Cell* **27**:1015–1025.
53. **Keseler IM, Mackie A, Santos-Zavaleta A, Billington R, Bonavides-Martínez C, Caspi R, Fulcher C, Gama-Castro S, Kothari A, Krummenacker M, Latendresse M, Muñiz-Rascado L, Ong Q, Paley S, Peralta-Gil M, Subhraveti P, Velázquez-Ramírez DA, Weaver D, Collado-Vides J, Paulsen I, Karp PD.** 2017. The EcoCyc database: reflecting new knowledge about *Escherichia coli* K-12. *Nucleic Acids Res* **45**:D543–D550.
54. **Supek F, Bošnjak M, Škunca N, Šmuc T.** 2011. REVIGO summarizes and visualizes long lists of Gene Ontology terms. *PLoS One* **6**:e21800.
55. **Mangat CS, Bharat A, Gehrke SS, Brown ED.** 2014. Rank ordering plate data facilitates data visualization and normalization in high-throughput screening. *J Biomol Screen* **19**:1314–1320.

Figures

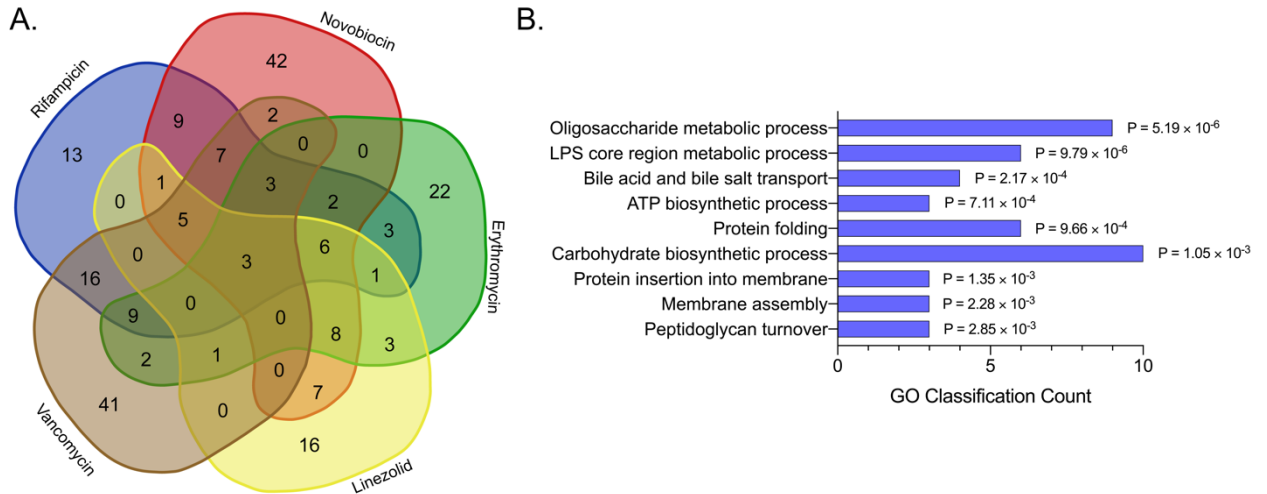


Figure 1: Genetic requirements for resistance to Gram-positive-targeting antibiotics in *E. coli*. (A.) Shown is a Venn diagram with the number of *E. coli* gene deletion mutants that were sensitive to the antibiotics rifampicin (blue), novobiocin (red), erythromycin (green), linezolid (yellow), and vancomycin (brown). The Keio and sRNA deletion collections were arrayed on solid media agar containing subinhibitory concentrations of each antibiotic. Colonies which grew less than 2σ below the mean in each antibiotic were defined as sensitive. (B.) Gene deletion strains which were sensitive to at least two of the antibiotics were categorized by GO terms for biological process. The topmost enriched and non-redundant GO terms are shown, where the GO classification count is the number of genes present belonging to each GO term. GO term enrichment and P value calculations (using a Fisher exact test) were performed using EcoCyc (53).

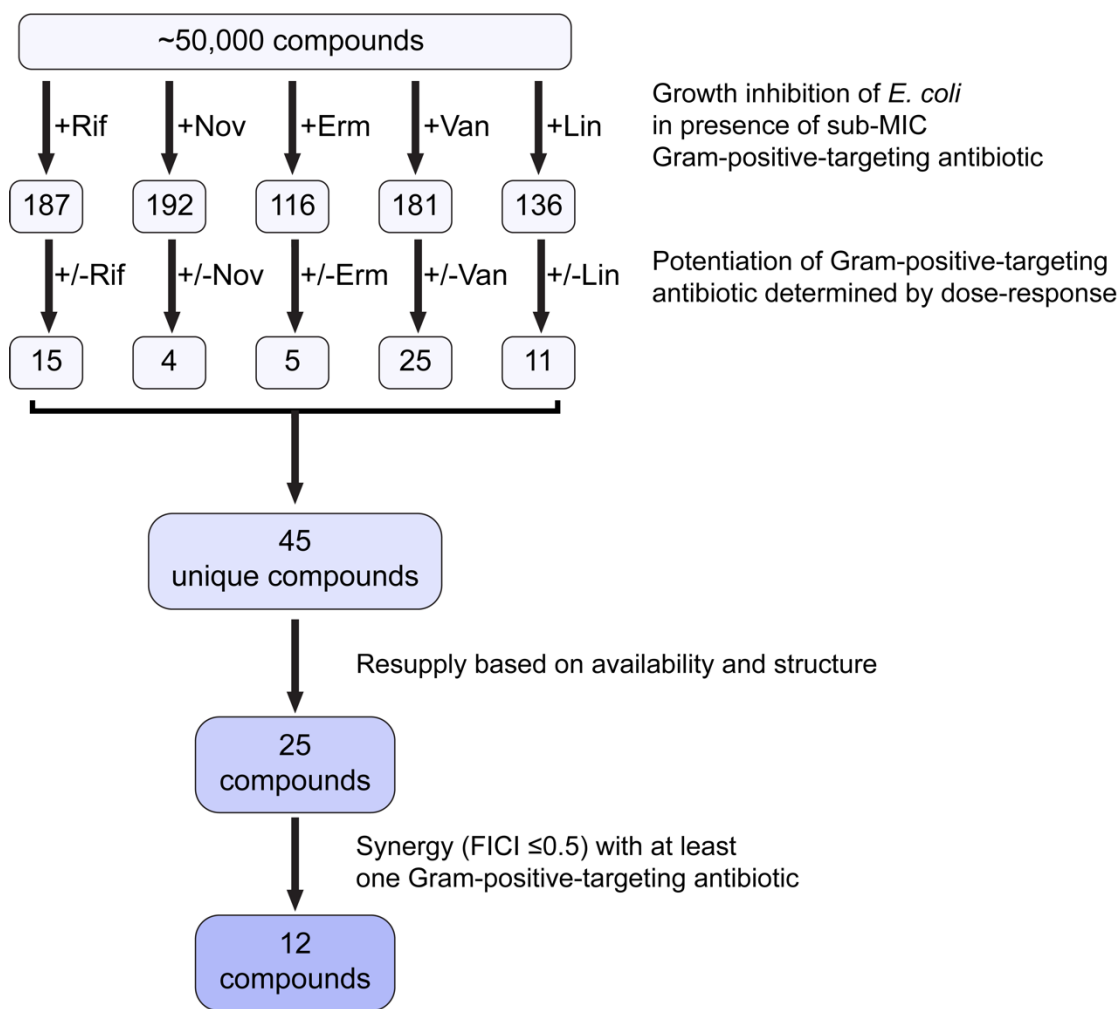


Figure 2: Workflow of the chemical screens for potentiation of Gram-positive-targeting antibiotics. A collection of ~50,000 compounds was screened for growth inhibition in rich microbiological media with subinhibitory concentrations (1/4 MIC) of each of the antibiotics, rifampicin (Rif), novobiocin (Nov), erythromycin (Erm), vancomycin (Van), and linezolid (Lin), against *E. coli*. Active compounds from the primary screens were subsequently tested for growth inhibitory activity against *E. coli* alone and in the presence of the corresponding Gram-positive-targeting antibiotic. Of those, 45 compounds had MICs at least two-fold more potent in the presence of the antibiotic. The resupplied compounds were assessed for synergy with rifampicin, novobiocin, vancomycin, erythromycin, and linezolid using checkerboard broth microdilution assays and 12 compounds showed synergy (FICI ≤ 0.5) with at least one of the antibiotics.

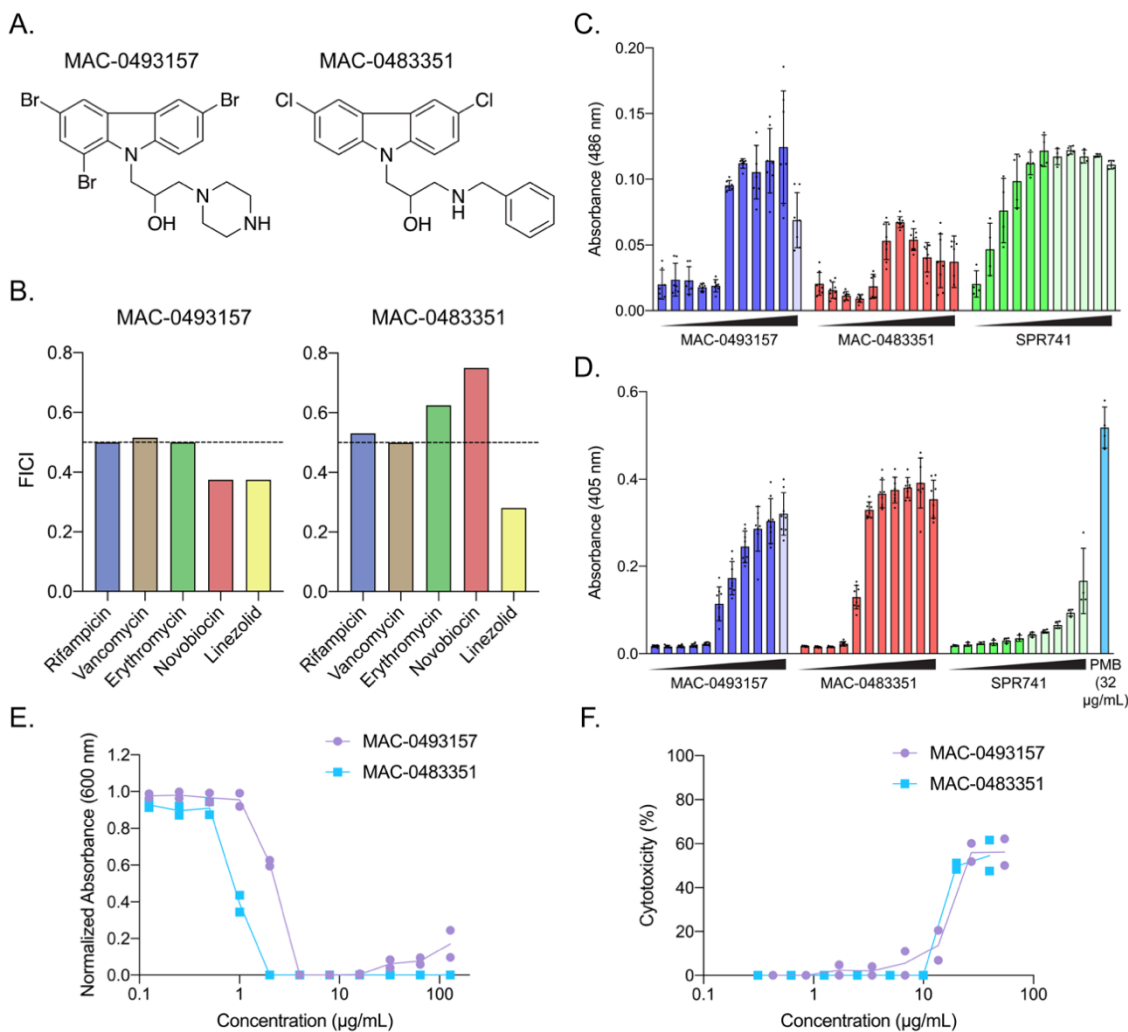


Figure 3: MAC-0493157 and MAC-0483351 potentiate the activity of linezolid against *E. coli* through outer and inner membrane disruption. (A.) Shown are chemical structures of MAC-0493157, an active in the linezolid and novobiocin potentiation screens, and MAC-0483351, an active in the linezolid potentiation screen. (B.) Fractional inhibitory concentration indices (FICIs) calculated from checkerboard broth microdilution assays confirmed synergy between linezolid and the two compounds, MAC-0493157 and MAC-0483351, against *E. coli* in rich microbiological media. MAC-0493157 has an MIC of 128 µg/mL alone, and MAC-0483351 has an MIC of >64 µg/mL alone. The dashed line at FICI=0.5 indicates the cutoff value for synergy. The FICI value shown is representative of two replicates. (C.) Disruption of the OM was measured by a β -lactamase assay in *E. coli*, where increased absorbance indicated nitrocefin hydrolysis by periplasmic β -lactamase. Concentrations of each compound shown are two-fold dilutions from 0 (left) to 128 (right) µg/mL, and those concentrations above the MIC of the compound have been coloured with an opacity of 25%. SPR741, a known OM disruptor, was used as a positive control. (D.) Disruption of the IM was measured

by a β -galactosidase assay in *E. coli*, in which increased absorbance at 405 nm indicates ONPG hydrolysis by cytoplasmic β -galactosidase. SPR741 is known to have minimal activity on the IM and is less IM active than the high control, 32 μ g/mL of polymyxin B (PMB). (E.) Potency analysis of MAC-0493157 and MAC-0483351 in *S. aureus* reveals single digit MIC for both compounds. (F.) Cytotoxicity of MAC-0493157 and MAC-0483351 in HEK293 as determined by LDH release assay.

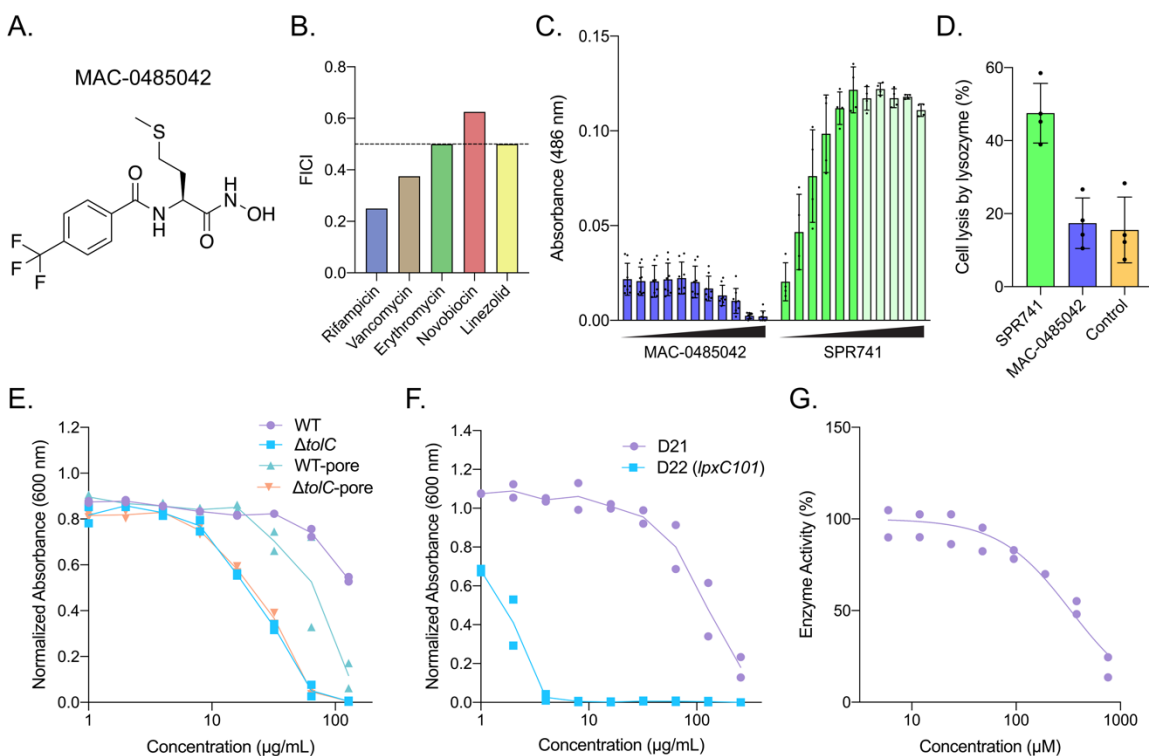


Figure 4: MAC-0485042 potentiates rifampicin and vancomycin activity in *E. coli* through inhibition of LpxC. (A.) Chemical structure of MAC-0485042, an active from the vancomycin potentiation screen. (B.) FICIs calculated from checkerboard broth microdilution assays revealed synergy between MAC-0485042 and four of the five the Gram-positive-targeting antibiotics, against *E. coli* in rich microbiological media. MAC-0485042 has an MIC of 256 $\mu\text{g}/\text{mL}$ alone. The dashed line at FICI=0.5 indicates the cutoff value for synergy. The FICI value shown is representative of two replicates. (C.) Disruption of the OM was measured by a β -lactamase assay in *E. coli*, where increased absorbance indicates nitrocefin hydrolysis by periplasmic β -lactamase. Concentrations of each compound shown are two-fold dilutions from 0 (left) to 128 (right) $\mu\text{g}/\text{mL}$, and those above the MIC of the compound have been coloured with an opacity of 25%. SPR741, which is known to disrupt the OM, was used as a positive control. (D.) Disruption of OM integrity was measured by permeability of lysozyme in *E. coli* using subinhibitory concentrations of SPR741 (2 $\mu\text{g}/\text{mL}$) and MAC-0485042 (64 $\mu\text{g}/\text{mL}$). The control was cell lysis by lysozyme in the absence of compound. (E.) Potency analysis of MAC-0485042 in wild type, efflux-deficient ($\Delta tolC$), and hyperporinated (pore) strains of *E. coli* reveal susceptibility to efflux. (F.) Potency analysis of MAC-0485042 in D21 (parent of *lpxC101* mutant) and D22 (*lpxC101* mutant) strains of *E. coli* shows sensitivity of D22 to the compound. (G.) *In vitro* inhibition of *E. coli* LpxC by MAC-0485042.

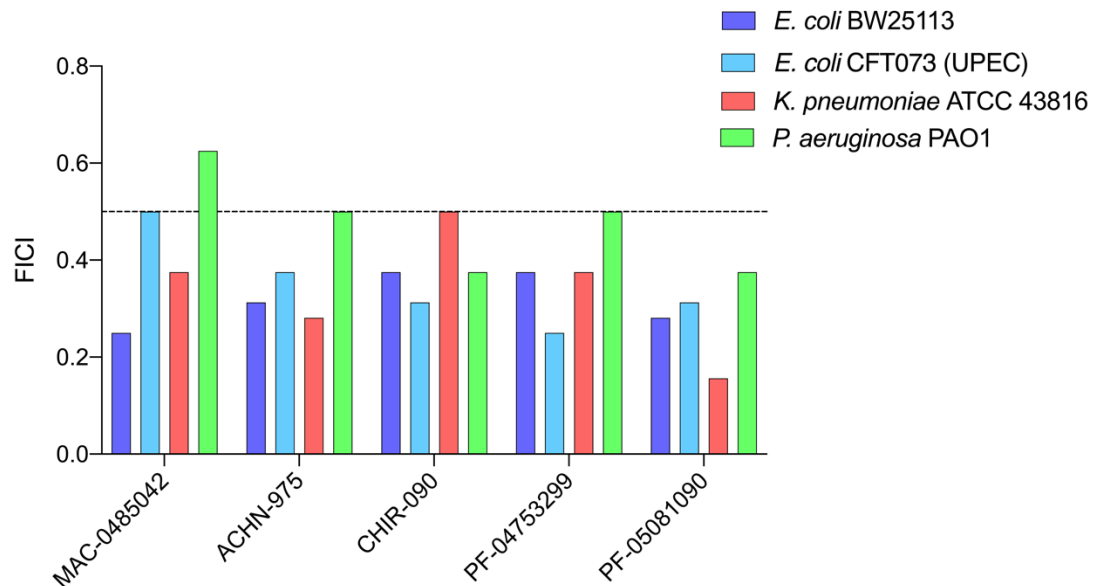


Figure 5: LpxC inhibitors can be used to potentiate the activity of rifampicin in pathogens. Shown are FICIs calculated from checkerboard broth microdilution assays of MAC-0485042 and commercially available LpxC inhibitors (ACHN-975, CHIR-090, PF-04753299, PF-05081090) in combination with rifampicin in *E. coli* BW25113, *E. coli* CFT073, *K. pneumoniae* ATCC 43816, and *P. aeruginosa* PAO1. The MICs of all commercially available LpxC inhibitors are $\leq 8 \mu\text{g/mL}$ and MICs of MAC-0485042 are $\geq 256 \mu\text{g/mL}$ for all strains tested. The dashed line at FICI=0.5 indicates the cutoff value for synergy. Values shown are representative of two replicates.

Tables

Table 1: Minimum inhibitory concentrations of Gram-positive-targeting antibiotics in wild type (WT), hyperporinated (pore), and efflux-deficient ($\Delta toIC$) strains of *E. coli* BW25113.

Antibiotic	Minimum Inhibitory Concentration ($\mu\text{g/mL}$)			
	WT	WT-Pore	$\Delta toIC$	$\Delta toIC$ -Pore
Rifampicin	4	≤ 0.125	4	≤ 0.125
Vancomycin	128	≤ 4	256	≤ 4
Novobiocin	64	4-8	≤ 1	≤ 1
Erythromycin	32	1	2	≤ 0.5
Linezolid	128-256	32	≤ 4	≤ 4

Supplementary Material

Figures

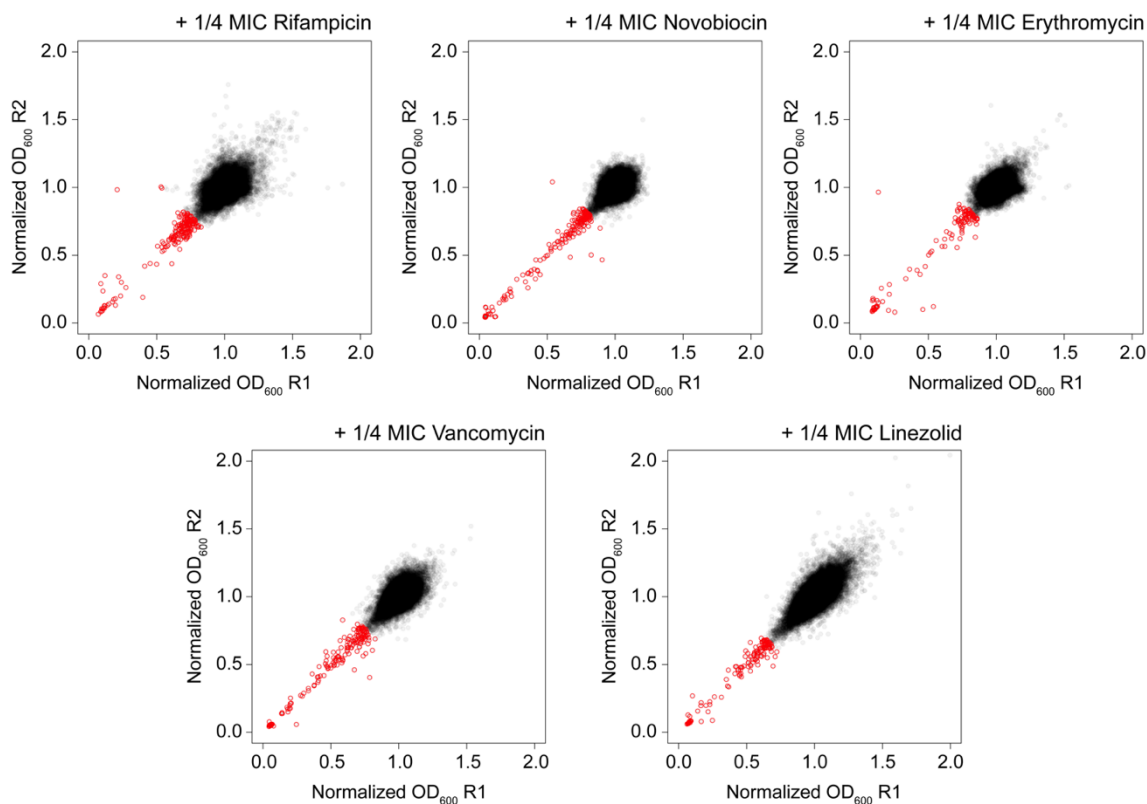


Figure S1: Replica plots of normalized *E. coli* growth in all five primary chemical screens performed in duplicate. Growth was measured by absorbance at 600 nm (OD₆₀₀) and normalization was performed as described in Mangat *et al* (55). Active compounds, shown as red circles, were defined as those which resulted in growth less than 4 σ below the mean.

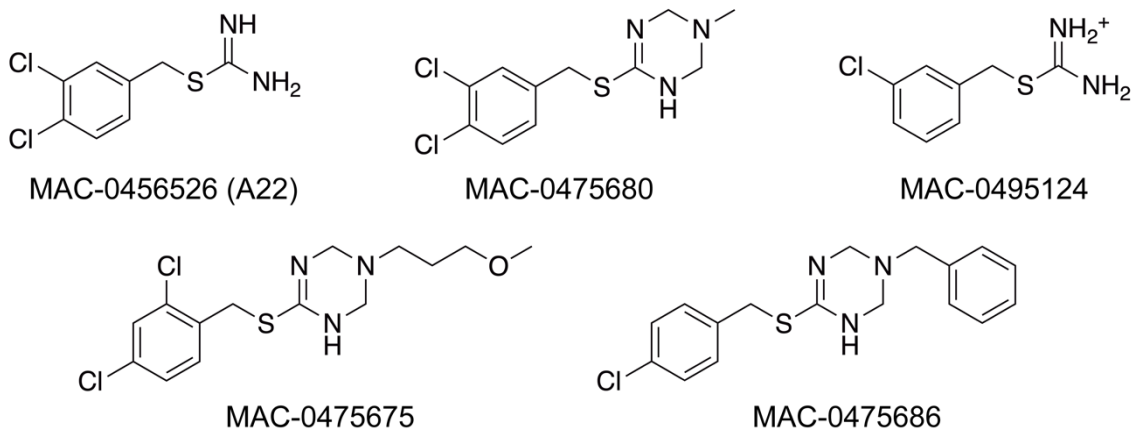


Figure S2: Chemical structures of A22 analogues detected as actives from the primary potentiation screens.

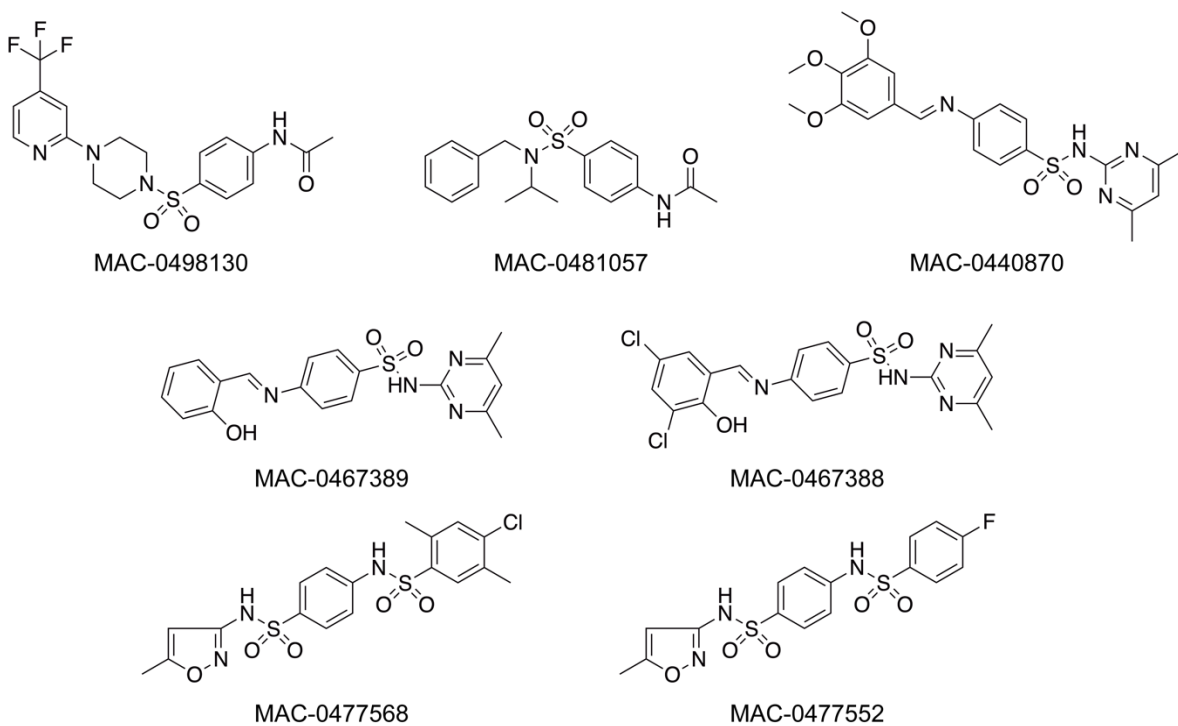


Figure S3: Chemical structures of sulfonamides detected as actives from the primary vancomycin potentiation screen.

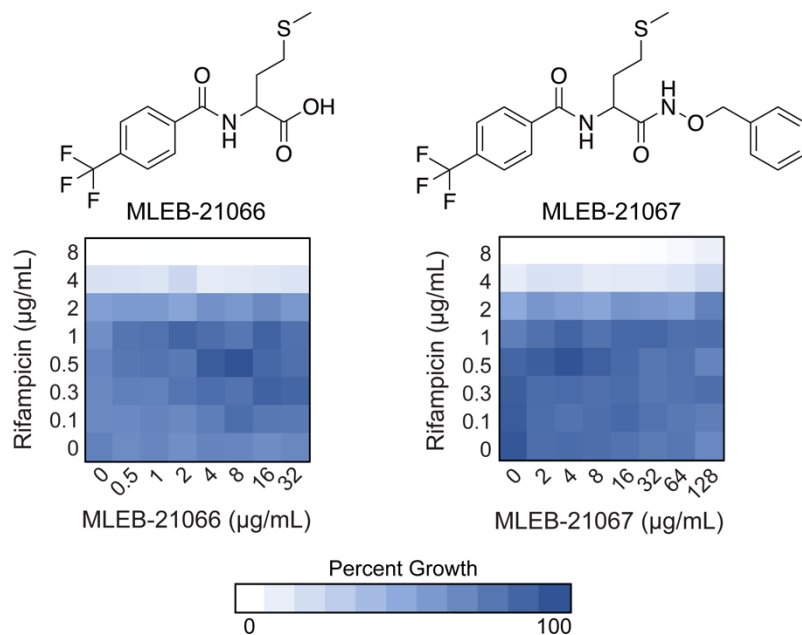


Figure S4: The hydroxamate moiety is required for potentiation activity of MAC-0485042. Shown are checkerboard broth microdilution assays of MAC-0485042 and two structural analogues lacking the hydroxamic acid group, MLEB-21066 and MLEB-21067, in combination with rifampicin in *E. coli* BW25113.

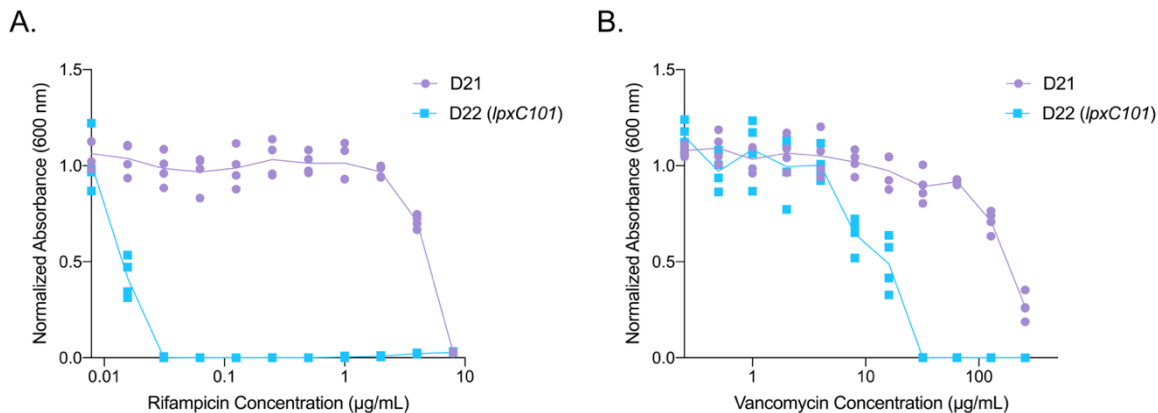
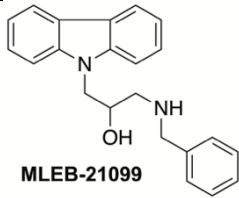
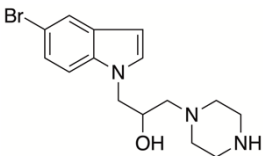
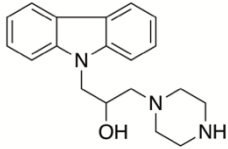
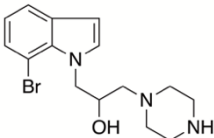
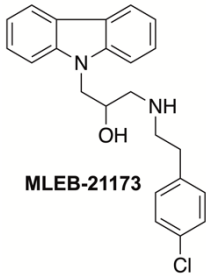
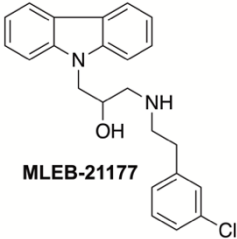


Figure S5: The *E. coli lpxC101* D22 mutant is hypersensitive to (A) rifampicin and (B) vancomycin, compared to the parental D21 strain.

Tables

Table S1: Potentiation activity of MAC-0493157 and MAC-0483351 analogues in *E. coli* BW25113.

Compound	MIC ($\mu\text{g/mL}$)	FICI ^a	Compound	MIC ($\mu\text{g/mL}$)	FICI ^a
 MLEB-21099	128	0.75	 MLEB-21184	>128	≤ 0.75
 MLEB-21100	>128	≤ 0.62	 MLEB-21185	>128	≤ 0.75
 MLEB-21173	16	0.56	 MLEB-21177	32	1

^a FICI data reported are for compounds in combination with linezolid. Refer to the Methods section for FICI determination.

CHAPTER V – Conclusion

Summary

The work presented in this thesis explores genetic and chemical avenues to increase the permeability of the Gram-negative OM to large-scaffold antibiotics in studies of basic bacterial biology and preclinical drug discovery. Chapter 2 describes the crossing of 39 OM-related query gene deletion strains with non-essential gene and sRNA deletions strains to generate ~155,400 double deletion strains in *E. coli*. The growth of these double deletion strains was quantified alone and in the presence of subinhibitory concentrations of the large-scaffold antibiotics rifampicin and vancomycin to probe both genetic interactions and permeability of the strains. SSL interactions between *yhdP*, an enigmatic gene implicated in ECA regulation, and LPS inner core biosynthetic genes revealed a connection between these two processes in the maintenance of OM and peptidoglycan integrity. Chapter 3 describes the implementation of a chemical screening platform for antagonism of vancomycin activity at cold temperatures in *E. coli*. This led to the discovery of liproxstatin-1 and MAC-0568743 as compounds which are specifically active on the OM, while sparing the integrity of the IM, fulfilling a need for OM-specific probes to study OM permeability in Gram-negative pathogens. Lastly, chapter 4 describes the genetic determinants for resistance to five Gram-positive-targeting antibiotics in *E. coli* to build a target list for chemical screens for antibiotic potentiators. These chemical screens led to the characterization of two linezolid potentiating compounds that were analogues of one another, which were found to be active on both the OM and IM. Furthermore,

a hydroxamate-containing compound was found to potentiate the activity of rifampicin and vancomycin likely through weak inhibition of LpxC. This prompted investigations of other known LpxC inhibitors as antibiotic potentiators in Gram-negative bacteria. This thesis work using both genetic and chemical perturbations has shown that targeting OM permeability is certainly promising for antibiotic potentiation efforts. Here, I hope to address some of the lessons I have learned, prospective avenues for future work, and outlook for the field.

Lessons learned

Although chapter 2 was presented in such a way where the focus was on characterizing novel biology of the OM, it was not the sole intention behind this project. The query gene deletion strains used for the SGAs were chosen because they were shown to antagonize the activity of vancomycin at cold temperatures (1), and in theory were the genetic targets for the compound screen of the same phenotype performed in chapter 3. The genetic interaction fingerprints of the query gene deletions generated in the SGAs were intended to be a tool for uncovering the mechanism of action for compounds with the same vancomycin antagonism phenotype. Despite the discovery of pentamidine as a physical membrane disruptor in the pilot chemical screen (2), we did not expect that the compounds uncovered would almost exclusively be membrane active. This may simply be due to the difficulty in finding enzyme inhibitors with whole cell activity due to susceptibility to efflux or lack of permeability (3). For instance, previously

reported inhibitors of LPS core biosynthesis have lacked any whole cell activity (4–6). If physical OM disruptors are not the desired compounds of this screening platform, investigators would benefit from secondary screening for membrane activity using assays such as those used throughout chapters 3 and 4 on cherry picked amounts of compound prior to the resupply stage.

Additionally, the potentiator compounds in chapters 3 and 4 of this thesis were discovered in screens of *E. coli* BW25113. Recognizing the ease of working with a model Gram-negative organism and all the genetic tools and databases that exist for *E. coli*, screening with a lab strain has pitfalls. Most importantly, investigators must be aware of the risk that results may not translate to other Gram-negatives, or even other pathogenic strains of *E. coli*. This is particularly true for OM related phenotypes, as *E. coli* K-12 lacks O-antigen (7). Many of the actives found in chapter 4 were only active on *E. coli* and none of the other Gram-negatives tested. For drug discovery efforts, it is important to consider which organisms have the highest need for treatments to increase the chances of compounds ever advancing past the preclinical discovery phase.

Future directions

The study presented in chapter 2 contains a wealth of synthetic interaction data that has not been extensively explored. Of the ~1000 detected SSL conditions in the no drug condition, we have only characterized a subset of four interactions in depth relating to our described phenotype between $\Delta yhdP$ and

deletions of LPS inner core biosynthetic genes and the sensitivity of these double deletion strains to vancomycin (8). Further experiments could be pursued in the realm of this subset of interactions, as well as the other interactions yet to be explored. For instance, YhdP has yet to be fully characterized. Since the publication of our work, recent work from Ruiz *et al.* (9) and Grimm *et al.* (10) has proposed that YhdP is also involved in anterograde phospholipid transport. The exact role of YhdP in phospholipid transport and ECA regulation, as well as the interplay between these processes requires additional investigations.

Since publishing this work, I have collected preliminary data which suggests that the susceptibility of the $\Delta yhdP$ Δ LPS inner core double mutants can be exploited to find compounds that either bind to LPS inner core or inhibit LPS biosynthesis. In this case, replacing the LPS inner core gene deletion with a compound that either binds LPS or inhibits its biosynthesis phenocopies this three-way SSL interaction between vancomycin, $\Delta yhdP$, and LPS perturbation. Compounds that physically bind to the inner core of LPS, including pentamidine, liproxstatin-1, and MAC-0568743, as well as an inhibitor of LpxC, PF-05081090, are synergistic with vancomycin in *E. coli* $\Delta yhdP$, but not in WT (Figure 1). While more compounds should be tested to confirm this observation and its specificity, this interaction could form the basis of a screen to find compounds that target LPS. A chemical screen could be performed in $\Delta yhdP$ in a subinhibitory concentration of vancomycin to find compounds that result in growth inhibition. Actives would need to be counter-screened for lack of growth inhibition in the

same conditions but in WT. Alternatively, this interaction could be used as a tool to help elucidate the mechanism of action of a compound known to increase OM permeability to reveal whether the target is LPS or some other aspect of the OM.

The studies described in chapters 3 and 4 which employ the use of chemical screening platforms to uncover compounds which increase the permeability of the OM could also be expanded and improved to find more chemical matter that physically perturbs the OM or alters OM biosynthesis. Although the vancomycin cold antagonism screening platform is more selective, producing a lower hit rate, the higher hit rate of the potentiation screening platform, in my opinion, is more valuable as the compounds uncovered are not limited to non-lethal molecules. When paired with the appropriate follow up assays to eliminate undesired compounds, this has the potential to uncover inhibitors of both essential and non-essential OM biosynthetic processes.

Screening natural product libraries for antagonism of vancomycin activity or potentiation of Gram-positive-targeting antibiotics is an avenue which should be further investigated. One of the most well-known OM disruptors, polymyxin B, is a natural product antibiotic produced by the bacterium *Paenibacillus polymyxa* (11, 12). Our lab has previously tried screening crude natural product extracts for antagonism of vancomycin activity in the cold with limited success. However, recent progress with the development of fractionated and purified natural product libraries makes this worth revisiting, particularly with the membrane assays that the lab is now well-versed in.

Another direction that should be considered is antibiotic potentiation in host-mimicking conditions. Despite rich microbiological media being the standard for antibiotic susceptibility testing, it is not representative of the host environment where bacterial infections would take place (13). For instance, bicarbonate, which is the main buffer in human blood, alters the efficacy of antibiotics (14). If the goal is to find a potentiator compound that works *in vivo*, perhaps future screens should be done in the presence of bicarbonate or in human serum. Many of the compounds uncovered in the screens in chapters 3 and 4 were synergistic with rifampicin in standard rich media, however when bicarbonate was added to the media the synergy was abrogated, despite rifampicin itself only being antagonized by bicarbonate two-fold. The reason for this phenomenon is currently unknown but is important to consider if one hopes to find an antibiotic potentiator compound with clinical applications rather than a probe of biology.

Exploiting synthetic interactions in antibacterial drug discovery

Understanding the incredibly complex biology of the bacterial cell systems for which treatments are needed is of utmost importance for giving ourselves an advantage in the antibiotic evolutionary arms race. The study of SSL interactions is one unconventional avenue that can be used in drug discovery. Targeting specific gene pairs that are SSL is theoretically possible but exceedingly difficult in practice. As SSL interactions are often context and strain specific (15, 16), these target combinations would provide a narrow spectrum approach which

would be beneficial for sparing the microbiome. However, the practicality of finding two inhibitors of gene products that are SSL for use in combination therapy is faced with double the challenges of finding an inhibitor of a single gene product and ensuring it has whole cell activity, a low frequency of resistance, and lacks toxicity *in vivo*. This is difficult to justify for individually dispensable targets. However, targets that are individually important for viability and exhibit synergism in combination, or targets that increase sensitivity to an existing therapy, can be excellent opportunities for dose-sparing and hitting bacteria with a “one-two punch”.

Mapped SSL interaction networks can be incredible tools in preclinical drug discovery (16–19). SSL interactions are useful for mechanism of action investigation, which is a bottleneck in antimicrobial drug discovery. Comparing the chemical-genetic interaction profile of an antimicrobial compound with unknown mechanism of action to known genetic interaction profiles can help reveal information leading to the target of the compound. Uncovering idiosyncratic genetic interactions can also be used for designing chemical screens to enrich for compounds that target certain processes. The work described in chapter 2 mapping the interaction network of OM permeability genes contains a wealth of data that can be used for mechanism of actions studies and the described sensitivity of LPS inner core and *yhdP* double deletion strains can be leveraged for chemical screening purposes (Figure 1).

Research into SSL interaction networks can also help investigators prioritize targets and processes for drug discovery. Genes that have the most densely connected networks within cells should be prioritized as targets since their inhibition is more likely to impact other cellular processes and prevent resistance from arising (17). Genes categorized as essential tend to have more interactions than dispensable genes, based on the studies in yeast using temperature sensitive alleles (20). Furthermore, knowledge of genes that are conditionally essential in different infection environments can inform on *in vivo* relevant targets that would not be uncovered using traditional approaches to study gene essentiality in standard microbiological growth media (21, 22). Investigating chemical-genetic interactions of various pathogens in a multitude of infection relevant growth media in combination with antibiotics can help inform on optimal antibiotics to be used in different sites of infection (23). Another area that warrants further exploration is whether acquired resistance elements exhibit any SSL interactions with other bacterial genes, which when targeted result in decreased fitness of the drug resistant bacteria. Overall, the exploration of SSL interactions is useful for numerous facets of antimicrobial drug discovery and should not be overlooked as a tool.

Targeting the outer membrane for antibiotic potentiation in the clinic

As the antibiotic pipeline continues to dwindle, especially for Gram-negative infections, researching alternative approaches such as the use of

adjuvants to revive ineffective antibiotics is imperative. Expanding the spectrum of antibiotics which are already clinically used for treating Gram-positive infections would be beneficial given the rising resistance to antibiotics effective against Gram-negative bacteria. This is an approach that has gained increased attention from the drug discovery community in recent years (24). Thus far, the OM disrupting antibiotic potentiator discovered by Northern Antibiotics and licensed by Spero Therapeutics, SPR741, completed Phase I clinical trials in 2017 with promising results, however its advancement to Phase II is unknown (25). Our group has recently shown that physical OM perturbation is able to overcome antibiotic inactivation and efflux resistance mechanisms for rifamycins, aminocoumarins, and macrolides being potentiated (26). OM perturbation by physical and genetic disruption was also found to lower the frequency of spontaneous resistance to rifampicin (26). These findings have countered concerns that resistance to one of the two agents in the potentiator-antibiotic combination would render the therapy useless.

The goal of chapters 3 and 4 was to find compounds that either physically disrupt OM integrity or increase OM permeability through inhibition of its biosynthesis for the purpose of increasing the activity of impermeable antibiotics against Gram-negative bacteria. The probe compounds uncovered in chapter 3, liproxstatin-1 and MAC-0568743, despite having limited potential for use *in vivo* due to the high concentrations required for potentiation, show that it is indeed possible for compounds to act on the OM while sparing the IM. IM activity is often

associated with toxicity (24, 27), as evidenced with the membrane active compounds discussed in chapter 4, due to indiscriminate activity on all membranes including those of mammalian cells. However, it is possible for compounds to be active on the Gram-negative IM while sparing mammalian membranes. Song *et al.* (28) reported a short linear antibacterial peptide that potentiated the activity of antibiotics by binding to LPS in the OM and phosphatidylglycerol in the IM. Despite its disruption of the IM, it exhibited no substantial toxicity to mammalian cell lines tested (28). Thus, although specificity for the OM over the IM is valuable for compounds to be used as biological probes, compounds that are active on the IM but are nontoxic to mammalian cells should not be discarded.

In chapter 4, we also demonstrate the prospects of inhibitors of lipid A biosynthesis being used in combination with large-scaffold antibiotics such as rifampicin. While LpxC inhibitors have been extensively explored as monotherapies, their capacity to be used as antibiotic potentiators has been acknowledged but not comprehensively characterized (29). Achaogen's LpxC inhibitor, ACHN-975, is the first and only LpxC inhibitor to enter Phase I clinical trials, however it was found to have an insufficient therapeutic window due to cardiovascular toxicity (30). ACHN-975 has been shown to be synergistic with vancomycin in both *in vitro* and *in vivo* models (31, 32). Our work demonstrates that the synergism between various LpxC inhibitors and Gram-positive-targeting antibiotics should not be overlooked and has the potential for dose-sparing. With

lower doses required for antibiotic potentiation, the toxicity of LpxC inhibitors can be minimized. Based on the genetic perturbation of *waaC* resulting in a lower rate of spontaneous resistance to rifampicin (26), one would expect that perturbation of *lpxC* should exhibit a similar effect. Further work should characterize the impact of both genetic and chemical perturbation of LpxC on acquired and spontaneous resistance to partner Gram-positive-targeting antibiotics to validate the feasibility of LpxC inhibitors as antibiotic potentiators for clinical applications.

Although combinations of agents that increase the permeability of the OM and antibiotics is promising for the treatment of Gram-negative infections, this approach is not without hurdles (24, 25). The justification of a combination of two compounds that lack activity alone is difficult for regulatory bodies. Issues such as routes of administration, pharmacokinetics, pharmacodynamics, and dosing regimens must be compatible for the two compounds being administered. Clinical trials for safety and efficacy of the combination must be tested on multiple concentrations of each compound to find the optimal therapeutic dose for each. Undeniably, these considerations are more challenging than for monotherapies.

Concluding remarks

The work presented in this thesis has aimed to increase our understanding of Gram-negative OM biology and permeability through SSL interactions and chemical probes. Indeed, we have uncovered interesting connections between ECA and LPS biosynthetic pathways through SSL interactions that illuminate

aspects of OM permeability that are not well characterized. We have also characterized several chemical probes of the OM and demonstrated the potential that OM targeting compounds hold as antibiotic adjuvants. The work presented in this thesis is exclusively *in vitro*, and the translation of synthetic lethality and antibiotic potentiator compounds into clinical use faces substantial challenges, as discussed throughout. Despite these challenges, both approaches are valuable tools to subvert bacterial survival strategies in a time where conventional strategies for antibiotic discovery have not been fruitful. I am especially hopeful that OM perturbation is not far from clinical relevance, due to the immense efforts in this field in recent years, including the advancements of a physical OM perturbant and an LpxC inhibitor into clinical trials.

References

1. **Stokes JM, French S, Ovchinnikova OG, Bouwman C, Whitfield C, Brown ED.** 2016. Cold stress makes *Escherichia coli* susceptible to glycopeptide antibiotics by altering outer membrane integrity. *Cell Chem Biol* **23**:267–277.
2. **Stokes JM, MacNair CR, Ilyas B, French S, Côté J-P, Bouwman C, Farha MA, Sieron AO, Whitfield C, Coombes BK, Brown ED.** 2017. Pentamidine sensitizes Gram-negative pathogens to antibiotics and overcomes acquired colistin resistance. *Nat Microbiol* **2**:17028.
3. **Tommasi R, Brown DG, Walkup GK, Manchester JI, Miller AA.** 2015. ESKAPEing the labyrinth of antibacterial discovery. *Nat Rev Drug Discov* **14**:529–542.
4. **De Leon GP, Elowe NH, Koteva KP, Valvano MA, Wright GD.** 2006. An *in vitro* screen of bacterial lipopolysaccharide biosynthetic enzymes identifies an inhibitor of ADP-heptose biosynthesis. *Chem Biol* **13**:437–441.
5. **Durka M, Tikad A, Périon R, Bosco M, Andaloussi M, Floquet S, Malacain E, Moreau F, Oxoby M, Gerusz V, Vincent SP.** 2011. Systematic synthesis of inhibitors of the two first enzymes of the bacterial heptose biosynthetic pathway: towards antivirulence molecules targeting

- lipopolysaccharide biosynthesis. *Chem Eur J* **17**:11305–11313.
6. **Moreau F, Desroy N, Genevard JM, Vongsouthi V, Gerusz V, Le Fralliec G, Oliveira C, Floquet S, Denis A, Escaich S, Wolf K, Busemann M, Aschenbrenner A.** 2008. Discovery of new Gram-negative antivirulence drugs: Structure and properties of novel *E. coli* WaaC inhibitors. *Bioorganic Med Chem Lett* **18**:4022–4026.
 7. **Liu D, Reeves PR.** 1994. *Escherichia coli* K12 regains its O antigen. *Microbiology* **140**:49–57.
 8. **Klobucar K, French S, Côté J-P, Howes JR, Brown ED.** 2020. Genetic and chemical-genetic interactions map biogenesis and permeability determinants of the outer membrane of *Escherichia coli*. *mBio* **11**:e00161-20.
 9. **Ruiz N, Davis RM, Kumar S.** 2021. YhdP, TamB, and YdbH are redundant but essential for growth. *mBio* **12**:e02714-21.
 10. **Grimm J, Shi H, Wang W, Mitchell AM, Wingreen NS, Huang KC, Silhavy TJ.** 2020. The inner membrane protein YhdP modulates the rate of anterograde phospholipid flow in *Escherichia coli*. *Proc Natl Acad Sci* **117**:26907–26914.
 11. **Ainsworth G, Brown A, Brownlee G.** 1947. ‘Aerosporin’, an antibiotic produced by *Bacillus aerosporus* Greer. *Nature* **160**:263.
 12. **Storm DR, Rosenthal KS, Swanson PE.** 1977. Polymyxin and related peptide antibiotics. *Annu Rev Biochem* **46**:723–763.
 13. **Brown ED, Wright GD.** 2016. Antibacterial drug discovery in the resistance era. *Nature* **529**:336–343.
 14. **Farha MA, French S, Stokes JM, Brown ED.** 2018. Bicarbonate alters bacterial susceptibility to antibiotics by targeting the proton motive force. *ACS Infect Dis* **4**:382–390.
 15. **van Opijnen T, Dedrick S, Bento J.** 2016. Strain dependent genetic networks for antibiotic-sensitivity in a bacterial pathogen with a large pan-genome. *PLoS Pathog* **12**:e1005869.
 16. **Klobucar K, Brown ED.** 2018. Use of genetic and chemical synthetic lethality as probes of complexity in bacterial cell systems. *FEMS Microbiol Rev* **42**:fux054.
 17. **Hogan AM, Cardona ST.** 2022. Gradients in gene essentiality reshape antibacterial research. *FEMS Microbiol Rev* fuac005.
 18. **Halder V, McDonnell B, Uthayakumar D, Usher J, Shapiro RS.** 2021. Genetic interaction analysis in microbial pathogens: unravelling networks of pathogenesis, antimicrobial susceptibility and host interactions. *FEMS Microbiol Rev* **45**:fuaa055.
 19. **Farha MA, French S, Brown ED.** 2021. Systems-level chemical biology to accelerate antibiotic drug discovery. *Acc Chem Res* **54**:1909–1920.
 20. **Costanzo M, VanderSluis B, Koch EN, Baryshnikova A, Pons C, Tan G, Wang W, Usaj M, Hanchard J, Lee SD, Pelechano V, Styles EB, Billmann M, van Leeuwen J, van Dyk N, Lin Z-Y, Kuzmin E, Nelson J,**

- Piotrowski JS, Srikumar T, Bahr S, Chen Y, Deshpande R, Kurat CF, Li SC, Li Z, Usaj MM, Okada H, Pascoe N, San Luis B-J, Sharifpoor S, Shuteriqi E, Simpkins SW, Snider J, Suresh HG, Tan Y, Zhu H, Malod-Dognin N, Janjic V, Przulj N, Troyanskaya OG, Stagljar I, Xia T, Ohya Y, Gingras A-C, Raught B, Boutros M, Steinmetz LM, Moore CL, Rosebrock AP, Caudy AA, Myers CL, Andrews B, Boone C.** 2016. A global genetic interaction network maps a wiring diagram of cellular function. *Science* **353**:aaf1420.
21. **Weber BS, De Jong AM, Guo ABY, Dharavath S, French S, Fiebig-Comyn AA, Coombes BK, Magolan J, Brown ED.** 2020. Genetic and chemical screening in human blood serum reveals unique antibacterial targets and compounds against *Klebsiella pneumoniae*. *Cell Rep* **32**:107927.
 22. **Carfrae LA, MacNair CR, Brown CM, Tsai CN, Weber BS, Zlitni S, Rao VN, Chun J, Junop MS, Coombes BK, Brown ED.** 2020. Mimicking the human environment in mice reveals that inhibiting biotin biosynthesis is effective against antibiotic-resistant pathogens. *Nat Microbiol* **5**:93–101.
 23. **Brown SA, Palmer KL, Whiteley M.** 2008. Revisiting the host as a growth medium. *Nat Rev Microbiol* **6**:657–666.
 24. **Klobucar K, Brown ED.** 2021. New potentiators of ineffective antibiotics: Targeting the Gram-negative outer membrane to overcome intrinsic resistance. *Curr Opin Chem Biol* **66**:102099.
 25. **Vaara M.** 2019. Polymyxin derivatives that sensitize Gram-negative bacteria to other antibiotics. *Molecules* **24**:249.
 26. **MacNair CR, Brown ED.** 2020. Outer membrane disruption overcomes intrinsic, acquired, and spontaneous antibiotic resistance. *mBio* **11**:e01615-20.
 27. **Hyun S, Choi Y, Jo D, Choo S, Park TW, Park SJ, Kim S, Lee S, Park S, Jin SM, Cheon DH, Yoo W, Arya R, Chong YP, Kim KK, Kim YS, Lee Y, Yu J.** 2020. Proline hinged amphipathic α -helical peptide sensitizes Gram-negative bacteria to various Gram-positive antibiotics. *J Med Chem* **63**:14937–14950.
 28. **Song M, Liu Y, Huang X, Ding S, Wang Y, Shen J, Zhu K.** 2020. A broad-spectrum antibiotic adjuvant reverses multidrug-resistant Gram-negative pathogens. *Nat Microbiol* **5**:1040–1050.
 29. **Erwin AL.** 2016. Antibacterial drug discovery targeting the lipopolysaccharide biosynthetic enzyme LpxC. *Cold Spring Harb Perspect Med* **6**:a025304.
 30. **Cohen F, Aggen JB, Andrews LD, Assar Z, Boggs J, Choi T, Dozzo P, Easterday AN, Haglund CM, Hildebrandt DJ, Holt MC, Joly K, Jubb A, Kamal Z, Kane TR, Konradi AW, Krause KM, Linsell MS, Machajewski TD, Miroshnikova O, Moser HE, Nieto V, Phan T, Plato C, Serio AW, Seroogy J, Shakhmin A, Stein AJ, Sun AD, Sviridov S, Wang Z, Wlasichuk K, Yang W, Zhou X, Zhu H, Cirz RT.** 2019. Optimization of

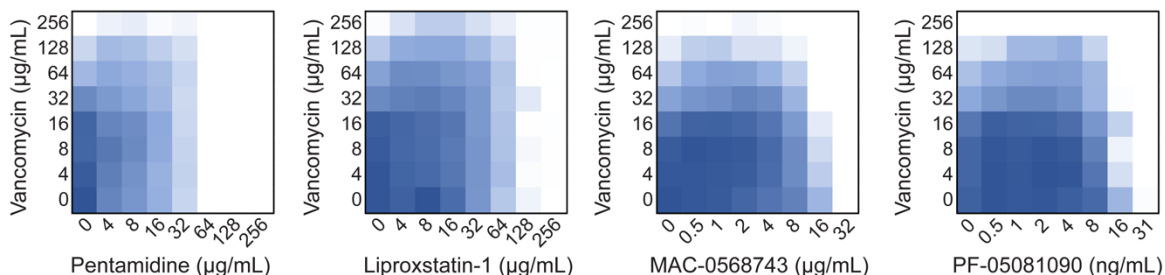
LpxC inhibitors for antibacterial activity and cardiovascular safety.

ChemMedChem **14**:1560–1572.

31. **Patten P, Armstrong E.** 2011. Combinations comprising a LpxC inhibitor and an antibiotic for use in the treatment of infections caused by Gram-negative bacteria. Patent WO 2011005355. USA.
32. **Kasar R, Linsell M, Aggen J, Lu Q, Wang D, Church T, Moser H, Patten P.** 2012. Hydroxamic acid derivatives and their use in the treatment of bacterial infections. Patent WO 2012154204. USA.

Figures

WT:



$\Delta yhdP$:

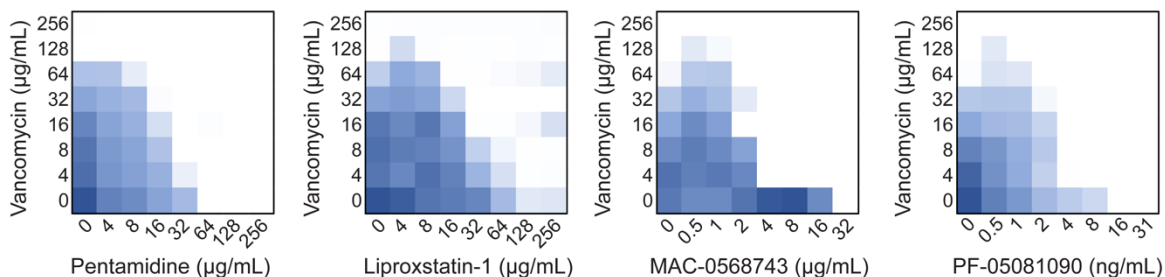


Figure 1: Compounds that target LPS, both physically and its biosynthesis, are synergistic with vancomycin in a $\Delta yhdP$ background. Shown are checkerboard broth microdilution assays between compounds which physically interact with LPS (pentamidine, liproxstatin-1, MAC-0568743) or inhibit LPS biosynthesis (PF-05081090) and vancomycin in *E. coli* BW25113 wild type (top) and $\Delta yhdP$ (bottom). Darker blue represents regions of higher growth and white represents growth inhibition.